GL01492

H.R. copy orig. illust.

UNIVERSITY OF UTAH RESEARCH INSTITUTE

UURI

EARTH SCIENCE LABORATORY
391 CHIPETA WAY, SUITE C
SALT LAKE CITY, UTAH 84108—1295
TELEPHONE 801-524-3422

December 23, 1985

MEMORANDUM

TO: Marshall Reed
GHTD, DOE

FROM: Howard Ross
ESL/UURI

SUBJECT: Preliminary evaluation of electrical resistivity data base, Soufriere geothermal area, St. Lucia, Caribbean Sea

Introduction

The initial electrical resistivity survey on St. Lucia was completed by geophysicists from the Institute of Geological Sciences (IGS), Great Britain, in 1974. The survey included 13 lines of dipole-dipole resistivity using a standard electrode separation (a) of 200 m. The distribution of survey lines and geothermal test wells is shown in Figure 1. The survey is described in detail by Greenwood and Lee (1976). A review of this report, the detailed topographic map and the numerical data for each line (which you provided to us), suggest that the survey was completed in a competent manner. The survey lines were selected to provide reasonable coverage of the thermal area and much of the caldera while making good use of existing access and minimizing topographic effects. Resistivity values were recorded for separations (n) of 2 to 10 by the IGS terminology (corresponds to n=1 to 9 in the SEG terminology).

Although these data appear to be quite reliable, the pseudosection plots are somewhat misleading as they are presented in terms of depth instead of

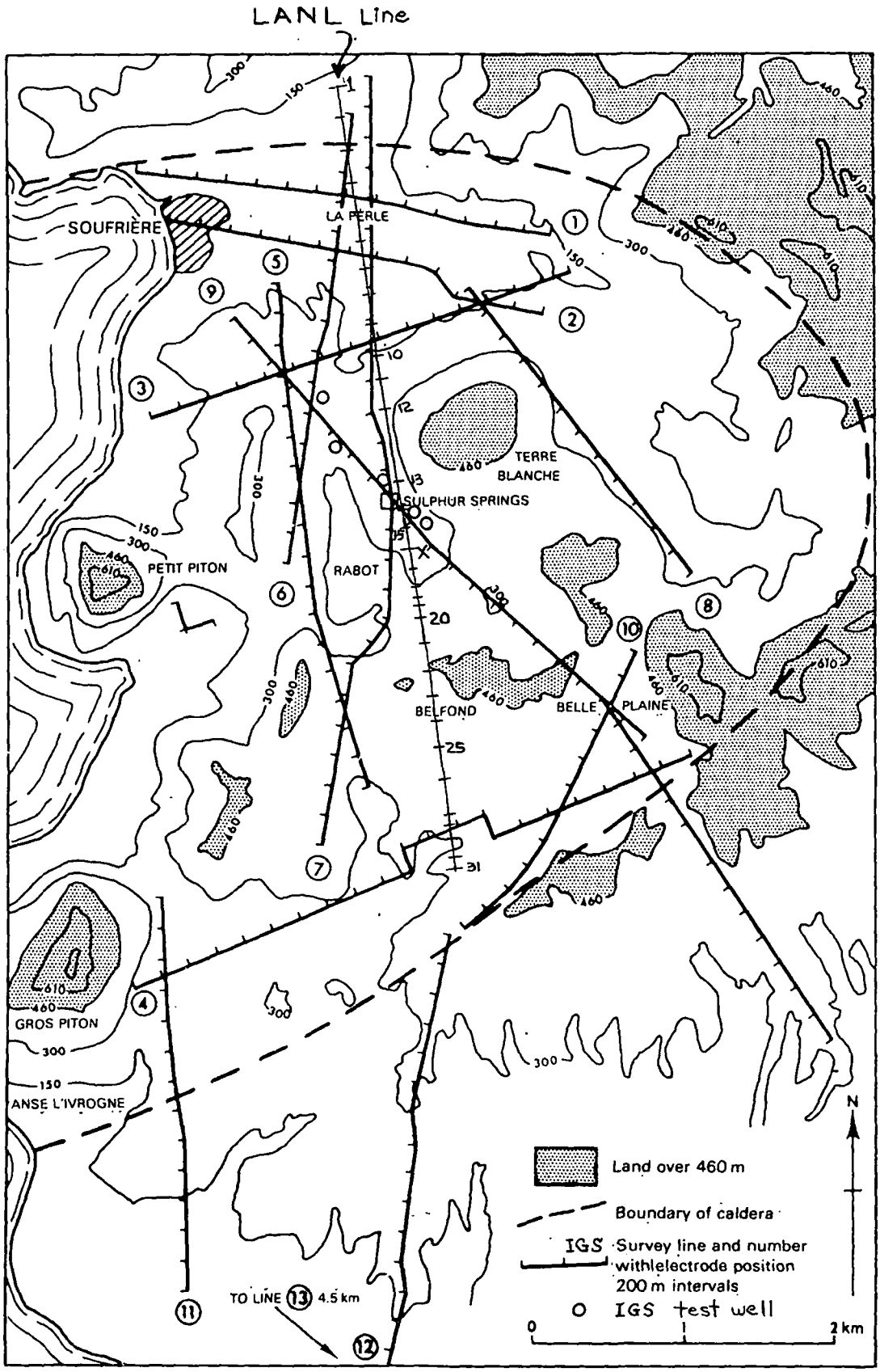

Fig. 1 Soufrière area, St Lucia showing geophysical survey lines

electrode separation (i.e. Figure 2c). The suggested depth equivalence (n=2=200 m, 3=300 m, 4=400 m, etc.) is not generally accepted or considered valid. The maximum reliable depths of resistivity mapping, assuming two-dimensional resistivity distribution perpendicular to the survey line with n=2-8 (IGS), and numerical modeling of the data has been shown to be approximately 2a to 2.5a.

In the case of the IGS data considered here this would correspond to depths of 400-500 m instead of the 800-1000 m indicated by depth scales on the pseudosections. Although the data were recorded to greater separations (n=2-10, IGS) the lateral effects associated with three-dimensional resistivity distributions and topography, and the lack of even two-dimensional numerical modeling, preclude an accurate mapping of resistivities for depths exceeding 400 m. The geologic interpretation of the data, excepting the depth considerations, seem reasonable and well considered.

Numerical Modeling, Line 9

Subsequent to reporting the field surveys, the IGS contracted to Geotronics Corp (U.S.A.) for a number of forward numerical model calculations simulating the resistivity distribution of the northern half of line 9 (dipoles 4-15) which crosses the Sulphur Springs area (Lee and Greenwood, 1976). Although none of the six models presented achieve a good fit to the observed data, model 6 (shown as Figure 2a, 2b) provides a fair indication of the near surface (0-200 m) resistivity distribution, and indicates the large scale resistivity distribution to depths of about 400 m. The models allow Lee and Greenwood to infer three deeper resistivity units of approximately 15 Ω•m, 30 Ω•m, and 5 Ω•m. The numerical model results lead the authors to the generally accepted resistivity depth-of-resolution values noted above, i.e. 2a-2.5a. The authors also correctly cautioned that three-dimensional subsurface and topographic effects, and the strong influence of near surface resistivities on the data set, severely limited interpretation for depths exceeding about 400 m. Numerical model 6 shows a good correlation with near surface geology. High temperature wells 3, 4 and 5 are sited in low (2-5 Ω•m) near surface resistivity bodies.

The resistivity modeling program used by Geotronics Corp. (RESCAL) was an early modeling algorithm and several important improvements have been incor-

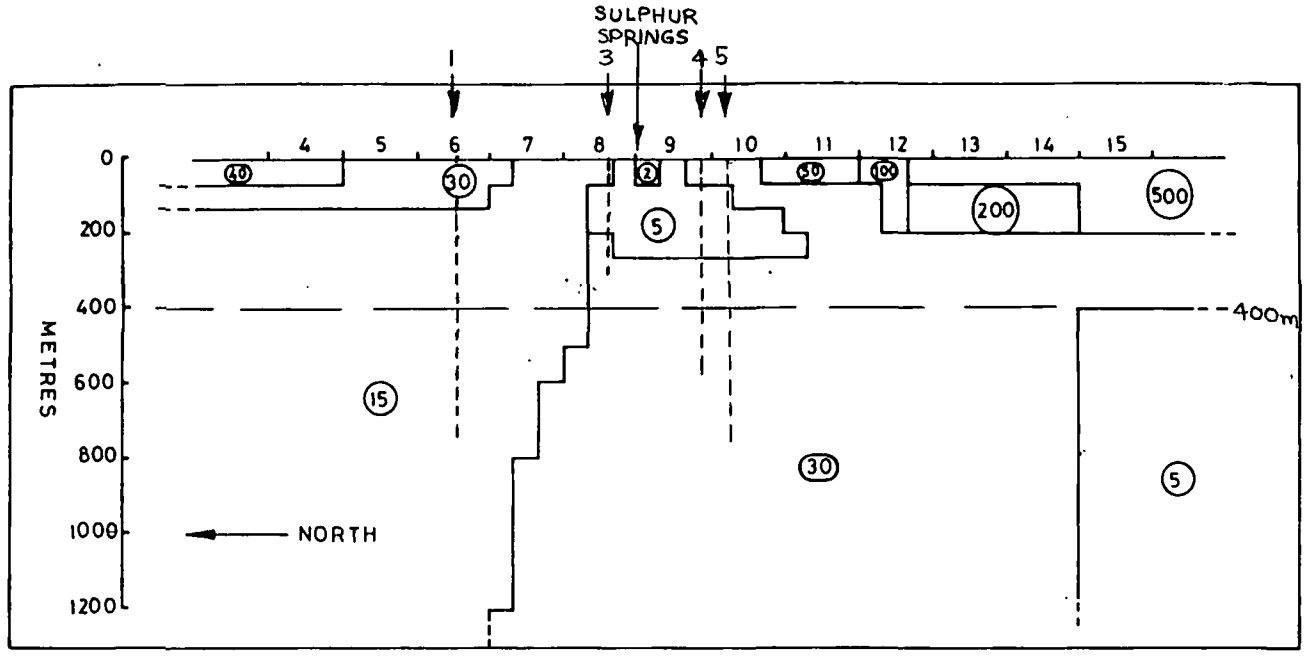

Fig. 2a Line 9 - true resistivity model 6

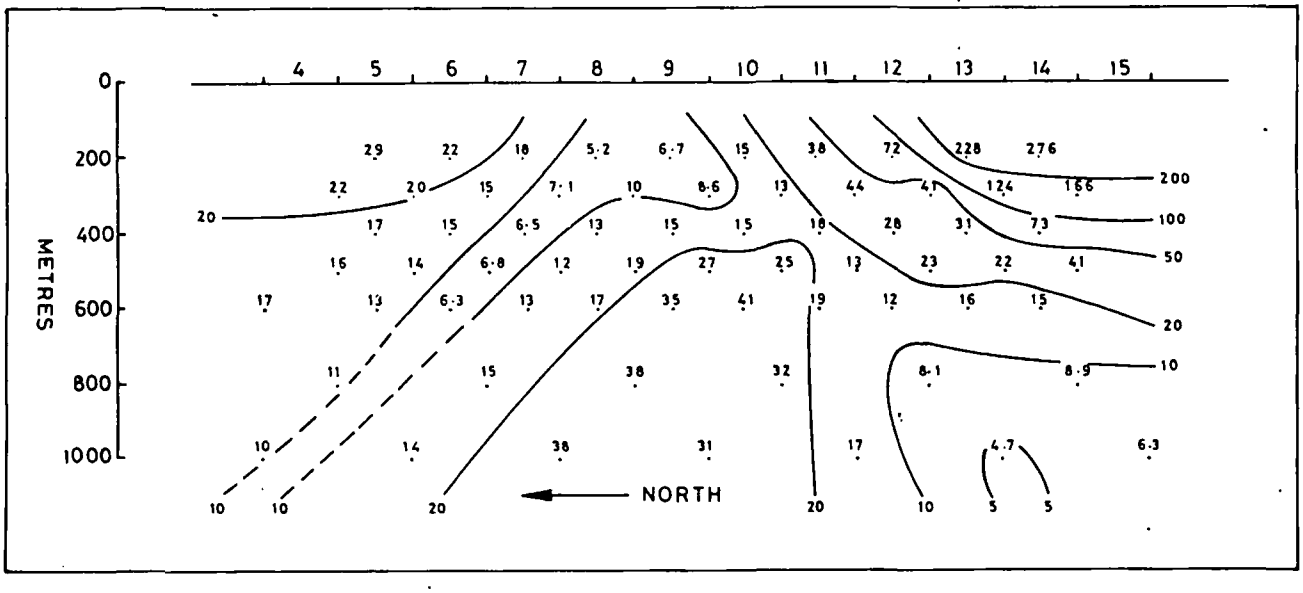

Fig. 2b Line 9 - computer generated section due to model 6

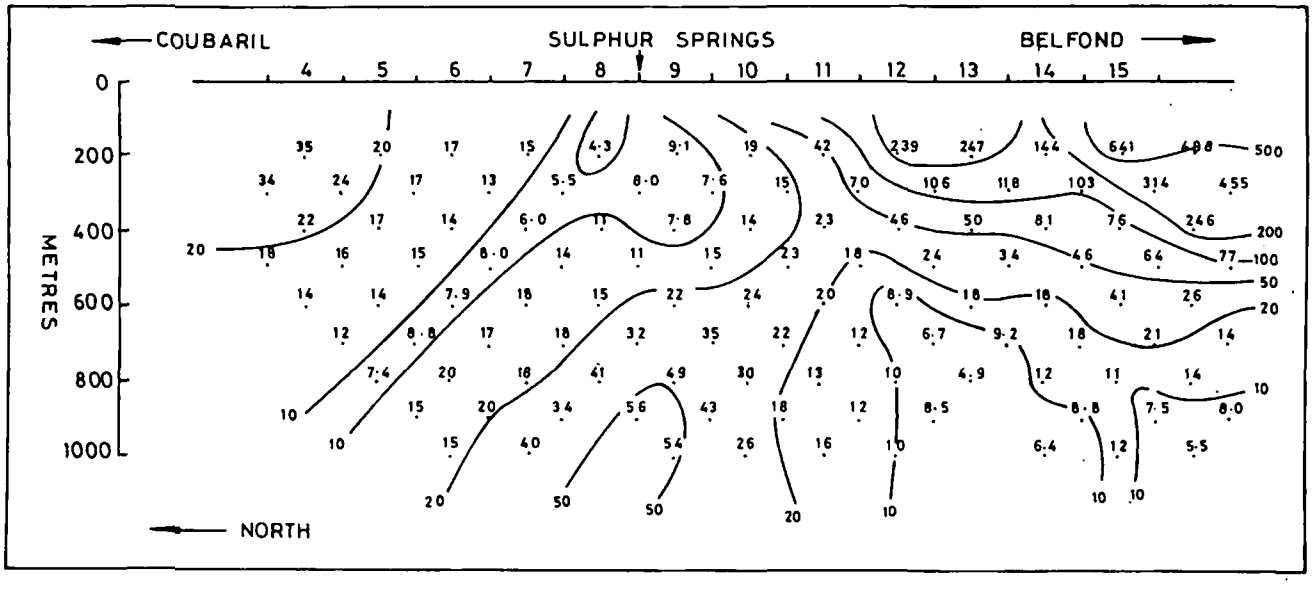

Fig. 2c Line 9 - apparent resistivity cross-section - observed

porated in later programs, such as RIP2 developed by ESL/UURI. The RIP2 algorithm is more efficient and permits a greater subdivision of the model (higher geometric resolution), calculation for separations n=2, 3, 4, 5, 6, 7 (as compared to n=2, 3, 4, 5, 6), and allows for modeling (2-D) topographic effects. As a result substantially more accurate interpretations, to depths of 2a-2.5a, are possible at present.

LANL Resistivity Profile

In January 1984, Los Alamos National Laboratory (LANL) completed one additional resistivity profile of total length 5.2 km (Ander et al., 1984). As shown in Figure 1, the northern half of the line is almost a complete duplication of the earlier IGS lines 6 and 7. The line location and electrode separation were chosen after evaluating the existing data of Greenwood and Lee (1976). The LANL survey profile attempted to achieve resistivity data to a depth of 2 km and simultaneously maintain a high spatial resolution consistent with 200 m dipoles. In an attempt to achieve these conflicting goals, they read voltages to separations as great as n=24 and 25. In order to read the small voltages which result from short transmitting and receiving dipoles, they developed their own 35-KW trailer-mounted DC transmitter driven by a 60-KW diesel generator.

The current flow path is primarily a function of the three-dimensional resistivity distribution and the separation of the current electrodes (i.e. the transmitting dipole length), and the use of short dipoles (200 m to less than 100 m) constrained most of the current flow to a near surface hemispherical volume with $r \leq 2a$ as shown schematically in Figure 3. Inherent to recording such extremely large transmitter-receiver separations as $n > 10$ are noisy data resulting from low induced voltages, which are then multiplied by large geometric factors. In addition, the current is not constrained to a simple flow path between transmitting and receiving dipoles, but is distributed inversely with resistivity for current paths lateral to the survey profile. As Lee and Greenwood (1976) and Greenwood and Lee (1976) reported earlier, the resistivity distribution in the subject area is certainly three-dimensional and topographic variations are also large. The Caribbean Sea is a low resistivity body only 1-2 km west of the survey profile. Thus the interpretation of these data to depths greater than 400 m to 500 m is very specu-

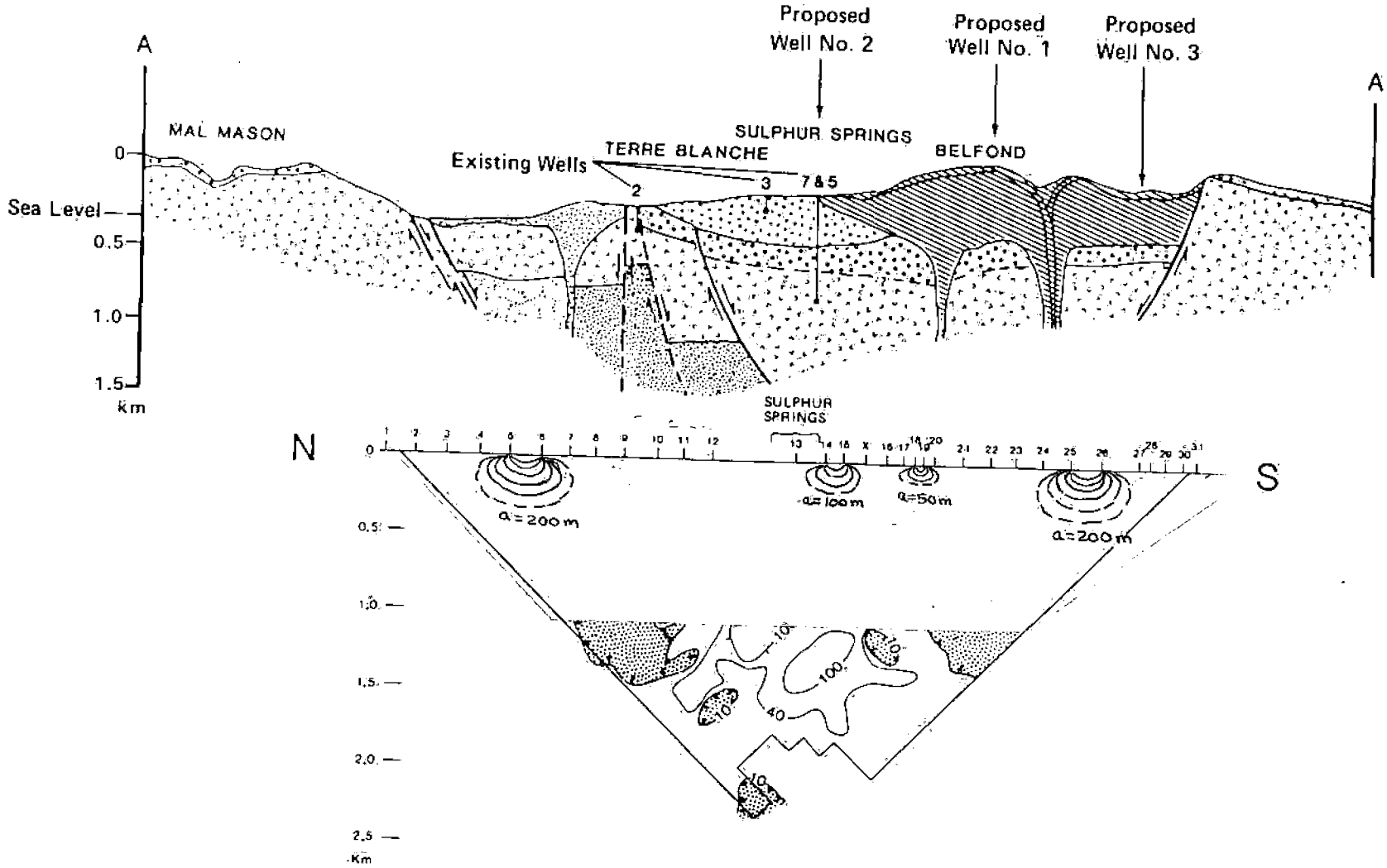

Figure 3. Schematic illustration of current distribution as a function of transmitting dipole length, for the LANL line.

lative.

The southern half of the LANL line does not duplicate earlier IGS coverage but is a real mix of different dipole lengths, from 200 m to less than 100 m (Figure 4), and hence of variable current depth penetration. A major data gap (or single 500 m dipole?) which occurs in the pseudosection (stations 12-13) is contoured as data comparable to the rest of the line. As a general rule the resistivity data could be interpreted through numerical modeling to determine the vertical resistivity distribution to depths of 400 m at most; less where the dipole length was 150 m or less.

Anders et al. (1984) present a very limited discussion of the LANL resistivity data, reproduced here as Figure 4. They note that "the upper 700 m of the pseudosection shows similar characteristics to the British dipole-dipole data" with 40 Ω•m resistivities common north of Sulphur Springs. They also note high apparent resistivities beneath the Belfond area and interpret a zone of very low resistivity, less than 1 ohm-m, underlying the Etangs area. They interpret a zone of higher apparent resistivity (40-150 Ω•m) starting at a depth of 600 m beneath the Sulphur Springs area. The remainder of the interpretation is a correlation with surface and geologic features. Based on the interpretation of the "deep" resistivity data they suggest three geothermal well locations 1, 2, and 3 (see Figure 4) where they expect to encounter geothermal brines at depths of approximately 900 m, 1800 m, and 1000 m, respectively.

Our limited review of these data suggest that the LANL interpretation is simplistic, and quite probably incorrect. As noted earlier, the probable maximum depth of reliable resistivity interpretation is about 400 m. Inspection of Figure 4, now annotated with the plotting diagonals, shows that the (apparent) deep low resistivity zones beneath Sulphur Springs and Belfond are more likely primarily due to reinforcement at the intersection of diagonals from low resistivity surface areas 1-5 and 26-27, and 13-15 and 26-31, respectively. There are no data to suggest the continuation of low resistivities near proposed Well No. 3 (electrodes 26-31) to depths below 200 m. It is uncertain from our reading of the LANL report if data were taken for the 12-13 dipole, or if this represents two large data gaps in the pseudosection. In addition, there is no numerical modeling to support an interpretation of the LANL data. In any case, we would never rely on one deep

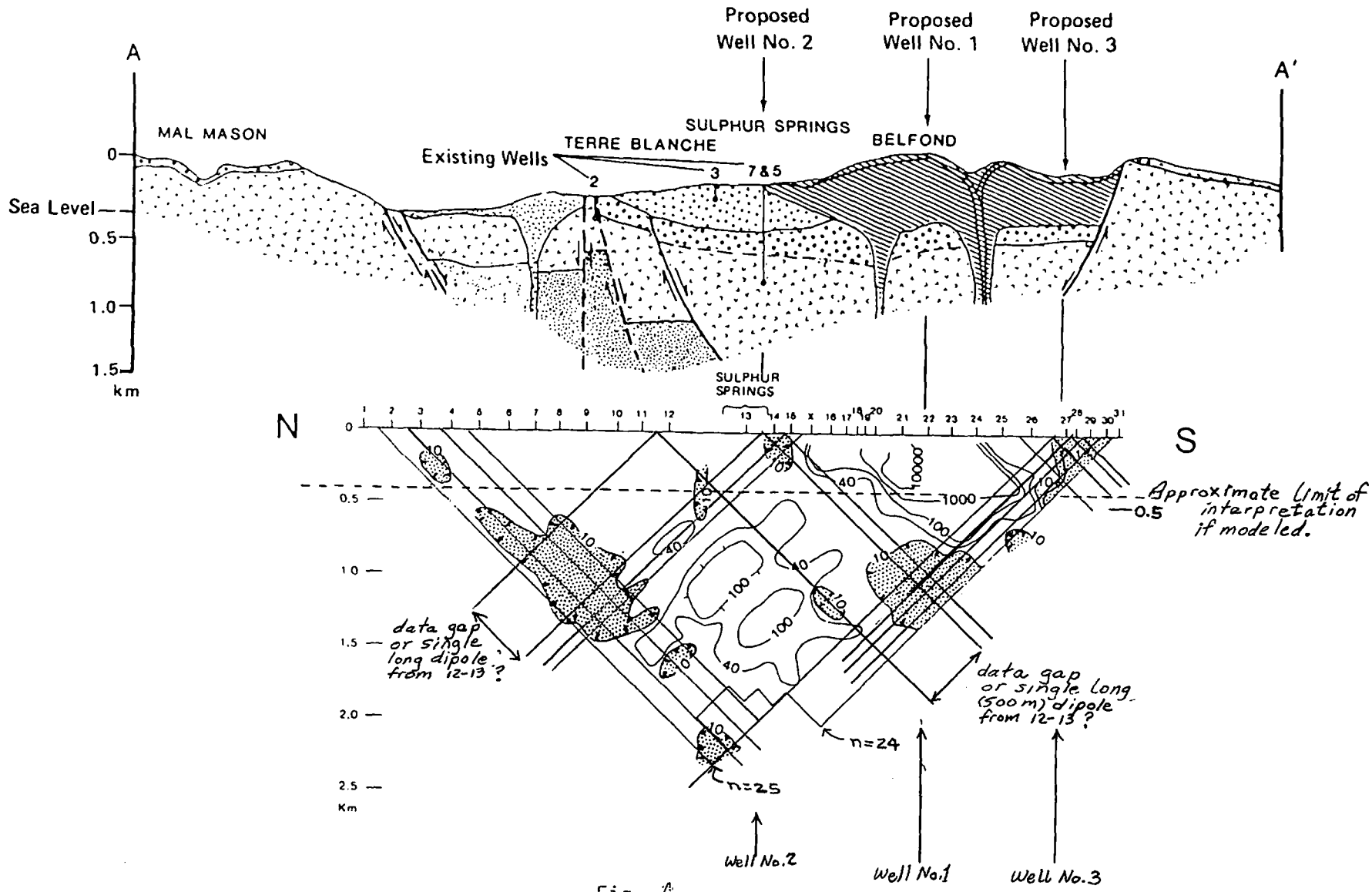

Fig. 4

Apparent resistivity data from the dipole-dipole survey plotted as a function of depth. Resistivity values are in ohm-m and are shown beneath the appropriate geologic cross section. Shaded areas depict resistivity contours of 10 ohm-m or less.

resistivity line since effects from beneath a single resistivity line cannot be separated from effects originating off to the side. There is thus no assurance at all that the low resistivity portions of the LANL profile indicate actual low earth resistivity at the depths they indicate directly beneath the line. We therefore recommend that the resistivity data of this line be given little weight in selecting drill sites for future testing of the geothermal resource.

Recommendation

Numerical modeling of several lines of the IGS resistivity survey could provide substantial information on resistivity distributions and hence possible faults, lithologic changes, and geothermal fluids, to depths of 400-500 m. Resistivity lines pertinent to siting of future drill holes include lines 4, 5, 6, 7, 8, 9, and 10. Topographic variations could be modeled, if severe enough to warrant the additional time and expense. Although the resistivity interpretation would not be valid for depths below 500 m, the structure from 0-500 m depths, when correlated with geologic data, would provide the best indication of deeper features, and hence the best basis on which to site future drill holes.

References

Ander, M., Goff, F., Hanold, B., Heiken, G., Vuataz, F., and Wohletz, K., 1984, Evaluation of the St. Lucia geothermal resource: Los Alamos Natl. Lab. rept., LA-10234-MS, 91 p.

Greenwood, P. G., and Lee, M. K., 1976, Geophysical surveys in St. Lucia for geothermal resources: Institute of Geological Sciences rept. no. 26, 30 p.

Lee, M. K., and Greenwood, P. G., 1976, The interpretation of resistivity surveys for geothermal resources in St. Lucia: Institute of Geological Sciences, rept. no. 31, 9 p.

Howard Ross

Howard P. Ross
Section Head/Geophysics

HPR/jp

Geophysical Surveys in St Lucia for Geothermal Resources

P. G. Greenwood and M. K. Lee

1. INTRODUCTION

The Soufrière region of the island of St Lucia in the Caribbean Sea has been regarded for the past few decades as a potential area for geothermal energy. Since the early nineteen-fifties well documented geological and geothermal studies of selected parts of the Soufriere region have been made by various authors, but no geophysical measurements, apart from a few temperature determinations, had been recorded.

In response to a request received by the Overseas Development Ministry (ODM) in London from the Government of St Lucia for assistance in an exploration programme for geothermal resources, experts from the Institute of Geological Sciences (IGS) and Merz and McLellan (M and M) visited St Lucia during April of 1974 to evaluate the surface emanations and recommend an exploratory programme. The IGS report recommended the application of geophysical, geochemical and hydrogeological investigations and that the combined conclusions from these disciplines be used to site a series of exploratory boreholes drilled by a contractor responsible to M and M. Some hydrogeochemical field studies were completed during September 1974 (Morgan-Jones and Edmunds,1974) and further field studies commenced in February 1975.

Geophysical investigations using the resistivity method were undertaken by Messrs P. G. Greenwood and M. K. Lee of the IGS Applied Geophysical Unit from September to December 1974 on behalf of ODM. This report presents the geophysical data collected and some tentative interpretations in terms of geothermal reservoir potential are made.

The resistivity results suggest that the Soufrière geothermal system is vapour dominated and that the subsurface structure of the system is complex. Without geological control (in the form of boreholes) it is not easy to infer either a unique or simple model for the geothermal reservoir, and it should be noted that resistivity interpretation techniques for the study of vapour dominated systems are less well advanced compared to those for hot water systems. However, the resistivity survey has successfully delineated anomalous zones but the full significance of the data will not be known until more extensive geochemical and hydrogeological surveys are completed and at least one exploratory borehole is logged.

2. FIELDWORK AND ORGANISATION

2.1 Organisation

The geophysical survey was conducted in co-operation with the St Lucia Government Lands and Survey Department who arranged for the necessary local support facilities. The field crew comprised the two IGS Geophysicists, a local surveyor, and a local labour force which varied according to the work available but usually exceeded twenty men. Initially two vehicles, but later three, were required to transport the large numbers of staff and the bulky resistivity equipment. The Sub Collector in Soufrière was appointed Liaison Officer and was responsible for the recruitment and payment of the labour force and the supply of fuel and minor contingencies. The use of radio transceivers was essential during the resistivity field measurements and without them the survey could never have been satisfactorily completed. Initially, considerable problems were encountered with these transceivers due to their use under jungle conditions (where the leaf surface of the thick vegetation act as innumerable radio wave reflectors thus scattering the transmitted signal) and invaluable assistance was received from both a detachment of Royal Signals from the British Army (on an exercise in the Caribbean) and the Radio Communication Department of the St Lucia Police Force.

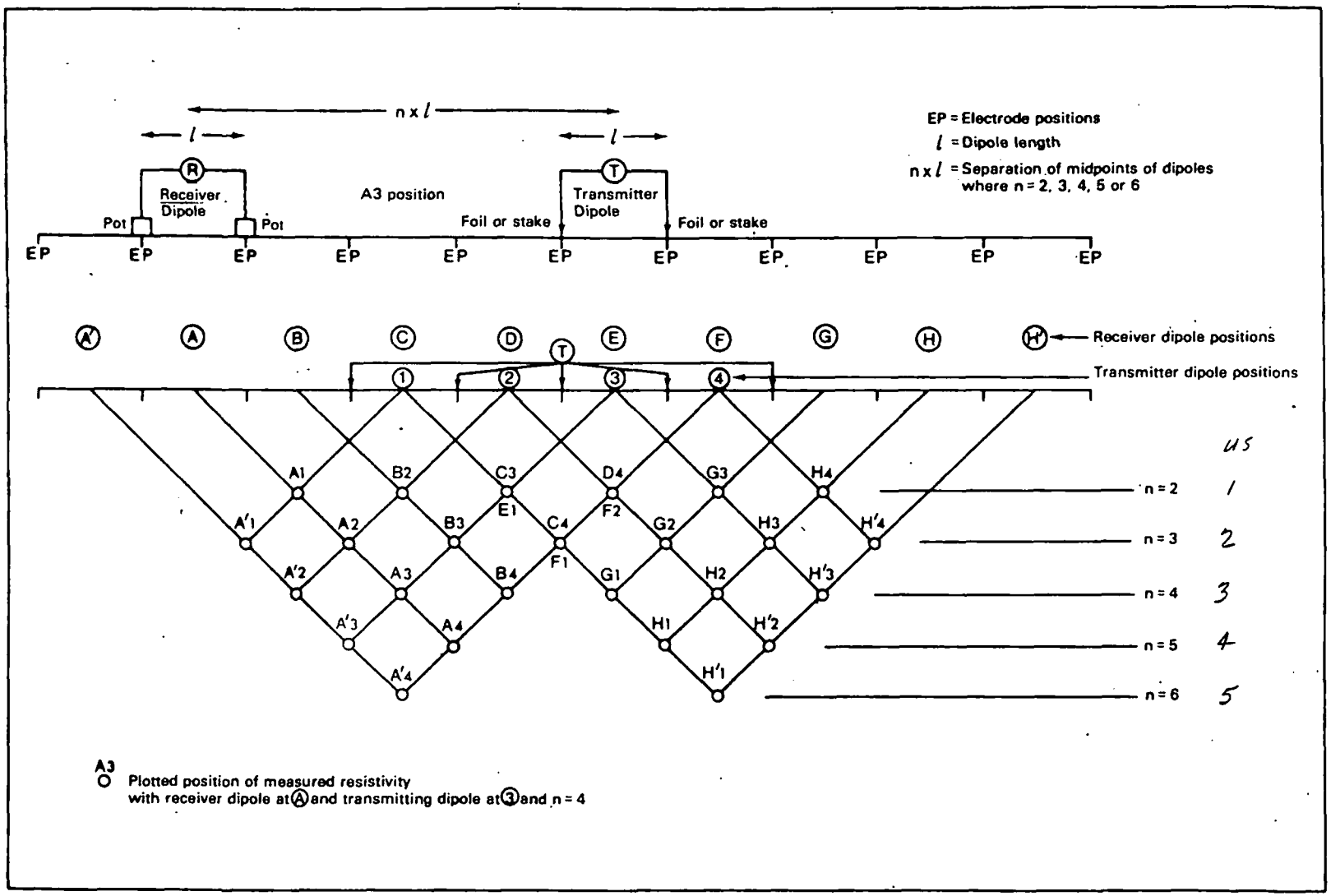

Fig. 3 A field 'set up' illustrating the method of plotting results for the dipole-dipole configuration (after Zohdy et al 1973)

APPENDIX III

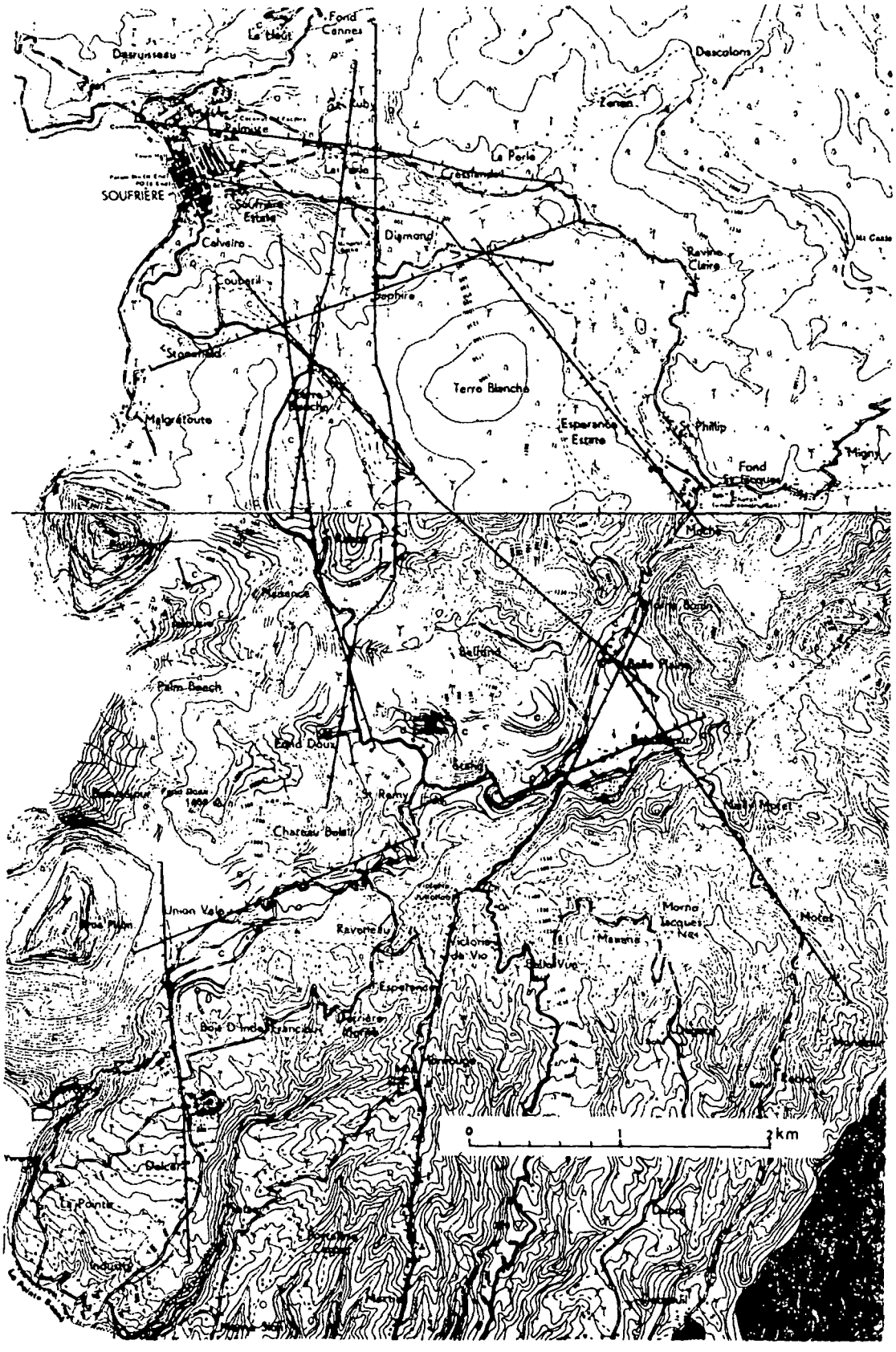

Soufriere area, St Lucia, showing geophysical survey lines
(Fig. 2 derives from this map)

APPENDIX III

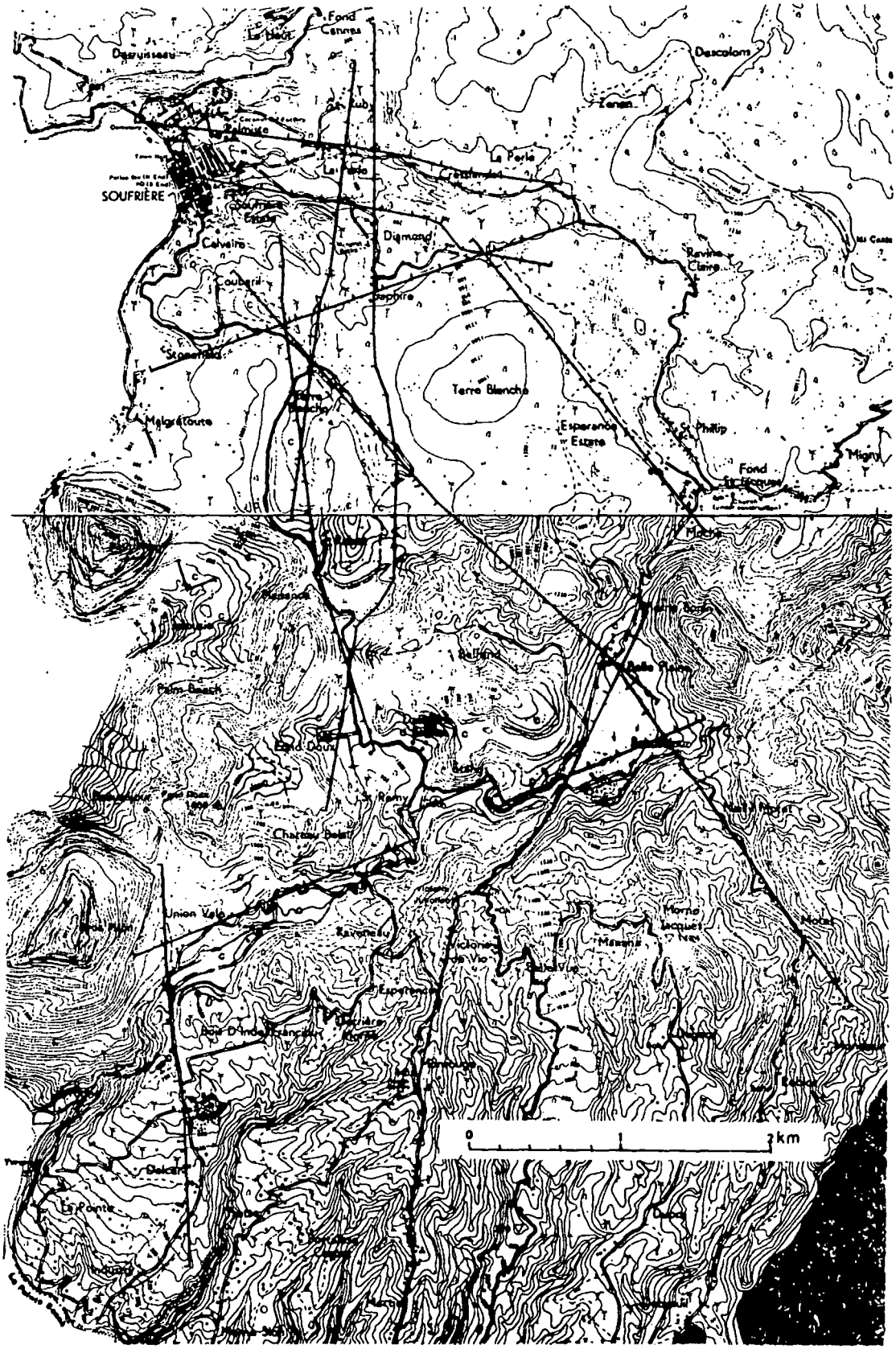

Soufriere area, St Lucia, showing geophysical survey lines
(Fig. 2 derives from this map)

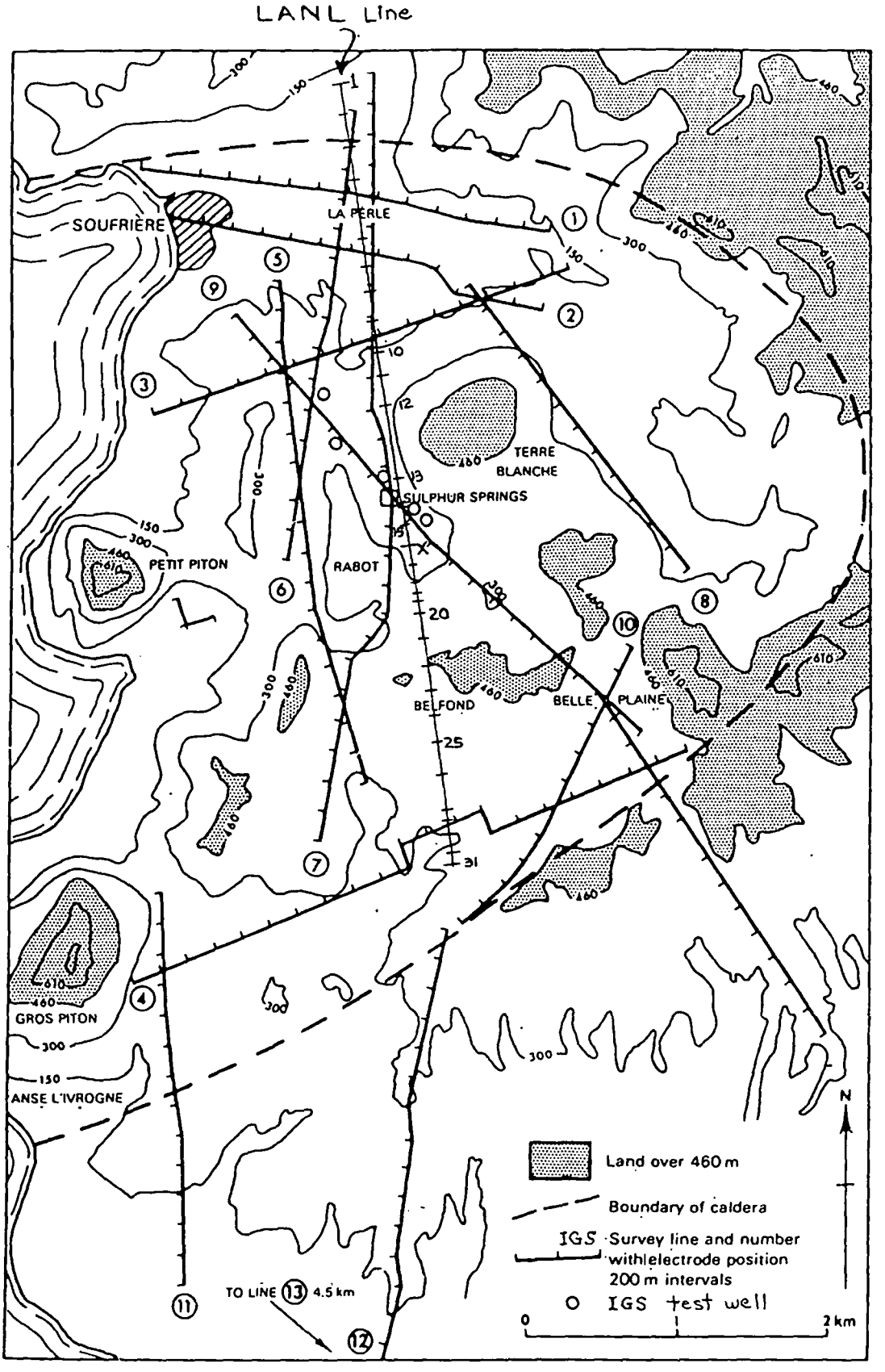

Fig. 1 Soufrière area, St Lucia showing geophysical survey lines

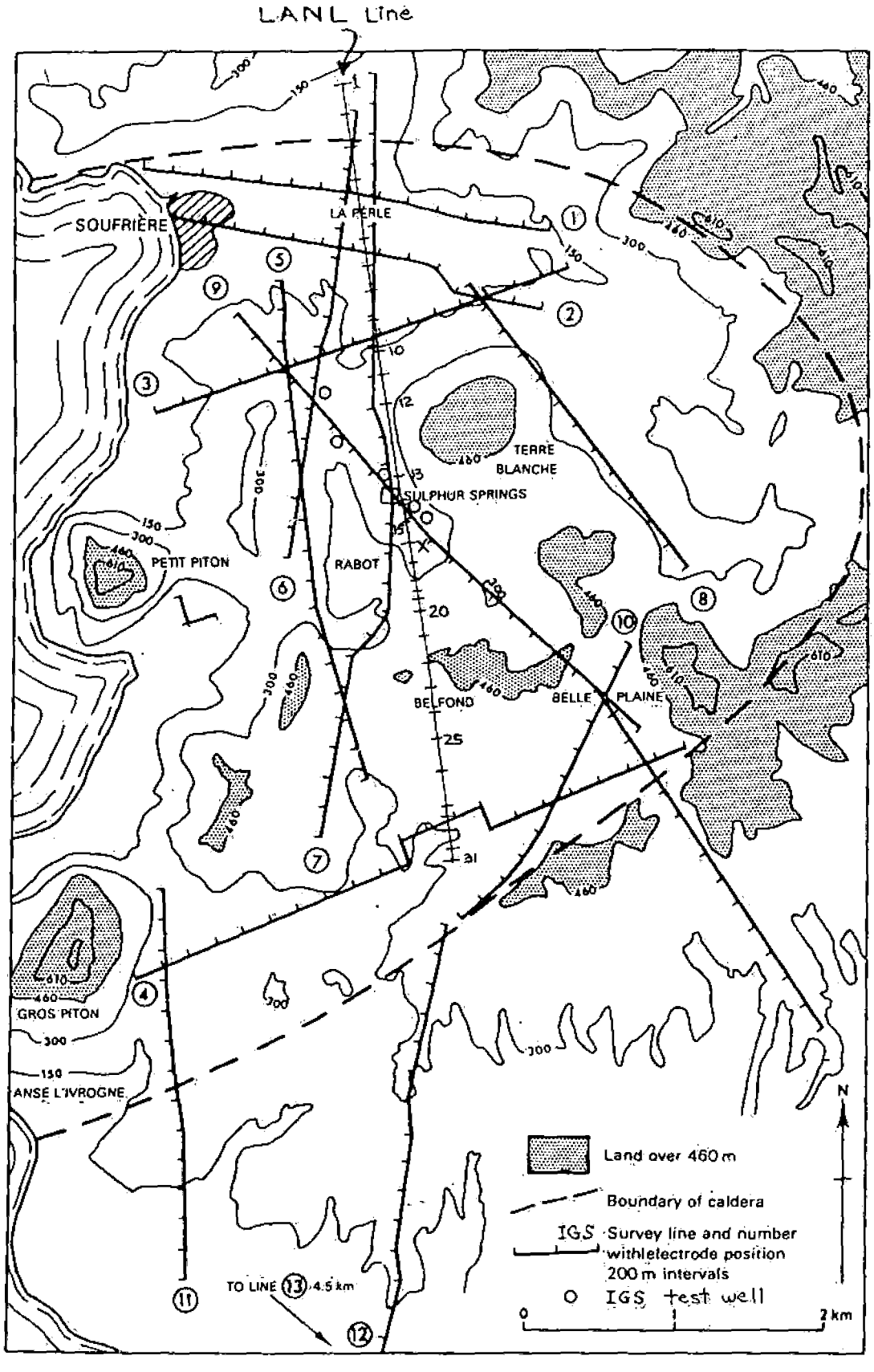

Fig. 1 Soufrière area, St Lucia showing geophysical survey lines

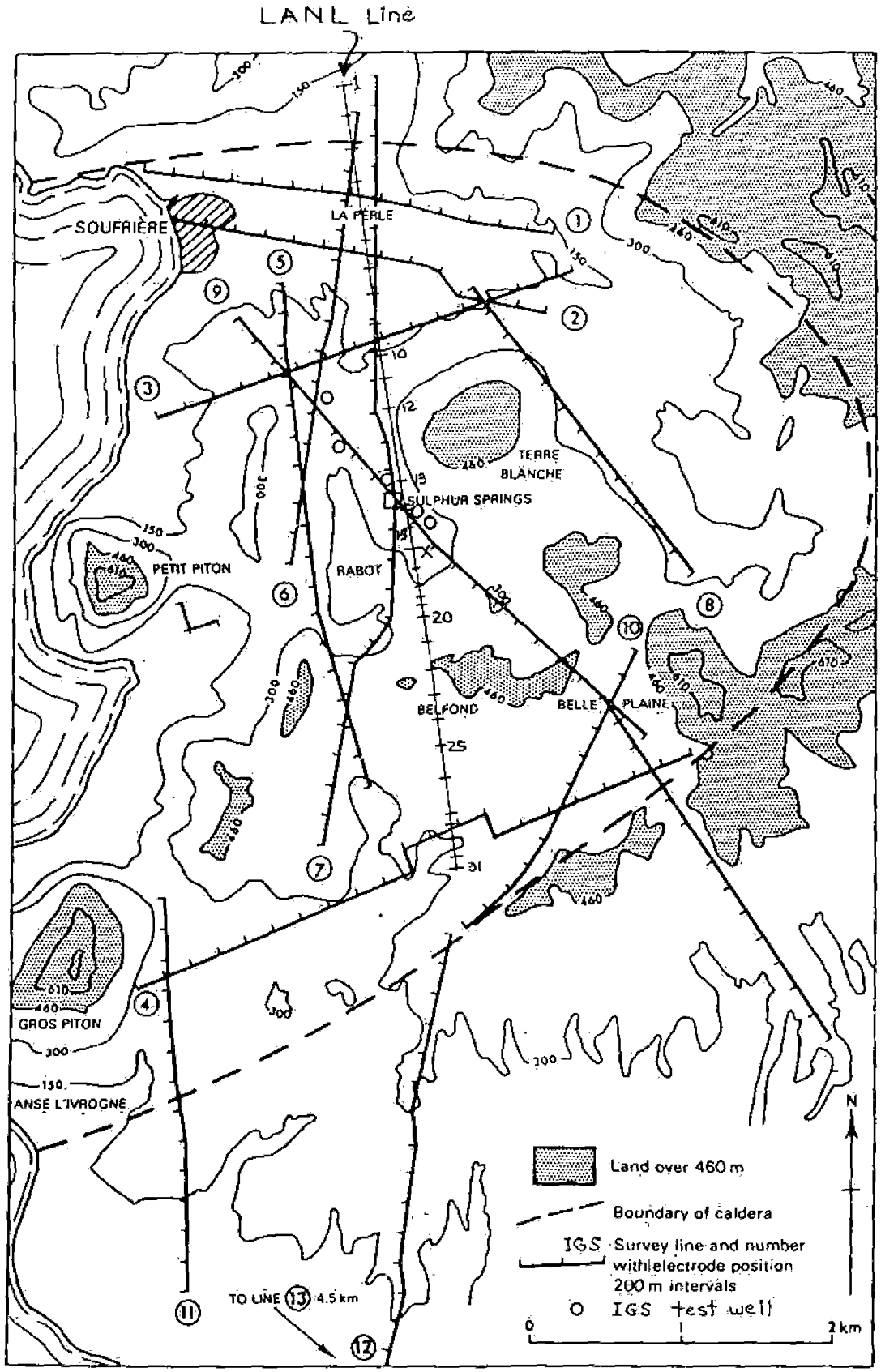

Fig. 1 Soufrière area, St Lucia showing geophysical survey lines.

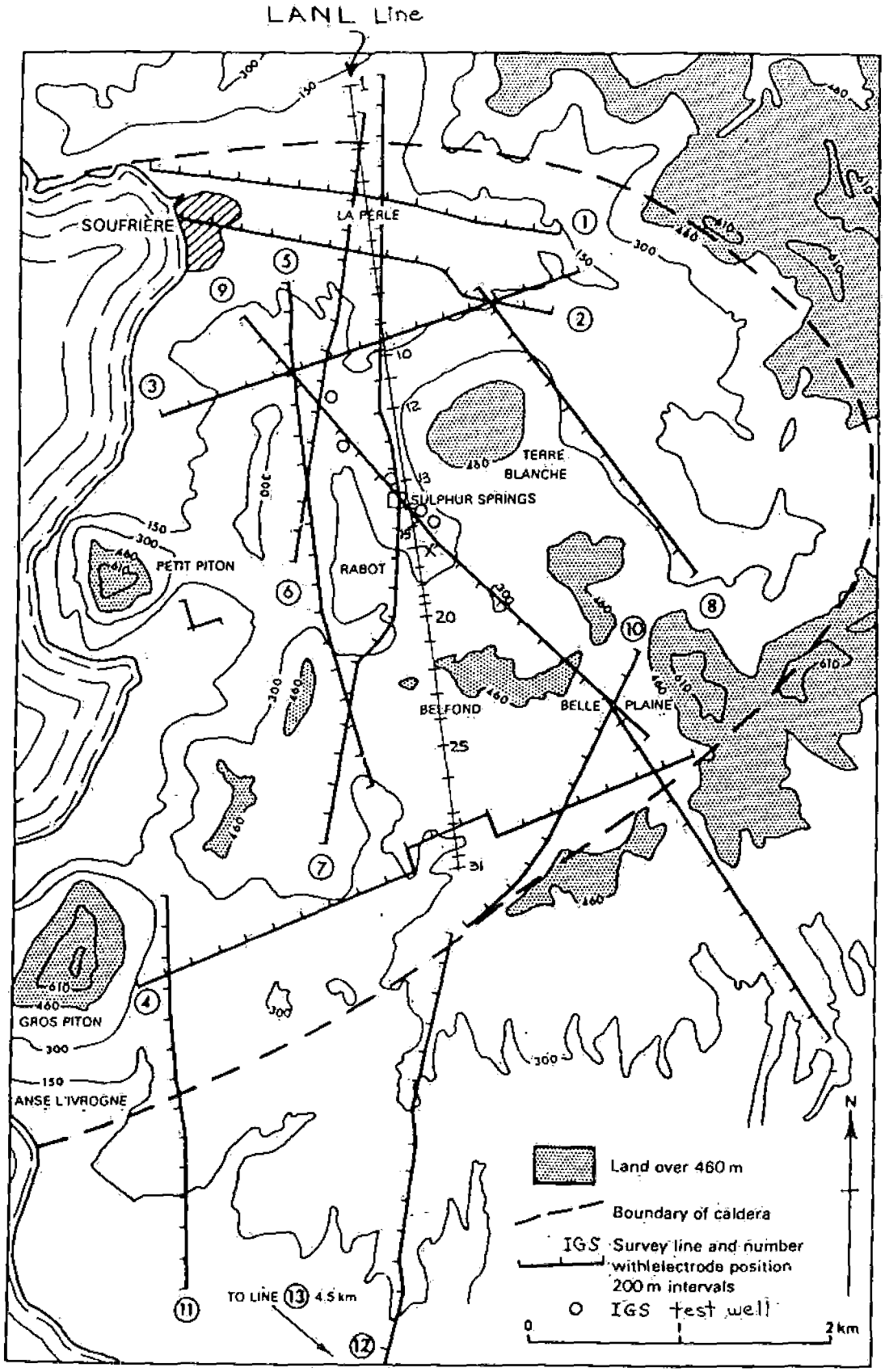

Fig. 1 Soufrière area, St Lucia showing geophysical survey lines

EARTH SCIENCE LABORATORY
UNIVERSITY of UTAH RESEARCH INSTITUTE

DIPOLE - DIPOLE ARRAY
APPARENT RESISTIVITY

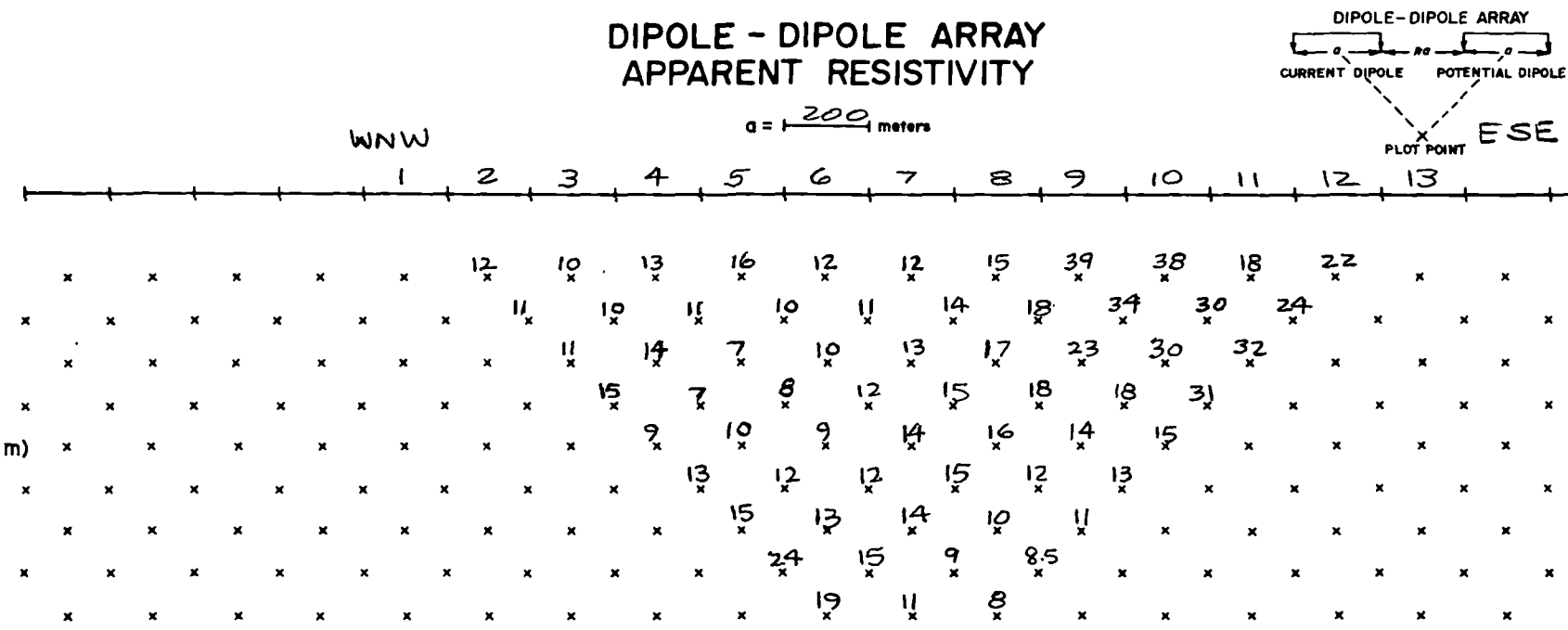

AREA St. Lucia STATE W. Indies LINE 2 DATA BY IGS DATE _____ TRANSMITTER _____ RECEIVER _____

EARTH SCIENCE LABORATORY
UNIVERSITY of UTAH RESEARCH INSTITUTE

DIPOLE - DIPOLE ARRAY
APPARENT RESISTIVITY

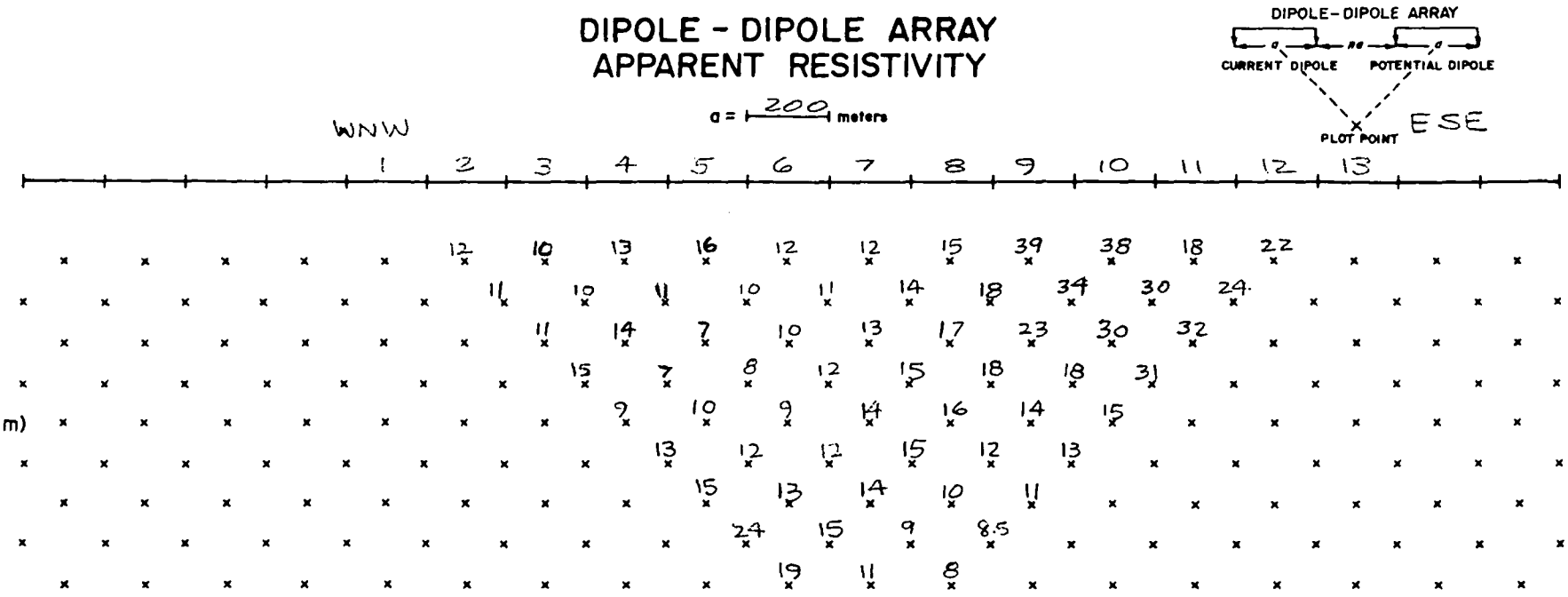

AREA St. Lucia STATE W. Indies LINE 2 DATA BY IGS DATE _____ TRANSMITTER _____ RECEIVER _____

EARTH SCIENCE LABORATORY
UNIVERSITY of UTAH RESEARCH INSTITUTE

DIPOLE - DIPOLE ARRAY
APPARENT RESISTIVITY

a = 200 meters

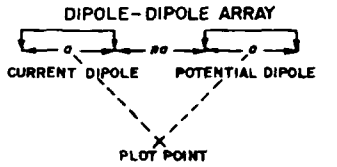

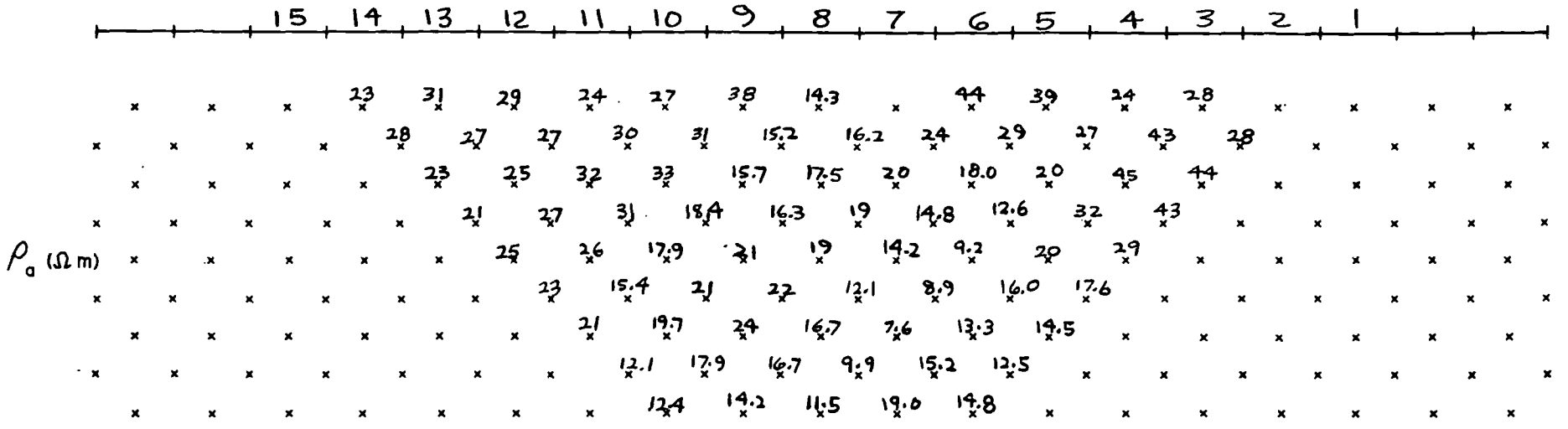

AREA St. Lucia STATE W. Indies LINE 3 DATA BY IGS DATE _____ TRANSMITTER _____ RECEIVER _____

EARTH SCIENCE LABORATORY
UNIVERSITY of UTAH RESEARCH INSTITUTE

DIPOLE - DIPOLE ARRAY
APPARENT RESISTIVITY

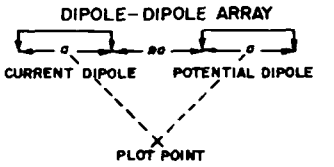

a = 200 meters

1 2 3 4 5 6 7 8 9 10 12 13 14 16 17 18 19 20 21 22

ρ_a (Ω m)

			19.4	20	26	44	35	32	54	75	192	74	70	1675	36	135					
		15.1	12.7	19.5	25	34	26	20	32	50	52	29	87	45	21	72					
	11.2	12.9	17.4	13.7	17.7	21	17.3	14.6	26	16.5	23	38	17.3	26	13.8	106					
		9.9	16.9	14.7	8.6	10.8	12.4	12.8	13.5	12.0	8.5	29	12.7	13.5	18.2	14.4					
			11.9	14.1	8.9	5.2	5.5	9.7	13.0	7.2	6.9	14.2	10.7	10.1	10.7	18.3					
			9.5	7.7	4.8	4.1	5.6	8.5	8.8	4.2	11.0	5.3	8.2	8.6	10.7						
			6.2	4.8	4.0	3.4	7.7	6.5	4.7	8.7	4.8	4.6	7.6	7.0							
				4.9	4.5	3.2	4.1	4.9	4.0	10.2	3.6	4.9	3.8	7.3							
					3.2	3.2	4.2	1.4	3.9	7.3	4.6	3.7	4.7	3.9							

AREA St. Lucia STATE W. Indies LINE 4 DATA BY IGS DATE _____ TRANSMITTER _____ RECEIVER _____

EARTH SCIENCE LABORATORY
UNIVERSITY of UTAH RESEARCH INSTITUTE

DIPOLE - DIPOLE ARRAY
APPARENT RESISTIVITY

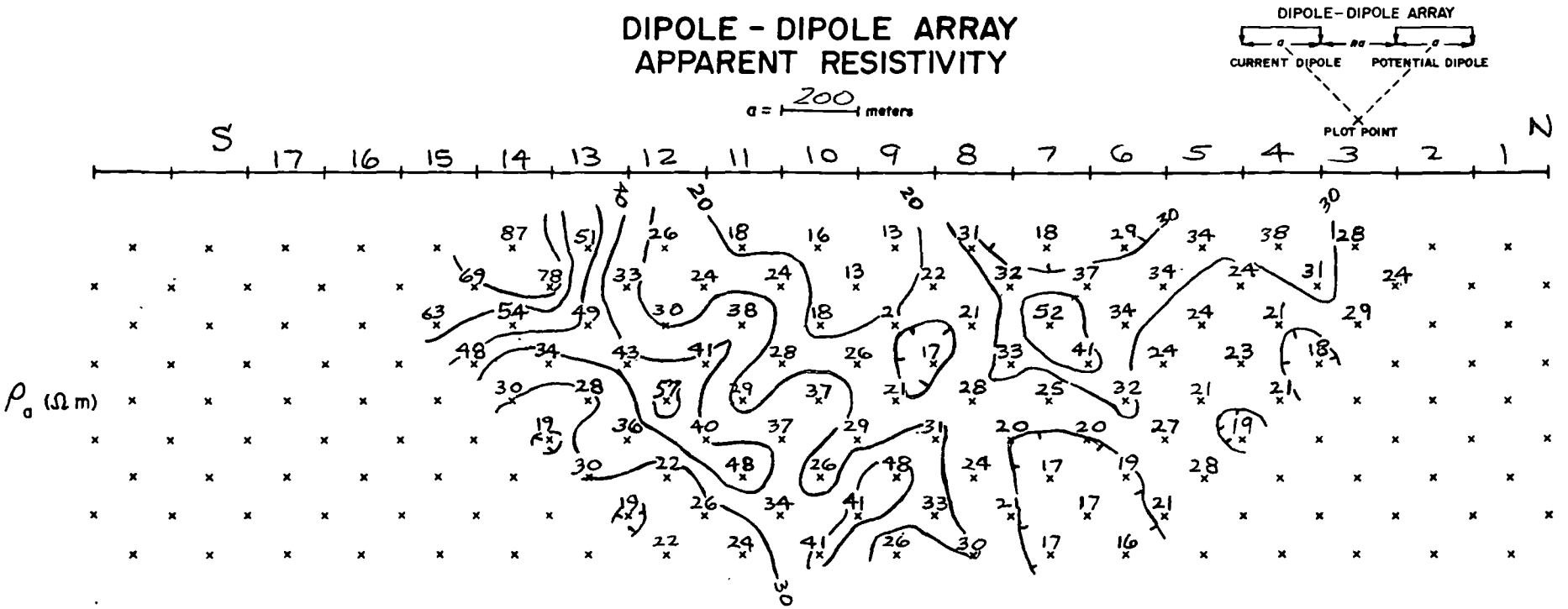

AREA St. Lucia STATE W. Indies LINE 5 DATA BY IGS DATE _____ TRANSMITTER _____ RECEIVER _____

EARTH SCIENCE LABORATORY
UNIVERSITY of UTAH RESEARCH INSTITUTE

DIPOLE - DIPOLE ARRAY
APPARENT RESISTIVITY

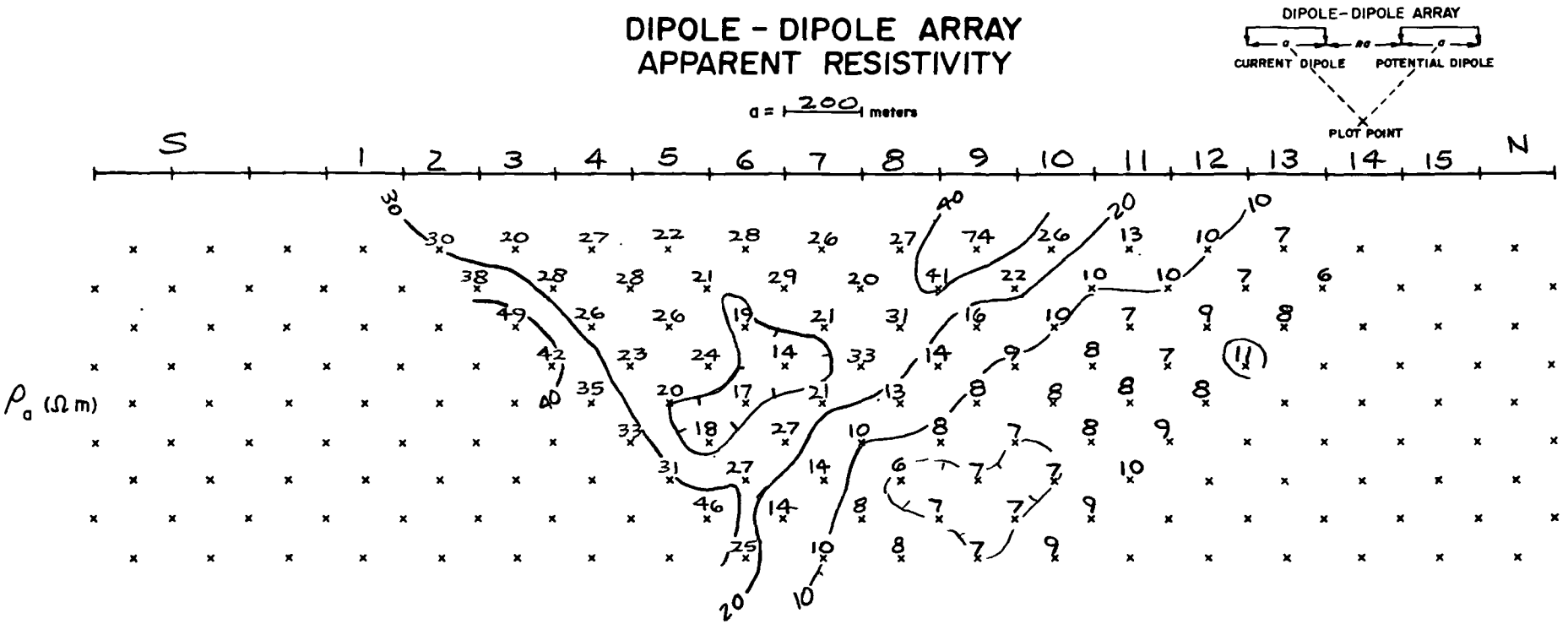

AREA St. Lucia STATE W. Indies LINE 6 DATA BY IGS DATE _____ TRANSMITTER _____ RECEIVER _____

EARTH SCIENCE LABORATORY
UNIVERSITY of UTAH RESEARCH INSTITUTE

DIPOLE - DIPOLE ARRAY
APPARENT RESISTIVITY

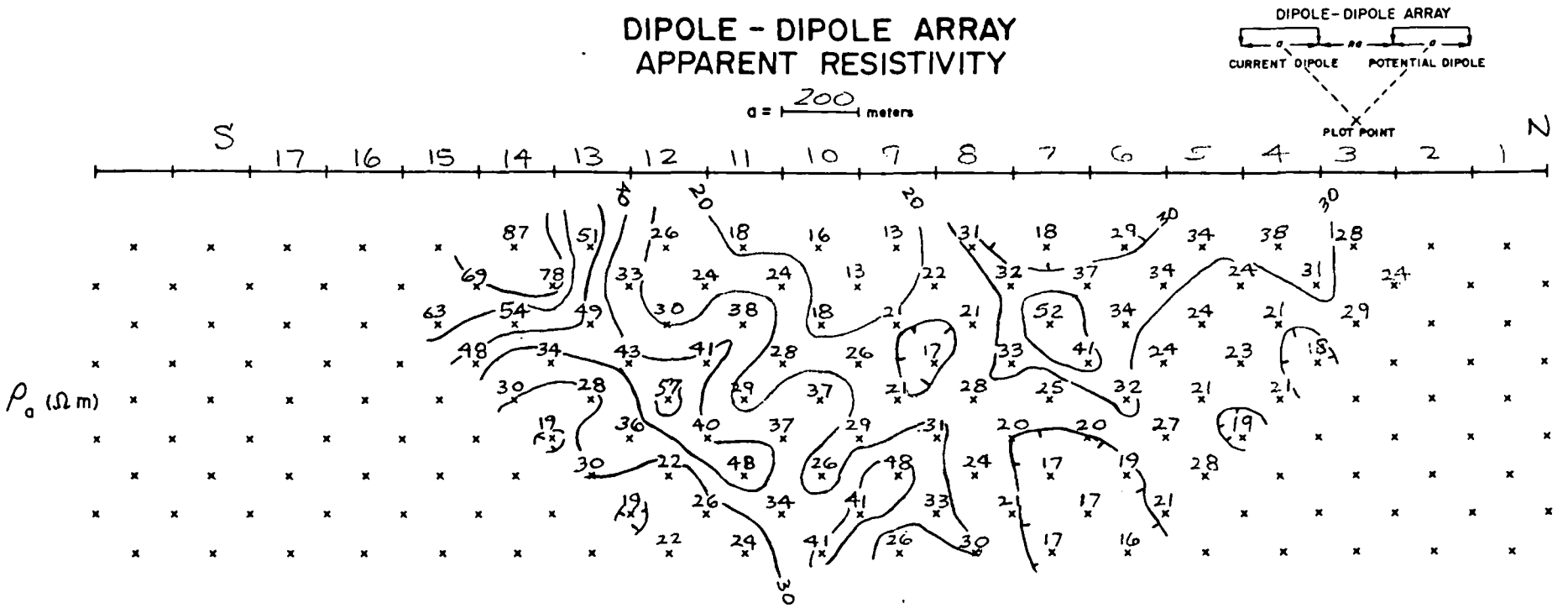

AREA St. Lucia STATE W. Indies LINE 5 DATA BY IGS DATE _____ TRANSMITTER _____ RECEIVER _____

EARTH SCIENCE LABORATORY
UNIVERSITY of UTAH RESEARCH INSTITUTE

DIPOLE - DIPOLE ARRAY
APPARENT RESISTIVITY

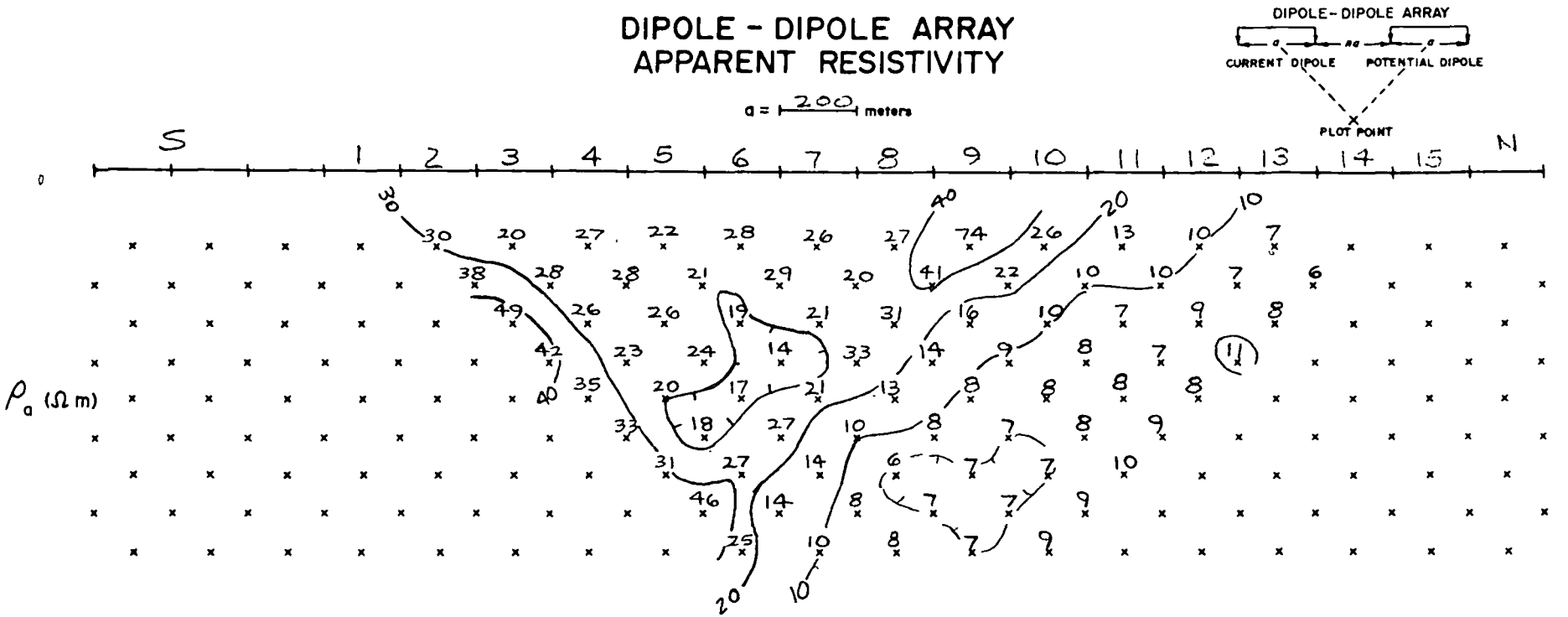

AREA St. Lucia STATE W. Indies LINE 6 DATA BY IGS DATE _____ TRANSMITTER _____ RECEIVER _____

EARTH SCIENCE LABORATORY
UNIVERSITY of UTAH RESEARCH INSTITUTE

DIPOLE - DIPOLE ARRAY
APPARENT RESISTIVITY

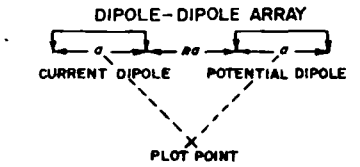

a = 200 meters

17 16 15 14 13 12 11 10 9 8 7 6 5 4 3 2 1

ρ_a (Ω m)

IGS

n=2: 9.7 5.1 6.0 4.5 8.5 31 270 175 252 120 270 124 68 92

n=3: 13.9 11.3 5.6 5.4 7.8 10.6 19.8 95 78 122 53 159 33 36 26

n=4: 13.3 15.4 12.8 4.4 9.0 8.7 17.5 12.5 54 46 63 38 55 21 19.7

n=5: 16.3 16.5 10.0 7.2 12.6 18.1 15.6 21 38 35 53 15.8 35 22

n=6: 18.2 14.3 18.7 9.4 19 15.6 30 18.8 34 38 23 11.5 36

n=7: 14.5 27 24 21 30 24 22 36 15.7 14.7 12.8

n=8: 27 31 24 28 21 28 22 14.4 10.6 18.4

n=9: 34 24 26 7.9 9.2 14

n=10: 30 55 ? 9.1 6.1 11.5

AREA St. Lucia STATE W. Indies LINE 7 DATA BY IGS DATE _____ TRANSMITTER _____ RECEIVER _____

EARTH SCIENCE LABORATORY
UNIVERSITY of UTAH RESEARCH INSTITUTE

DIPOLE - DIPOLE ARRAY
APPARENT RESISTIVITY

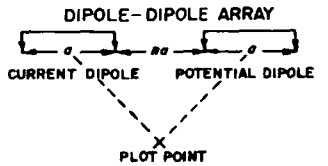

a = 200 meters

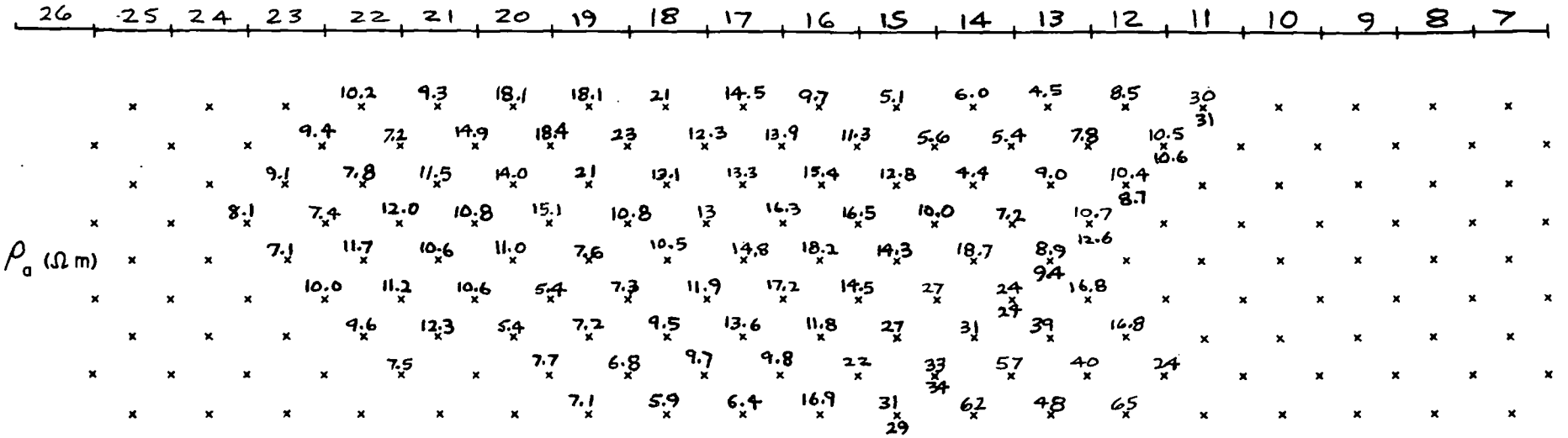

AREA St. Lucia STATE W. Indies LINE 7 DATA BY IGS DATE _____ TRANSMITTER _____ RECEIVER _____

EARTH SCIENCE LABORATORY
UNIVERSITY of UTAH RESEARCH INSTITUTE

DIPOLE - DIPOLE ARRAY
APPARENT RESISTIVITY

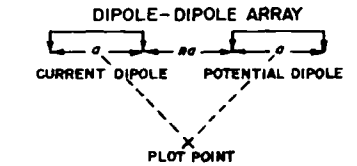

a = 200 meters

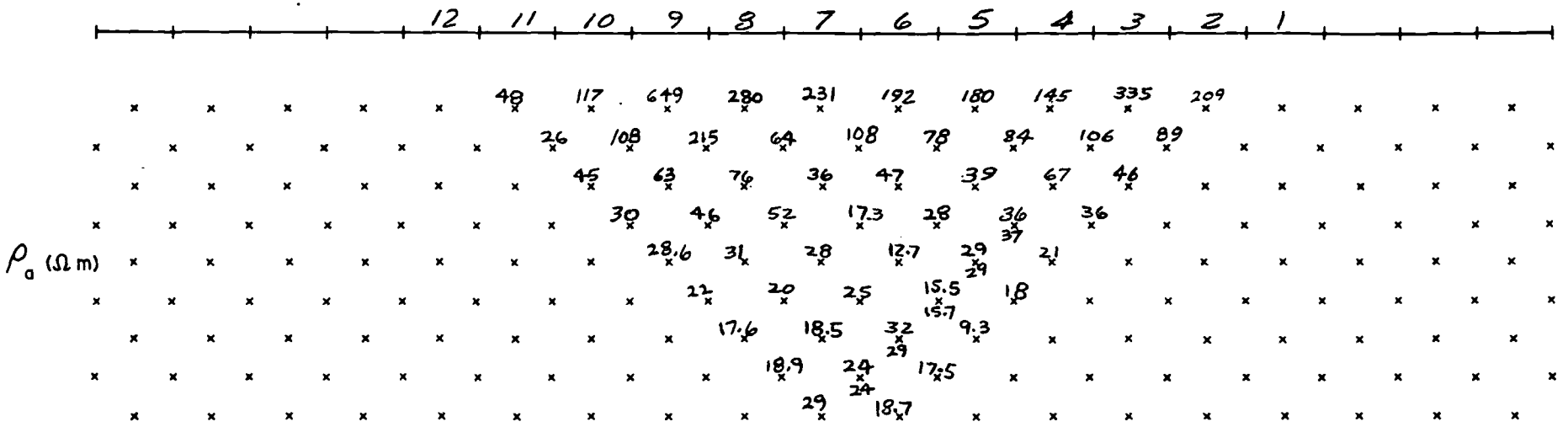

AREA St. Lucia STATE W. Indies LINE 8 DATA BY IGS DATE _____ TRANSMITTER _____ RECEIVER _____

EARTH SCIENCE LABORATORY
UNIVERSITY of UTAH RESEARCH INSTITUTE

DIPOLE - DIPOLE ARRAY
APPARENT RESISTIVITY

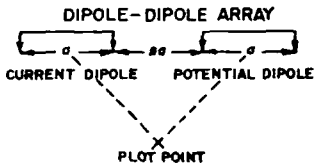

a = 200 meters

12 13 14 15 16 17 18 19 20 21 22 23 24 25 26 27 28 29 30 31

ρ_a (Ω m)

								58	143	23.3	61	31	43	82	69				
							18.5	23.4	25	25.3	43	35	46	121	213				
							13.9	16.3	11.6	27	20.8	42	29	54	84	72			
							15.8	11.2	10.8	14.7	21.1	20.1	35	32	35	28.6	39		
							10.2	13.7	7.0	15.1	12.5	19.6	15.6	37	21.4	14.7	19.9		
						12.6	10.6	8.6	8.2	10.5	13.0		17.4	22.5	9.1	12.2			
					10.2	13.4	6.7	10.0	7.6	11.0				10.4	9.4				
				8.0	12.3	10.3	8.0	9.7	6.4				6.4	9.4					
				5.5	9.4	8.1	12.0	10.7	7.0					8.1					

AREA St. Lucia STATE W. Indies LINE 9ext DATA BY BGS DATE _____ TRANSMITTER _____ RECEIVER _____

EARTH SCIENCE LABORATORY
UNIVERSITY of UTAH RESEARCH INSTITUTE

DIPOLE - DIPOLE ARRAY
APPARENT RESISTIVITY

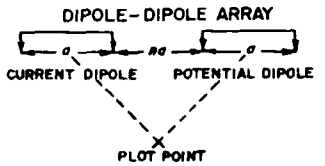

a = 200 meters

1 2 3 4 5 6 7 8 9 10 11 12 13 14 15 16 17 18 19 20 21

ρ_a (Ω m)

		23	35	20.5	17	14.6	4.3	9.1	18.9	42	239	247	144	641	498	1198	257		58	143
	21.5	34	23.5	16.8	12.9	5.5	8.0	7.6	14.7	70	106	119	103	314	455	320	44	18.5	23.4	
	29	22	17.5	13.8	6.0	11.4	7.8	14.4	22.8	46	50	81	76	247	123	47	13.9	16.3		
	18	16.3	14.7	8.0	13.8	10.9	15.4	23	17.6	24	34	46	64	77	23	15.8	11.2			
	13.7	14.2	7.9	17.9	14.9	22.2	24	20.2	8.9	18.3	18.2	41.1	26	20	10.2	13.7				
	11.6	8.8	17.4	18.1	32	35	22	11.9	6.7	9.2	18.3	21.1	13.7	12.6	10.6	8.6				
	7.4	19.9	17.5	4.1	4.9	30	13.5	10.4	4.9	12.3	10.6	14.3	10.2	13.4	6.7	10.0				
	14.9	20.4	34	56	43	17.8	12.0	8.5		8.8	7.5	9.0	12.3	10.3	8.0					
	15.1	40.5		54	26.5	16.3	10.3		6.4	12.1	5.5	9.4	8.1	12.0						

AREA St. Lucia STATE W. Indies LINE 9 DATA BY BGS DATE _____ TRANSMITTER _____ RECEIVER _____

EARTH SCIENCE LABORATORY
UNIVERSITY of UTAH RESEARCH INSTITUTE

DIPOLE - DIPOLE ARRAY
APPARENT RESISTIVITY

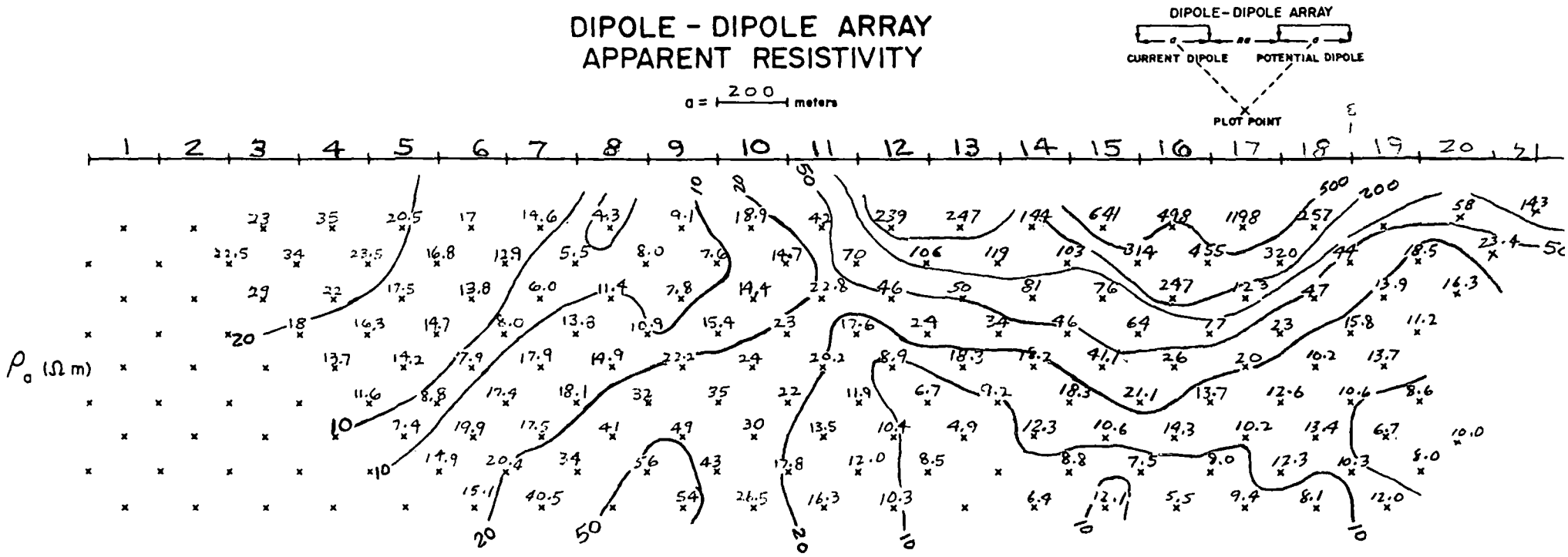

AREA St. Lucia STATE W. Indies LINE 9 DATA BY BGS DATE _____ TRANSMITTER _____ RECEIVER _____

EARTH SCIENCE LABORATORY
UNIVERSITY of UTAH RESEARCH INSTITUTE

DIPOLE - DIPOLE ARRAY
APPARENT RESISTIVITY

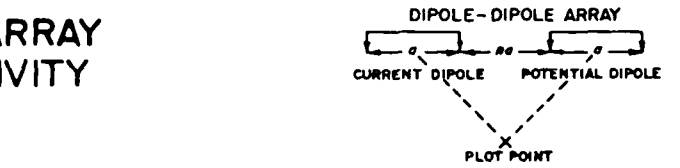

a = 200 meters

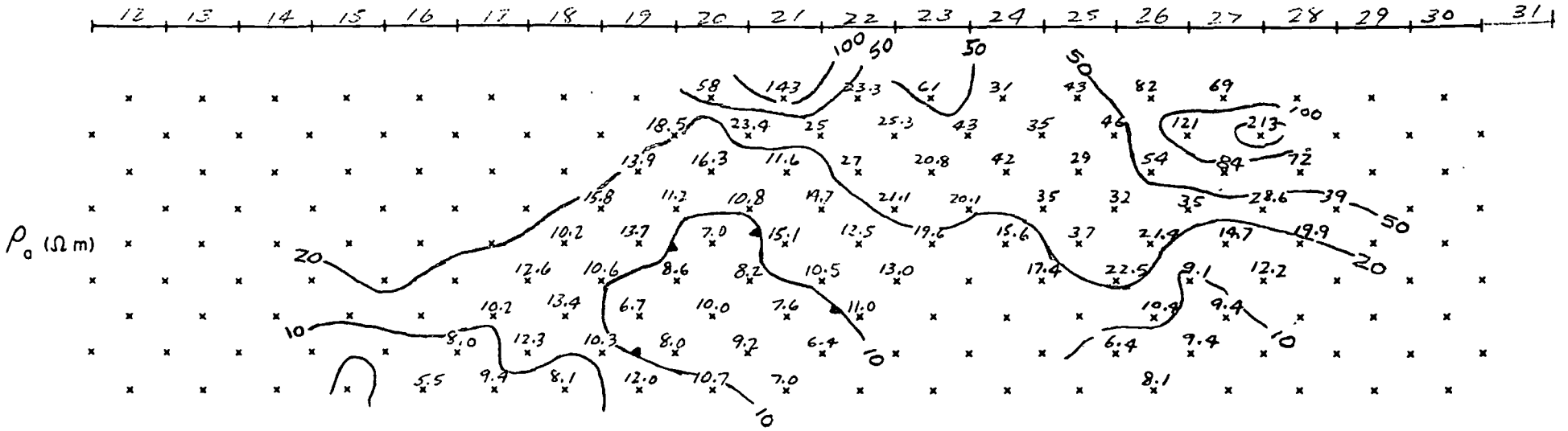

AREA St. Lucia STATE W. Indies LINE 9ext DATA BY BGS DATE _____ TRANSMITTER _____ RECEIVER _____

EARTH SCIENCE LABORATORY
UNIVERSITY of UTAH RESEARCH INSTITUTE

DIPOLE - DIPOLE ARRAY
APPARENT RESISTIVITY

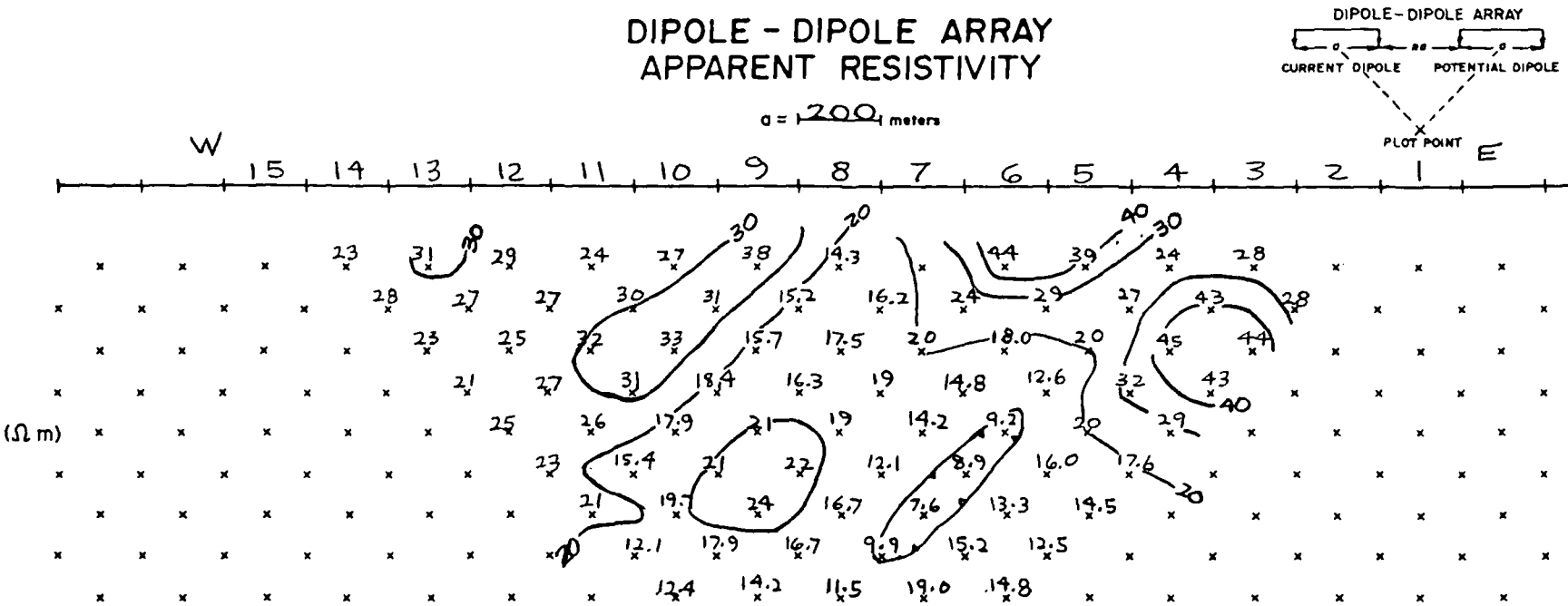

AREA St. Lucia STATE W. Indies LINE 3 DATA BY IGS DATE _____ TRANSMITTER _____ RECEIVER _____

EARTH SCIENCE LABORATORY
UNIVERSITY of UTAH RESEARCH INSTITUTE

DIPOLE - DIPOLE ARRAY
APPARENT RESISTIVITY

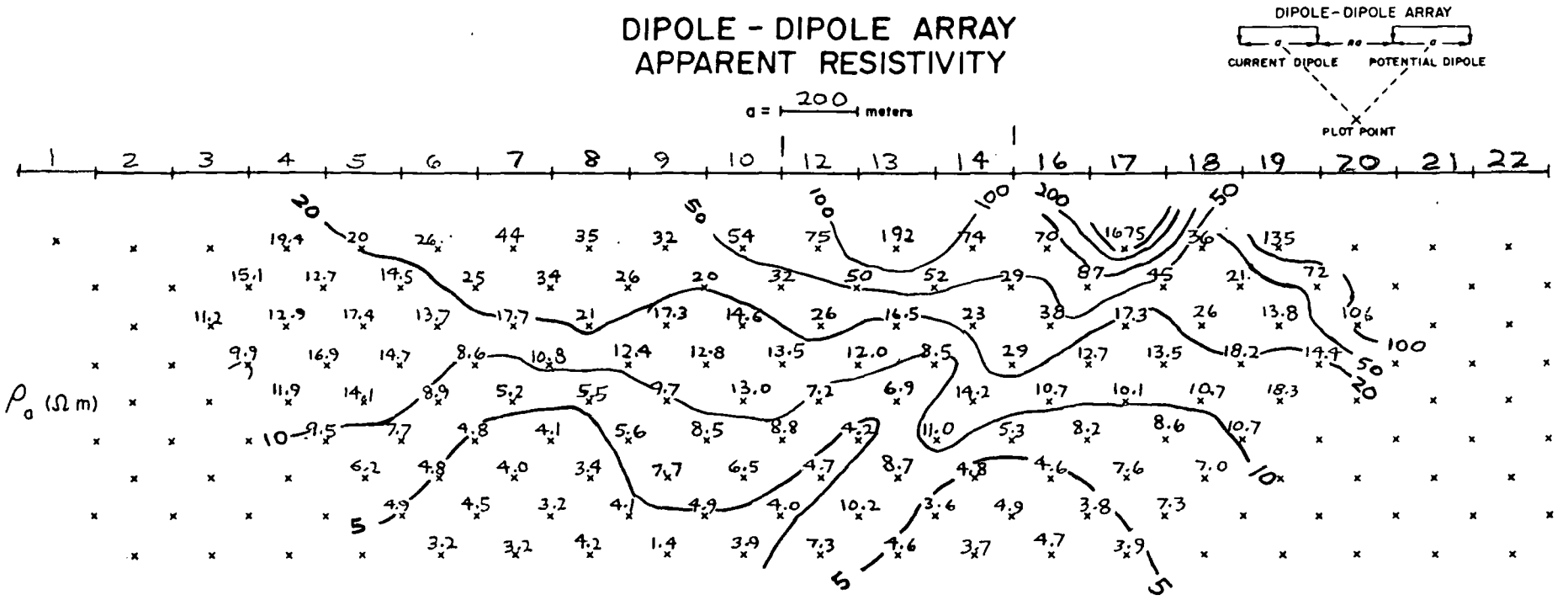

AREA St. Lucia STATE W. Indies LINE 4 DATA BY IGS DATE _____ TRANSMITTER _____ RECEIVER _____

EARTH SCIENCE LABORATORY
UNIVERSITY of UTAH RESEARCH INSTITUTE

DIPOLE - DIPOLE ARRAY
APPARENT RESISTIVITY

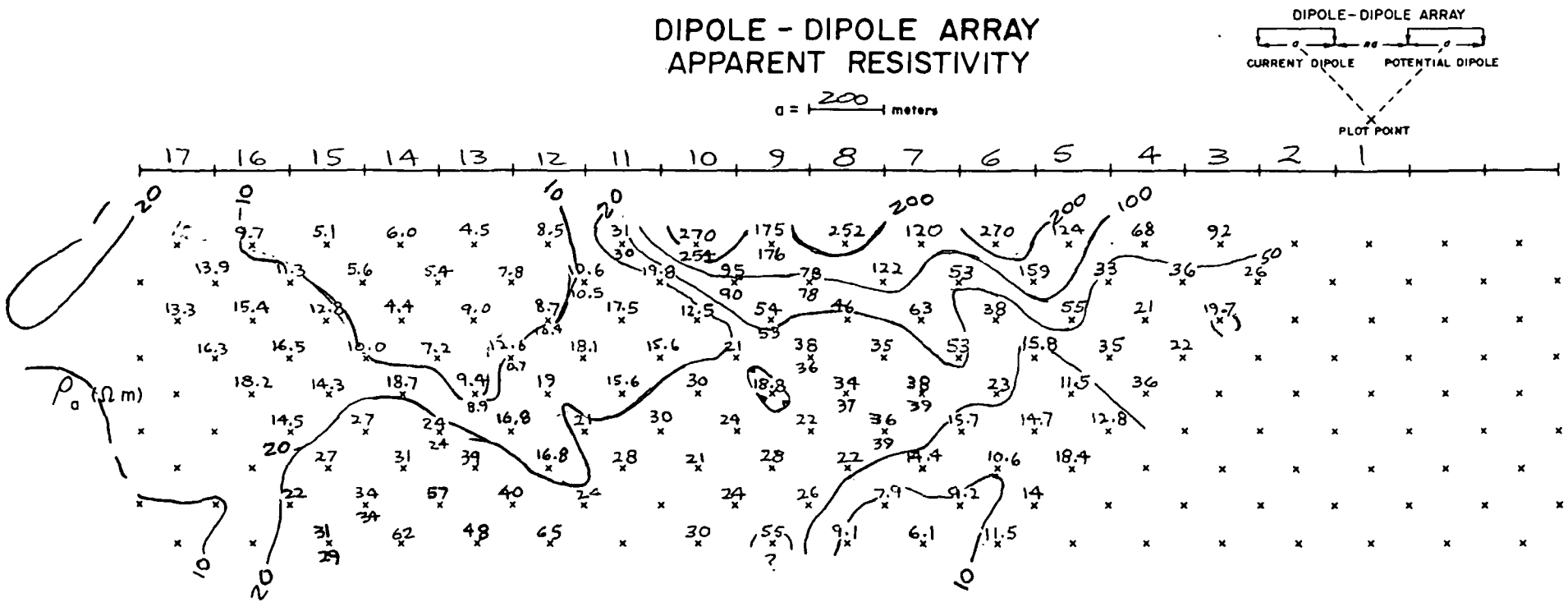

AREA St. Lucia STATE W. Indies LINE 7 DATA BY IGS DATE _____ TRANSMITTER _____ RECEIVER _____

EARTH SCIENCE LABORATORY
UNIVERSITY of UTAH RESEARCH INSTITUTE

DIPOLE - DIPOLE ARRAY
APPARENT RESISTIVITY

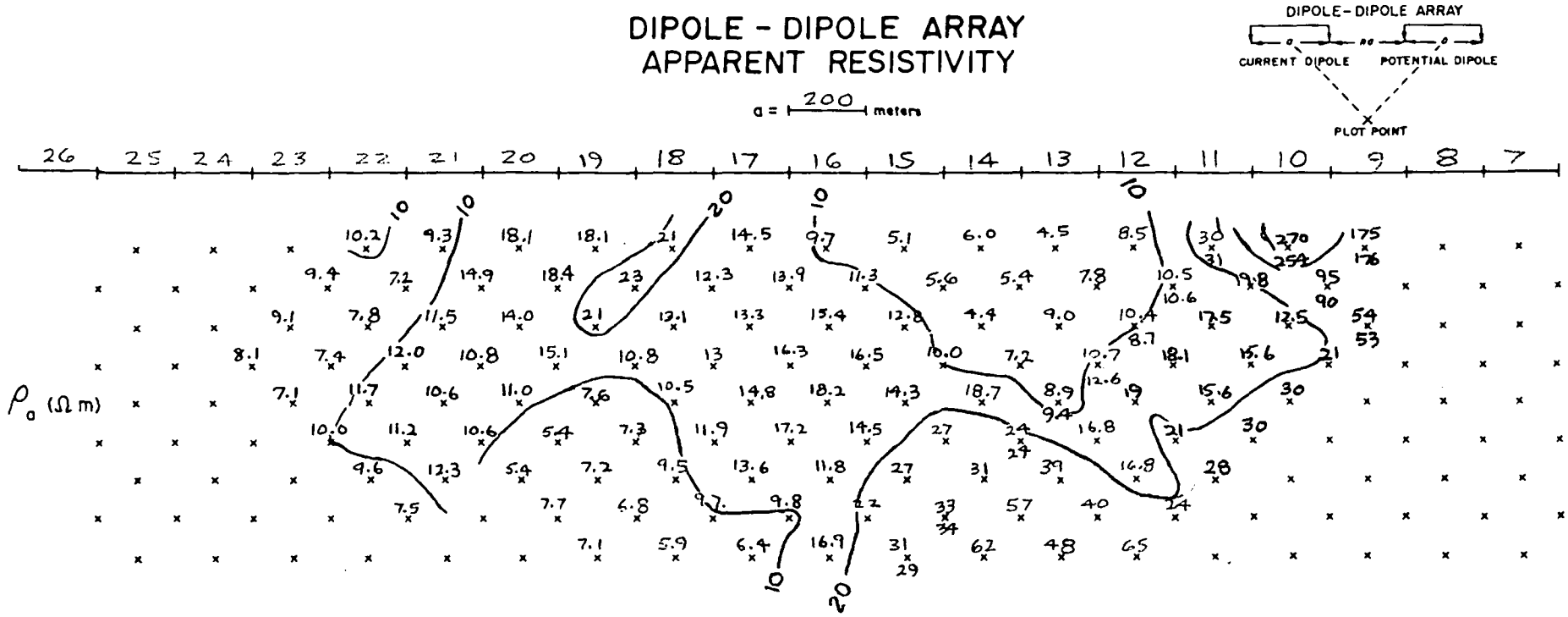

AREA St. Lucia STATE W. Indies LINE 7 DATA BY IGS DATE _____ TRANSMITTER _____ RECEIVER _____

EARTH SCIENCE LABORATORY
UNIVERSITY of UTAH RESEARCH INSTITUTE

DIPOLE - DIPOLE ARRAY
APPARENT RESISTIVITY

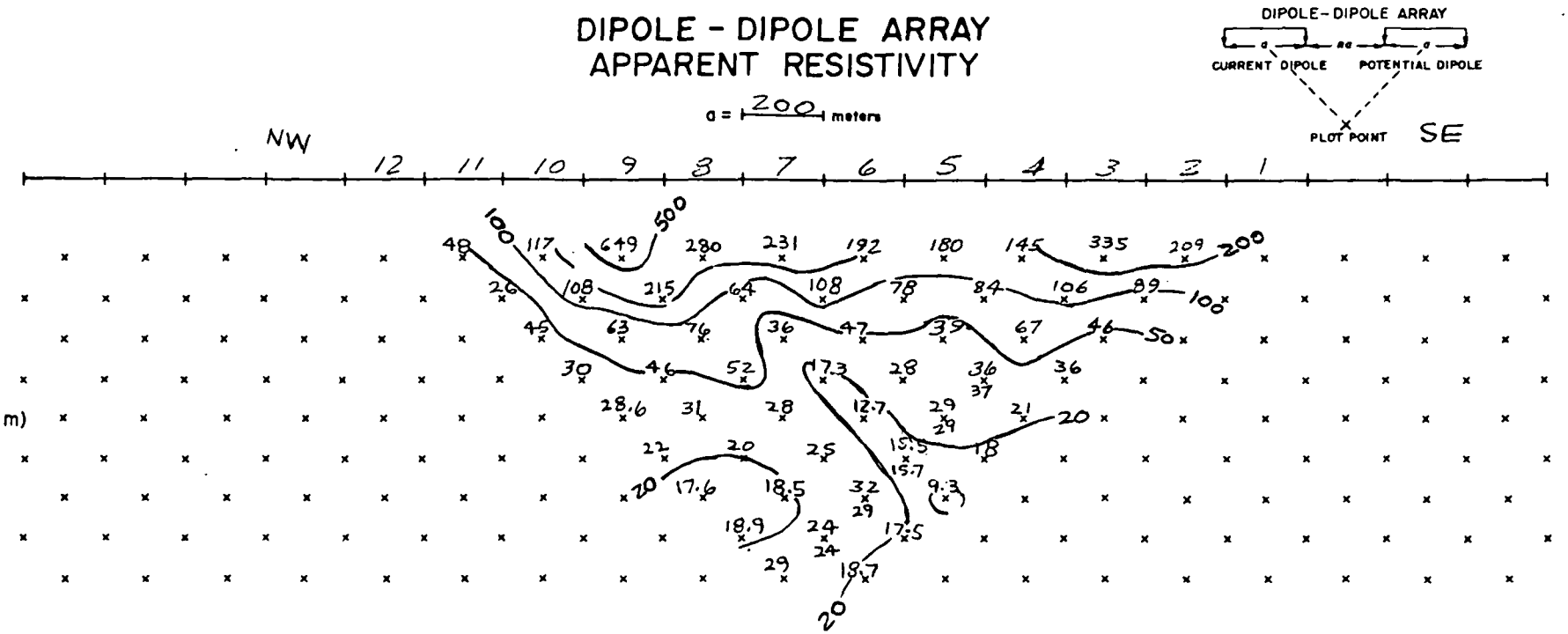

AREA St. Lucia STATE W. Indies LINE 8 DATA BY IGS DATE _____ TRANSMITTER _____ RECEIVER _____

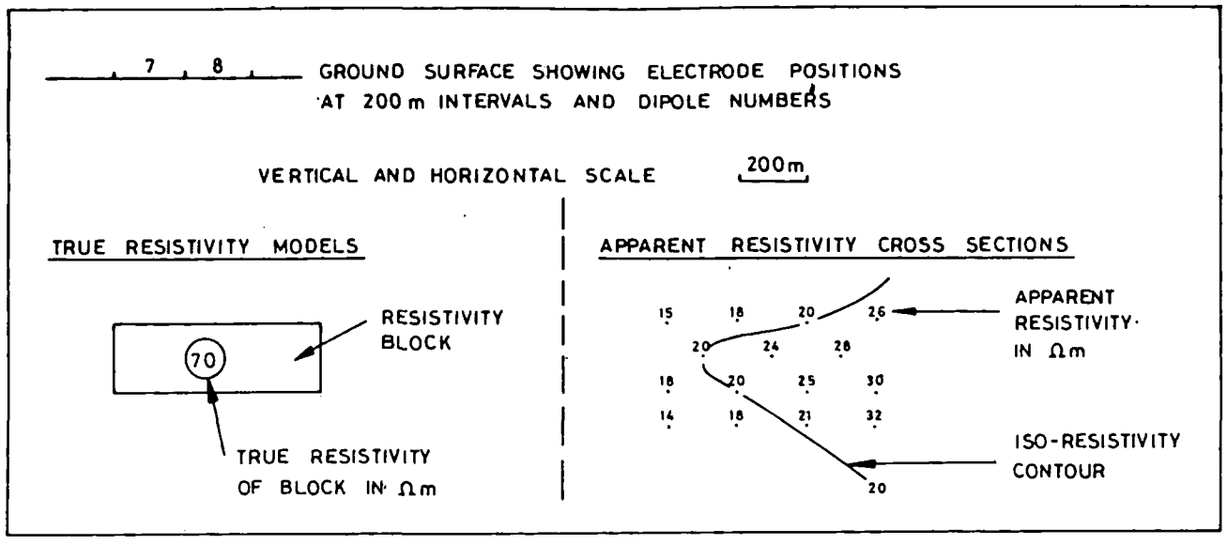

Fig. 1. Key to Figs. 2 to 14

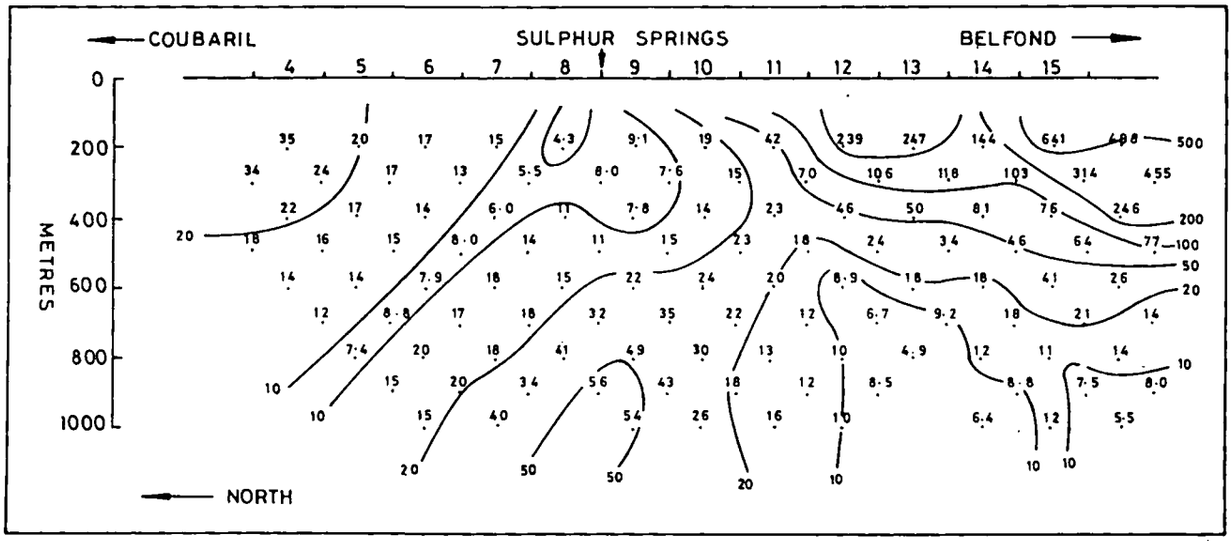

Fig. 2. Line 9 - apparent resistivity cross-section

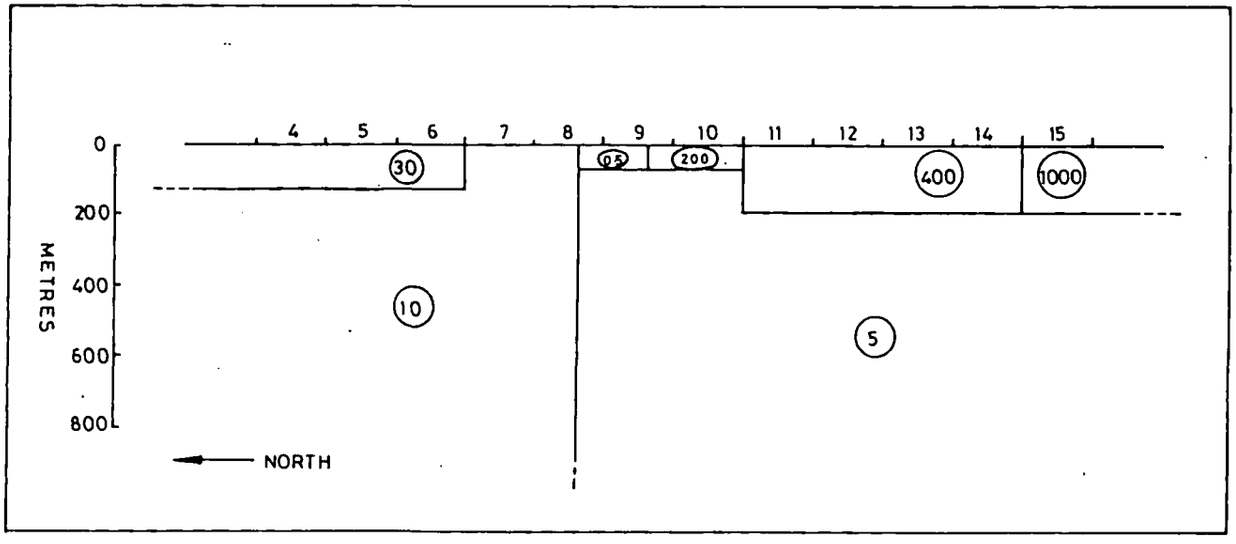

Fig. 3. Line 9 - true resistivity model 1

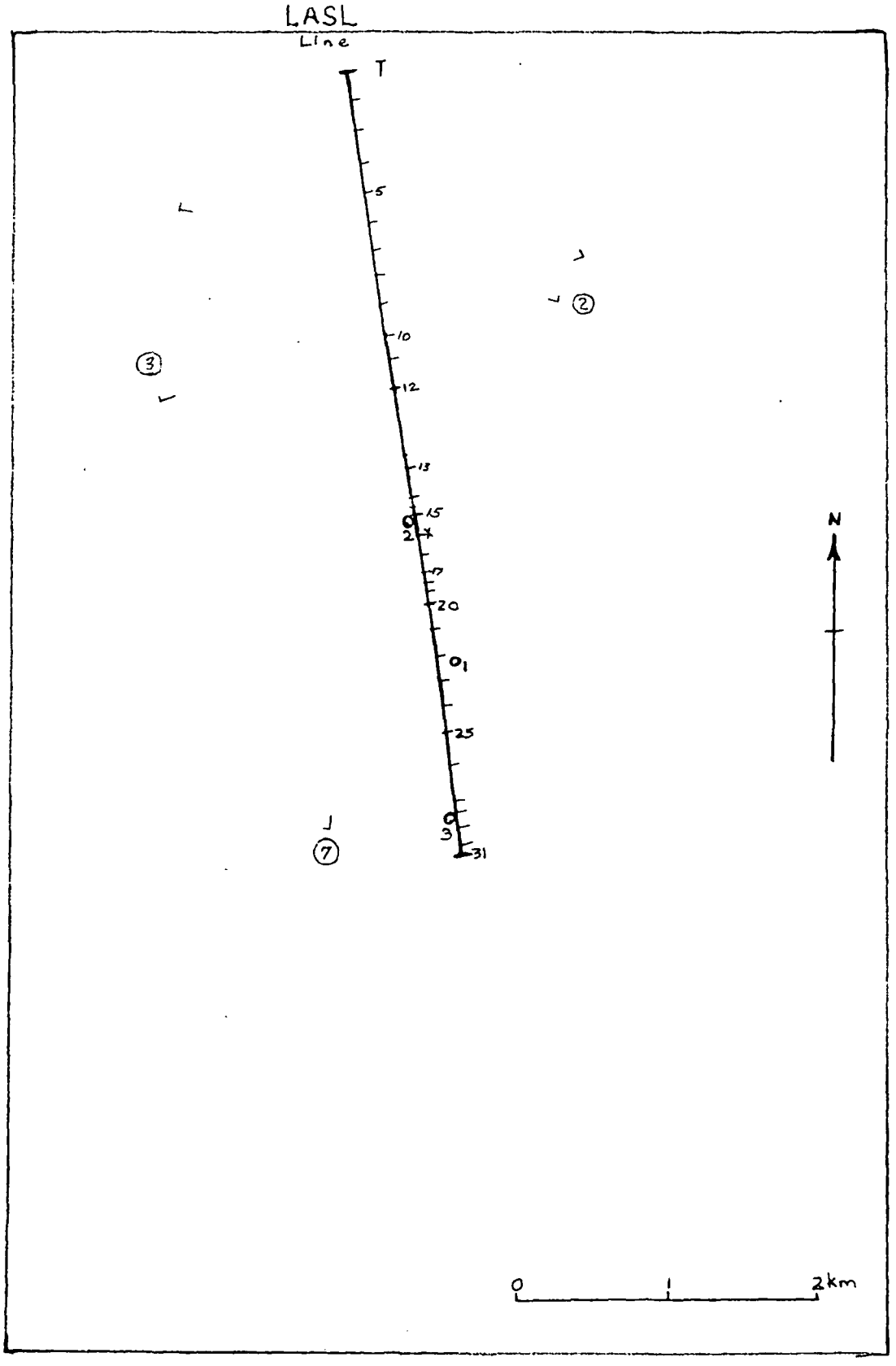
LASL
Line
T
5
10
12
13
15
20
25
31
N
0
1
2km

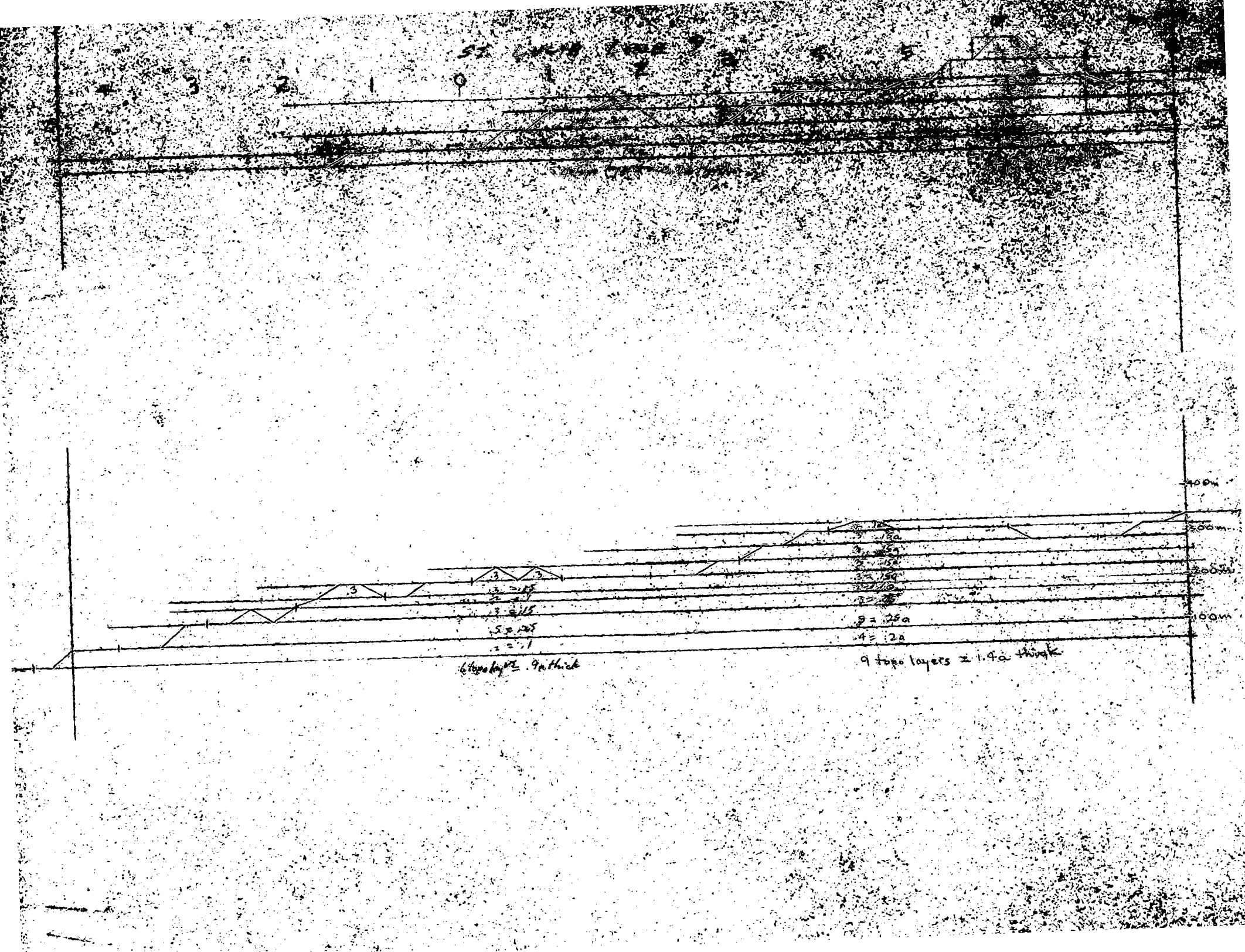
400m
200m
100m
6 topo layers = .9a thick
9 topo layers = 1.4a thick

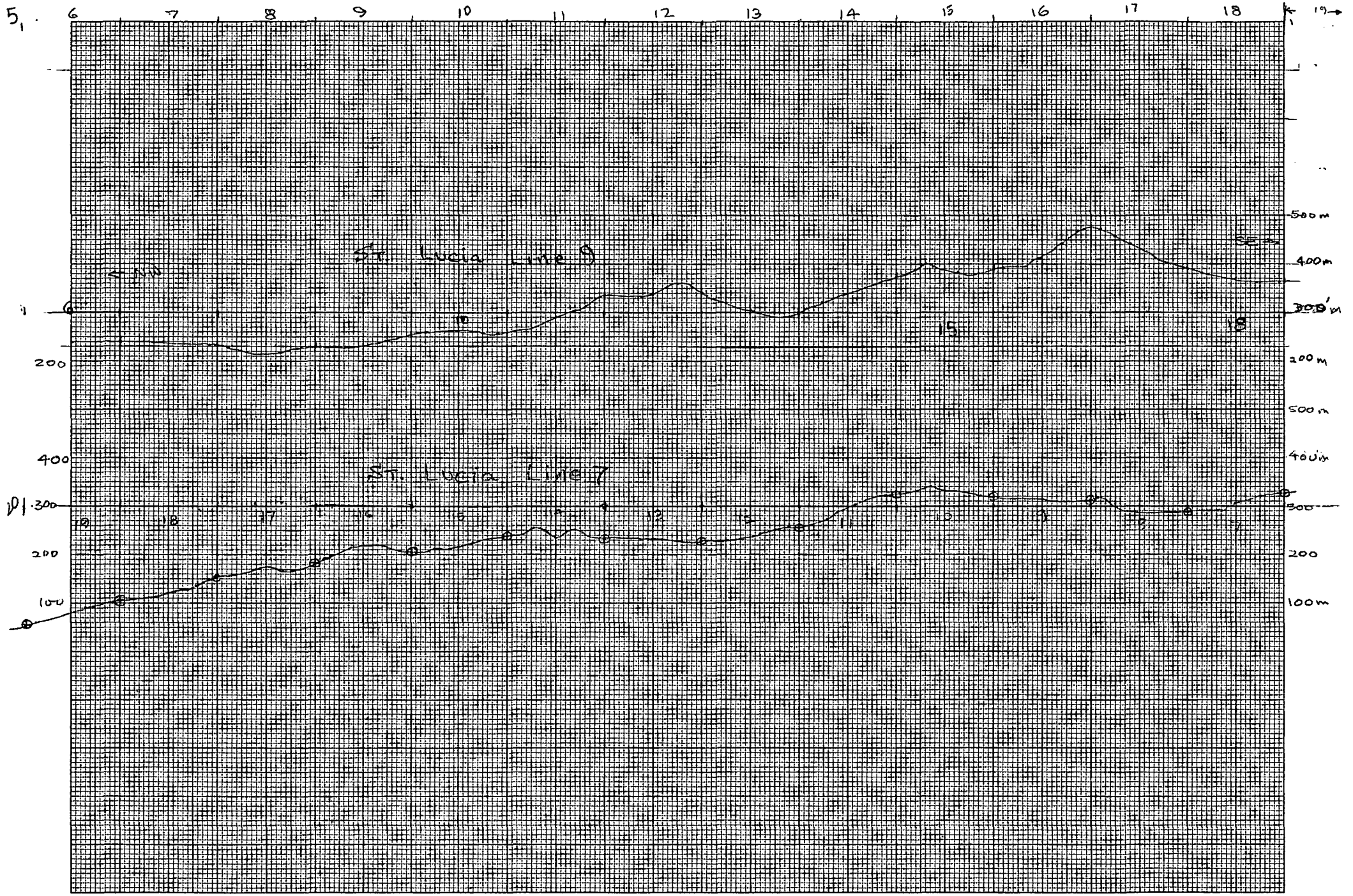
6
7
8
9
10
11
12
13
14
15
16
17
18
19
500m
400m
300m
200m
500m
400m
300
200
100
ST. Lucia Line 8
ST. Lucia Line 7

Coding form : 2-D Finite Element Model (Standard Mesh) Line 9

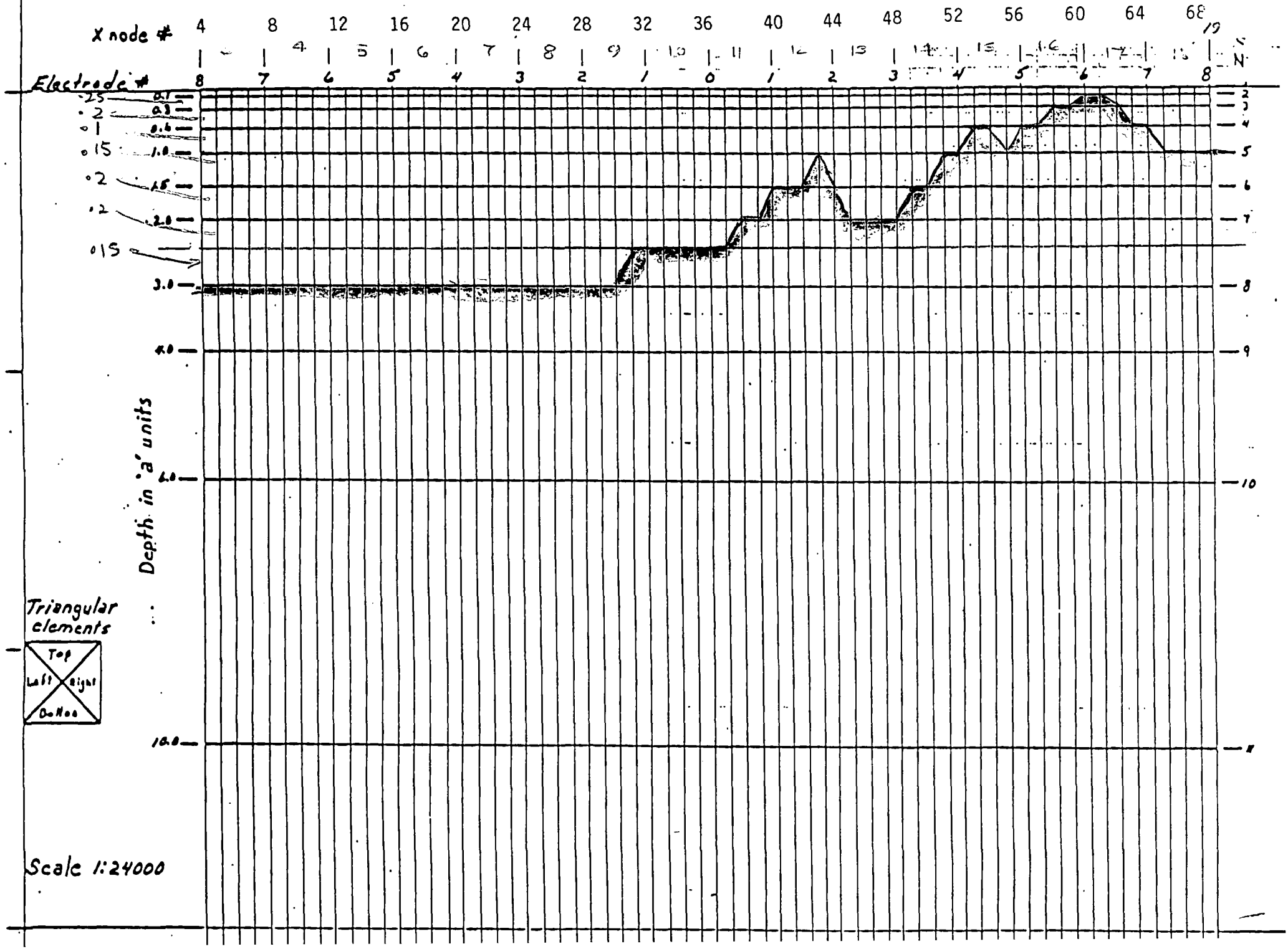

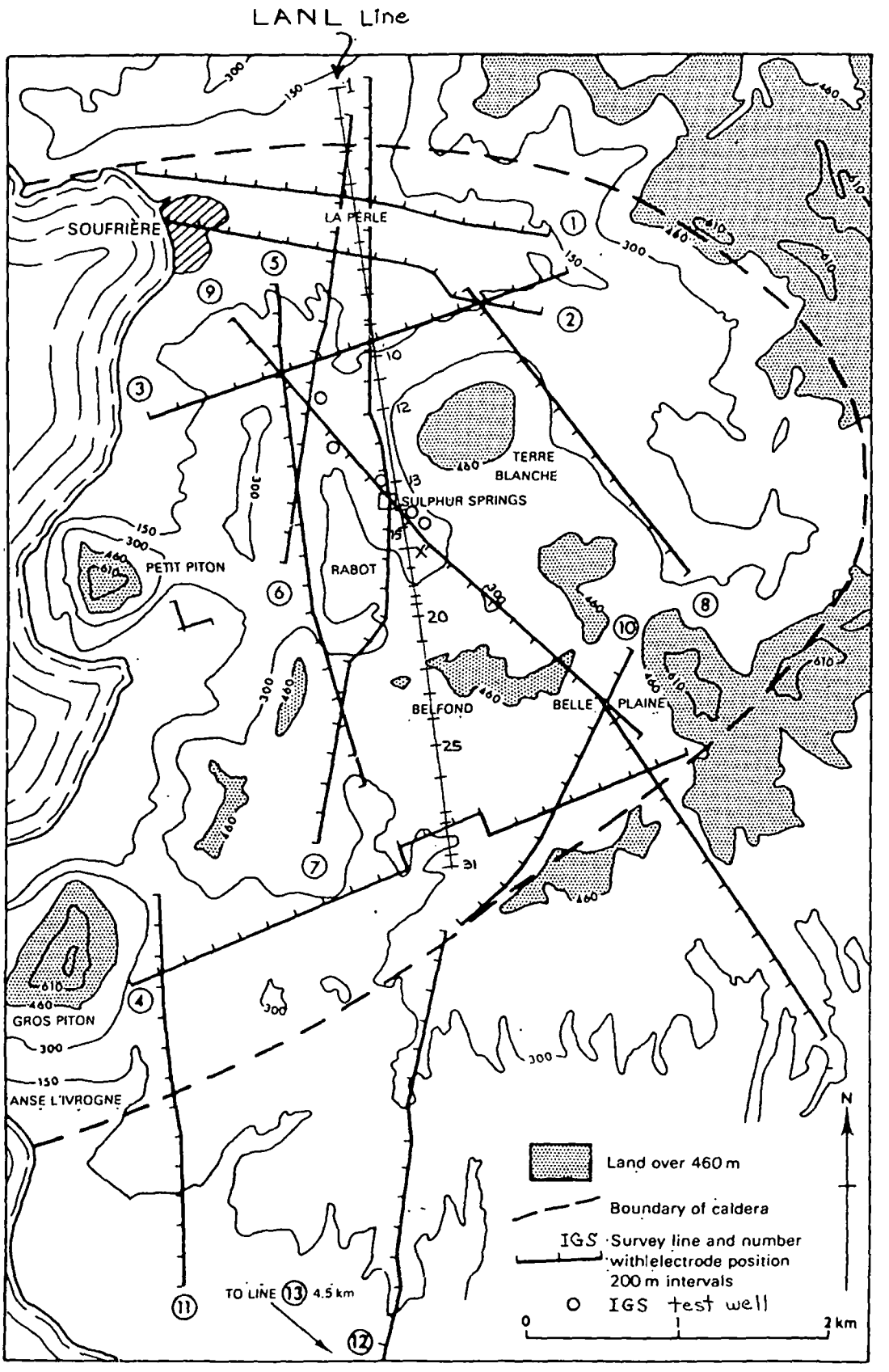

Fig. 1 Soufrière area, St Lucia showing geophysical survey lines

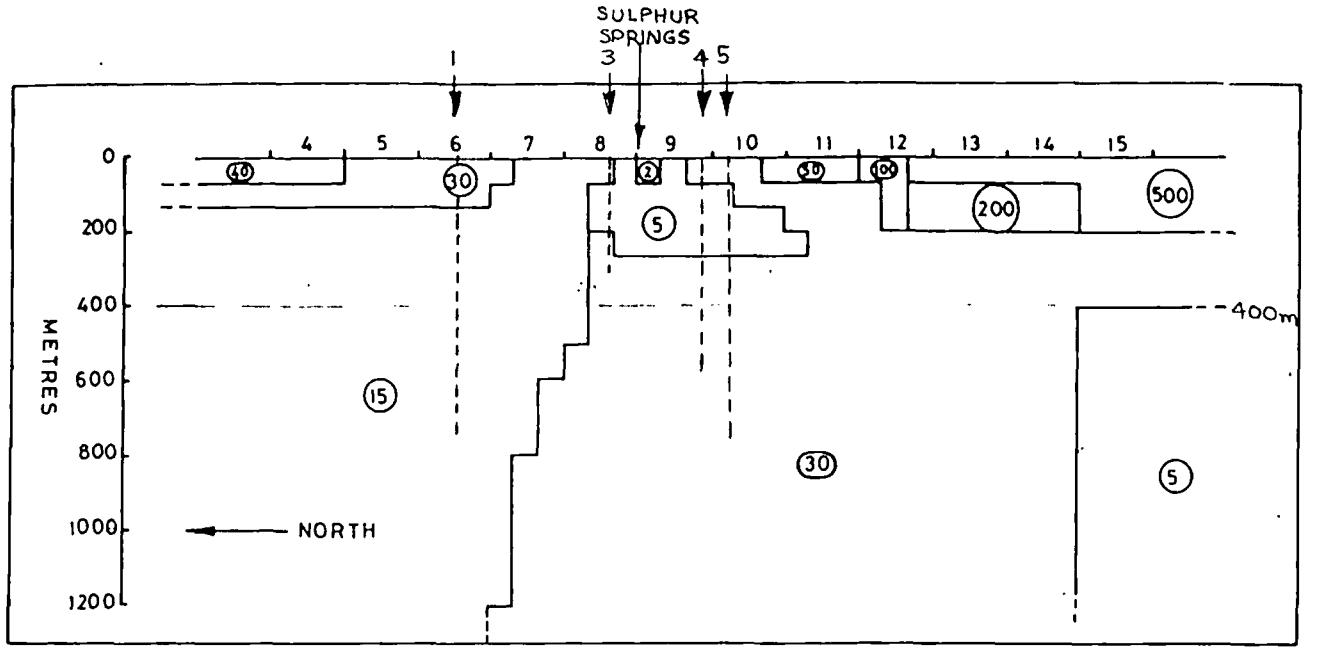

Fig. 2a Line 9 - true resistivity model 6

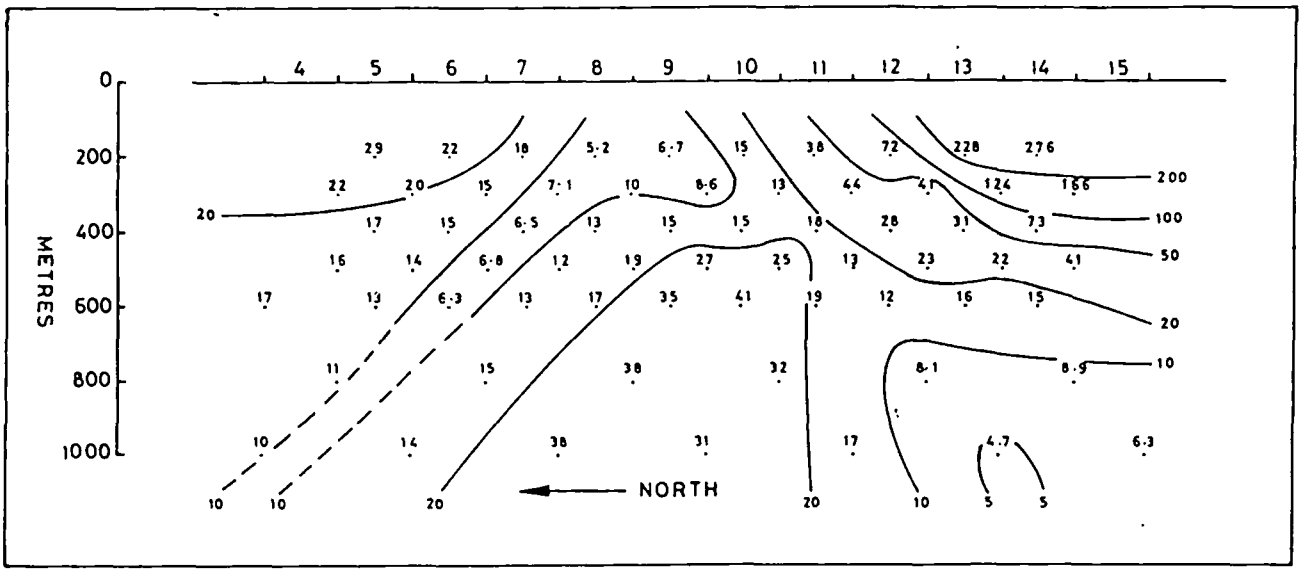

Fig. 2b Line 9 - computer generated section due to model 6

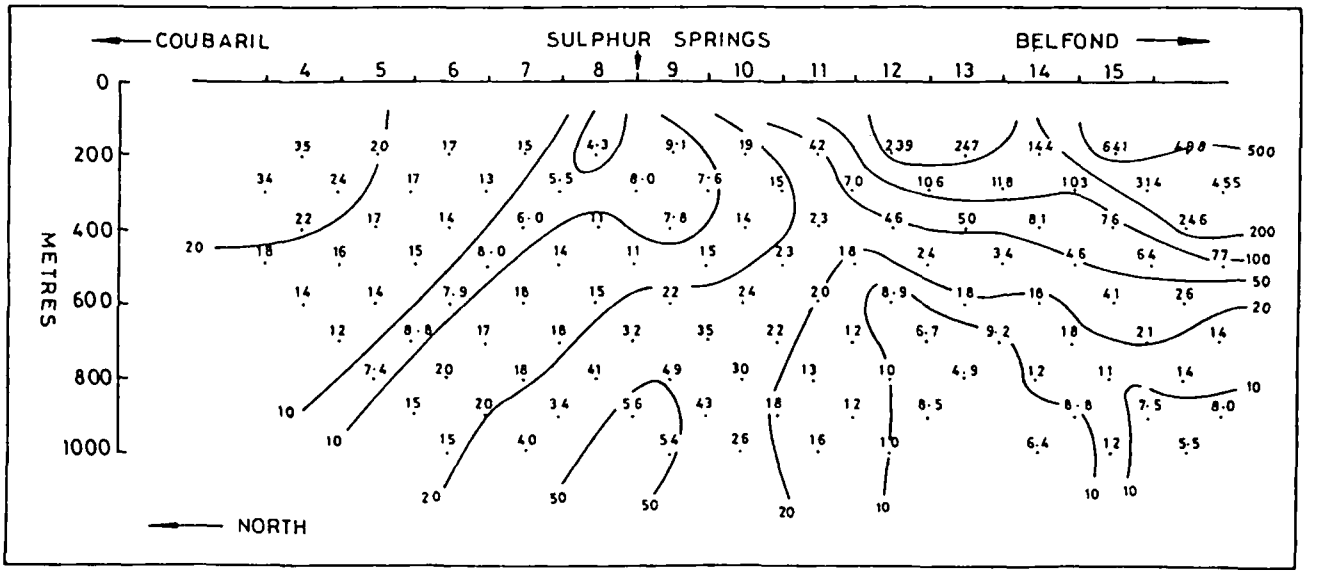

Fig. 2c Line 9 - apparent resistivity cross-section - observed

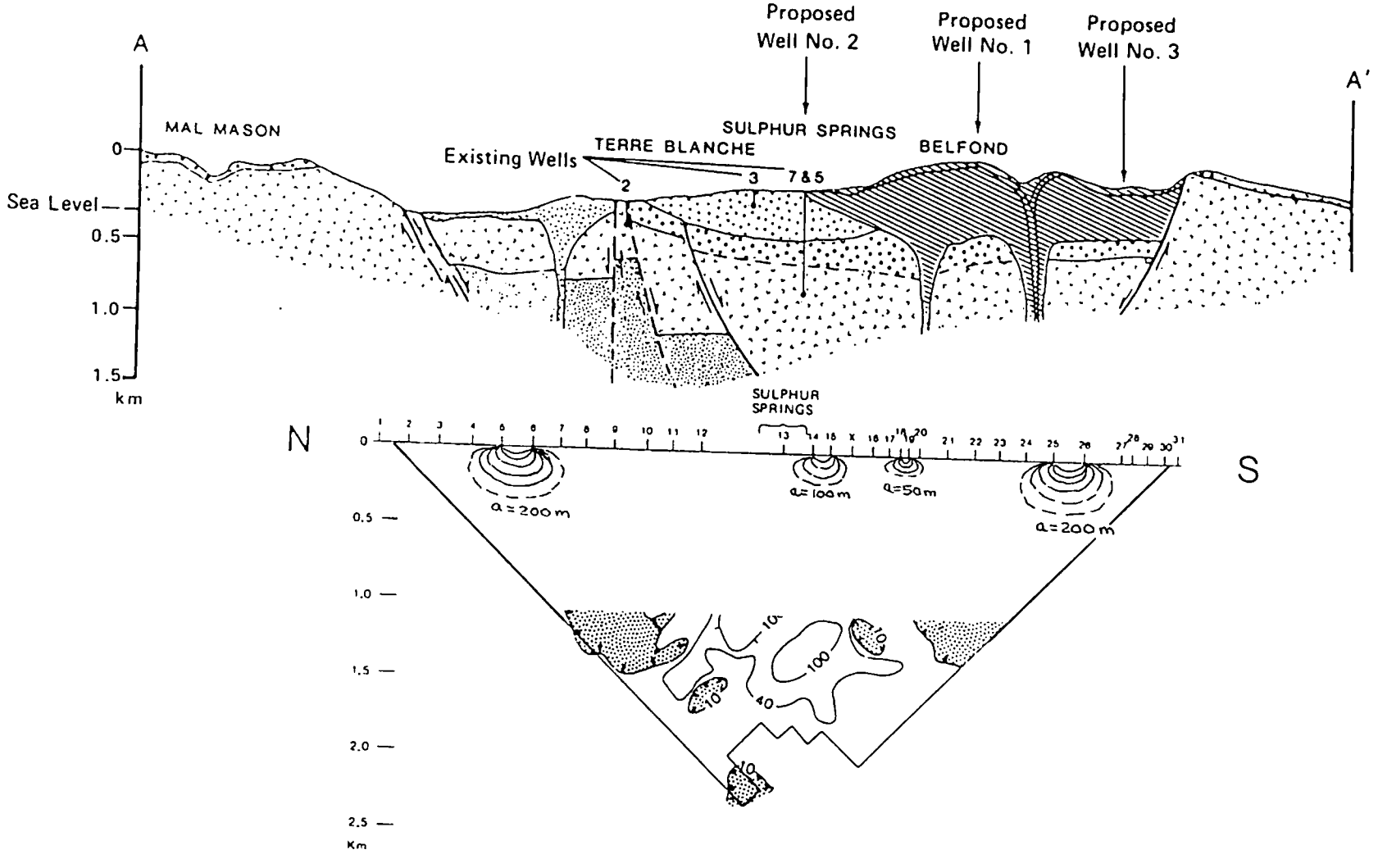

Fig. 3 Schematic illustration of current distribution as a function of transmitting dipole length, for the LANL line.

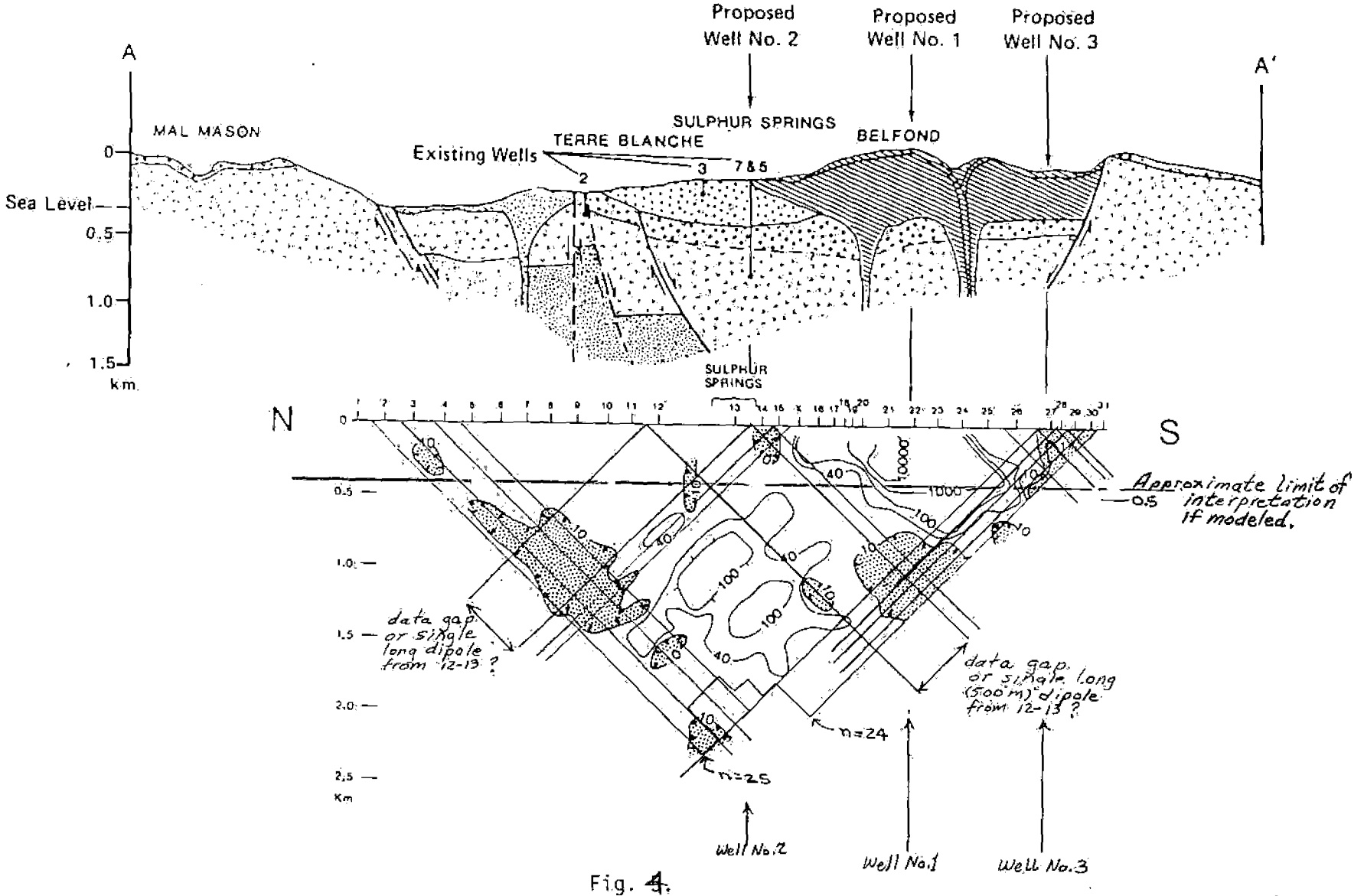

Fig. 4.

Apparent resistivity data from the dipole-dipole survey plotted as a function of depth. Resistivity values are in ohm-m and are shown beneath the appropriate geologic cross section. Shaded areas depict resistivity contours of 10 ohm-m or less.

UNITED NATIONS REVOLVING FUND
FOR NATURAL RESOURCES EXPLORATION

FONDS AUTORENOUVELABLE DES NATIONS UNIES
POUR L'EXPLORATION DES RESSOURCES NATURELLES

TELEPHONE: 212-906-6123
212-906-6120

UNRFNRE
One United Nations Plaza
New York, N.Y. 10017

CABLE ADDRESS: UNDEVPRO • NEW YORK
TELEX: 422862 UNDEVPRO-NYK

REFERENCE:

9 September 1985

Dear Marshall,

As I told you in Kona, the expected BGS geophysical data was on my desk when I got back. I am passing it on herewith, and hope that it will be suitable for combining with the LANL Resistivity data to produce some useful 3-D modelling at Utah.

Yours sincerely,

Peter R. Donovan

Mr. Marshall Reed
U.S. Department of Energy CE 324
Washington D.C. 20585

NRC/STL/GEN
NR/PER/GEN

British Geological Survey

Keyworth
Nottingham NG12 5GG

Telephone Plumtree (06 077) 6111
Telex 378173 BGSKEY G

PD

UN REVOLVING FUND

'85 AUG -6 10:03

P M Fozzard Esq
Technical Manager
UN Revolving Fund
1 United Nations Plaza.
Room FF914
NEW YORK
NY 10017
UNITED STATES OF AMERICA

Your reference

Our reference GF/AG/72/62

26 July 1985

Dear Peter

BGS GEOPHYSICAL SURVEYS FOR GEOTHERMAL RESOURCES IN ST LUCIA

When I passed through New York earlier this month Peter Donovan asked for the original resistivity data from the BGS survey in St Lucia in 1974. Please find enclosed a copy of the reports on the survey (number 26) and the interpretation (Number 31) together with the original data and an explanation of these data. There is an explanation of the data and at the beginning of each line of data. The orientation of the line is given together with the disposition of the dipoles. The position of the lines on St Lucia are given in the figures in the reports. This information should be sufficient for any geophysicist to decipher the basic information for any reprocessing. I am copying this letter, but not contents, to Mike Lewis in case you need any clarification regarding geophysics, but do not hesitate to request any further information from us if necessary. Peter Greenwood has only just returned from a spell away from England and Mike Lee is currently away, hence the delay in getting the information to you.

All the air freight from Peru in early July is now finally with us in Keyworth although the portable computer was missing but we got another similar unit to edit the original data before reading it into the main computer here. The majority of the resistivity curves are now reinterpreted and plotted on A4 size. We have been striving for a report deadline for the end of the month but it may slip a few days, but at least a preliminary report was left in Arequipa. Air freight both ways return UK and Peru is certainly a problem as we found on the way out.

With best wishes.

Yours sincerely

Rob

ROB EVANS

Peter I will try to phone you early next week

EXPLANATION OF TITLES ON DATA SHEETS.

DIPL	DIPOLE NUMBER.
ANG	AZIMUTH IN DEGREES OF DIPOLE.
LENGTH	LENGTH OF DIPOLES IN METRES.
TX	DIPOLE NUMBER AT WHICH TRANSMITTER IS LOCATED.
RX	DIPOLE NUMBER AT WHICH RECEIVER IS LOCATED.
RANGE	} VOLTAGE MEASURED BY RX.
MULT	
I	TRANSMITTED CURRENT. AMPS.
DEPTH	PLOTTING DEPTH ON PSUEDO-SECTION.
RES	APPARENT RESISTIVITY. OHM. METRES

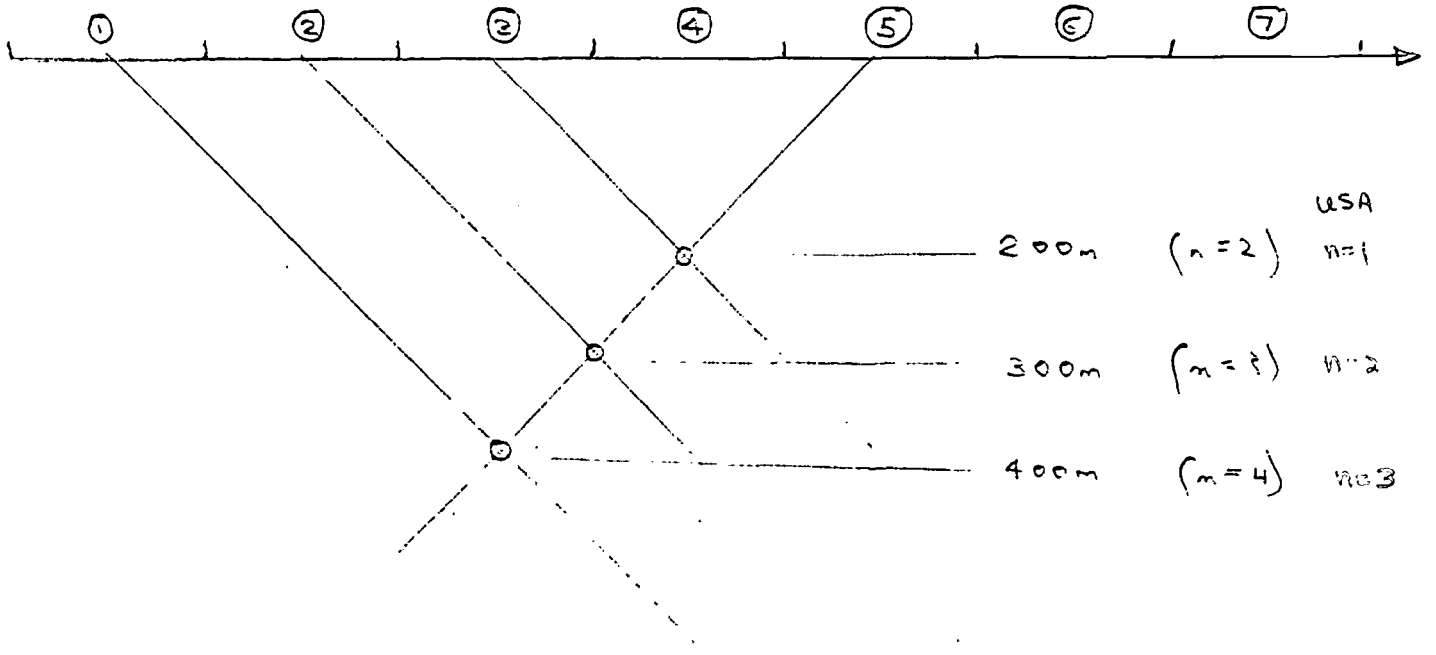

ARRAY: COLINEAR DIPOLE-DIPOLE.

WHERE LINES ARE BENT THE SEPARATION BETWEEN RX AND TX DIPOLE CENTRES IS CALCULATED AS:

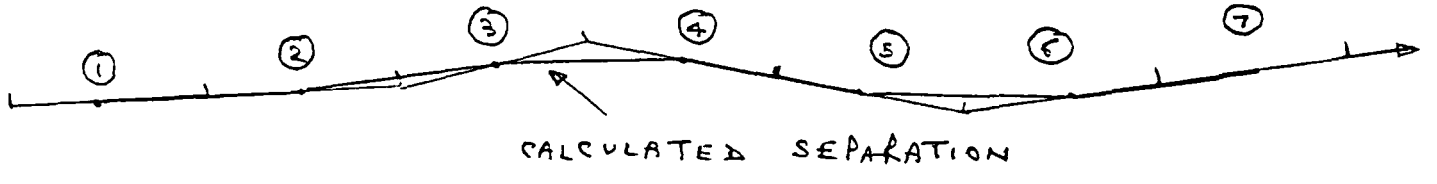

LINE 1 LM PERLE

DIPL	ANG	LENGTH
1	97.	200. 0
2	97.	200. 0
3	97.	200. 0
4	97.	200. 0
5	97.	200. 0
6	97.	200. 0
7	97.	200. 0
8	100.	200. 0
9	100.	200. 0
10	105.	200. 0
11	105.	200. 0
12	97.	200. 0
13	97.	200. 0
14	97.	200. 0

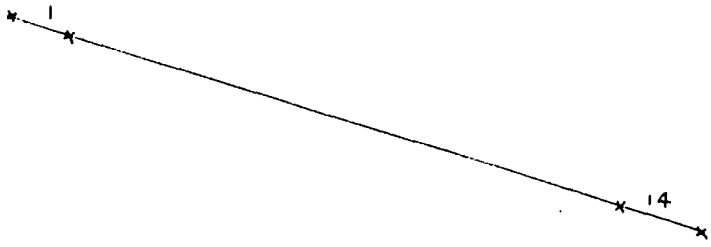

TX	RX	RANGE	MULT	I	DEPTH (m)	N (S=4)	RES
4	6	10. 000	1. 08	3. 45	200. 0	1	11. 80
4	7	1. 000	1. 20	3. 40	300. 0	2	5. 32
5	7	3. 000	2. 94	2. 94	200. 0	1	11. 31
4	8	0. 300	1. 40	3. 42	400. 0	3	4. 63
5	8	1. 000	1. 26	2. 97	300. 0	2	6. 40
4	9	0. 300	1. 00	3. 45	500. 0	4	6. 55
5	9	0. 300	2. 12	3. 00	400. 0	3	7. 99
4	10	0. 240	1. 00	3. 45	600. 5	5	9. 20
5	10	0. 300	1. 47	3. 00	500. 5	4	11. 11
4	11	0. 150	1. 00	3. 50	700. 5	6	9. 04
5	11	0. 250	1. 00	3. 02	600. 5	5	10. 91
4	12	0. 170	1. 00	3. 55	797. 8	7	15. 14
5	12	0. 200	1. 00	3. 03	697. 8	6	13. 93
6	8	3. 000	2. 67	3. 25	200. 0	1	9. 29
6	9	1. 000	1. 35	3. 30	300. 0	2	6. 16
7	9	3. 000	2. 20	3. 00	200. 0	1	8. 30
6	10	0. 300	2. 90	3. 20	400. 5	3	10. 26
7	10	1. 000	1. 88	3. 00	300. 5	2	9. 46
6	11	0. 300	1. 22	3. 23	500. 5	4	8. 53
7	11	0. 300	2. 98	3. 05	400. 5	3	11 04
6	12	0. 300	1. 45	3. 23	597. 8	5	17. 80
7	12	0. 300	1. 29	3. 05	497. 8	4	9. 62
6	13	0. 120	1. 00	3. 25	697. 8	6	7. 79
7	13	0. 160	1. 00	3. 05	597. 8	5	6. 93
6	14	0. 100	1. 00	3. 30	797. 8	7	9. 58
7	14	0. 120	1. 00	3. 05	697. 8	6	8. 30
11	8	1. 000	2. 81	3. 05	300. 0	2	13. 87
12	8	1. 000	1. 39	3. 30	398. 8	3	15. 93
13	8	0. 300	1. 36	3. 05	498. 8	4	10. 07
14	8	0. 280	1. 00	3. 50	598. 8	5	10 52
11	9	10. 000	3. 03	3. 05	200. 0	1	37. 47
12	9	3. 000	3. 00	3. 30	298. 8	2	41. 40
13	9	1. 000	2. 16	3. 10	398. 8	3	26. 22
14	9	0. 300	4. 00	3. 50	498. 8	4	25. 74
12	10	30. 000	1. 66	3. 30	200. 0	1	56. 98
13	10	3. 000	2. 50	3. 10	300. 0	2	36. 32
14	10	3. 000	1. 40	3. 55	400. 0	3	44. 44
13	11	30. 000	1. 38	3. 10	200. 0	1	50. 42
14	11	3. 000	3. 00	3. 55	300. 0	2	38. 35
14	12	10. 000	4. 00	3. 55	200. 0	1	42. 48
11	7	0. 300	2. 00	3. 05	400. 5	3	7. 41
12	7	0 300	1. 53	3. 30	497. 8	5	10. 54
13	7	0. 150	1. 00	3. 05	597. 8	6	6. 50

					Depth	n (SEGs)	
14	7	0.120	1.00	3.50	697.8	6	7.24
1	3	10.000	1.95	6.15	200.0	1	11.95
1	4	3.000	2.01	6.15	300.0	2	14.79
2	4	10.000	1.56	5.75	200.0	1	10.23
1	5	1.000	1.43	6.15	400.0	3	8.77
2	5	1.000	2.33	5.75	300.0	2	6.11
3	5	10.000	1.46	4.80	200.0	1	11.47
1	6	0.300	1.44	6.10	500.0	4	5.34
2	6	0.300	1.98	5.75	400.0	3	3.89
3	6	1.000	1.40	4.80	300.0	2	4.40
4	6	10.000	1.42	4.15	200.0	1	12.90
1	7	0.230	1.00	6.15	600.0	5	4.93
2	7	0.280	1.00	5.75	500.0	4	3.67
3	7	0.300	1.59	4.80	400.0	3	3.75
4	7	1.000	1.64	4.15	300.0	2	5.96
5	7	10.000	1.28	4.00	200.0	1	12.06
1	8	0.160	1.00	6.15	700.0	6	5.50
2	8	0.140	1.00	5.75	600.0	5	3.22
3	8	0.240	1.00	4.80	500.0	4	3.77
4	8	0.300	1.80	4.15	400.0	3	4.91
5	8	1.000	1.59	4.00	300.0	2	6.00
1	9	0.160	1.00	6.15	800.0	7	8.24
2	9	0.160	1.00	5.75	700.0	6	5.87
3	9	0.200	1.00	4.80	600.0	5	5.50
4	9	0.300	1.28	4.15	500.0	4	6.97
5	9	0.300	2.81	4.00	400.0	3	7.94
1	10	0.210	1.00	6.15	900.5	8	15.52
2	10	0.180	1.00	5.75	800.5	7	9.95
3	10	0.180	1.00	4.80	700.5	6	7.94
4	10	0.300	1.10	4.15	600.5	5	10.52
5	10	0.300	1.96	4.00	500.5	4	11.11
1	11	0.110	1.00	6.15	1000.5	9	11.14
2	11	0.080	1.00	5.75	900.5	8	6.30
3	11	0.100	1.00	4.80	800.5	7	6.60
4	11	0.180	1.00	4.15	700.5	6	9.15
5	11	0.280	1.00	4.00	600.5	5	9.22
2	12	0.130	1.00	5.70	997.8	9	14.16
3	12	0.130	1.00	4.80	897.8	8	12.23
4	12	0.180	1.00	4.15	797.8	7	13.72
5	12	0.280	1.00	4.00	697.8	6	14.77
3	13	0.070	1.00	4.80	997.8	9	9.05
4	13	0.070	1.00	4.15	897.8	8	7.62
5	13	0.100	1.00	4.00	797.8	7	7.91
4	14	0.080	1.00	4.15	997.8	9	11.96
5	14	0.100	1.00	4.00	897.8	8	11.29

LINE 2 SOUFRIERE-DIAMOND

DIPL	ANG	LENGTH
1	100.	200. 0
2	100.	200. 0
3	100.	200. 0
4	100.	200. 0
5	100.	200. 0
6	100.	200. 0
7	100.	200. 0
8	100.	200. 0
9	107.	200. 0
10	141.	200. 0
11	100.	200. 0
12	100.	200. 0
13	100.	200. 0

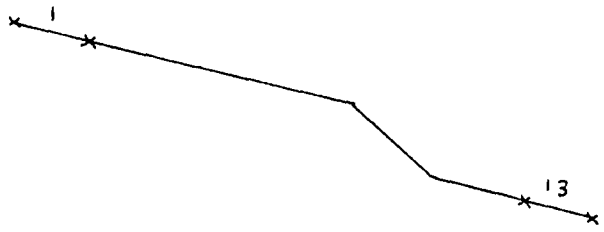

TX	RX	RANGE	MULT	I	DEPTH	RES
3	1	10. 000	1. 33	4. 20	200. 0	11. 94
4	1	1. 000	2. 93	4. 00	300. 0	11. 05
5	1	1. 000	1. 24	4. 20	400. 0	11. 13
6	1	0. 300	2. 71	4. 20	500. 0	14. 59
7	1	0. 300	1. 00	4. 20	600. 0	9. 42
4	2	10. 000	1. 08	3. 93	200. 0	10. 36
5	2	1. 000	2. 67	4. 20	300. 0	9. 59
6	2	1. 000	1. 53	4. 20	400. 0	13. 73
7	2	0. 300	1. 39	4. 20	500. 0	7. 49
5	3	10. 000	1. 44	4. 22	200. 0	12. 86
6	3	1. 000	3. 11	4. 22	300. 0	11. 11
7	3	0. 300	2. 51	4. 21	400. 0	6. 74
6	4	10. 000	1. 75	4. 20	200. 0	15. 71
7	4	1. 000	2. 86	4. 20	300. 0	10. 27
7	5	10. 000	1. 35	4. 20	200. 0	12. 12
6	8	10. 000	1. 36	4. 22	200. 0	12. 15
5	8	3. 000	1. 05	4. 24	300. 0	11. 20
4	8	1. 000	1. 05	4. 00	400. 0	9. 90
3	8	0. 300	1. 51	4. 23	500. 0	8. 07
7	9	10. 000	1. 66	4. 20	200. 0	14. 92
6	9	3. 000	1. 32	4. 21	300. 0	14. 22
5	9	1. 000	1. 46	4. 23	400. 0	13. 06
4	9	0. 300	2. 15	4. 00	500. 0	12. 21
3	9	0. 300	1. 00	4. 21	600. 0	9. 44
7	10	3. 000	1. 60	4. 20	304. 1	18. 39
6	10	1. 000	1. 69	4. 20	404. 5	16. 79
5	10	0. 300	2. 48	4. 22	504. 8	15. 11
4	10	0. 300	1. 20	4. 00	605 0	13. 78
3	10	0. 210	1. 00	4. 21	705. 2	12. 40
7	11	1. 000	2. 71	4. 20	374. 3	22. 83
6	11	1. 000	1. 10	4. 20	474. 5	18. 32
5	11	0. 300	1. 81	4. 21	574. 6	15. 80
4	11	0. 300	1. 00	4. 00	674. 7	14. 75
3	11	0. 200	1. 00	4. 20	774. 7	14 12
7	12	1. 000	1. 10	4. 18	474. 3	18. 41
6	12	0. 300	1. 63	4. 20	574. 6	14. 26
5	12	0. 250	1. 00	4. 21	674. 7	11. 68
4	12	0. 140	1. 00	4. 00	774. 7	10. 37
3	12	0. 090	1. 00	4. 20	874. 7	9. 11
7	13	0. 300	1. 67	4. 19	574. 6	14. 64
6	13	0. 250	1. 00	4. 20	674. 7	13. 11

5	13	0.150	1.00	4.20	774.7	10.58
4	13	0.080	1.00	4.00	874.7	8.50
3	13	0.055	1.00	4.20	974.7	7.69
11	13	10.000	2.73	4.75	200.0	21.67
10	13	3.000	2.26	4.75	300.5	23.64
9	13	1.000	3.78	4.00	379.4	31.78
8	13	1.000	1.85	4.18	474.5	30.96
10	12	10.000	2.20	4.70	200.1	18.42
9	12	3.000	2.89	4.00	279.3	29.69
8	12	1.000	3.48	4.10	374.3	30.03
9	11	10.000	3.58	4.00	178.0	38.31
8	11	3.000	3.08	4.12	273.6	33.68
8	10	30.000	1.38	4.13	203.6	58.59
8	2	0.300	1.00	4.15	600.0	9.54
9	2	0.230	1.00	4.00	700.0	12.20
10	2	0.160	1.00	4.63	805.3	13.06
11	2	0.160	1.00	4.60	874.7	14.79
12	2	0.080	1.00	4.40	974.7	10.67
8	1	0.240	1.00	4.02	700.0	12.60
9	1	0.180	1.00	3.95	800.0	14.51
10	1	0.200	1.00	4.60	905.4	23.74
11	1	0.150	1.00	4.61	974.7	19.09

LINE 3 STONEFIELD-SAPPHIRE

DIPL	ANG	LENGTH
1	0.	200. 0
2	0.	200. 0
3	0.	200. 0
4	0.	200. 0
5	0.	200. 0
6	0.	200. 0
7	0.	200. 0
8	0.	200. 0
9	0.	200. 0
10	0.	200. 0
11	0.	200. 0
12	0.	200. 0
13	0.	200. 0
14	0.	200. 0
15	0.	200. 0

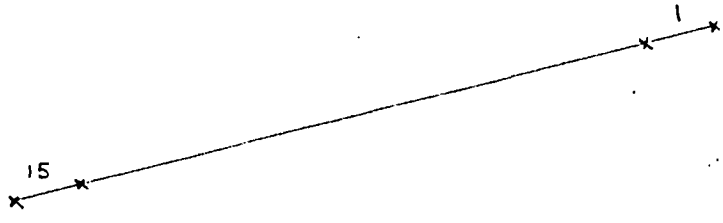

TX	RX	RANGE	MULT	I	DEPTH	RES
4	1	3. 000	1. 62	2. 58	300. 0	28. 41
5	1	1. 000	3. 00	2. 58	400. 0	43. 84
6	1	1. 000	1. 25	2. 21	500. 0	42. 65
7	1	0. 300	1. 48	2. 05	600. 0	28. 58
8	1	0. 270	1. 00	3. 23	700. 0	17. 65
4	2	10. 000	1. 91	2. 58	200. 0	27. 91
5	2	3. 000	2. 46	2. 57	300. 0	43. 30
6	2	1. 000	2. 63	2. 20	400. 0	45. 07
7	2	0. 300	2. 88	2. 05	500. 0	31. 75
8	2	0. 300	1. 65	3. 22	600. 0	20. 28
5	3	10. 000	1. 56	2. 50	200. 0	23. 52
6	3	3. 000	1. 31	2. 20	300. 0	26. 94
7	3	1. 000	1. 10	2. 05	400. 0	20. 23
8	3	0. 300	1. 84	3. 30	500. 0	12. 61
6	4	10. 000	2. 30	2. 20	200. 0	39. 41
7	4	3. 000	1. 31	2. 05	300. 0	28. 91
8	4	1. 000	1. 55	3. 25	400. 0	17. 98
7	5	10. 000	2. 42	2. 05	200. 0	44. 50
8	5	3. 000	1. 79	3. 35	300. 0	24. 17
8	14	0. 300	2. 22	3. 40	600. 0	25. 85
7	14	0. 160	1. 00	2. 20	700. 0	15. 35
6	14	0. 140	1. 00	2. 25	800. 0	19. 70
5	14	0. 100	1. 00	2. 53	900. 0	17. 88
4	14	0. 060	1. 00	2. 62	1000. 0	14. 24
8	15	0. 300	1. 20	3. 28	700. 0	23. 17
7	15	0. 140	1. 00	2. 10	800. 0	21. 11
6	15	0. 060	1. 00	2. 25	900. 0	12. 64
5	15	0. 050	1. 00	2. 50	1000. 0	12. 44
13	15	30. 000	1. 19	5. 85	200. 0	23. 01
12	15	3. 000	2. 84	4. 55	300. 0	28. 24
11	15	1. 000	2. 61	4. 20	400. 0	23. 43
10	15	0. 300	4. 00	4. 35	500. 0	20. 80
9	15	0. 300	3. 11	4. 90	600. 0	25. 12
12	14	30. 000	1. 26	4. 55	200. 0	31. 32
11	14	3. 000	2. 47	4. 15	300. 0	26. 93
10	14	1. 000	2. 83	4. 33	400. 0	24. 64
9	14	1. 000	1. 77	4. 90	500. 0	27. 24
11	13	30. 000	1. 08	4. 15	200. 0	29. 43
10	13	3. 000	2. 61	4. 33	300. 0	27. 27
9	13	3. 000	1. 39	4. 82	400. 0	32. 62
10	12	10. 000	2. 76	4. 25	200. 0	24. 48
9	12	3. 000	3. 24	4. 82	300. 0	30. 41

9	11	10.000	3.45	4.80	200.0	27.10
10	8	30.000	1.43	4.28	200.0	37.79
11	8	3.000	2.81	4.15	300.0	30.68
12	8	1.000	4.00	4.54	400.0	33.21
13	8	1.000	2.45	5.90	500.0	31.30
9	7	10.000	1.86	4.90	200.0	14.31
10	7	3.000	1.46	4.33	300.0	15.25
11	7	1.000	1.70	4.17	400.0	15.37
12	7	0.300	3.70	4.55	500.0	18.39
13	7	0.300	2.67	5.90	600.0	17.21
9	6	3.000	1.72	4.80	300.0	16.21
10	6	1.000	2.02	4.35	400.0	17.51
11	6	0.300	3.00	4.17	500.0	16.27
12	6	0.300	2.39	4.55	600.0	20.79
13	6	0.300	1.98	5.93	700.0	21.15
9	5	1.000	2.58	4.80	400.0	20.26
10	5	0.300	3.62	4.32	500.0	18.95
11	5	0.300	2.00	4.17	600.0	18.99
12	5	0.300	1.61	4.55	700.0	22.41
13	5	0.300	1.52	5.95	800.0	24.27
9	4	0.300	3.15	4.80	500.0	14.84
10	4	0.300	1.54	4.30	600.0	14.18
11	4	0.240	1.00	4.19	700.0	12.09
12	4	0.240	1.00	4.55	800.0	16.70
13	4	0.220	1.00	5.95	900.0	16.73
9	3	0.300	1.12	4.80	600.0	9.24
10	3	0.180	1.00	4.28	700.0	8.88
11	3	0.100	1.00	4.15	800.0	7.63
12	3	0.100	1.00	4.55	900.0	9.94
13	3	0.110	1.00	5.93	1000.0	11.54
9	2	0.300	1.20	4.75	700.0	16.00
10	2	0.180	1.00	4.30	800.0	13.24
11	2	0.140	1.00	4.17	900.0	15.19
12	2	0.140	1.00	4.58	1000.0	19.01
9	1	0.220	1.00	4.80	800.0	14.51
10	1	0.120	1.00	4.35	900.0	12.48
11	1	0.100	1.00	4.20	1000.0	14.81

LINE 4 GROS PITON-BEAUSEJOUR DIPOLES 11 AND 15 ARE DUMMIES ✓

DIPL	ANG	LENGTH
1	68.	200. 0
2	68.	200 0
3	68.	200. 0
4	68.	200. 0
5	68.	200. 0
6	68.	200. 0
7	68.	200. 0
8	68.	200. 0
9	68.	200. 0
10	68.	200. 0
11	338.	188. 0
12	68.	200. 0
13	68.	200. 0
14	68.	200. 0
15	0.	1. 0?
16	111.	275. 0
17	68.	200. 0
18	68.	200 0
19	68.	200. 0
20	68.	200. 0
21	68.	200. 0
22	68.	200. 0

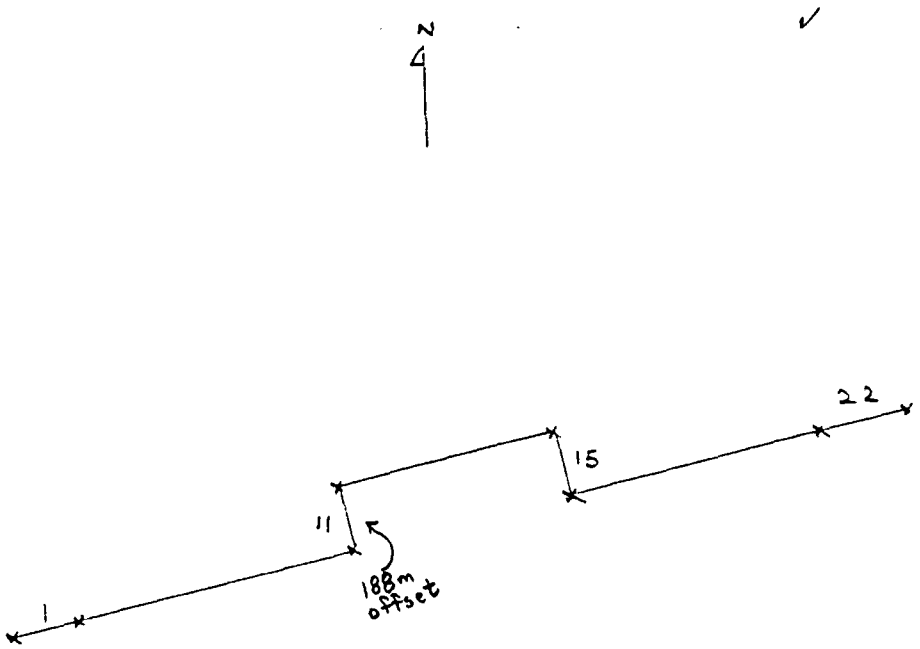

TX	RX	RANGE	MULT	I	DEPTH	RES
18	22	10 000	1. 54	5. 50	400. 0	105. 56
17	22	0. 300	3. 34	5. 25,	500. 0	14 39
16	22	0. 300	2. 25	4. 50	620. 3	18. 31
14	22	0. 220	1. 00	4. 58	700. 6	10. 74
13	22	0. 120	1. 00	5. 70	800. 7	6. 97
12	22	0. 100	1. 00	6. 45	900. 7	7. 26 ✓
18	21	10. 000	2. 57	5. 42	300. 0	71. 50
17	21	1. 000	1. 91	5. 21	400. 0	13. 82
16	21	0. 300	4. 00	4. 55	520. 0	18. 25
14	21	0. 300	1. 10	4. 40	600. 5	10. 70
13	21	0. 220	1. 00	5. 75	700. 6	8. 56
12	21	0. 150	1. 00	6. 53	800 7	7. 60 ✓
18	20	100. 000	1. 94	5. 42	200. 0	134. 94
17	20	3. 000	2. 44	5. 21	300. 0	21. 19
16	20	3. 000	1. 15	4. 55	419. 7	26. 02
14	20	0. 300	2. 34	4. 40	500. 4	13 46
13	20	0. 300	1. 35	5. 73	600. 5	10. 07
12	20	0. 240	1. 00	6. 55	700. 6	8. 20
17	19	30. 000	1 65	5. 21	200. 0	35. 82
16	19	10. 000	1. 49	4 55	319. 2	44. 67
14	19	1. 000	1 69	4. 40	400. 0	17 34
13	19	0. 300	2. 68	5. 73	500 4	12. 74
12	19	0. 300	1 65	6. 58	600. 5	10. 74
16	18	1000. 002	2. 22	4. 55	216. 6	1675. 47 —?
14	18	10. 000	1. 82	4. 40	299. 0	87. 19
13	18	3. 000	1. 60	5. 75	400 0	37. 70
12	18	1. 000	2. 26	6. 58	500. 4	22. 02
14	17	10. 000	3. 51	4 40	194. 6	70. 43
13	17	3. 000	2. 64	5. 75	299. 0	29. 06
12	17	1. 000	3. 30	6. 60	400. 0	22. 58
12	14	100. 000	3. 39	6. 65	200. 0	192. 18
12	1	0. 035	1. 00	6 90	1000. 0	3. 24
12	2	0. 065	1. 00	6. 80	899. 9	4 47
13	2	0. 080	1. 00	5. 95	1000. 0	8. 22
12	3	0. 050	1. 00	6. 40	799. 8	1. 01

13	3	0.040	1.00	5.85	899.9	5.20
14	3	0.030	1.00	4.60	1000.0	4.17
12	4	0.120	1.00	6.60	699.9	4.06
13	4	0.060	1.00	5.90	799.9	3.36
14	4	0.040	1.00	4.60	899.9	4.07
16	4	0.010	1.00	4.80	976.6	1.40
5	1	1.000	1.94	6.50	400.0	11.25
6	1	0.300	3.05	6.98	500.0	9.88
7	1	0.300	2.04	6.80	600.0	11.88
8	1	0.230	1.00	5.10	700.0	9.52
9	1	0.090	1.00	4.60	800.0	6.20
10	1	0.050	1.00	4.60	900.0	4.92
5	2	3.000	2.14	6.42	300.0	15.08
6	2	1.000	2.34	6.83	400.0	12.92
7	2	1.000	1.49	6.65	500.0	16.89
8	2	0.300	1.76	4.95	600.0	14.07
9	2	0.160	1.00	4.40	700.0	7.68
10	2	0.070	1.00	4.57	800.0	4.85
5	3	10.000	3.21	6.25	200.0	19.36
6	3	3.000	1.89	6.75	300.0	12.67
7	3	1.000	3.06	6.62	400.0	17.43
8	3	0.300	3.19	4.90	500.0	14.73
9	3	0.300	1.00	4.45	600.0	8.90
10	3	0.105	1.00	4.57	700.0	4.85
6	4	30.000	1.22	6.78	200.0	20.35
7	4	3.000	2.12	6.60	300.0	14.53
8	4	1.000	1.76	4.85	400.0	13.68
9	4	0.300	1.70	4.45	500.0	8.64
10	4	0.180	1.00	4.58	600.0	5.19
7	5	30.000	1.51	6.50	200.0	26.27
8	5	3.000	2.69	4.83	300.0	25.20
9	5	1.000	2.06	4.38	400.0	17.73
10	5	0.300	2.20	4.59	500.0	10.84
8	6	30.000	1.87	4.80	200.0	44.06
9	6	3.000	3.25	4.38	300.0	33.57
10	6	1.000	2.58	4.58	400.0	21.24
9	7	30.000	1.33	4.35	200.0	34.58
10	7	3.000	2.60	4.59	300.0	25.63
10	8	10.000	3.86	4.59	200.0	31.70
9	12	10.000	2.79	4.55	193.5	54.38
8	12	3.000	1.61	4.98	298.2	20.41
7	12	1.000	2.55	6.65	399.2	17.27
6	12	1.000	1.00	6.82	499.6	12.35
5	12	0.250	1.00	6.41	599.8	5.54
10	13	30.000	1.38	4.90	193.5	74.93
9	13	3.000	2.32	4.55	298.2	32.19
8	13	1.000	1.60	4.95	399.2	14.56
7	13	0.300	3.34	6.60	499.6	12.79
6	13	0.300	1.55	6.80	599.8	9.74
5	13	0.160	1.00	6.42	699.9	8.56
10	14	10.000	1.10	4.65	298.2	49.78
9	14	1.000	2.67	4.57	399.2	26.31
8	14	0.300	2.66	4.98	499.6	13.50
7	14	0.300	2.00	6.55	599.8	13.04
6	14	0.260	1.00	6.85	699.9	8.47
5	14	0.150	1.00	6.40	799.9	7.74
10	17	0.300	1.80	4.80	500.7	8.52
9	17	0.240	1.00	4.62	600.8	6.88
8	17	0.100	1.00	5.10	700.7	4.15
7	17	0.100	1.00	6.70	800.8	4.74
6	17	0.060	1.00	6.82	900.8	3.99
5	17	0.040	1.00	6.45	1000.8	3.87
10	18	0.300	1.72	4.80	600.7	14.24
9	18	0.240	1.00	4.62	700.8	11.00
8	18	0.140	1.00	5.10	800.7	8.72
7	18	0.150	1.00	6.70	900.8	10.15

6	18	0.050	1.00	6.80	1000.8	7.53
10	19	0.120	1.00	4.80	700.7	5.39
9	19	0.070	1.00	4.62	800.8	4.61
8	19	0.040	1.00	5.10	900.7	5.06
7	19	0.050	1.00	6.70	1000.8	4.65
10	20	0.070	1.00	4.80	800.7	4.63
9	20	0.050	1.00	4.62	900.8	4.91
8	20	0.030	1.00	5.10	1000.7	3.67
10	21	0.040	1.00	4.80	900.7	3.78
9	21	0.035	1.00	4.68	1000.8	4.66
10	22	0.030	1.00	4.82	1000.7	3.86

LINE 4 CONT

DIPL	ANG	LENGTH
1	68.	200. 0
2	68.	200. 0
3	68.	200. 0
4	68	200. 0
5	68.	200. 0
6	68.	200 0
7	68.	200 0
8	68	200 0
9	68.	200 0
10	68	200 0
11	338	188. 0 —
12	68.	200. 0
13	68.	200. 0
14	68	200 0
15	158.	188. 0 →
16	68	200. 0
17	68.	200. 0
18	68.	200. 0
19	68.	200. 0
20	68.	200. 0
21	68.	200. 0
22	68.	200. 0

TX	RX	RANGE	MULT	I	DEPTH	RES
13	16	30 000	1. 61	5. 80	198. 5	73. 86
12	16	10 000	1. 65	6 65	298. 2	52. 22
10	16	1. 000	2. 12	4. 85	400. 0	16. 48
9	16	0. 300	2. 50	4. 70	500. 0	12. 08
8	16	0. 280	1. 00	5. 10	600. 0	7. 24
7	16	0. 280	1. 00	6. 70	700. 0	8. 82
6	16	0. 140	1. 00	6. 85	800. 0	6. 47
5	16	0. 070	1. 00	6. 50	900. 0	4. 87

LINE 2 COUGAR1L-RABUT-DAUPHINE

DIPL	ANG	LENGTH
1	172.	200. 0
2	172.	200. 0
3	172.	200. 0
4	172.	200. 0
5	172.	200. 0
6	172.	200. 0
7	172.	200. 0
8	172.	200 0
9	172.	200. 0
10	172.	200. 0
11	172.	200. 0
12	162.	200. 0
13	162.	200. 0
14	162.	200. 0
15	162.	200. 0
16	162.	200 0
17	162.	200. 0

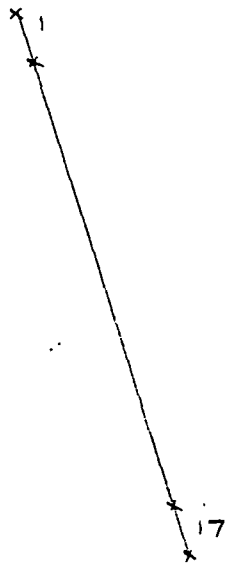

TX	RX	RANGE	MULT	I	DEPTH	RES
4	1	3. 000	2. 69	5. 00	298. 5	24. 23
5	1	1. 000	4. 02	5 17	398. 5	29. 15
6	1	1. 000	1. 26	5. 15	498. 5	18. 35
7	1	0. 300	2. 60	4. 80	596. 5	21. 33
8	1	0. 300	1. 29	4. 21	698. 5	19. 32
4	2	30. 000	1. 20	4. 85	200. 0	28. 05
5	2	10. 000	1. 06	5. 13	300. 0	31. 31
6	2	1. 000	2. 75	5. 07	400. 0.	20. 59
7	2	1. 000	1. 45	4. 75	500. 0	23. 20
8	2	0. 300	2. 18	4. 20	600. 0	20. 73
5	3	30. 000	1 70	5. 10	200. 0	17. 70
6	3	3. 000	1. 63	5. 03	300. 0	13. 65
7	3	3. 000	1. 03	4. 80	400. 0	24. 27
8	3	1. 000	1. 36	4. 20	500. 0	24. 41
6	4	30. 000	1. 53	5. 03	200. 0	34. 40
7	4	10. 000	1. 10	4. 81	300. 0	34. 49
8	4	3. 000	1. 28	4. 21	400. 0	34. 39
7	5	30. 000	1. 22	4 80	200. 0	38. 75
8	5	10. 000	1. 04	4. 21	300 0	37. 25
8	6	10. 000	2. 05	4. 15	200. 0	18. 44
7	9	10. 000	3. 94	4. 81	200. 0	30. 86
6	9	10. 000	1. 10	5. 15	300. 0	32. 21
5	9	3. 000	2. 38	5. 20	400 0	51. 76
4	9	1. 000	2. 75	5 03	500 0	41 22
8	10	10 000	1 50	4 25	200. 0	13. 31
7	10	3. 000	2. 40	4. 98	300. 0	12. 57
6	10	1. 000	1. 33	5. 15	400. 0	20 72
5	10	1 000	2. 26	5. 20	500. 0	32. 77
4	10	0 300	3. 13	5. 03	600. 0	24. 63
8	11	1. 000	3. 80	4. 15	300. 0	13. 45
7	11	1. 000	2. 70	4. 85	400. 0	20. 99
6	11	1. 000	1. 17	5. 20	500. 0	16. 96
5	11	0 300	2. 67	5. 20	600. 0	27. 94
4	11	0. 300	1. 68	5. 05	700. 0	20. 44
8	12	1. 000	2. 07	4 26	400. 0	18. 36
7	12	1. 000	1. 63	4. 85	500. 0	25. 55
6	12	0. 300	2. 69	5. 20	600. 0	20. 67
5	12	0. 300	2. 56	5. 20	700. 0	31. 49
4	12	0. 300	1. 24	5. 06	800. 0	23. 52
8	13	1. 000	1. 58	4 28	500 0	27 73

7	13	1.000	1.35	4.35	600.0	36.67
6	13	0.300	2.39	5.10	700.0	19.12
5	13	0.300	2.60	5.20	800.0	47.58
4	13	0.200	1.22	5.06	900.0	32.68
8	14	0.300	3.12	4.25	600.0	38.56
7	14	0.300	2.86	4.85	700.0	36.75
6	14	0.300	1.43	5.20	800.0	12.02
5	14	0.300	1.56	5.20	900.0	41.12
4	14	0.210	1.00	5.09	1000.0	25.67
8	15	0.300	2.70	4.20	700.0	40.41
7	15	0.300	2.46	4.83	800.0	48.04
6	15	0.300	1.29	5.18	900.0	33.56
5	15	0.300	1.15	5.20	1000.0	41.05
8	16	0.300	1.00	4.50	800.0	21.93
7	16	0.290	1.00	4.83	900.0	26.05
6	16	0.120	1.00	5.20	1000.0	14.25
8	17	0.160	1.00	4.22	900.0	19.17
7	17	0.170	1.00	4.81	1000.0	21.82
13	17	10.000	1.07	6.45	400.0	62.54
12	17	1.000	2.85	4.45	500.0	48.29
11	17	0.300	2.88	3.85	600.0	29.85
10	17	0.300	1.80	4.45	700.0	18.51
9	17	0.300	1.09	3.40	800.0	30.33
13	16	10.000	2.89	6.30	300.0	69.17
12	16	3.000	2.11	4.43	400.0	53.87
11	16	1.000	1.70	3.85	500.0	33.57
10	16	0.300	2.45	3.48	600.0	27.83
9	16	0.300	1.95	3.40	700.0	36.12
13	15	100.000	1.45	6.25	200.0	87.46
12	15	10.000	2.28	4.43	300.0	77.61
11	15	3.000	1.67	3.85	400.0	49.39
10	15	1.000	2.02	3.50	500.0	43.30
9	15	1.000	1.48	3.40	600.0	37.04
12	14	30.000	2.00	4.42	200.0	51.18
11	14	3.000	2.78	3.85	300.0	32.83
10	14	1.000	2.72	3.45	400.0	29.55
9	14	1.000	1.87	3.40	500.0	41.16
11	13	10.000	2.59	3.83	200.0	25.55
10	13	3.000	1.84	3.45	300.0	23.95
9	13	1.000	3.41	3.40	400.0	37.59
10	12	10.000	1.63	3.40	200.0	18.12
9	12	3.000	1.79	3.35	300.0	24.29
9	11	10.000	1.46	3.35	200.0	16.48
9	1	0.300	1.00	3.40	798.5	27.82
10	1	0.160	1.00	3.48	898.5	16.72
11	1	0.100	1.00	3.81	998.5	16.27
9	2	0.300	1.44	3.37	700.0	27.33
10	2	0.200	1.00	3.45	800.0	18.55
11	2	0.140	1.00	3.83	900.0	16.72
12	2	0.120	1.00	4.42	1013.8	17.07
9	3	0.300	2.70	3.39	600.0	31.53
10	3	0.300	1.07	3.41	700.0	19.87
11	3	0.200	1.00	3.81	800.0	16.62
12	3	0.200	1.00	4.42	900.0	20.69
13	3	0.300	1.00	6.35	1000.0	29.50

LINE 6 RABOT-DH1-RUBY

DIPL	ANG	LENGTH
1	8.	200. 0
2	8.	200. 0
3	8.	200. 0
4	8.	200. 0
5	8.	200. 0
6	8.	200. 0
7	8.	200. 0
8	18.	200. 0
9	8.	200. 0
10	8.	200. 0
11	8.	200. 0
12	8.	200. 0
13	8.	200. 0
14	8.	200. 0
15	8.	200. 0

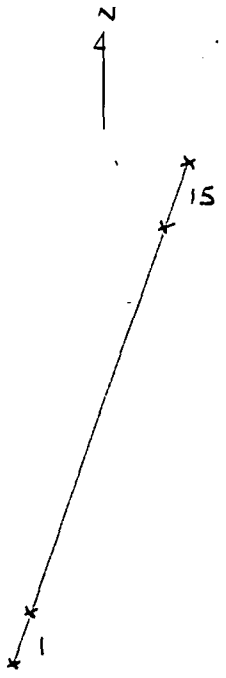

TX	RX	RANGE	MULT	I	DEPTH	RES
3	1	10. 000	2. 24	2. 82	200. 0	29. 95
4	1	3. 000	2. 72	3. 20	300. 0	38. 45
5	1	1. 000	4. 00	3. 10	400. 0	48. 64
6	1	1. 000	2. 05	3. 70	500. 0	41. 77
7	1	0. 300	3. 85	4. 37	600. 0	34. 87
4	2	10. 000	1. 68	3. 20	200. 0	19. 79
5	2	3. 000	1. 95	3. 15	300. 0	28. 01
6	2	1. 000	2. 60	3. 70	400. 0	26. 49
7	2	1. 000	1. 32	4. 37	500. 0	22. 77
5	3	10. 000	2. 25	3. 15	200. 0	26. 93
6	3	3. 000	2. 33	3. 75	300. 0	28. 11
7	3	1. 000	2. 99	4. 37	400. 0	25. 79
6	4	10. 000	2. 14	3. 75	200. 0	21. 51
7	4	3. 000	2. 07	4. 37	300. 0	21. 43
7	5	10. 000	3. 30	4. 38	200. 0	28. 40
3	8	0. 300	2. 95	2. 85	500. 0	23. 60
4	8	1. 000	1. 62	3. 20	400. 0	19. 22
5	8	3. 000	2. 03	3. 19	300. 0	28. 93
6	8	10. 000	2. 57	3. 75	200. 0	25. 90
3	9	0. 300	1. 26	2. 95	598. 5	16. 82
4	9	0. 300	2. 05	3. 25	498. 5	14. 19
5	9	1. 000	1. 80	3. 19	398. 5	21. 15
6	9	3. 000	1. 70	3. 75	298. 5	20. 42
7	9	10. 000	3. 15	4. 39	198. 5	27. 27
3	10	0. 300	1. 25	2. 95	698. 5	26. 71
4	10	0. 300	1. 74	3. 28	598. 5	20. 89
5	10	1. 000	1. 42	3. 20	498. 5	33. 27
6	10	3. 000	1. 05	3. 75	398. 5	31. 49
7	10	10. 000	1. 20	4. 40	298. 5	40. 95
3	11	0. 130	1. 00	3. 00	798. 5	13. 66
4	11	0. 160	1. 00	3. 39	698. 5	9. 92
5	11	0. 300	1. 10	3. 22	598. 5	13. 45
6	11	0. 300	2. 28	3. 80	498. 5	13. 50
7	11	1. 000	1. 93	4. 40	328. 5	16. 44
3	12	0. 050	1. 00	3. 00	898. 5	7. 51
4	12	0. 070	1. 00	3. 40	798. 5	6. 49
5	12	0. 130	1. 00	3. 38	698. 5	8. 08
6	12	0. 240	1. 00	3. 80	598. 5	8. 29
7	12	0. 300	1. 84	4. 40	498. 5	9. 41

3	13	0.040	1.00	3.00	998.5	8.26
4	13	0.050	1.00	3.37	898.5	6.69
5	13	0.080	1.00	3.39	798.5	7.44
6	13	0.130	1.00	3.80	698.5	7.19
7	13	0.260	1.00	4.40	598.5	7.76
4	14	0.035	1.00	3.20	998.5	6.78
5	14	0.050	1.00	3.30	898.5	6.83
6	14	0.080	1.00	3.80	798.5	6.64
7	14	0.160	1.00	4.40	698.5	7.64
5	15	0.045	1.00	3.27	998.5	8.53
6	15	0.080	1.00	3.80	898.5	9.49
7	15	0.140	1.00	4.40	798.5	10.03
8	1	0.300	2.56	4.93	700.0	33.47
9	1	0.300	1.45	5.00	798.5	31.21
10	1	0.300	1.50	4.45	898.5	45.56
11	1	0.130	1.00	3.20	998.5	25.18
8	2	0.300	2.56	5.00	600.0	20.45
9	2	0.300	1.45	5.01	698.5	18.25
10	2	0.300	1.29	4.48	798.5	27.24
11	2	0.100	1.00	3.20	898.5	14.08
12	2	0.045	1.00	2.75	998.5	10.14
8	10	30.000	3.28	5.05	200.0	73.63
8	11	3.000	2.38	5.08	300.0	21.51
9	11	10.000	3.52	5.02	200.0	26.43
8	12	1.000	1.38	5.05	400.0	10.37
9	12	3.000	1.16	5.02	300.0	10.45
10	12	10.000	1.54	4.45	200.0	13.05
8	13	0.300	1.86	5.08	500.0	8.35
9	13	1.000	1.00	5.05	400.0	7.47
10	13	1.000	2.95	4.45	300.0	10.00
11	13	3.000	2.94	3.20	200.0	10.39
8	14	0.300	1.00	5.07	600.0	7.88
9	14	0.300	1.55	5.05	500.0	6.94
10	14	0.300	3.70	4.48	400.0	9.34
11	14	1.000	1.49	3.22	300.0	6.98
12	14	3.000	1.77	2.75	200.0	7.28
8	15	0.220	1.00	5.08	700.0	9.23
9	15	0.300	1.00	5.03	600.0	7.87
10	15	0.300	2.24	4.45	500.0	11.39
11	15	0.300	2.29	3.20	400.0	8.09
12	15	1.000	1.00	2.73	300.0	5.52

LINE 7 RUBY-SPRINGS-FOND DOUX

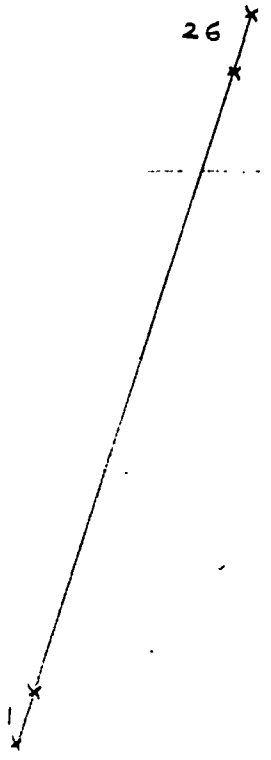

DIPL	ANG	LENGTH
1	9.	200. 0
2	9.	200. 0
3	9.	200. 0
4	9.	200. 0
5	9.	200. 0
6	9.	200. 0
7	45.	200. 0
8	32.	200. 0
9	1.	200. 0
10	1.	200. 0
11	1.	200. 0
12	1.	200. 0
13	351.	200. 0
14	351.	200. 0
15	338.	200. 0
16	355.	200. 0
17	0.	200. 0
18	0.	200. 0
19	0.	200. 0
20	0.	200. 0
21	0.	200. 0
22	0.	200. 0
23	0.	200. 0
24	0.	200. 0
25	0.	200. 0
26	0.	200. 0

TX	RX	RANGE	MULT	I	DEPTH	N	RES
4	1	3. 000	2. 00	3. 43	300. 0	3	26. 38
5	1	1. 000	1. 83	3. 50	400. 0	4	19. 71
6	1	0. 300	2. 79	2. 90	500. 0	5	21. 76
7	1	0. 300	2. 81	3. 47	600. 6	6	36. 40
8	1	0. 150	1. 00	2. 35	692. 9	7	12. 83
9	1	0. 140	1. 00	2. 35	765. 6	8	18. 37
4	2	30. 000	2. 78	3. 43	200. 0	2	91. 66
5	2	3. 000	2. 73	3. 40	300. 0	3	36. 32
6	2	1. 000	1. 57	2. 80	400. 0	4	21. 14
7	2	1. 000	1. 45	3. 47	500. 6	5	35. 33
8	2	0. 220	1. 00	2. 38	592. 8	6	11. 45
9	2	0. 170	1. 00	2. 38	665. 4	7	14. 71
5	3	30. 000	2. 03	3. 40	200. 0	2	67. 53
6	3	3. 000	2. 03	2. 80	300. 0	3	32. 80
7	3	3. 000	1. 53	3. 47	400. 4	4	54. 90
8	3	0. 300	1. 82	2. 40	492. 8	5	15. 84
9	3	0. 300	1. 43	2. 40	565. 2	6	23. 16
6	4	30. 000	3. 07	2. 80	200. 0	2	124. 00
7	4	30. 000	1. 14	3. 47	300. 3	3	159. 44
8	4	1. 000	2. 67	2. 40	392. 8	4	38. 11
9	4	1. 000	1. 68	2. 40	464. 8	5	52. 74
7	5	100. 000	2. 43	3. 50	200. 1	2	270. 35
8	5	3. 000	3. 09	2. 40	292. 8	3	52. 90
9	5	3. 000	1. 27	2. 40	363. 8	4	62. 57
8	6	30. 000	2. 44	2. 42	192. 8	2	120. 32
9	6	10. 000	1. 63	2. 42	261. 2	3	121. 18
9	7	100. 000	1. 60	2. 42	206. 1	2	252. 36
8	10	100. 000	1. 11	2. 45	200. 0	2	174. 87

X	C						
7	10	10.000	1.90	3.50	305.8	3	77.55
6	10	1.000	3.54	2.82	364.8	4	46.09
5	10	1.000	1.65	3.42	465.3	5	34.72
4	10	0.300	3.46	3.43	565.5	6	37.25
9	11	100.000	1.73	2.42	200.0	2	269.50
8	11	10.000	1.47	2.45	300.2	3	95.20
7	11	3.000	1.72	3.55	406.4	4	53.95
6	11	1.000	1.55	2.85	465.7	5	37.57
5	11	0.300	3.16	3.42	565.8	6	33.76
4	11	0.300	2.08	3.43	665.9	7	35.73
11	6	1.000	1.90	3.70	465.7		35.47
12	6	0.300	2.51	4.75	565.9		18.82
13	6	0.300	1.74	4.25	662.2		24.17
14	6	0.080	1.00	1.10	762.4		20.86
10	7	10.000	2.08	3.80	305.8		78.20
11	7	3.000	1.81	3.80	406.4		53.03
12	7	1.000	1.31	4.80	507.0		21.12
13	7	0.300	3.15	4.30	636.7		30.20
14	7	0.140	1.00	1.07	738.2		29.55
15	7	0.070	1.00	0.85	898.6		28.12
10	8	100.000	1.69	3.70	200.0		176.30
11	8	10.000	2.16	3.80	300.2		90.19
12	8	1.000	1.48	4.80	400.2		12.46
13	8	0.300	2.78	4.30	519.8		15.56
14	8	0.120	1.00	1.10	620.2		15.56
15	8	0.080	1.00	0.85	762.1		21.47
10	1	0.120	1.00	3.70	865.8		14.05
11	1	0.070	1.00	3.60	966.0		11.47
10	2	0.130	1.00	3.70	765.8		10.61
11	2	0.080	1.00	3.70	865.9		9.22
12	2	0.050	1.00	4.80	966.0		6.07
10	3	0.290	1.00	3.70	665.7		15.74
11	3	0.180	1.00	3.70	765.9		14.44
12	3	0.090	1.00	4.80	866.0		7.89
13	3	0.065	1.00	4.30	962.2		9.08
10	4	1.000	1.14	3.70	565.5		38.64
11	4	0.300	2.47	3.70	665.9		39.34
12	4	0.300	1.20	4.80	766.0		21.91
13	4	0.260	1.00	4.30	862.2		26.17
14	4	0.100	1.00	1.05	962.4		55.32 -?
12	5	0.300	1.81	4.80	666.0		21.78
13	5	0.300	1.36	4.30	762.2		28.42
14	5	0.060	1.00	1.05	862.4		23.81
15	5	0.040	1.00	0.82	965.3		29.55
11	5	1.000	1.16	3.80	565.8		37.18
11	9	100.000	2.56	3.80	200.0		253.97
12	9	3.000	2.10	4.80	300.0		19.79
13	9	1.000	2.00	4.35	400.0		17.45
14	9	0.260	1.00	1.08	500.0		18.09
15	9	0.120	1.00	0.85	604.1		18.97
12	10	30.000	1.32	4.80	200.0		31.10
13	10	3.000	1.00	4.30	300.0		10.57
14	10	0.250	1.00	1.08	400.0		8.68
15	10	0.140	1.00	0.85	504.0		12.56 ✓
14	16	3.000	1.12	2.55	196.6		5.06
13	16	1.000	1.35	3.65	296.6		5.56
12	16	0.300	1.83	4.80	392.8		4.37
11	16	0.300	1.25	3.90	492.8		7.18
10	16	0.280	1.00	3.85	592.9		9.42 ✓
15	17	3.000	1.54	1.80	201.3		9.72
14	17	1.000	2.00	2.65	296.0		11.26
13	17	1.000	1.30	3.80	396.0		12.82
12	17	0.300	2.09	4.80	489.0		10.04
11	17	0.300	1.86	3.95	589.1		18.67
10	17	0.300	1.48	3.95	689.1		23.57 ✓
15	18	1.000	1.63	1.80	301.3		13.86 ✓

Tx	Rc					n		
14	18	0.300	3.78	2.70	396.0	4	15.42	
13	18	0.300	2.90	3.90	496.0		16.51	
12	18	0.300	1.73	4.80	589.1		14.33	
11	18	0.300	1.71	4.00	689.1		26.94	
10	18	0.300	1.32	4.00	789.1	8	31.04	
15	19	0.300	2.06	1.80	401.4	4	13.26	
14	19	0.300	2.00	2.70	496.0		16.29	
13	19	0.300	1.86	3.95	596.0		18.23	
12	19	0.300	1.10	4.80	689.1		14.47	
11	19	0.300	1.13	3.95	789.1		26.95	
10	19	0.300	1.00	3.95	889.2	9	33.97	
15	20	0.300	1.00	1.80	501.4	5	12.97	
14	20	0.300	1.00	2.60	596.0		14.83	
13	20	0.300	1.10	3.95	696.0		17.25	
12	20	0.180	1.00	4.80	789.1		11.79	
11	20	0.200	1.00	4.00	889.2		22.39	
10	20	0.200	1.00	3.95	989.2	10	31.12	✓
15	21	0.140	1.00	1.82	601.4	6	10.54	
14	21	0.150	1.00	2.60	696.0		11.89	
13	21	0.175	1.00	4.00	796.0		13.56	
12	21	0.105	1.00	4.80	889.2		9.81	
11	21	0.110	1.00	4.00	989.2	10	16.91	✓
15	22	0.060	1.00	1.80	701.4	7	7.34	
14	22	0.080	1.00	2.60	796.0		9.54	
13	22	0.090	1.00	4.10	896.0		9.74	
12	22	0.050	1.00	4.80	989.2	10	6.41	✓
15	23	0.040	1.00	1.85	801.4	8	7.16	
14	23	0.040	1.00	2.60	896.0		6.83	
13	23	0.040	1.00	4.15	996.0	10	5.89	✓
15	24	0.030	1.00	1.85	901.4	9	7.70	
14	24	0.030	1.00	2.60	996.0	10	7.06	✓
16	7	0.080	1.00	1.75	904.5	9	23.94	
17	7	0.150	1.00	1.75	968.7	10	65.33	✓
16	8	0.080	1.00	1.72	793.3	8	16.76	
17	8	0.130	1.00	1.75	867.7		39.66	
18	8	0.210	1.00	3.20	967.8	10	48.10	
16	9	0.140	1.00	1.72	692.9	7	16.81	
17	9	0.220	1.00	1.75	789.1		39.37	
18	9	0.300	1.34	3.15	889.2		57.02	
19	9	0.300	1.39	4.10	989.2	10	62.45	✓
16	10	0.120	1.00	1.75	592.9	6	8.88	
17	10	0.200	1.00	1.75	689.1		23.96	
18	10	0.300	1.00	3.05	789.1		30.84	
19	10	0.300	1.00	4.10	889.2		32.73	
20	10	0.200	1.00	4.20	989.2	10	29.26	✓
10	12	10.000	3.00	3.80	200.0	2	29.76	✓
10	13	1.000	2.78	3.95	300.0	3	10.47	
11	13	3.000	2.85	3.80	200.0	2	8.50	✓
10	14	0.300	3.64	3.95	400.0	4	10.36	
11	14	1.000	2.00	3.85	300.0		7.78	
12	14	3.000	1.90	4.75	200.0	2	4.53	✓
10	15	0.300	1.85	3.95	504.0	5	10.72	
11	15	0.300	3.03	3.85	404.0		8.95	
12	15	1.000	1.70	4.75	304.0		5.43	
13	15	3.000	1.85	3.50	200.0	2	6.00	✓
16	18	3.000	2.24	1.75	200.0	2	14.48	✓
16	19	1.000	1.45	1.78	300.0	3	12.30	
17	19	3.000	3.33	1.80	200.0	2	20.92	✓
16	20	0.300	2.00	1.73	400.0	4	13.10	
17	20	1.000	2.75	1.80	300.0		23.04	
18	20	10.000	1.54	3.20	200.0	2	18.14	✓
16	21	0.250	1.00	1.75	500.0	5	10.79	
17	21	1.000	1.00	1.80	400.0		20.94	
18	21	3.000	1.30	3.20	300.0		18.38	
19	21	10.000	1.92	4.00	200.0	2	18.10	✓
16	22	0.100	1.00	1.75	600.0	6	7.56	

Tx	Rx						
17	22	0.300	1.20	1.80	500.0	5	15.08
18	22	1.000	1.19	3.20	400.0		14.02
19	22	1.000	4.00	4.05	300.0		14.89
20	22	3.000	3.46	4.20	200.0	2	9.32 ✓
16	23	0.045	1.00	1.75	700.0	7	5.44
17	23	0.150	1.00	1.80	600.0		11.00
18	23	0.300	1.53	3.22	500.0		10.75
19	23	1.000	1.25	4.10	400.0		11.49
20	23	1.000	2.02	4.20	300.0		7.25
21	23	3.000	2.81	3.10	200.0	2	10.25 ✓
16	24	0.030	1.00	1.75	800.0	8	5.44
17	24	0.090	1.00	1.80	700.0		10.56
18	24	0.260	1.00	3.22	600.0		10.65
19	24	0.300	2.22	4.18	500.0		12.01
20	24	0.300	2.90	4.20	400.0		7.81
21	24	1.000	1.94	3.12	300.0	3	9.38 ✓
17	25	0.070	1.00	1.80	800.0	8	12.31
18	25	0.170	1.00	3.22	700.0		11.15
19	25	0.300	1.24	4.20	600.0		11.69
20	25	0.300	1.38	4.20	500.0		7.43
21	25	0.300	2.61	3.23	400.0	4	9.14 ✓
17	26	0.030	1.00	1.82	900.0	9	7.46
18	26	0.100	1.00	3.30	800.0		9.60
19	26	0.200	1.00	4.20	700.0		10.05
20	26	0.230	1.00	4.25	600.0		7.14
21	26	0.300	1.15	3.20	500.0	5	8.13 ✓

LINE 8 ESPERANCE

DIPL	ANG	LENGTH
1	0.	200.0
2	0.	200.0
3	0.	200.0
4	0.	200.0
5	0.	200.0
6	0.	200.0
7	0.	200.0
8	0.	200.0
9	0.	200.0
10	0.	200.0
11	0.	200.0
12	0.	200.0

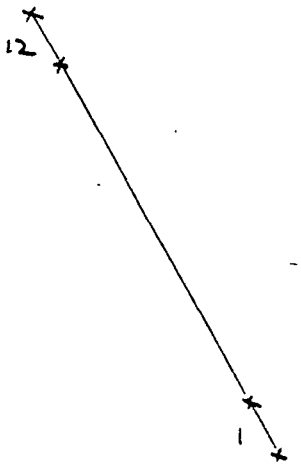

TX	RX	RANGE	MULT	I	DEPTH	RES
3	1	100.000	1.32	2.38	200.0	209.09
4	1	10.000	1.16	1.97	300.0	88.79
5	1	1.000	2.68	2.20	400.0	45.92
6	1	1.000	1.32	2.78	500.0	35.80
4	2	100.000	1.75	1.97	200.0	334.89
5	2	10.000	1.58	2.24	300.0	106.37
6	2	3.000	1.65	2.78	400.0	67.13
5	3	30.000	2.86	2.23	200.0	145.05
6	3	10.000	1.53	2.76	300.0	83.59
6	4	100.000	1.35	2.83	200.0	179.84
5	7	30.000	3.80	2.24	200.0	191.86
4	7	3.000	3.41	1.98	300.0	77.91
3	7	1.000	2.41	2.36	400.0	38.50
2	7	1.000	1.42	3.00	500.0	35.69
6	8	100.000	1.70	2.78	200.0	230.53
5	8	10.000	1.60	2.23	300.0	108.19
4	8	1.000	2.41	1.95	400.0	46.59
3	8	0.300	2.92	2.36	500.0	27.99
2	8	0.300	2.21	3.00	600.0	29.16
6	9	10.000	1.18	2.77	300.0	64.24
5	9	1.000	2.11	2.23	400.0	35.67
4	9	0.300	1.53	2.00	500.0	17.30
3	9	0.220	1.00	2.39	600.0	12.70
2	9	0.220	1.00	3.00	700.0	15.48
6	10	3.000	1.89	2.80	400.0	76.34
5	10	1.000	1.56	2.25	500.0	52.28
4	10	0.300	1.41	2.00	600.0	27.91
3	10	0.280	1.00	2.40	700.0	24.63
2	10	0.300	1.00	3.00	800.0	31.67
6	11	1.000	1.73	2.83	500.0	46.09
5	11	0.300	1.80	2.28	600.0	31.25
4	11	0.190	1.00	2.00	700.0	20.06
3	11	0.140	1.00	2.40	800.0	18.47
2	11	0.160	1.00	3.00	900.0	24.13
6	12	0.300	2.04	2.82	600.0	23.64
5	12	0.240	1.00	2.28	700.0	22.22
4	12	0.110	1.00	1.98	800.0	17.59
3	12	0.100	1.00	2.39	900.0	18.93
2	12	0.140	1.00	3.02	1000.0	28.84 ✓
7	1	0.300	1.00	1.92	600.0	20.62
8	1	0.170	1.00	1.98	700.0	18.13
9	1	0.060	1.00	2.04	800.0	9.31
10	1	0.050	1.00	1.29	900.0	17.53
11	1	0.050	1.00	1.66	1000.0	18.74
7	9	100.000	1.54	2.07	200.0	230.47 ✓

8	10	100.000	3.29	1.91	200.0	649.37
7	10	10.000	2.95	2.07	300.0	214.90
9	11	30.000	2.28	2.20	200.0	117.21
8	11	10.000	1.40	1.95	300.0	108.26
7	11	3.000	1.15	2.07	400.0	62.83
10	12	10.000	1.82	1.42	200.0	48.32
9	12	3.000	1.26	2.20	300.0	25.91
8	12	1.000	2.32	1.95	400.0	44.85
7	12	0.300	2.80	2.08	500.0	30.45
7	2	0.300	3.18	1.92	500.0	37.46
8	2	0.300	1.40	1.92	600.0	28.86
9	2	0.160	1.00	2.15	700.0	15.71
10	2	0.130	1.00	1.42	800.0	28.99
11	2	0.090	1.00	1.73	900.0	23.53

LINE 9 COUBARIL-SPRINGS-BELLE PLAINE-MOTET

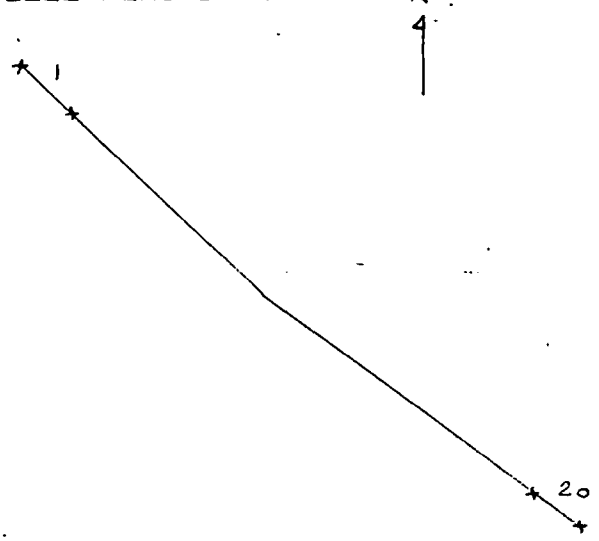

DIPL	ANG	LENGTH
1	138.	200. 0
2	138.	200. 0
3	138.	200. 0
4	138.	200. 0
5	138.	200. 0
6	138.	200. 0
7	138.	200. 0.
8	138.	200. 0
9	138.	200. 0
10	138.	200. 0
11	132.	200. 0
12	132.	200. 0
13	132.	200. 0
14	132.	200. 0
15	132.	200. 0
16	132.	200. 0
17	132.	200. 0
18	132.	200. 0
19	132.	200. 0
20	132.	200. 0

TX	RX	RANGE	MULT	I	DEPTH (m)	n (SEG)	RES
4	1	3. 000	2. 61	5. 25	300. 0	2	22. 49
5	1	1. 000	3. 28	4. 30	400. 0	3	28. 76
6	1	0. 300	3. 10	3. 85	500. 0	4	18. 21
7	1	0. 300	1. 30	3. 75	600. 0	5	13. 72
8	1	0. 230	1. 00	4. 20	700. 0	6	11. 56
4	2	10. 000	3. 17	5. 20	200. 0	1	22. 98
5	2	3. 000	3. 22	4. 25	300. 0	2	34. 28
6	2	1. 000	2. 26	3. 82	400. 0	3	22. 30
7	2	0. 300	2. 70	3. 75	500. 0	4	16. 29
8	2	0. 300	1. 51	4. 21	600. 0	5	14. 20
5	3	10. 000	3. 87	4. 20	200. 0	1	34. 74
6	3	3. 000	1. 98	3. 80	300. 0	2	23. 57
7	3	1. 000	1. 73	3. 75	400. 0	3	17. 39
8	3	0. 300	2. 74	4. 21	500. 0	4	14. 72
6	4	10. 000	2. 06	3. 80	200. 0	1	20. 44
7	4	3. 000	1. 39	3. 75	300. 0	2	16. 77
8	4	1. 000	1. 54	4. 21	400. 0	3	13. 79
7	5	10. 000	1. 66	3. 67	200. 0	1	17. 05
8	5	3. 000	1. 20	4. 21	300. 0	2	12. 89
8	6	10. 000	1. 63	4. 21	200. 0	1	14. 60
7	9	3. 000	1. 43	3. 75	200. 0	1	4. 31
6	9	1. 000	1. 38	3. 81	300. 0	2	5. 46
5	9	0. 300	2. 26	4. 25	400. 0	3	6. 01
4	9	0. 300	1. 84	5. 20	500. 0	4	8. 00
8	10	3. 000	3. 40	4. 21	200. 0	1	9. 13
7	10	1. 000	1. 98	3. 75	300. 0	2	7. 96
6	10	1. 000	1. 15	3. 81	400. 0	3	11. 38
5	10	0. 300	2. 60	4. 25	500. 0	4	13. 84
4	10	0. 300	2. 35	5. 20	600. 0	5	17. 89
8	11	1. 000	2. 12	4. 21	300. 0	2	7. 61
7	11	0. 300	2. 58	3. 75	400. 0	3	7. 80
6	11	0. 300	1. 83	3. 81	500. 0	4	10. 90
5	11	0. 300	1. 59	4. 25	600. 0	5	14. 86
4	11	0. 300	1. 48	5. 21	700. 0	6	18. 05
8	12	1. 000	1. 61	4. 22	400. 0	3	14. 35
7	12	0. 300	2. 57	3. 77	500. 0	4	15. 40
6	12	0. 300	2. 14	3. 81	600. 0	5	22. 22

5	12	0.300	2.16	4.25	700.0	6	32.19
4	12	0.300	2.25	5.20	800.0	7	41.13
8	13	1.000	1.30	4.25	500.0	4	23.00
7	13	0.300	2.28	3.75	600.0	5	24.01
6	13	0.300	2.13	3.80	700.0	6	35.43
5	13	0.300	2.14	4.15	800.0	7	48.91
4	13	0.300	2.15	5.20	900.0	8	56.05
8	14	0.300	2.18	4.25	600.0	5	20.25
7	14	0.300	1.30	3.75	700.0	6	21.90
6	14	0.300	1.19	3.80	800.0	7	29.67
5	14	0.300	1.35	4.21	900.0	8	43.42
4	14	0.300	1.50	5.20	1000.0	9	53.72
8	15	0.240	1.00	4.25	700.0	6	11.90
7	15	0.160	1.00	3.75	800.0	7	13.48
6	15	0.150	1.00	3.81	900.0	8	17.76
5	15	0.180	1.00	4.22	1000.0	9	26.46
8	16	0.140	1.00	4.25	800.0	7	10.42
7	16	0.100	1.00	3.75	900.0	8	12.04
6	16	0.100	1.00	3.81	1000.0	9	16.28
8	17	0.080	1.00	4.25	900.0	8	8.51
7	17	0.060	1.00	3.62	1000.0	9	10.29
17	20	3.000	3.15	3.22	300.0	2	44.26
16	20	3.000	1.42	3.45	400.0	3	46.55
15	20	1.000	1.33	4.45	500.0	4	22.53
14	20	0.300	2.43	4.80	600.0	5	20.04
13	20	0.130	1.00	2.00	700.0	6	13.72
17	19	100.000	2.18	3.20	200.0	1	256.82
16	19	30.000	2.42	3.42	300.0	2	320.11
15	19	10.000	1.44	4.43	400.0	3	122.54
14	19	3.000	1.63	4.80	500.0	4	76.81
13	19	0.300	1.33	2.00	600.0	5	26.32
16	18	1000.002	1.08	3.40	200.0	1	1197.50
15	18	100.000	1.33	4.41	300.0	2	454.78
14	18	30.000	1.05	4.80	400.0	3	247.40
13	18	1.000	1.71	2.01	500.0	4	64.14
15	17	300.000	1.96	4.45	200.0	1	498.14
14	17	100.000	1.00	4.81	300.0	2	313.51
13	17	1.000	4.02	2.00	400.0	3	75.77
14	16	300.000	2.72	4.80	200.0	1	640.88
13	16	10.000	1.36	2.00	300.0	2	102.54
13	15	30.000	2.54	2.00	200.0	1	143.63
14	12	100.000	3.14	4.80	200.0	1	246.61
15	12	30.000	1.16	4.43	300.0	2	118.46
16	12	3.000	2.45	3.43	400.0	3	80.78
17	12	1.000	1.95	3.21	500.0	4	45.80
13	11	100.000	1.27	2.00	200.0	1	239.39
14	11	30.000	1.13	4.81	300.0	2	106.28
15	11	3.000	1.97	4.43	400.0	3	50.29
16	11	1.000	1.59	3.50	500.0	4	34.25
17	11	0.300	1.48	3.22	600.0	5	18.19
13	10	3.000	3.10	2.01	300.0	2	69.90
14	10	3.000	1.96	4.80	400.0	3	46.29
15	10	1.000	1.41	4.45	500.0	4	23.96
16	10	0.300	1.61	3.50	600.0	5	18.27
17	10	0.140	1.00	3.23	700.0	6	9.18
13	9	1.000	1.22	2.01	400.0	3	22.83
14	9	0.300	3.73	4.80	500.0	4	17.55
15	9	0.300	1.00	4.45	600.0	5	8.89
16	9	0.110	1.00	3.47	700.0	6	6.69
17	9	[illegible]	[illegible]	[illegible]	[illegible]	7	4.50

9	2	0.160	1.00	3.82	700.0	6	8.84
10	2	0.190	1.00	3.02	800.0	7	19.92
11	2	0.130	1.00	2.90	900.0	8	20.36
12	2	0.130	1.00	2.00	1000.0	9	40.49
9	3	0.230	1.00	3.85	600.0	5	7.88
10	3	0.250	1.00	3.03	700.0	6	17.42
11	3	0.160	1.00	2.90	800.0	7	17.53
12	3	0.150	1.00	2.00	900.0	8	33.96
12	20	0.090	1.00	2.00	800.0	7	14.25
11	20	0.050	1.00	3.00	900.0	8	7.54
10	20	0.060	1.00	3.10	1000.0	9	12.09
12	19	0.200	1.00	2.00	700.0	6	21.11
11	19	0.100	1.00	3.00	800.0	7	10.56
10	19	0.060	1.00	3.10	900.0	8	8.79
9	19	0.040	1.00	3.90	1000.0	9	6.39
12	18	0.300	1.92	1.85	600.0	5	41.08
11	18	0.240	1.00	3.00	700.0	6	18.30
10	18	0.120	1.00	3.10	800.0	7	12.30

LINE 9 EXTENSION

DIPL	ANG	LENGTH
1	138.	200. 0
2	138.	200. 0
3	138.	200. 0
4	138.	200. 0
5	138.	200. 0
6	138.	200. 0
7	138.	200. 0
8	138.	200. 0
9	138.	200. 0
10	138.	200. 0
11	132.	200. 0
12	132.	200. 0
13	132.	200. 0
14	132.	200. 0
15	132.	200. 0
16	132.	200. 0
17	132.	200. 0
18	132.	200. 0
19	145.	200. 0
20	145.	200. 0
21	145.	200. 0
22	145.	200. 0
23	145.	200. 0
24	145.	300. 0
25	145.	200. 0
26	145.	200. 0
27	145.	200. 0
28	145.	200. 0
29	145.	200. 0
30	145.	200. 0
31	145.	200. 0

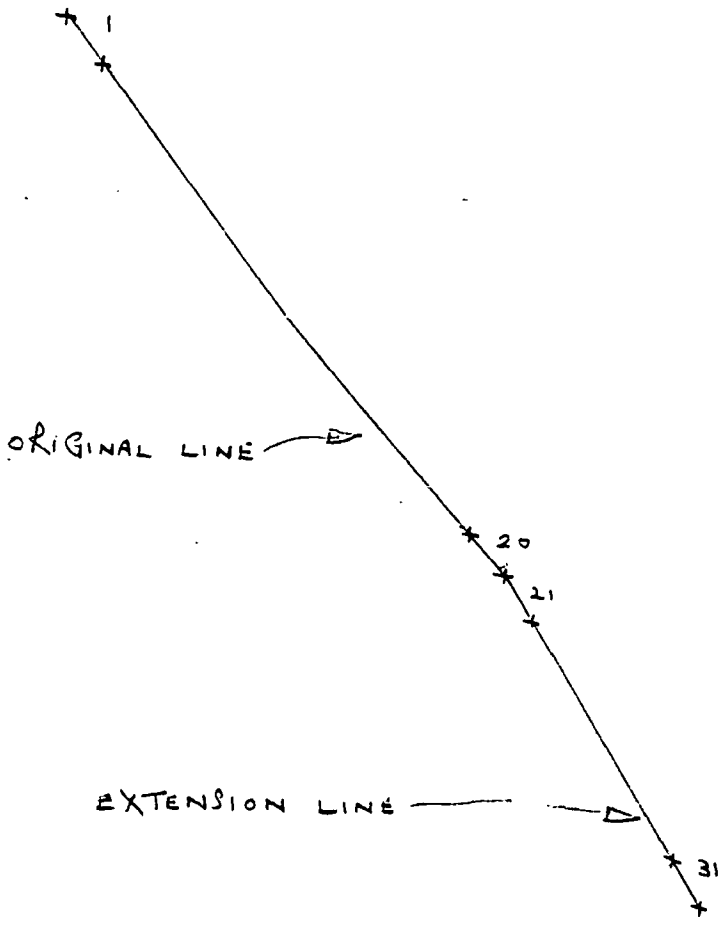

TX	RX	RANGE	MULT	I	DEPTH	N (SEG)	RES
26	24	30. 000	2. 06	4. 70	225. 0	1	42. 84
25	23	10. 000	1. 55	4. 10	250. 0	1	31. 18
26	23	3. 000	2. 18	4. 65	350. 0	2	34. 80
24	22	30. 000	2. 85	4. 55	225. 0	1	61. 22
25	22	3. 000	2. 36	4. 10	350. 0	2	42. 72
26	22	1. 000	3. 61	4. 65	450. 0	3	42. 25
23	21	10. 000	3. 90	6. 30	200. 0	1	23. 34
24	21	3. 000	3. 15	4. 55	325. 0	2	25. 30
25	21	1. 000	1. 55	4. 05	450. 0	3	20. 83
26	21	0. 300	3. 08	4. 65	550. 0	4	20. 09
22	20	100. 000	2. 45	6. 44	200. 0	1	143. 42
23	20	10. 000	1. 04	6. 30	300. 0	2	24. 89
24	20	3. 000	1. 40	4. 55	425. 0	3	27. 02
25	20	0. 300	2. 84	4. 07	550. 0	4	21. 16
26	20	0. 300	1. 80	4. 65	650. 0	5	19. 56
21	19	30. 000	3. 39	6. 60	200. 0	1	58. 09
22	19	10. 000	1. 00	6. 45	300. 0	2	23. 38
23	19	1. 000	1. 92	6. 25	400. 0	3	11. 58
24	19	0. 300	3. 91	4. 55	525. 0	4	14. 71
25	19	0. 300	1. 00	4. 05	650. 0	5	12. 48
26	19	0. 230	1. 00	4. 60	750. 0	6	13. 02
21	18	3. 000	2. 68	6. 60	300. 0	1	18. 53
22	18	1. 000	2. 80	6. 55	400. 0	3	16. 30
23	18	0. 300	2. 93	6. 25	500. 0	4	10. 73
24	18	0. 300	2. 31	4. 53	625. 0	5	15. 07
25	18	0. 160	1. 00	4. 05	750. 0	6	10. 44

Tx	Rc					n (SEG)	
26	18	0.130	1.00	4.60	850.0	7	10.95
21	17	1.000	2.46	6.60	400.0	3	13.91
22	17	0.300	3.26	6.55	500.0	4	11.19
23	17	0.300	1.12	6.35	600.0	5	6.96
24	17	0.240	1.00	4.55	725.0	6	8.17
25	17	0.080	1.00	4.05	850.0	7	7.55
26	17	0.055	1.00	4.60	950.0	8	6.41
21	16	1.000	1.40	6.60	500.0	4	15.79
22	16	0.300	2.30	6.55	600.0	5	13.74
23	16	0.260	1.00	6.35	700.0	6	8.56
24	16	0.200	1.00	4.55	825.0	7	10.02
25	16	0.070	1.00	4.05	950.0	8	9.17
26	16	0.045	1.00	4.60	1050.0	9	7.04
21	15	0.300	1.77	6.80	600.0	5	10.18
22	15	0.300	1.11	6.55	700.0	6	10.60
23	15	0.130	1.00	6.05	800.0	7	6.72
24	15	0.110	1.00	4.40	925.0	8	8.05
25	15	0.060	1.00	4.00	1050.0	9	10.72
21	14	0.300	1.35	6.75	700.0	6	12.55
22	14	0.280	1.00	6.55	800.0	7	13.37
23	14	0.140	1.00	6.05	900.0	8	10.33
24	14	0.120	1.00	4.40	1025.0	9	11.96
21	13	0.220	1.00	6.80	800.0	7	10.17
22	13	0.180	1.00	6.55	900.0	8	12.30
23	13	0.080	1.00	6.05	1000.0	9	8.12
21	12	0.120	1.00	6.78	900.0	8	7.97
22	12	0.100	1.00	6.55	1000.0	9	9.41
21	11	0.060	1.00	6.75	1000.0	9	5.51
25	27	30.000	3.05	4.20	200.0	1	82.13
24	27	10.000	1.60	4.20	325.0	2	46.40
23	27	1.000	3.25	6.15	430.0	3	28.76
22	27	1.000	2.15	6.25	550.0	4	34.77
21	27	0.300	1.92	6.20	650.0	5	15.65
26	28	30.000	2.78	4.55	200.0	1	69.10
25	28	30.000	1.07	4.00	300.0	2	121.01
24	28	3.000	2.60	4.20	425.0	3	54.36
23	28	1.000	1.96	6.15	550.0	4	32.21
22	28	1.000	1.39	6.25	650.0	5	37.47
21	28	0.300	1.38	6.20	750.0	6	17.39
26	29	30.000	2.14	4.55	300.0	2	212.77
25	29	3.000	2.98	4.00	400.0	3	84.26
24	29	1.000	2.56	4.20	525.0	4	34.77
23	29	0.300	2.60	6.15	650.0	5	21.37
22	29	0.300	1.80	6.25	750.0	6	22.50
26	30	3.000	2.68	4.20	400.0	3	72.17
25	30	1.000	1.52	4.00	500.0	4	28.65
24	30	0.300	2.10	4.20	625.0	5	14.70
23	30	0.200	1.00	5.70	750.0	6	9.14
22	30	0.170	1.00	6.25	850.0	7	10.35
21	30	0.075	1.00	6.20	950.0	8	6.44
26	31	1.000	2.20	4.20	500.0	4	39.49
25	31	0.300	2.01	4.00	600.0	5	19.89
24	31	0.300	1.10	4.20	725.0	6	12.15
23	31	0.140	1.00	5.70	850.0	7	9.35
22	31	0.110	1.00	6.25	950.0	8	9.38
21	31	0.070	1.00	6.20	1050.0	9	8.14

LINE 10 BELLE PLAINE-VICTORIA JUNCTION

DIPL	ANG	LENGTH
1	205.	200. 0
2	205.	200. 0
3	205.	200. 0
4	205.	200. 0
5	205.	200. 0
6	205.	200. 0
7	205.	200. 0
8	213.	200. 0
9	219.	200. 0
10	228.	200. 0
11	228.	200. 0

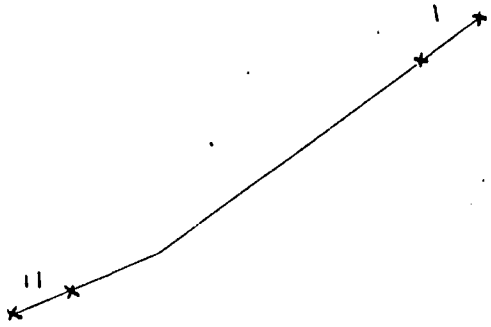

TX	RX	RANGE	MULT	I	DEPTH	RES
3	1	30. 000	3. 10	2. 20	200. 0	159. 36
4	1	3. 000	2. 60	2. 37	300. 0	49. 63
5	1	1. 000	1. 91	2. 80	400. 0	25. 72
6	1	0. 300	2. 62	3. 40	500. 0	17. 43
4	2	30. 000	2. 13	2. 37	200. 0	101. 64
5	2	3. 000	2. 43	2. 80	300. 0	39. 26
6	2	1. 000	1. 88	3. 42	400. 0	20. 72
5	3	100. 000	1. 43	2. 81	200. 0	191. 85
6	3	10. 000	1. 68	3. 42	300. 0	74. 08
6	4	100. 000	1. 34	3. 42	200. 0	147. 71
3	5	30. 000	3. 76	2. 20	200. 0	193. 29
3	6	3. 000	3. 73	2. 20	300. 0	76. 70
4	6	30. 000	3. 17	2. 37	200. 0	151. 27
3	7	1. 000	1. 25	2. 10	400. 0	22. 44
4	7	3. 000	2. 13	2. 35	300. 0	41. 00
5	7	30. 000	3. 09	2. 80	200. 0	124. 81
3	8	0. 300	1. 42	2. 20	500. 0	14. 68
4	8	1. 000	1. 20	2. 37	400. 0	19. 17
5	8	3. 000	1. 75	2. 80	300. 0	28. 36
6	8	10. 000	2. 80	3. 40	200. 0	31. 09
3	9	0. 200	1. 00	2. 20	600. 7	12. 10
4	9	0. 300	1. 56	2. 37	500. 7	14. 97
5	9	1. 000	1. 63	2. 81	400. 7	21. 91
6	9	3. 000	2. 00	3. 42	300. 7	26. 41
3	10	0. 100	1. 00	2. 20	703. 9	9. 78
4	10	0. 240	1. 00	2. 37	603. 8	13. 54
5	10	0. 300	2. 44	2. 81	503. 8	19. 76
6	10	1. 000	2. 14	3. 42	403. 8	23. 59
3	11	0. 060	1. 00	2. 20	803. 8	8. 57
4	11	0. 110	1. 00	2. 37	703. 7	9. 68
5	11	0. 300	1. 27	2. 81	603. 7	17. 60
6	11	0. 300	3. 10	3. 42	503. 7	20. 17
7	1	0. 200	1. 00	2. 80	600. 0	9. 42
8	1	0. 150	1. 00	3. 60	700. 0	8. 85
9	1	0. 120	1. 00	3. 43	800. 8	11. 22
7	2	0. 300	1. 20	2. 80	500. 0	9. 69
8	2	0. 220	1. 00	3. 60	600. 0	8. 11
9	2	0. 140	1. 00	3. 43	700. 8	8. 71
7	3	1. 000	1. 65	2. 80	400. 0	22. 22
8	3	0. 300	2. 25	3. 60	500. 0	14. 21
9	3	0. 300	1. 10	3. 43	600. 7	12. 80
7	4	3. 000	2. 60	2. 80	300. 0	42. 01
8	4	1. 000	1. 72	3. 62	400. 0	17. 99
9	4	0. 300	2. 22	3. 45	500. 7	14. 64
7	5	30. 000	3. 06	2. 80	200. 0	123. 60
8	5	3. 000	2. 74	3. 60	300. 0	29. 24

9	5	1.000	2.12	3.45	400.7	23.21
8	6	10.000	3.04	3.61	200.0	31.79
9	6	3.000	2.00	3.47	300.7	26.03
9	7	30.000	2.37	3.45	200.7	77.75
7	9	30.000	1.85	2.80	200.7	74.78
7	10	3.000	3.20	2.82	303.7	51.47
8	10	30.000	2.58	3.61	200.8	80.90
7	11	1.000	3.33	2.81	403.8	44.55
8	11	10.000	1.51	3.61	300.8	62.89
9	11	30.000	4.00	3.46	200.0	131.00
9	1	0.140	1.00	4.80	800.8	9.35
10	1	0.100	1.00	5.10	903.9	9.14
11	1	0.100	1.00	5.60	1003.9	11.15
9	2	0.180	1.00	4.80	700.8	8.00
10	2	0.100	1.00	5.05	803.9	6.43
11	2	0.090	1.00	5.60	903.8	7.24
9	3	0.300	1.54	4.78	600.7	12.86
10	3	0.280	1.00	5.05	703.9	11.94
11	3	0.180	1.00	5.60	803.8	10.11

LINE 11 GRID PTTON-DELLER

DIPL	ANG	LENGTH
1	177.	200. 0
2	177.	200. 0
3	177.	200. 0
4	177.	200. 0
5	174.	200. 0
6	174.	200. 0
7	170.	200. 0
8	170.	200. 0
9	178.	200. 0
10	178.	200. 0
11	178.	200. 0
12	178.	200. 0
13	178.	200. 0

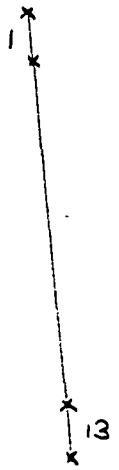

TX	RX	RANGE	MULT	I	DEPTH	RES
6	13	0. 300	2. 46	5. 55	699. 0	27. 93
5	13	0. 300	1. 50	6. 00	799. 0	23. 65
4	13	0. 240	1. 00	6. 60	897. 9	16. 41
3	13	0. 080	1. 00	4. 85	997. 9	10. 24
6	12	1. 000	1. 40	5. 55	599. 0	33. 11
5	12	0. 300	2. 45	5. 95	699. 0	25. 97
4	12	0. 300	1. 42	6. 60	797. 9	20. 40
3	12	0. 160	1. 00	4. 80	897. 9	15. 05
2	12	0. 060	1. 00	4. 40	997. 9	8. 46
6	11	1. 000	2. 03	5. 42	499. 0	28. 11
5	11	1. 000	1. 27	5. 92	599. 0	28. 21
4	11	0. 300	2. 64	6. 55	697. 9	25. 51
3	11	0. 240	1. 00	4. 80	797. 9	15. 82
2	11	0. 100	1. 00	4. 40	897. 9	10. 27
1	11	0. 010	1. 00	5. 05	997. 9	1. 23
6	10	3. 000	1. 00	5. 40	399. 0	20. 89
5	10	1. 000	1. 50	5. 85	499. 0	19. 30
4	10	0. 300	2. 85	6. 50	597. 9	17. 38
3	10	0. 240	1. 00	4. 80	697. 9	10. 56
2	10	0. 100	1. 00	4. 40	797. 9	7. 19
1	10	0. 010	1. 00	5. 00	897. 9	0. 90
6	9	10. 000	1. 58	5. 45	299. 0	43. 97
5	9	3. 000	1. 98	5. 85	399. 0	38. 42
4	9	1. 000	3. 12	6. 40	497. 9	36. 98
3	9	0. 300	2. 85	4. 80	597. 9	23. 57
2	9	0. 300	1. 18	4. 40	697. 9	17. 00
1	9	0. 050	1. 00	5. 05	797. 9	3. 14
6	8	30. 000	3. 14	5. 42	200. 0	65. 55
5	8	10. 000	1. 97	5. 90	300. 0	50. 29
4	8	3. 000	3. 17	6. 45	400. 4	55. 56
3	8	1. 000	2. 60	4. 80	500. 4	40. 79
2	8	0. 300	3. 40	4. 40	600. 4	30. 55
1	8	0. 180	1. 00	5. 03	700. 4	7. 55
5	7	30. 000	1. 77	5. 87	200. 0	34. 12
4	7	10. 000	1. 67	6. 55	300. 4	38. 47
3	7	3. 000	1. 24	4. 85	400. 4	28. 93
2	7	1. 000	1. 25	4. 42	500. 4	21. 35
1	7	0. 180	1. 00	5. 10	600. 4	4. 66
4	6	30. 000	2. 63	6. 55	200. 0	45. 42
3	6	10. 000	1. 05	4. 85	300. 0	32. 63
2	6	1. 000	3. 13	4. 41	400. 0	26. 74
1	6	0. 300	1. 30	5. 15	500. 0	5. 71
3	5	30. 000	1. 51	4. 82	200. 0	35. 44
2	5	3. 000	2. 91	4. 41	300. 0	39. 86

1	5	0.300	2.82	5.14	400.0	6.21
2	4	30.000	2.76	4.41	200.0	70.78
1	4	3.000	1.62	5.12	300.0	14.31
1	3	10.000	2.26	5.10	200.0	16.71

LINE 12 VICTORIA JUNCTION-LE RICHE

DIPL	ANG	LENGTH
1	192.	200. 0
2	192.	200. 0
3	192.	200. 0
4	192.	200. 0
5	192.	200. 0
6	192.	200. 0
7	171.	200. 0
8	186.	200. 0
9	186.	200. 0
10	186.	200. 0
11	186.	200. 0
12	168.	200. 0
13	193.	200. 0
14	193.	200. 0
15	193.	200. 0
16	193.	200. 0

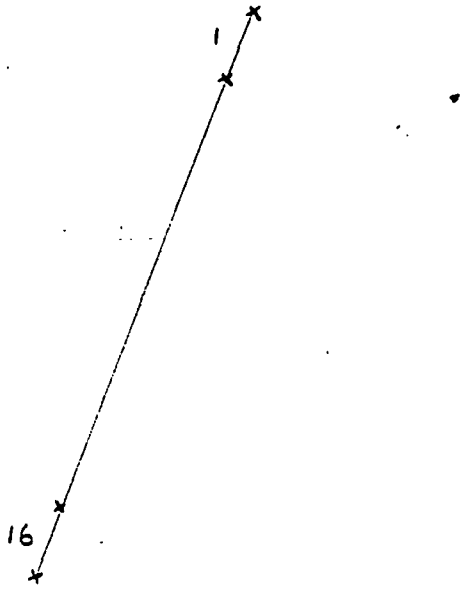

TX	RX	RANGE	MULT	I	DEPTH	RES
1	3	30. 000	1. 55	6. 20	200. 0	28. 27
1	4	10. 000	2. 64	6. 25	300. 0	63. 70
2	4	30. 000	2. 72	7. 60	200. 0	40. 48
1	5	10. 000	3. 78	6. 30	400. 0	226. 19
3	5	30. 000	2. 10	6. 80	200. 0	34. 93
1	6	1. 000	3. 46	6. 30	500. 0	41. 41
2	6	3. 000	1. 69	7. 80	400. 0	24. 50
3	6	10. 000	2. 32	6. 85	300. 0	51. 07
4	6	30. 000	3. 74	5. 00	200. 0	84. 60
1	7	1. 000	2. 69	6. 25	600. 1	59. 15
2	7	1. 000	1. 65	7. 80	500. 1	16. 55
3	7	3. 000	2. 06	6. 83	400. 0	35. 18
4	7	10. 000	2. 50	5. 00	300. 0	77. 12
5	7	100. 000	1. 43	5. 30	200. 0	102. 79
1	8	0. 300	2. 28	6. 40	695. 2	22. 04
2	8	0. 300	1. 56	7. 78	595. 2	7. 73
3	8	1. 000	1. 68	6. 80	495. 2	18. 09
4	8	3. 000	1. 96	5. 00	395. 2	42. 97
5	8	10. 000	2. 29	5. 30	295. 2	63. 39
6	8	30. 000	2. 28	5. 90	195. 2	44. 90
1	9	0. 300	1. 17	6. 22	795. 2	17. 51
2	9	0. 240	1. 00	7. 75	695. 2	6. 40
3	9	0. 300	2. 93	6. 80	595. 2	16. 66
4	9	1. 000	2. 89	4. 95	495. 2	42. 99
5	9	10. 000	1. 22	5. 25	395. 2	85. 88
6	9	30. 000	1. 16	5. 83	295. 2	89. 94
1	10	0. 110	1. 00	6. 22	895. 2	7. 86
2	10	0. 100	1. 00	7. 75	795. 2	4. 01
3	10	0. 270	1. 00	6. 80	695. 2	8. 22
4	10	0. 300	2. 83	5. 00	595. 2	21. 99
5	10	1. 000	3. 30	5. 30	495. 2	46. 24
6	10	3. 000	2. 66	5. 85	395. 2	51. 22
1	11	0. 140	1. 00	6. 22	995. 2	13. 78
2	11	0. 100	1. 00	7. 75	895. 2	5. 74
3	11	0. 300	1. 03	6. 80	795. 2	14. 16
4	11	1. 000	1. 11	4. 98	695. 3	46. 35
5	11	3. 000	1. 60	5. 25	595. 2	119. 21
6	11	10. 000	1. 37	5. 80	495. 2	177. 39
2	12	0. 060	1. 00	7. 75	1007. 7	4. 90
3	12	0. 180	1. 00	6. 80	907. 7	12. 12
4	12	0. 300	2. 01	4. 95	807. 6	29. 26

5	12	1.000	2.92	5.28	707.6	117.18
6	12	3.000	2.98	5.85	607.6	201.86
3	13	0.120	1.00	6.80	981.3	10.91
4	13	0.300	1.20	4 95	881.3	32.85
5	13	1.000	1.74	5.35	781.2	103.59
6	13	3.000	1.75	5.95	681.0	189.79
4	14	0.300	1.00	5.00	981.4	37.03
5	14	1.000	1.40	5.35	881.3	117.96
6	14	3.000	1.40	5.95	781.2	224.39
5	15	1.000	2.75	5.35	981.3	316.75
6	15	3.000	2.93	5.95	881.3	664.90
6	16	10.000	1.15	5.95	981.3	1189.55

LINE 13 GIRUD-LONDONDERRY-SAPHIRE

DIPL	ANG	LENGTH
1	149.	200. 0
2	149.	200. 0
3	175.	200. 0
4	188.	200. 0
5	198.	200. 0
6	198.	200. 0
7	215.	200. 0
8	195.	200. 0
9	185.	200. 0
10	213.	200. 0
11	222.	200. 0
12	208.	200. 0
13	208.	200. 0
14	251.	200. 0
15	210.	200. 0
16	206.	200. 0
17	204.	200. 0
18	221.	200. 0
19	218.	200. 0
20	182.	200. 0

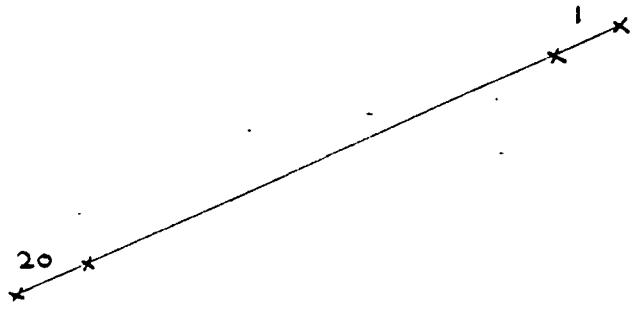

TX	RX	RANGE	MULT	I	DEPTH	RES
8	1	0. 260	1. 00	4. 35	688. 9	12. 06
9	1	0. 210	1. 00	4. 40	745. 2	15. 76
10	1	0. 140	1. 00	4. 18	979. 3	14. 96
11	1	0. 110	1. 00	3. 55	1131. 0	19. 33
8	2	0. 250	1. 00	4. 35	589. 5	8. 79
9	2	0. 200	1. 00	4. 37	638. 8	12. 34
10	2	0. 140	1. 00	4. 18	885. 3	11. 78
11	2	0. 110	1. 00	3. 55	1039. 4	15. 72
12	2	0. 100	1. 00	4. 75	1046. 7	15. 67
8	3	0. 300	2. 00	4. 30	487. 1	10. 82
9	3	0. 300	1. 60	4. 35	567. 6	15. 65
10	3	0. 260	1. 00	4. 20	724. 1	13. 06
11	3	0. 160	1. 00	3. 56	847. 1	14. 36
12	3	0. 140	1. 00	4. 75	901. 9	13. 34
13	3	0. 105	1. 00	5. 20	1002. 1	12. 73
8	4	0. 300	4. 02	4. 30	390. 8	10. 67
9	4	0. 300	2. 50	4. 35	482. 3	13. 44
10	4	0. 300	1. 23	4. 20	604. 3	11. 35
11	4	0. 220	1. 00	3. 57	714. 8	12. 88
12	4	0. 190	1. 00	4. 72	791. 4	12. 25
13	4	0. 140	1. 00	5. 18	891. 4	11. 86
8	5	1. 000	3. 51	4. 25	294. 8	12. 35
9	5	1. 000	1. 61	4. 33	392. 7	14. 03
10	5	0. 300	1. 92	4. 20	493. 1	10. 07
11	5	0. 270	1. 00	3. 58	595. 4	9. 80
12	5	0. 230	1. 00	4. 70	686. 8	9. 70
13	5	0. 170	1. 00	5. 18	786. 8	9. 84
8	6	10. 000	2. 37	4. 22	194. 8	21. 78
9	6	3. 000	1. 99	4. 32	292. 7	20. 79
10	6	1. 000	1. 28	4. 20	393. 1	11. 02
11	6	0. 300	1. 50	3. 58	495. 4	9. 18
12	6	0. 300	1. 25	4. 70	586. 8	9. 82
13	6	0. 250	1. 00	5. 20	686. 8	9. 58
9	7	30. 000	3. 07	4. 32	203. 0	80. 76
10	7	3. 000	2. 52	4. 20	280. 8	29. 62
11	7	1. 000	1. 07	3. 60	373. 8	11. 75
12	7	0. 300	3. 01	4. 70	484. 4	13. 58

13	7	0.300	1.86	5.20	584.4	13.43
10	8	30.000	2.00	4.20	195.7	55.57
11	8	3.000	1.18	3.60	296.8	14.20
12	8	1.000	1.52	4.65	389.4	11.36
13	8	0.300	2.73	5.17	489.4	11.26
11	9	30.000	1.75	3.60	203.8	55.63
12	9	3.000	2.36	4.65	289.7	24.71
13	9	1.000	2.59	5.10	389.8	20.48
12	10	30.000	1.88	4.60	198.1	46.73
13	10	3.000	2.60	5.10	298.1	22.77
13	11	30.000	2.26	5.10	200.0	50.35
12	14	30.000	1.45	4.70	200.1	34.59
11	14	3.000	2.00	3.60	280.5	29.36
10	14	1.000	2.39	4.21	393.0	23.55
9	14	1.000	1.18	4.35	564.7	22.05
8	14	0.300	1.35	4.25	633.5	13.77
13	15	30.000	2.14	5.19	171.9	54.93
12	15	10.000	1.10	4.73	273.8	32.04
11	15	1.000	2.99	3.62	381.5	27.10
10	15	1.000	1.38	4.25	475.1	22.39
9	15	0.300	2.49	4.35	551.7	24.19
8	15	0.300	1.00	4.30	657.9	13.22
13	16	3.000	2.87	5.18	270.8	23.75
12	16	1.000	2.80	4.70	371.4	20.51
11	16	1.000	1.07	3.62	482.2	19.84
10	16	0.300	2.13	4.25	573.2	18.38
9	16	0.300	1.26	4.35	638.1	20.00
8	16	0.170	1.00	4.26	750.0	11.69
13	17	1.000	2.66	5.17	371.5	17.50
12	17	1.000	1.18	4.70	471.6	17.13
11	17	0.300	1.56	3.63	582.2	15.27
10	17	0.300	1.10	4.23	673.3	15.19
9	17	0.200	1.00	4.33	738.9	15.73
8	17	0.100	1.00	4.26	850.1	9.89
13	18	0.300	2.68	5.15	480.3	10.34
12	18	0.300	1.43	4.70	580.3	10.75
11	18	0.180	1.00	3.65	672.2	9.53
10	18	0.140	1.00	4.25	777.3	9.53
9	18	0.110	1.00	4.33	897.8	11.54
8	18	0.075	1.00	4.25	984.1	10.05
13	19	0.300	1.38	5.15	578.0	9.58
12	19	0.250	1.00	4.67	678.0	10.27
11	19	0.140	1.00	3.65	774.3	11.15
10	19	0.110	1.00	4.23	876.1	10.83
9	19	0.080	1.00	4.30	985.1	11.92
13	20	0.180	1.00	5.15	640.7	8.15
12	20	0.130	1.00	4.67	741.2	9.66
11	20	0.080	1.00	3.67	903.2	10.14
10	20	0.060	1.00	4.25	953.3	9.55

scalar versus tensor estimates, theoretical versus observed field patterns over the survey area, and controls on near-field effects using CSAMT and natural field data both inside and outside the caldera.

303
(PB–92-172246/XAB)
In-situ measurement of thermal conductivity using the continuous-heating line-source method and WHOI outrigged probe. Technical report. Jemsek, J.; Von Herzen, R.; Andrew, P. (Woods Hole Oceanographic Institution, MA (United States)). Aug 1985. 77p. (WHOI–85-28). NTIS Prices: PC A05/MF A01.

Sponsored by National Science Foundation, Washington, DC.

The outrigged thermal probes of a 'pogo' marine geothermal probe have been adapted to measure thermal conductivity in-situ by the continuous-heating line source technique. The instrumental uncertainty in applying the analytical theory to a single-probe and double-probe configuration is found to be 3 and 6 percent, respectively. The in-situ outrigged single probe (.32 cm dia.) is essentially a scaled-up version of the needle probe (.08 cm dia.). The main advantage of the outrigged probe over a larger radius probe (e.g., violin-bow probe) is that for short-time temperatures (<2 min.), simple approximations to the exact solution for a perfectly conducting cylindrical probe are achieved. The continuous-heating compares favorably with the pulse-heating technique, the latter being more energy efficient. The continuous-heating method applied to the thin outrigged probe allows for accurate equilibrium in-situ temperature and thermal conductivity estimates in less than 15 minutes of recording time. The technique has been applied to several hundred marine heat flow stations. Comparison of in-situ measurements to needle probe measurements made on nearby piston cores indicate agreement to within 5%.

304
Developing natural convection in a fluid layer with localized heating and large viscosity variation. Hickox, C.E.; Chu, T.Y. pp. 75-82 of General topics in fluids engineering 1991. White, F.M.; Kamemoto, K. New York, NY (United States); American Society of Mechanical Engineers (1991). 148p. (CONF-910684–). Contract AC04-76DP00789.

From 1. American Society of Mechanical Engineers/Japan Society of Mechanical Engineers (ASME/JSME) fluids engineering conference; Portland, OR (United States) (23-26 Jun 1991).

Numerical simulations and laboratory experiments are used to elucidate aspects of transient natural convection in a magma chamber. This paper reports that the magma chamber is modeled as a horizontal fluid layer confined within an enclosure of square platform and heated from below by a strip heater centered on the lower boundary of the enclosure. The width of the strip heater and the depth of the fluid layer are one-fourth of the layer width. Corn syrup is used as the working fluid in order to approximate the large viscosity variation with temperature and the large Prandtl number typical of magma. The quiescent, uniform, fluid layer is subjected to instantaneous heating from the strip heater producing a transient flow which is dominated by two counter-rotating convective cells. Experimentally determine characteristics of the developing flow are compared with numerical simulations carried out with a finite element computer program.

305
Overview of geothermal exploration in Saint Lucia, West Indies. Barthelmy, A. pp. 227-234 of 1990 International Symposium on geothermal energy. Davis, CA (United States); Geothermal Resources Council (1990). 1710p. (CONF-900823–).

From Annual meeting of the Geothermal Resources Council and international symposium on geothermal energy; Kailua Kona, HI (United States) (20-24 Aug 1990).

A recent program of deep exploratory drilling conducted in the Qualibou Caldera in Soufriere, Saint Lucia has provided new but inconclusive information on the geothermal resource. Well SI-1 located in the Belfond area was drilled to a total depth of 7261 ft. This well encountered low permeability and high temperatures, with a maximum of 241°C at total depth. Following this unsuccessful attempt at penetrating the reservoir, the site at Etangs chosen for the location of well No 2 was abandoned and the second well SL-2 was drilled to a total depth of 4636 ft in the sulphur Springs area. SL-2 produced superheated steam with a very high gas content from what is assumed to be a vapor dominated zone overlying in a brine dominated reservoir. This paper reports that a long term flow test of SL-2 is required, specifically planned to investigate the chemistry of the geothermal fluid and to allow a more definite assessment of the well's permeability and drawdown characteristics.

306
Magnetic anomalies of the northern Gulf of California: Structural and thermal interpretations. Sanchez-Zamora, O.; Doguin, P.; Couch, R.W.; Ness, G.E. pp. 377-402 of The gulf and peninsular province of the Californias. Dauphin, J.P.; Simoneit, B.R.T. Tulsa, OK (United States); American Association of Petroleum Geologists (1991). 834p.

Geophysical surveys in the northern Gulf of California in 1981 and 1984 (GOLFO 81, GOLFO 84) provided the magnetic data for this study. The authors analyze the data using frequency domain techniques to determine the depth to the tops and bottoms of magnetic sources. The authors assume that the bottom of the deepest sources represent the Curie-point isotherm. The author's results indicate a shallow magnetic horizon with depths to source tops between 2.3 and 4.1 km below sea level; an intermediate-depth horizon between 3.6 and 6.4 km; and a deep magnetic horizon between 6.7 and 9.5 km. The author's computed depths to the bottom of the magnetized crust yield an average depth of 11.5 km below sea level. Using the individual computed depths to the Curie-point isotherm, and assuming a Curie-point temperature of 580° C, the authors determine an average thermal gradient of 51.8° C/km. Assuming a conductivity of 2.2 W/m° C, the average computed heat flow for the central part of the northern Gulf of California is 114 mW/m^2. This paper presents plots of fault traces which were determined using a deconvolution method based on Werner's simplified thin-dike assumption. The method presented automates the interpretation of magnetic profiles leading to the linearization of complex nonlinear magnetic problems.

307
Well logging results from three geothermal fields in Central America. Dennis, B.; Van Eeckhout, E. pp. 373-378 of 1990 International symposium on geothermal energy. Davis, CA (United States); Geothermal Resources Council (1990). 1710p. (CONF-900823–).

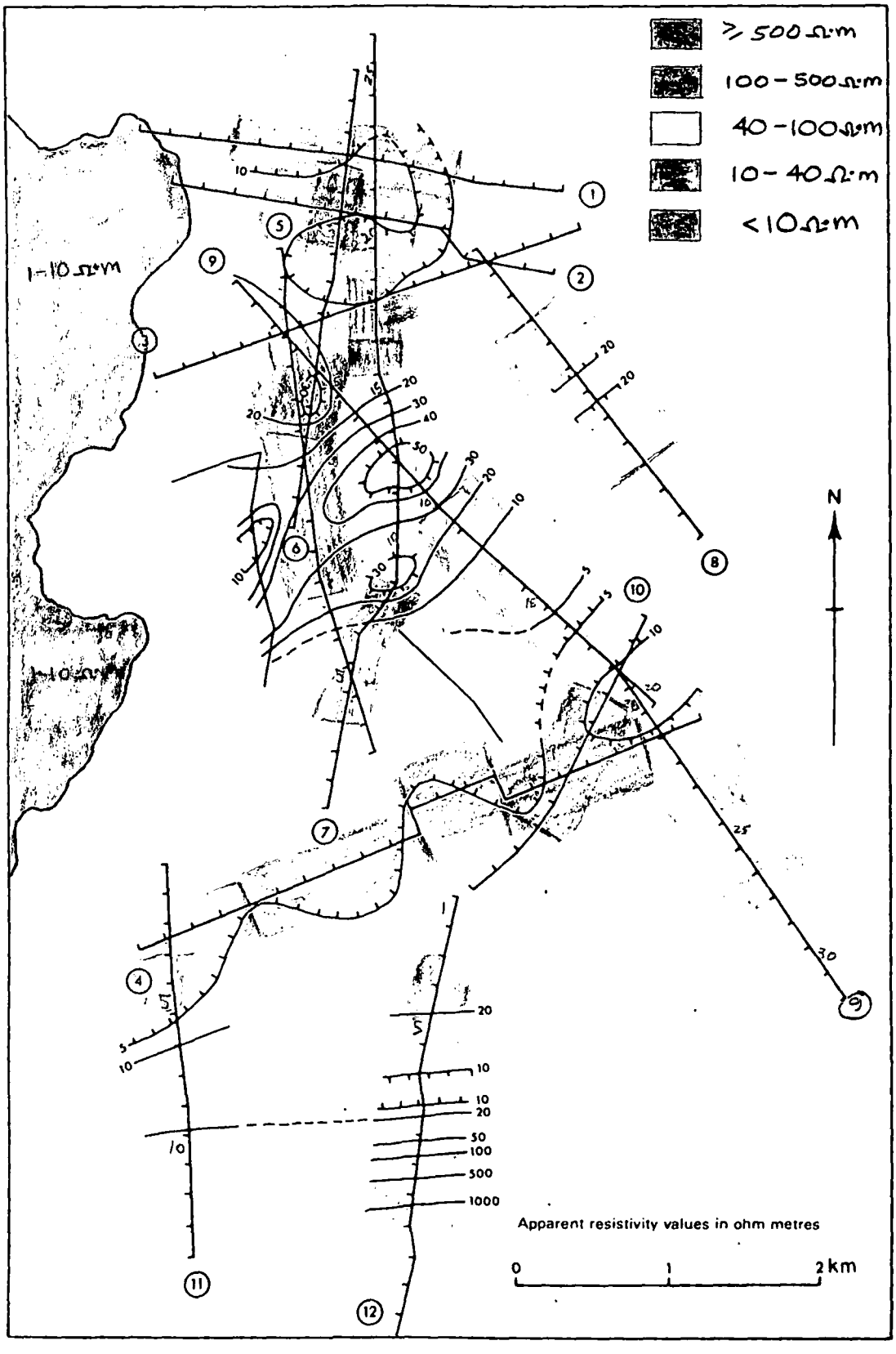

Fig. 5 Soufrière area: Apparent resistivity contours at ~~700m~~ below sea level
Estimated Intrinsic Resistivity, Deep, 1.5-2.5 @ depth 300 – 500 m

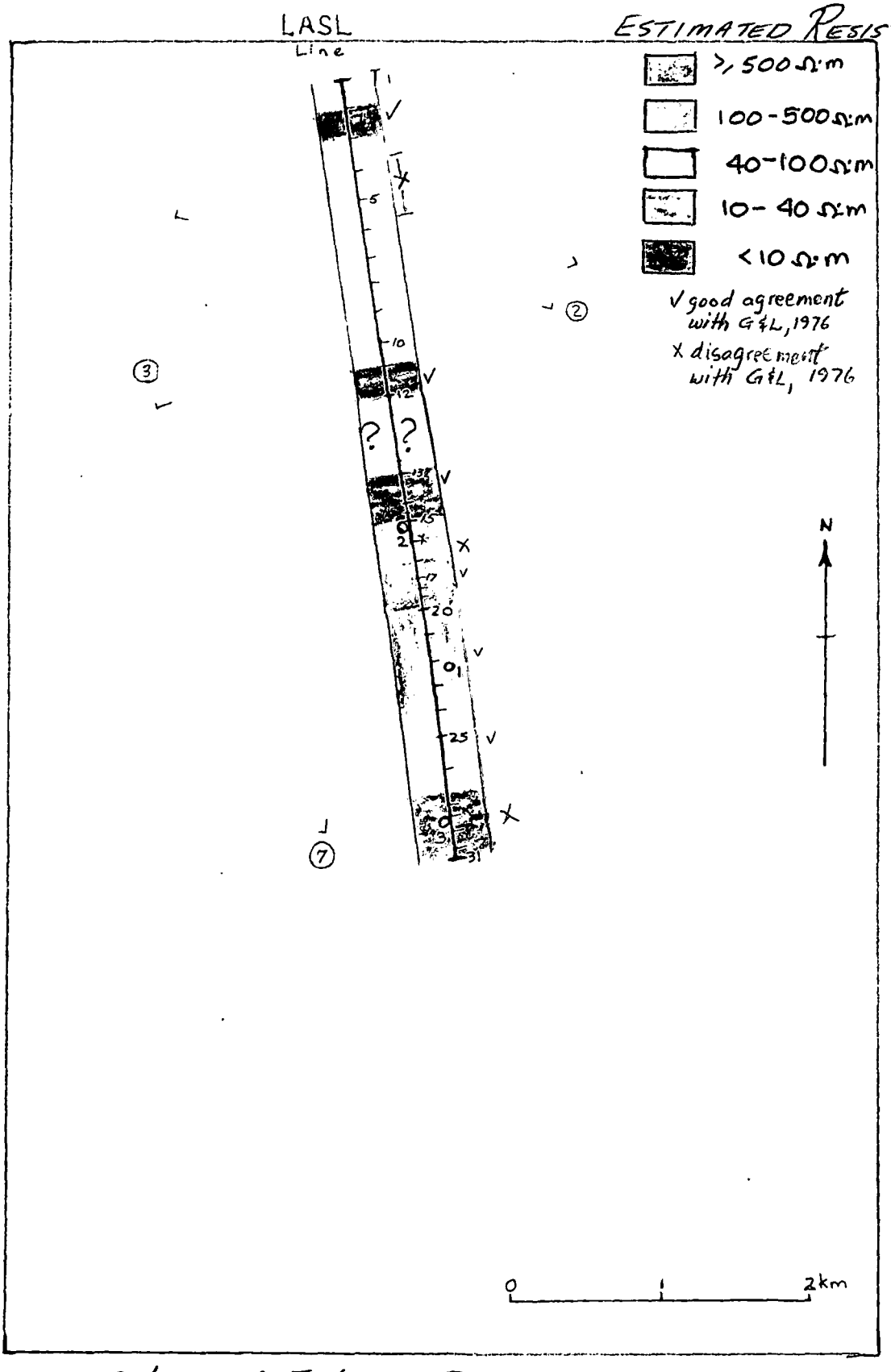

Estimated Intrinsic Resistivity, Shallow
0 - 1a depth
0 - 200m

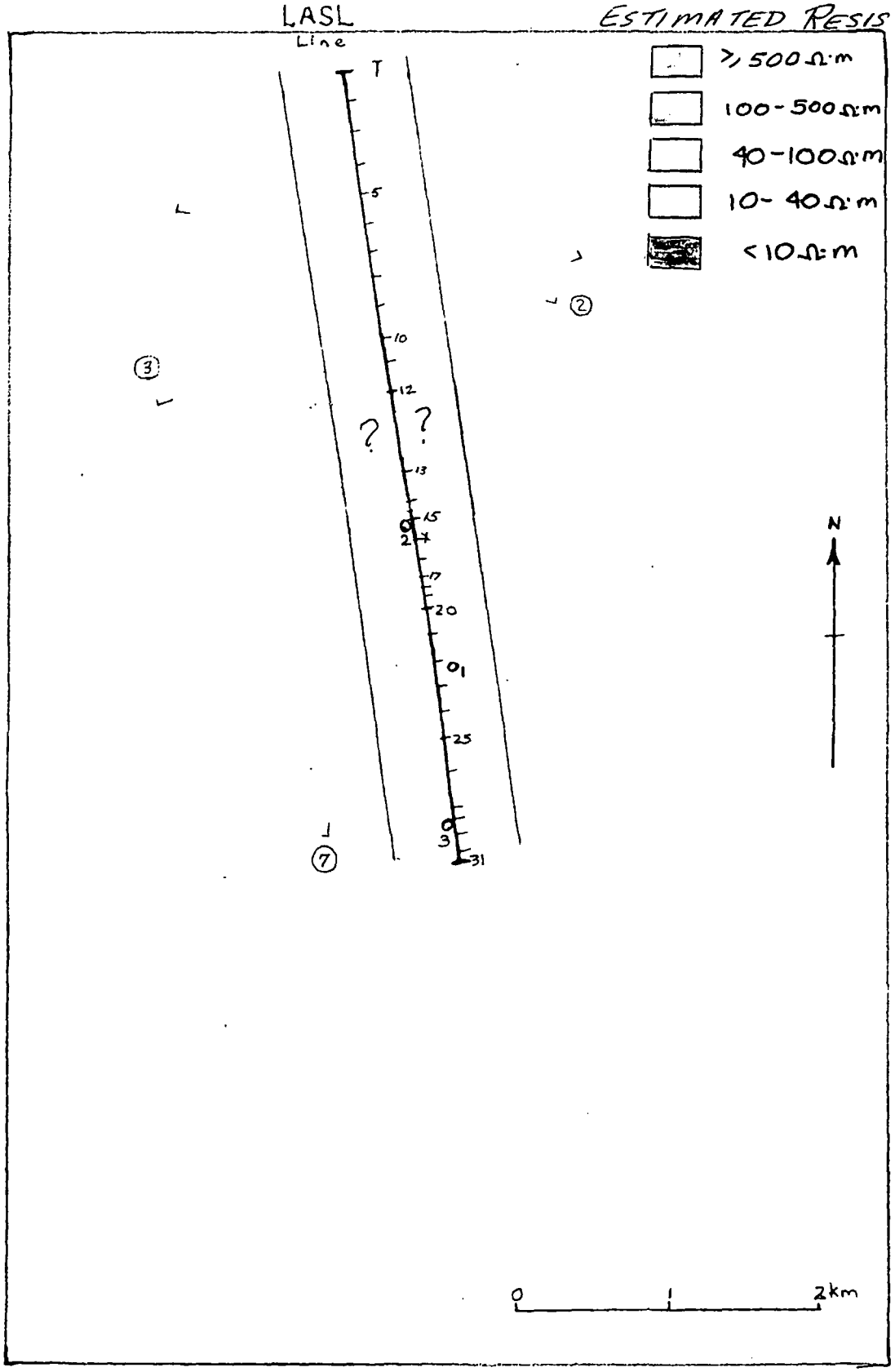

ESTIMATED INTRINSIC RESISTIVITY, Deep

1.5-2.5 a depth

300-500 m

EARTH SCIENCE LABORATORY
UNIVERSITY of UTAH RESEARCH INSTITUTE

DIPOLE - DIPOLE ARRAY
APPARENT RESISTIVITY

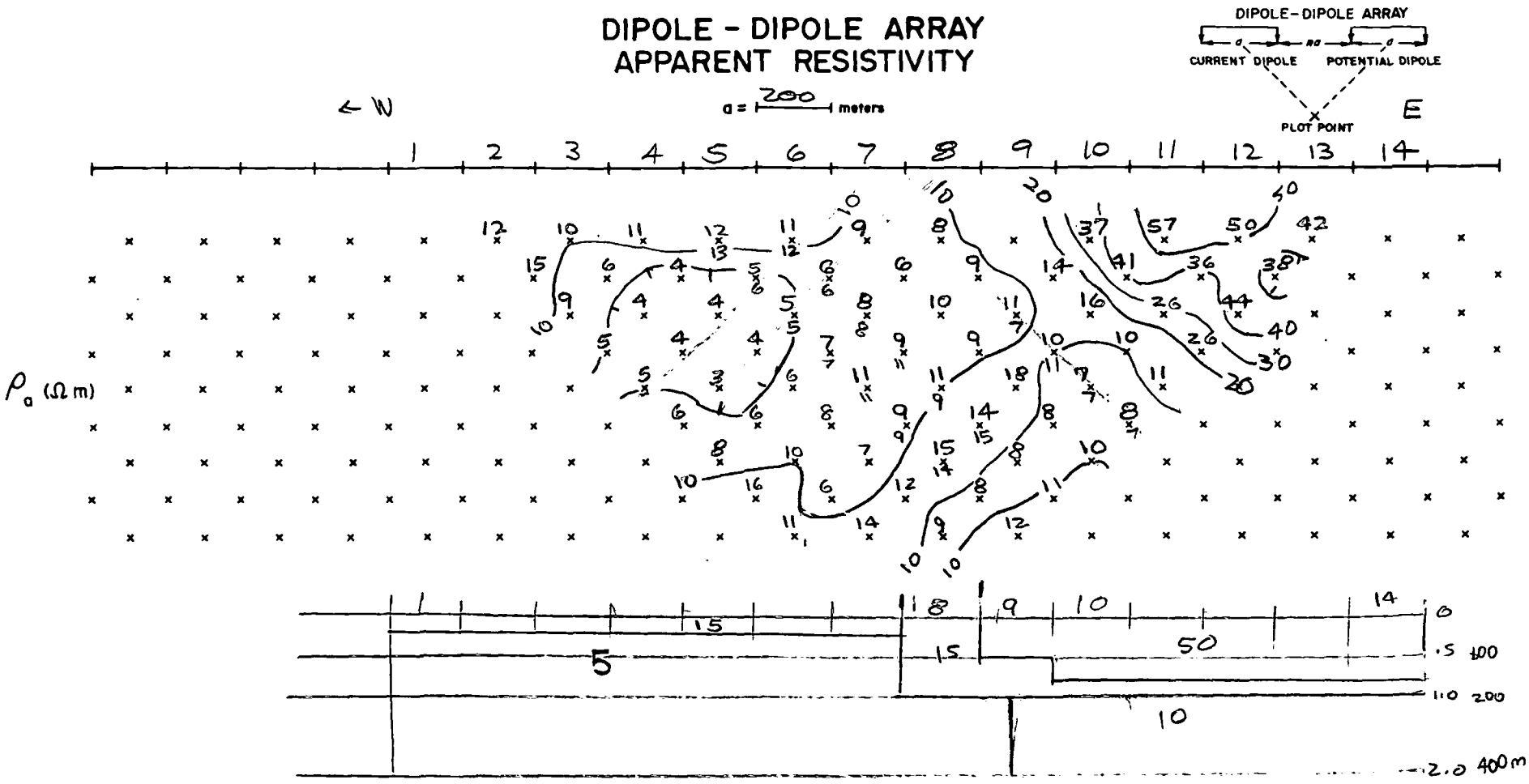

AREA St. Lucia STATE W. Indies LINE 1 DATA BY IGS DATE _____ TRANSMITTER _____ RECEIVER _____

EARTH SCIENCE LABORATORY
UNIVERSITY of UTAH RESEARCH INSTITUTE

DIPOLE - DIPOLE ARRAY
APPARENT RESISTIVITY

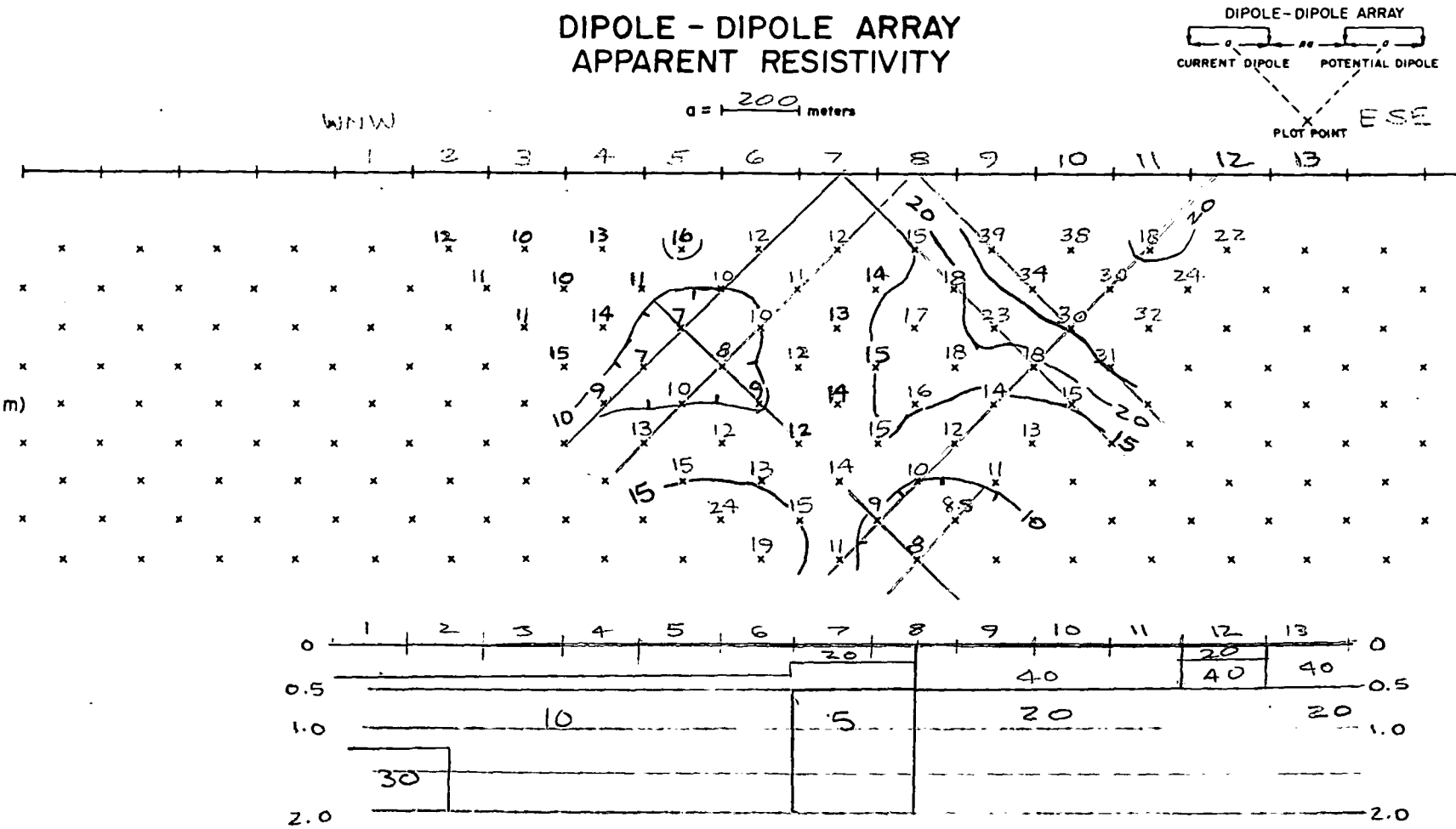

AREA St. Lucia STATE W. Indies LINE 2 DATA BY IGS DATE _____ TRANSMITTER _____ RECEIVER _____

EARTH SCIENCE LABORATORY
UNIVERSITY of UTAH RESEARCH INSTITUTE

DIPOLE - DIPOLE ARRAY
APPARENT RESISTIVITY

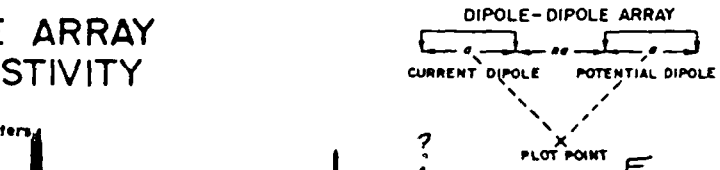

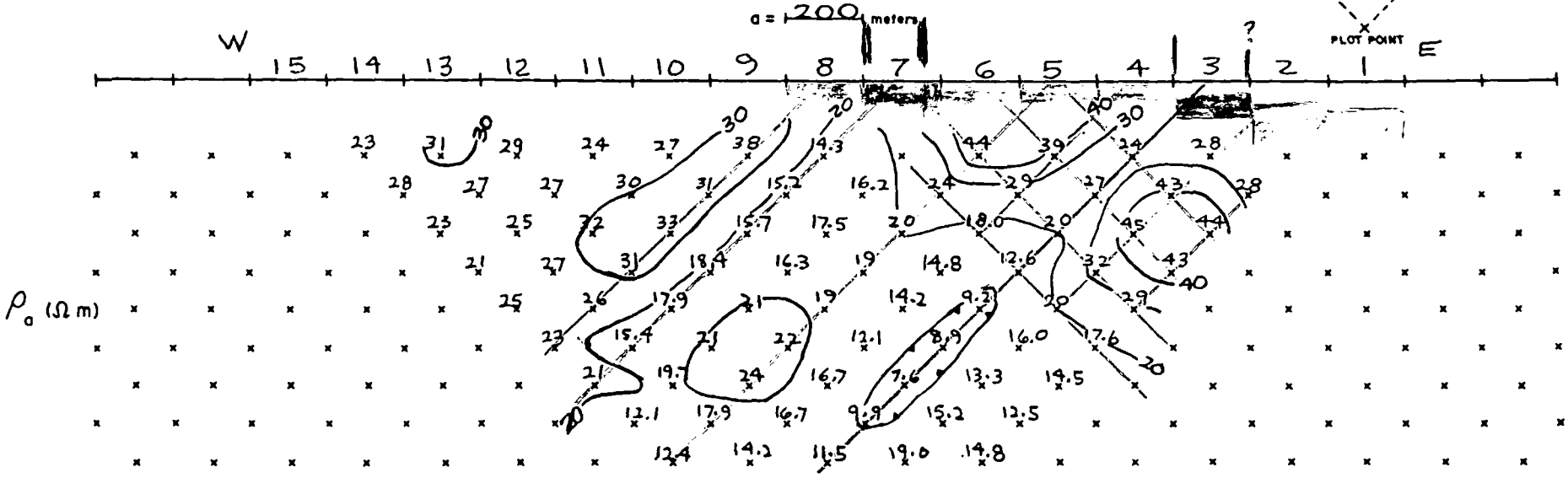

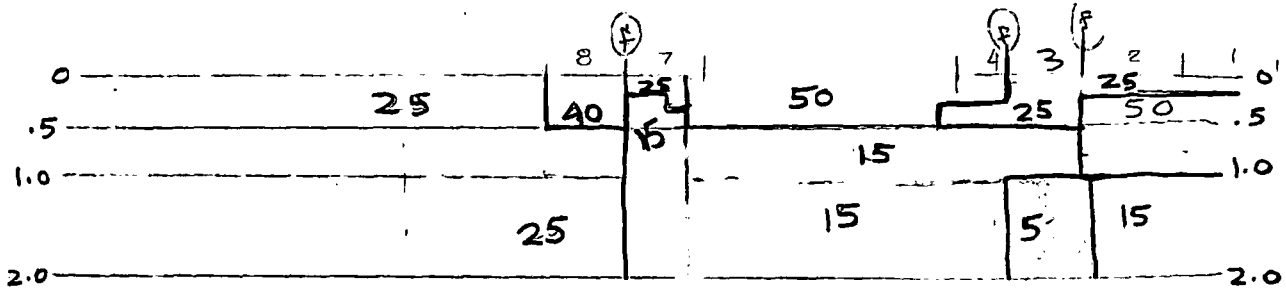

AREA St. Lucia STATE W. Indies LINE 3 DATA BY IGS DATE _____ TRANSMITTER _____ RECEIVER _____

EARTH SCIENCE LABORATORY
UNIVERSITY of UTAH RESEARCH INSTITUTE

DIPOLE - DIPOLE ARRAY
APPARENT RESISTIVITY

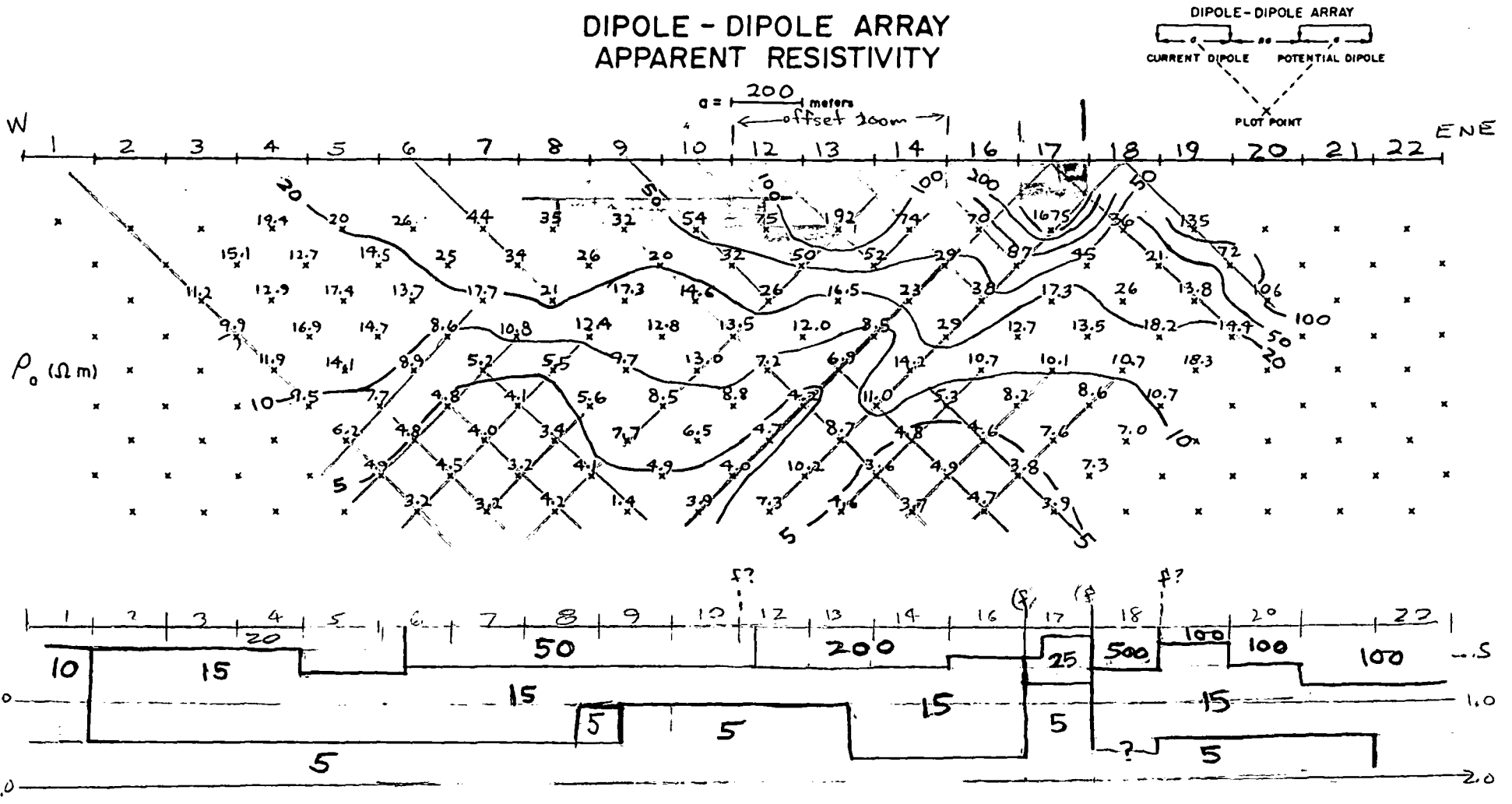

AREA St. Lucia STATE W. Indies LINE 4 DATA BY IGS DATE _____ TRANSMITTER _____ RECEIVER _____

EARTH SCIENCE LABORATORY
UNIVERSITY of UTAH RESEARCH INSTITUTE

DIPOLE - DIPOLE ARRAY
APPARENT RESISTIVITY

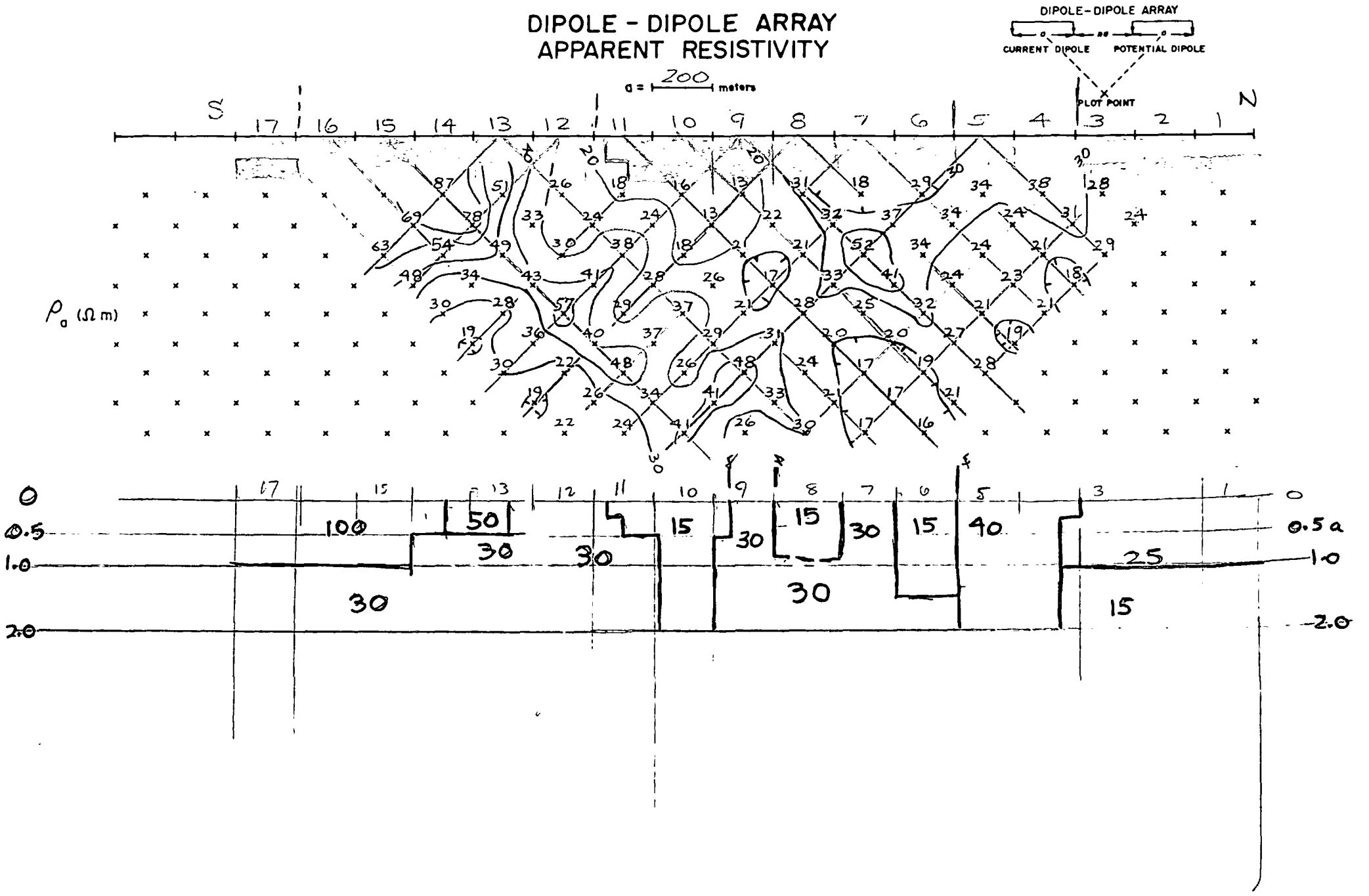

AREA St. Lucia STATE W. Indies LINE 5 DATA BY IGS DATE _____ TRANSMITTER _____ RECEIVER _____

EARTH SCIENCE LABORATORY
UNIVERSITY of UTAH RESEARCH INSTITUTE

DIPOLE - DIPOLE ARRAY
APPARENT RESISTIVITY

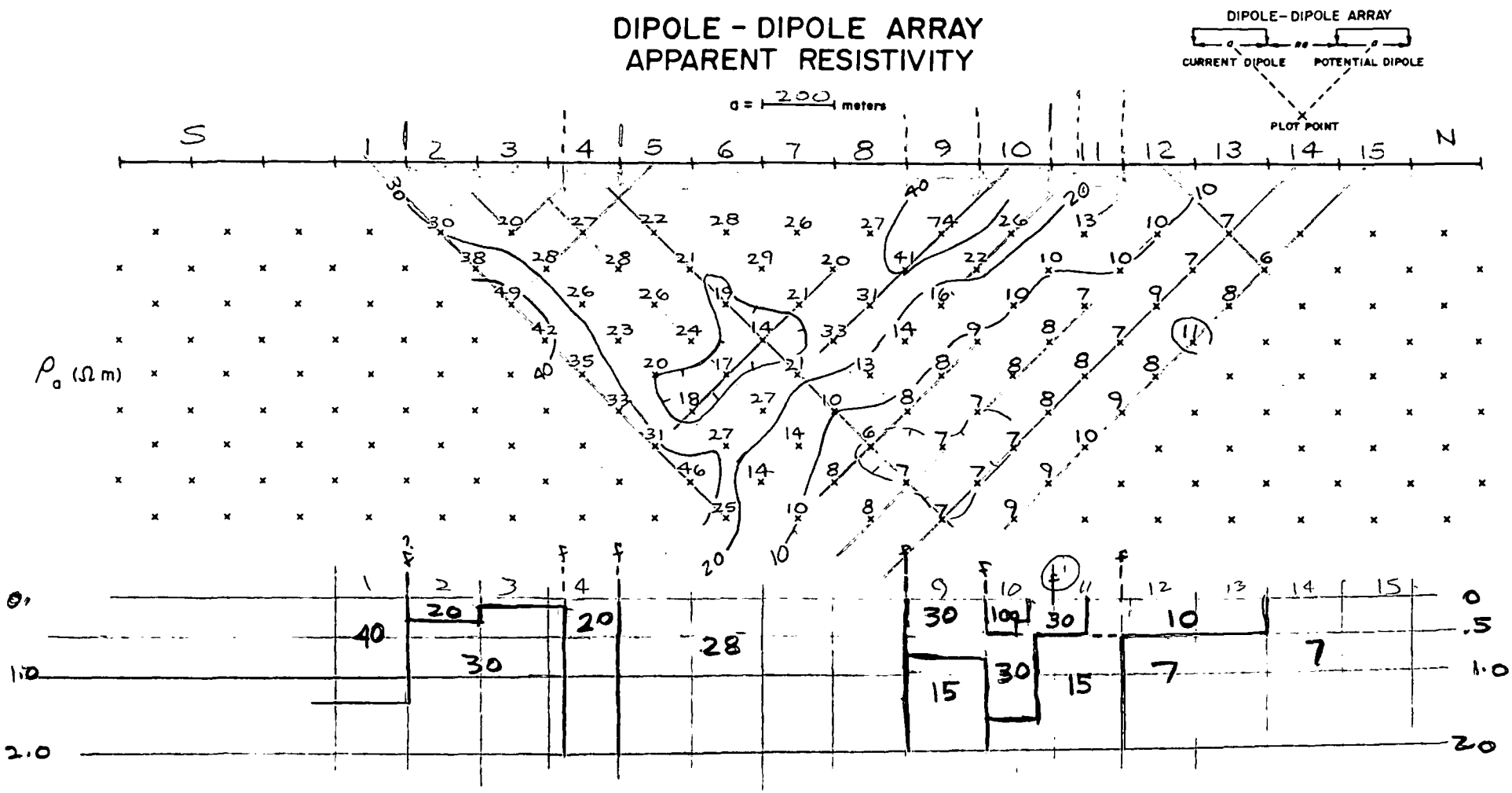

AREA St. Lucia STATE W. Indies LINE 6 DATA BY IGS DATE _____ TRANSMITTER _____ RECEIVER _____

EARTH SCIENCE LABORATORY
UNIVERSITY of UTAH RESEARCH INSTITUTE

DIPOLE - DIPOLE ARRAY
APPARENT RESISTIVITY

a = 200 meters

NW SE

12 11 10 9 8 7 6 5 4 3 2 1

ρ_a (Ω m)

100 500
48 117 649 286 231 192 180 145 335 209 200
24 108 215 64 108 78 84 106 89 100
45 63 76 96 47 39 67 46 50
30 46 52 17.3 28 36 36
28.6 31 28 12.7 29 21 20
22 20 25 15.5 18
20 17.6 18.5 32 9.3
18.9 24 17.5
29 18.7
20

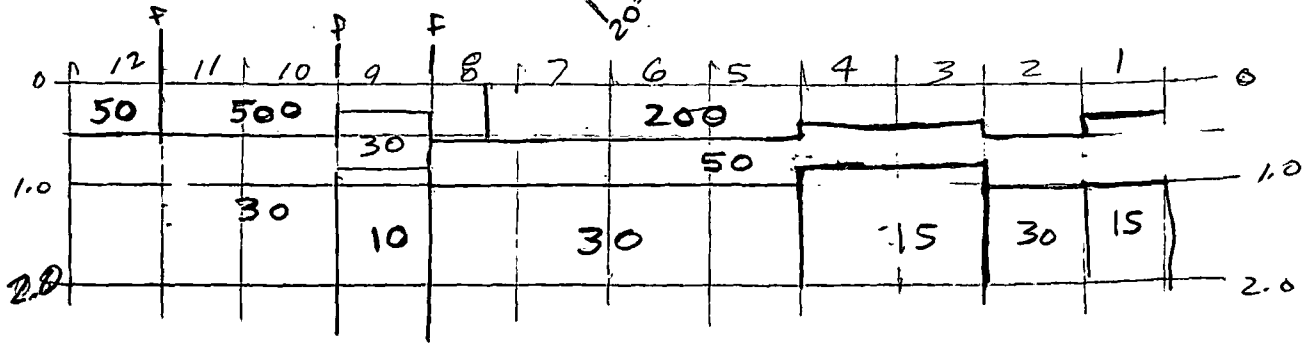

AREA St. Lucia STATE W. Indies LINE 8 DATA BY IGS DATE _____ TRANSMITTER _____ RECEIVER _____

EARTH SCIENCE LABORATORY
UNIVERSITY of UTAH RESEARCH INSTITUTE

DIPOLE - DIPOLE ARRAY
APPARENT RESISTIVITY

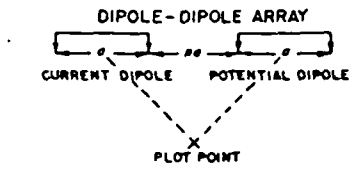

a = 200 meters

NNE

SSW

17 16 15 14 13 12 11 10 9 8 7 6 5 4 3 2 1

IGS

n = 2

n = 5

n = 10

ρ_a (Ω m)

12 11 10 9 8 7 6 5 4 3 2 1

0
.5
1.0
2.0

AREA St. Lucia STATE W. Indies LINE 7 DATA BY IGS DATE _____ TRANSMITTER _____ RECEIVER _____

EARTH SCIENCE LABORATORY
UNIVERSITY of UTAH RESEARCH INSTITUTE

DIPOLE - DIPOLE ARRAY
APPARENT RESISTIVITY

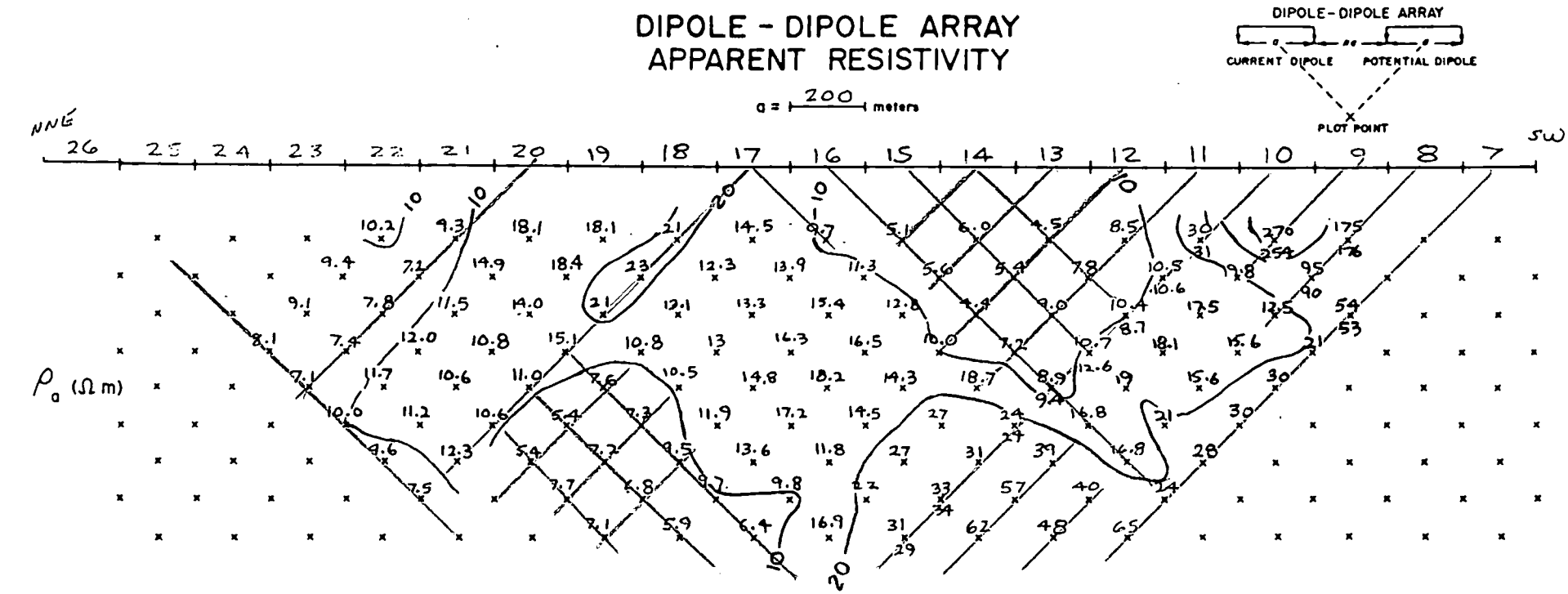

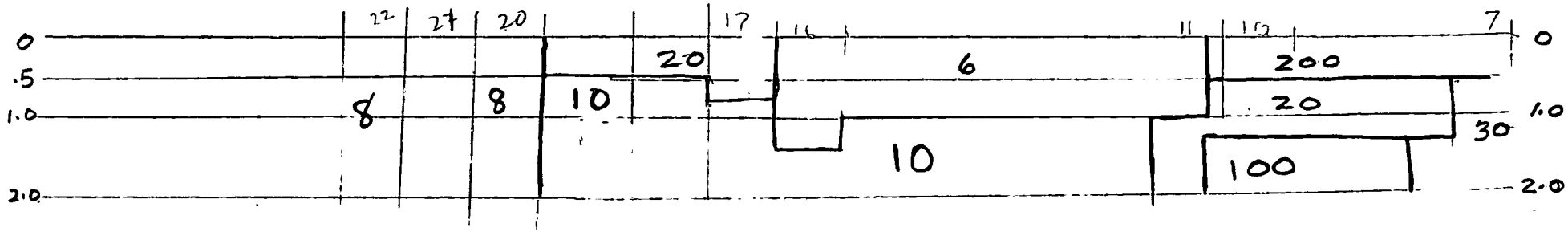

AREA St. Lucia STATE W. Indies LINE 7 Ext. DATA BY IGS DATE _____ TRANSMITTER _____ RECEIVER _____

EARTH SCIENCE LABORATORY
UNIVERSITY of UTAH RESEARCH INSTITUTE

DIPOLE - DIPOLE ARRAY
APPARENT RESISTIVITY

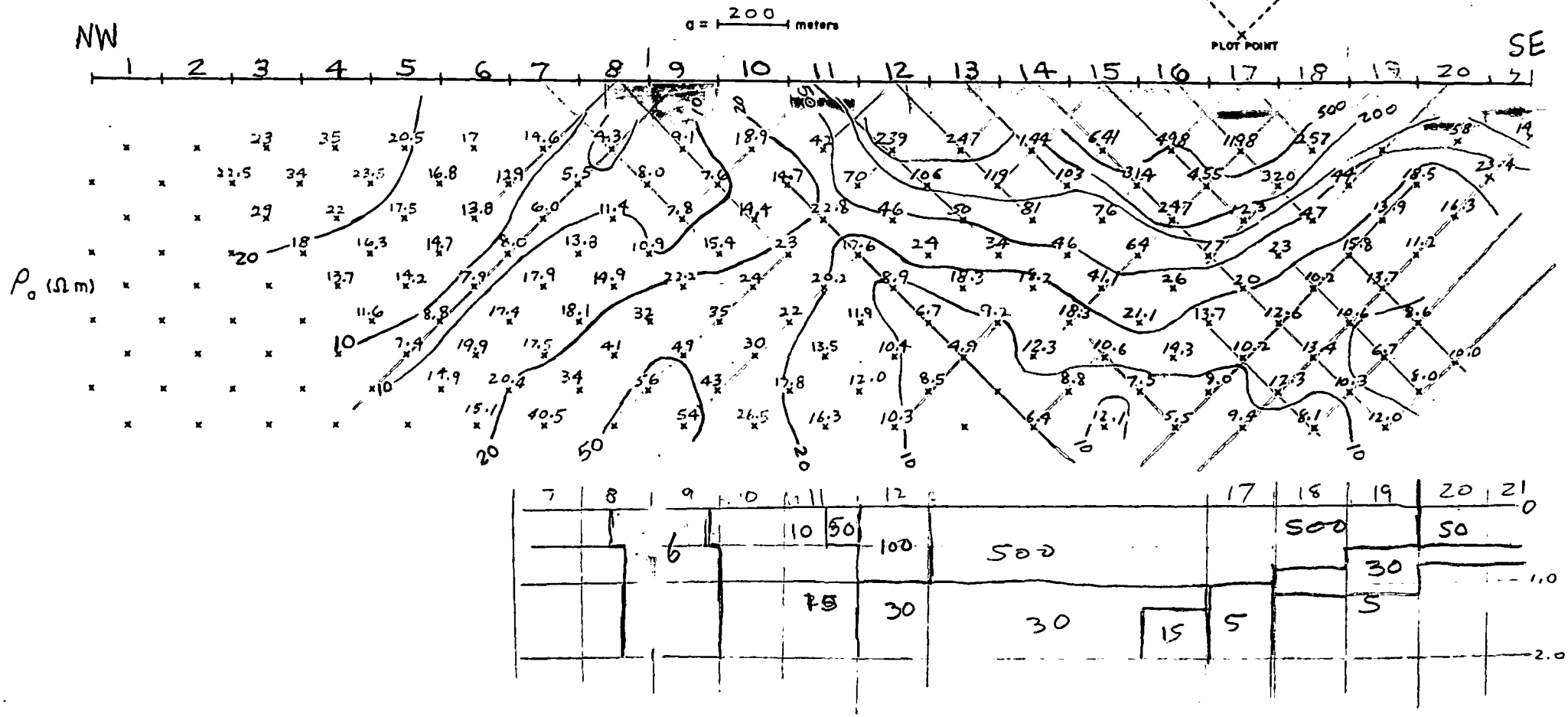

AREA St. Lucia STATE W. Indies LINE 9 DATA BY BGS DATE _____ TRANSMITTER _____ RECEIVER _____

EARTH SCIENCE LABORATORY
UNIVERSITY of UTAH RESEARCH INSTITUTE

DIPOLE - DIPOLE ARRAY
APPARENT RESISTIVITY

← NW

a = 200 meters

SE →

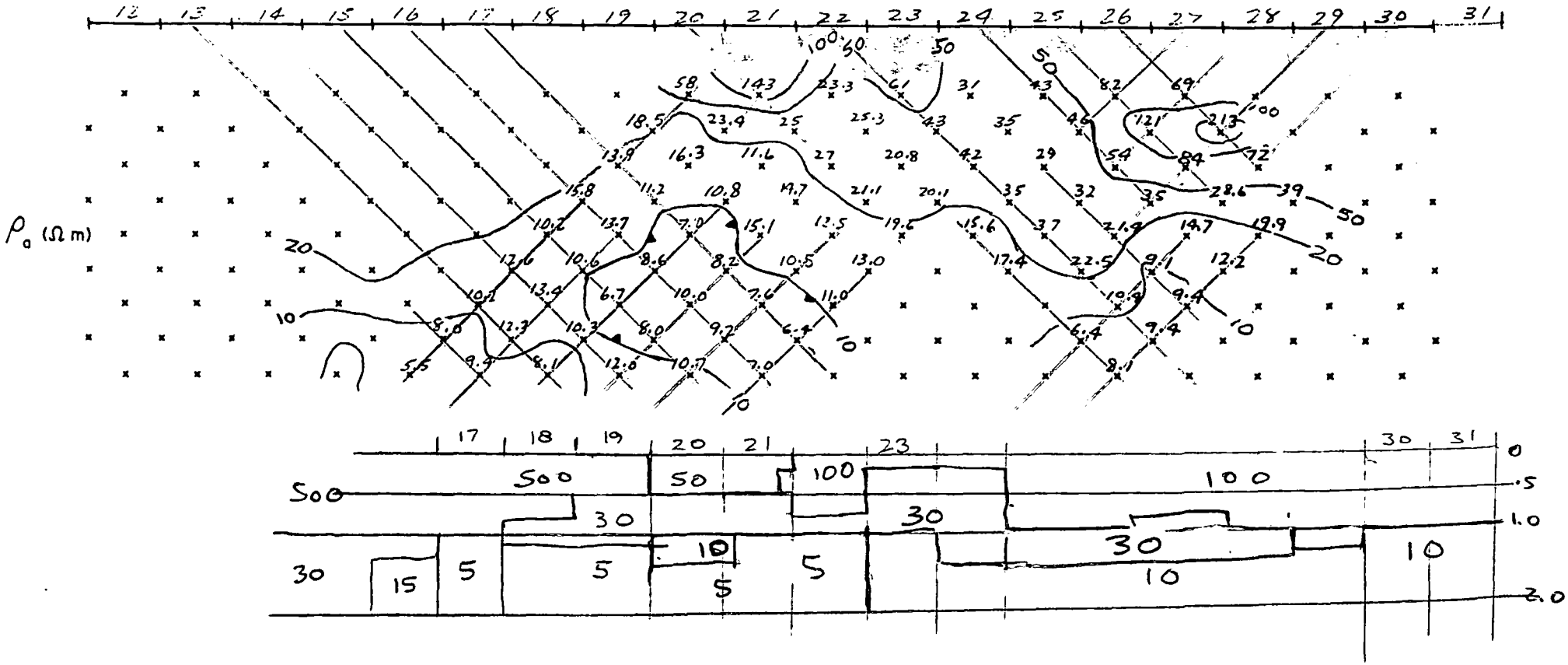

AREA St. Lucia STATE W. Indies LINE 9ext DATA BY BGS DATE _____ TRANSMITTER _____ RECEIVER _____

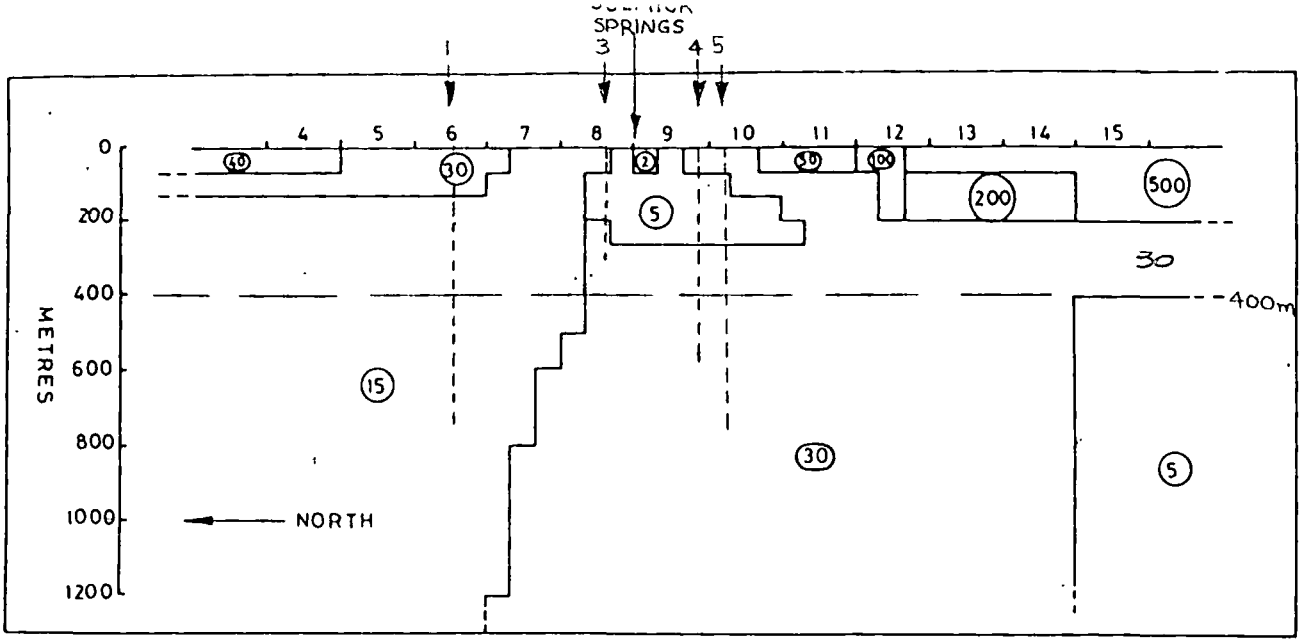

Fig. 2a Line 9 - true resistivity model 6

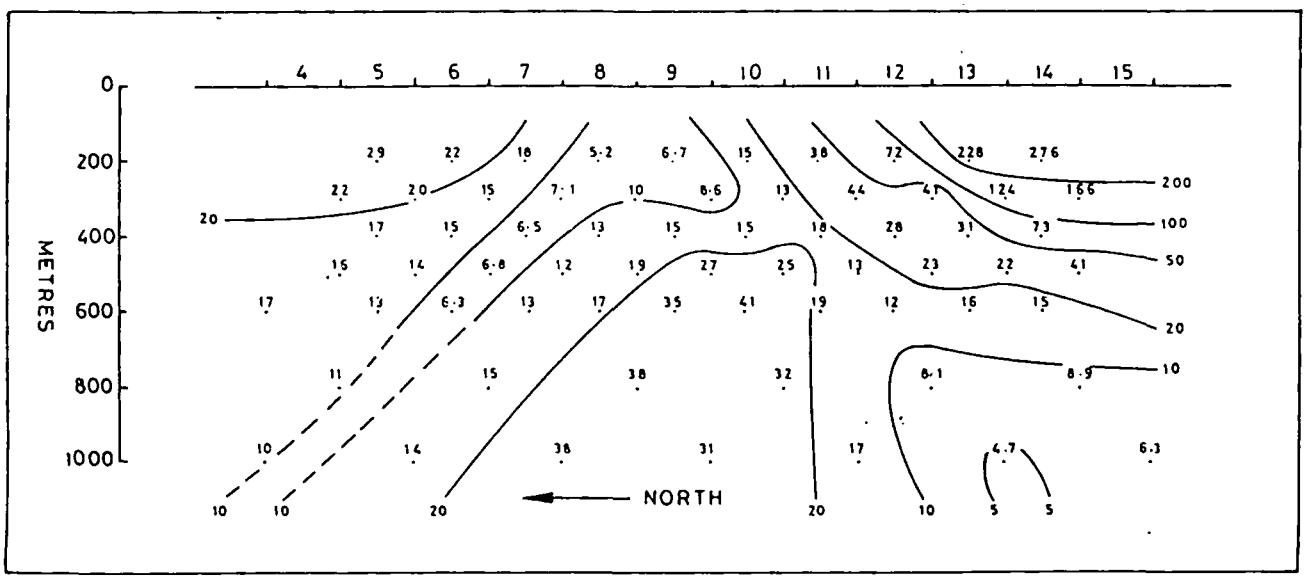

Fig. 2b Line 9 - computer generated section due to model 6

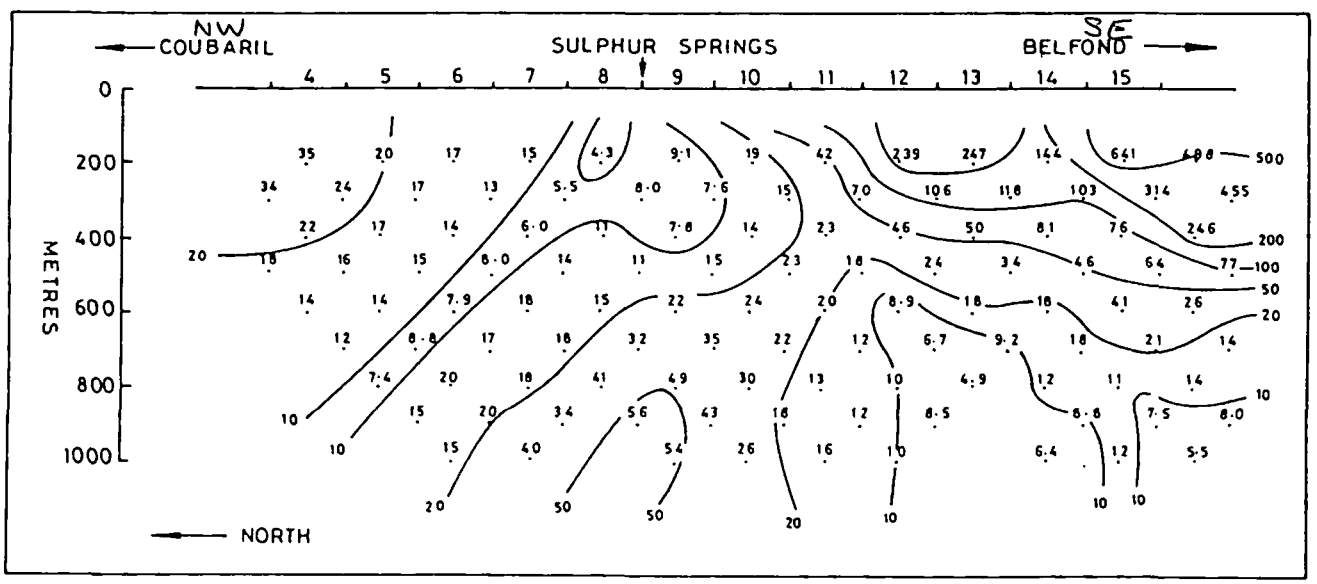

Fig. 2c Line 9 - apparent resistivity cross-section - observed

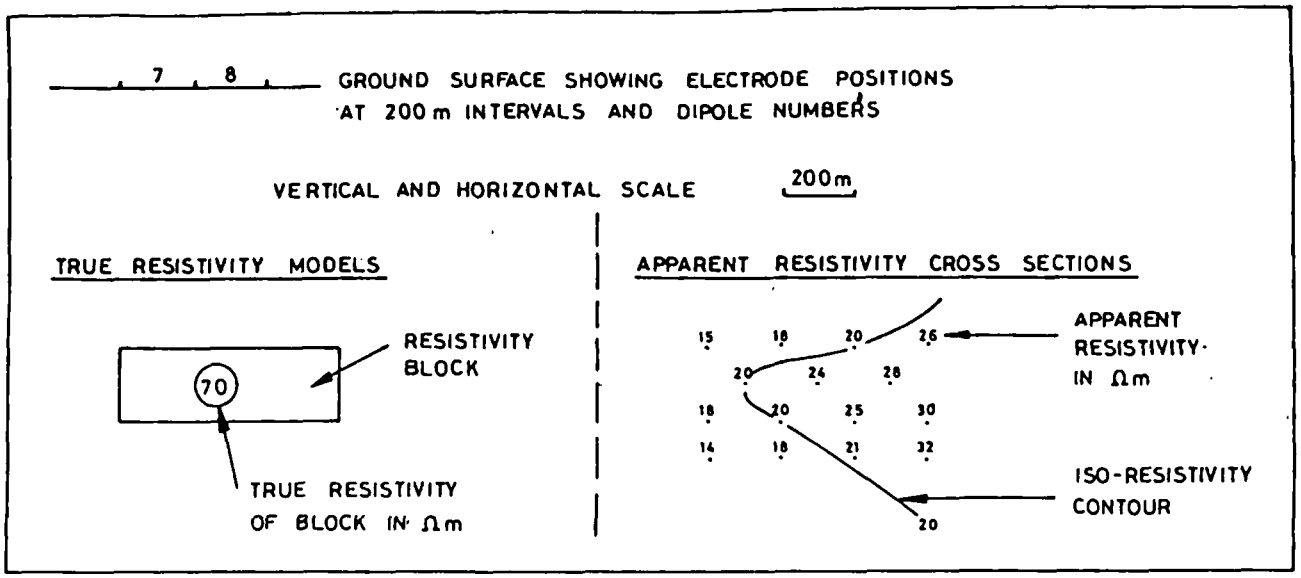

Fig. 1. Key to Figs. 2 to 14

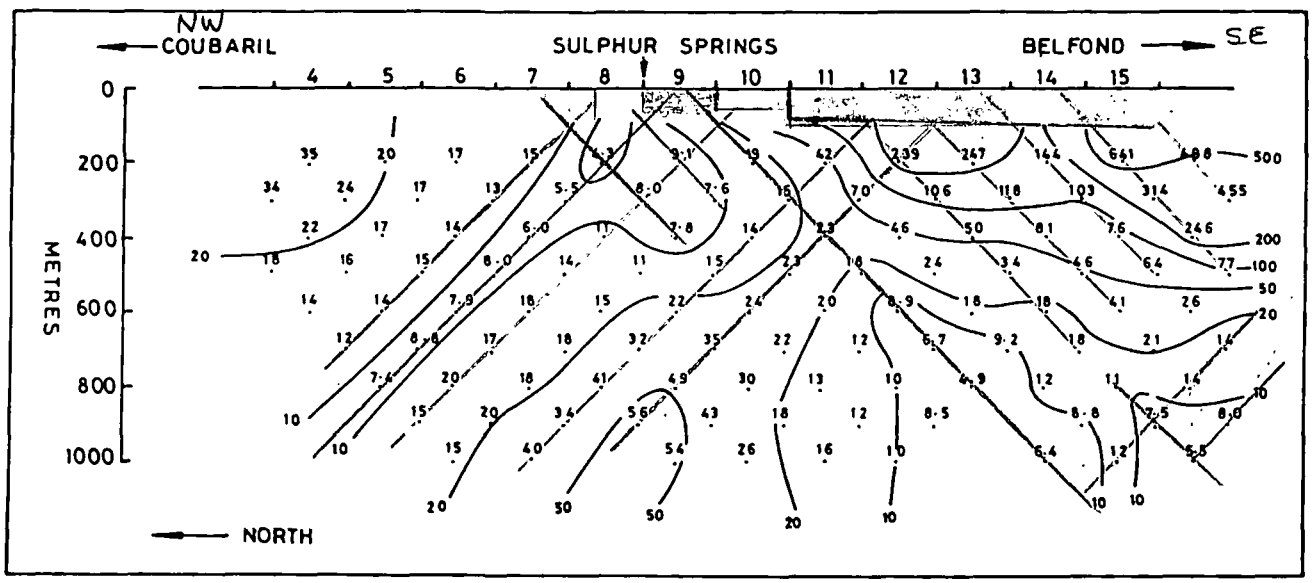

Fig. 2. Line 9 - apparent resistivity cross-section

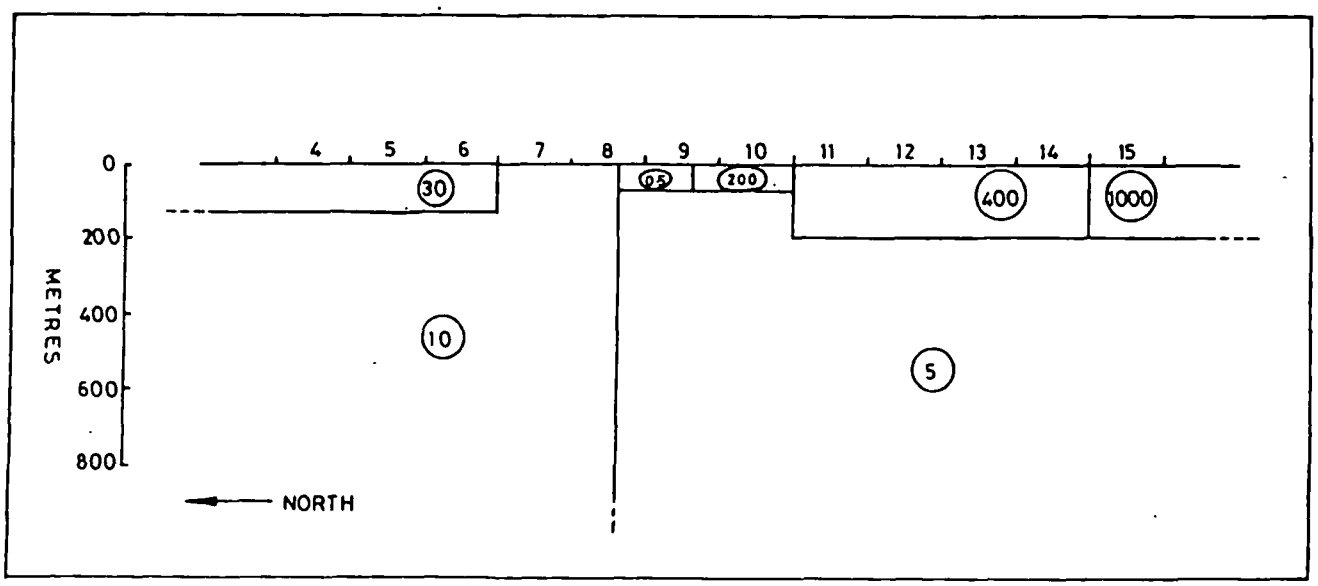

Fig. 3. Line 9 - true resistivity model 1

EARTH SCIENCE LABORATORY
UNIVERSITY of UTAH RESEARCH INSTITUTE

DIPOLE - DIPOLE ARRAY
APPARENT RESISTIVITY

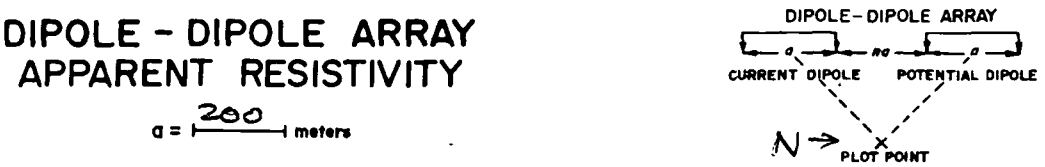

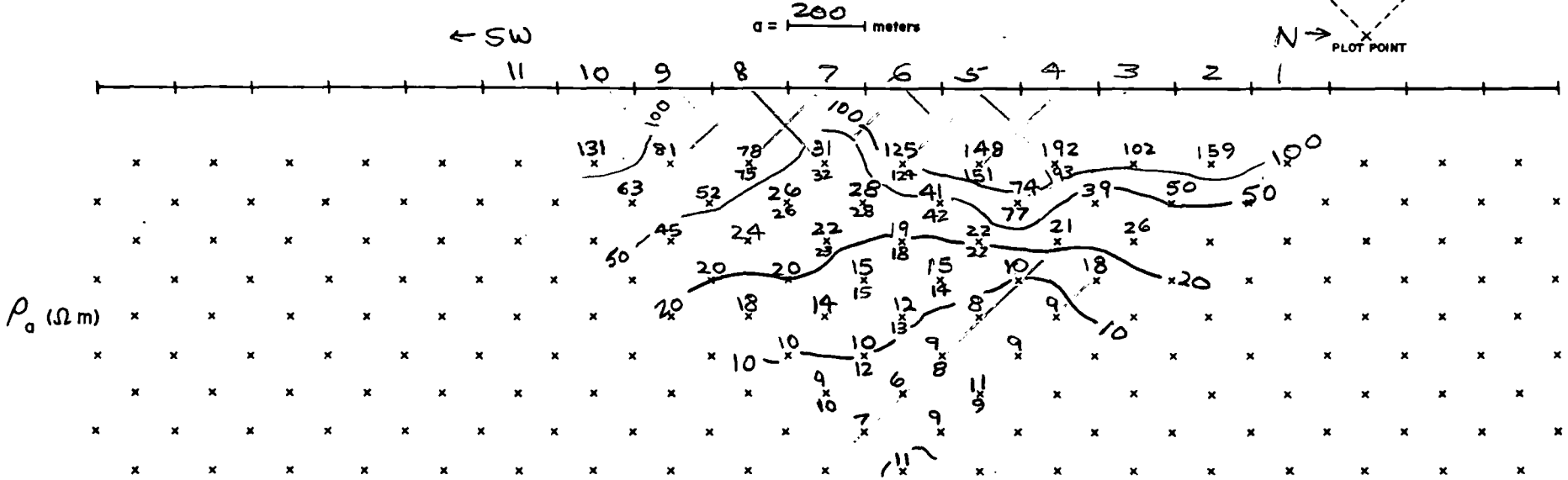

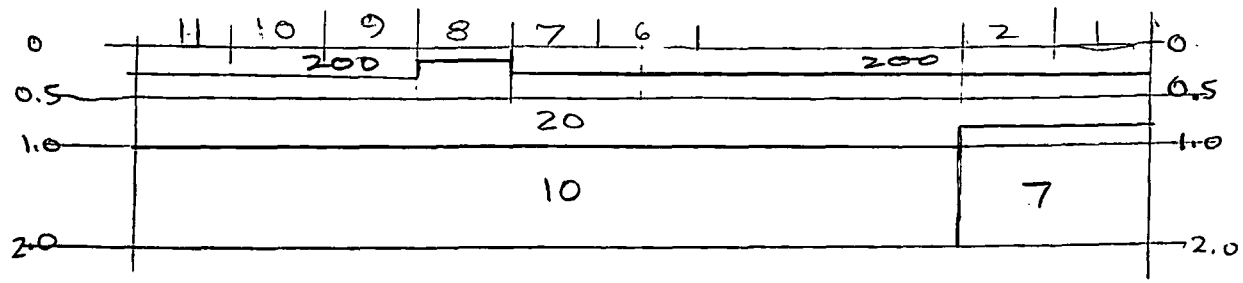

AREA St. Lucia STATE West Indies LINE 10 DATA BY IGS DATE _____ TRANSMITTER _____ RECEIVER _____

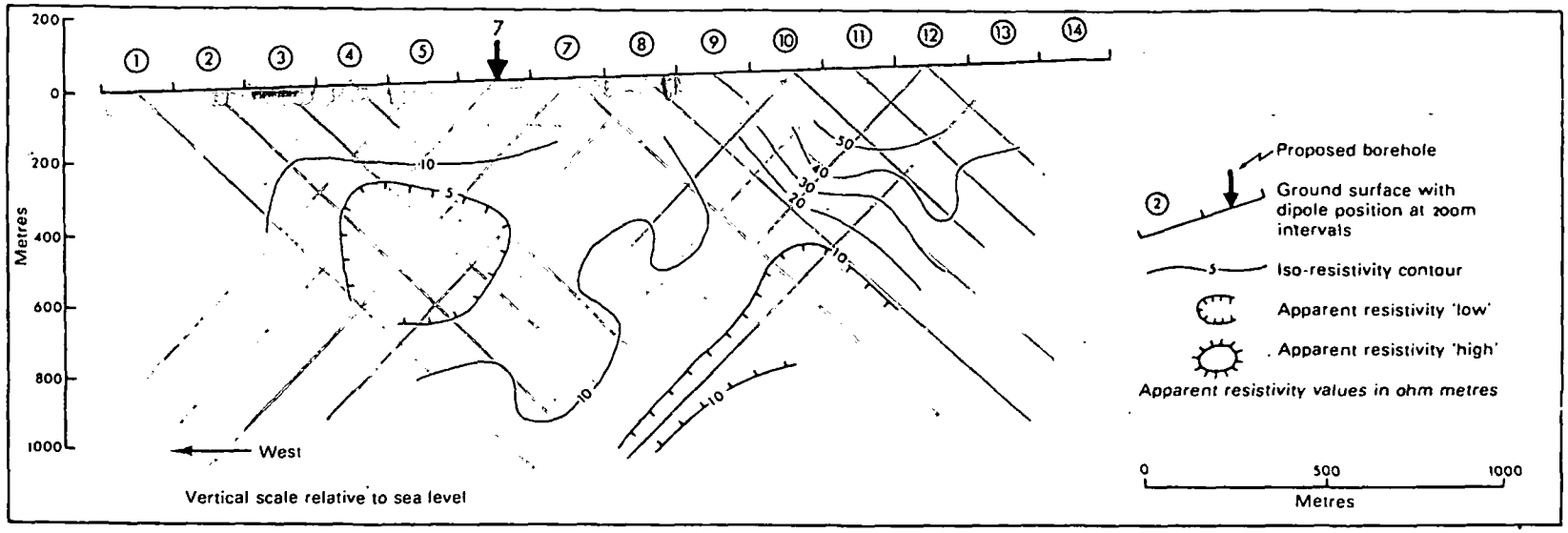

Fig. 6 Apparent resistivity cross section: Line 1, La Perle

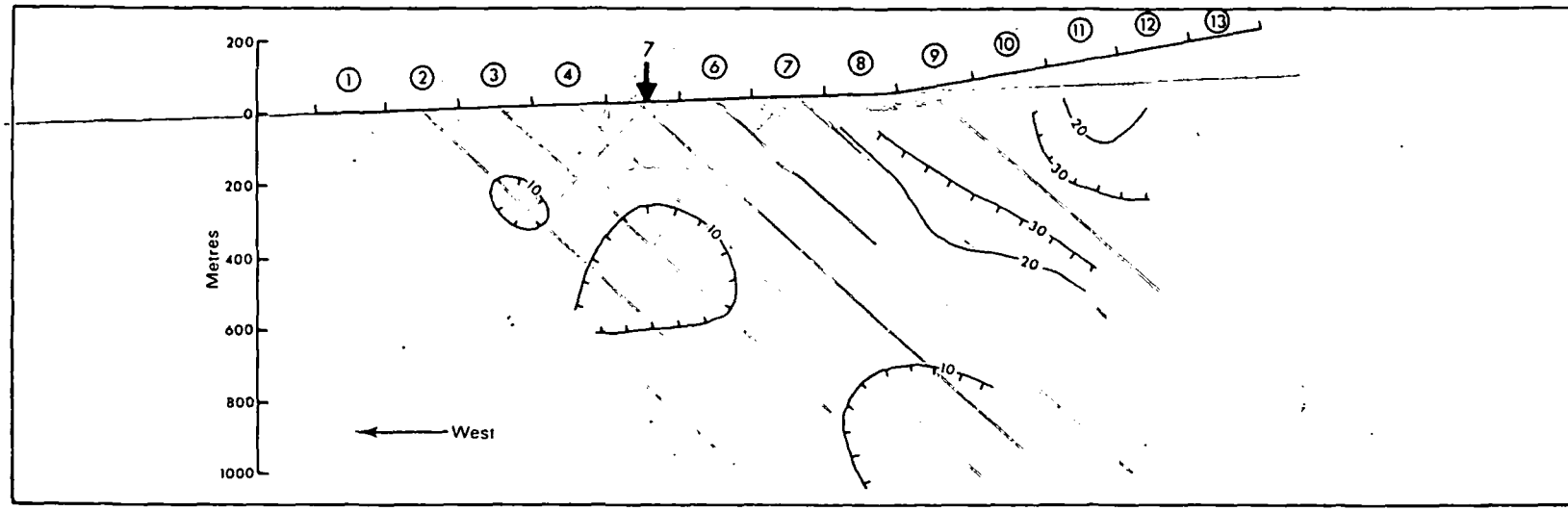

Fig. 7 Apparent resistivity cross section: Line 2, Soufriere - Diamond

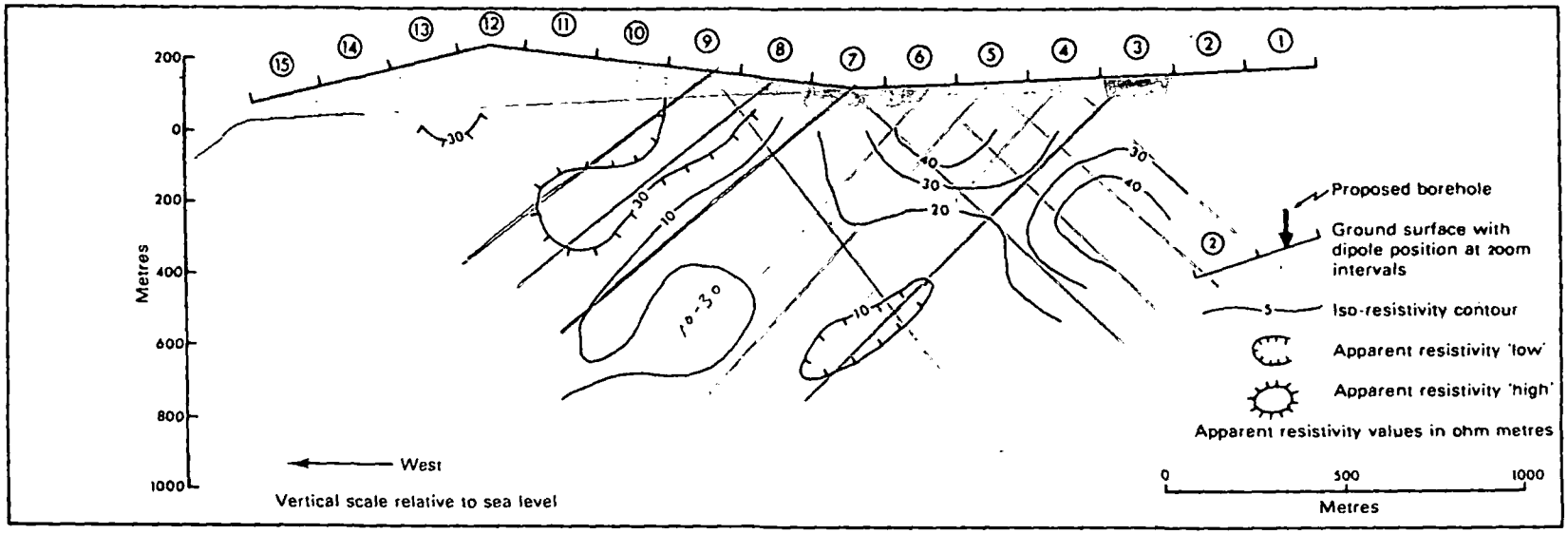

Fig. 8 Apparent resistivity cross section: Line 3, Stonefield - Saphire

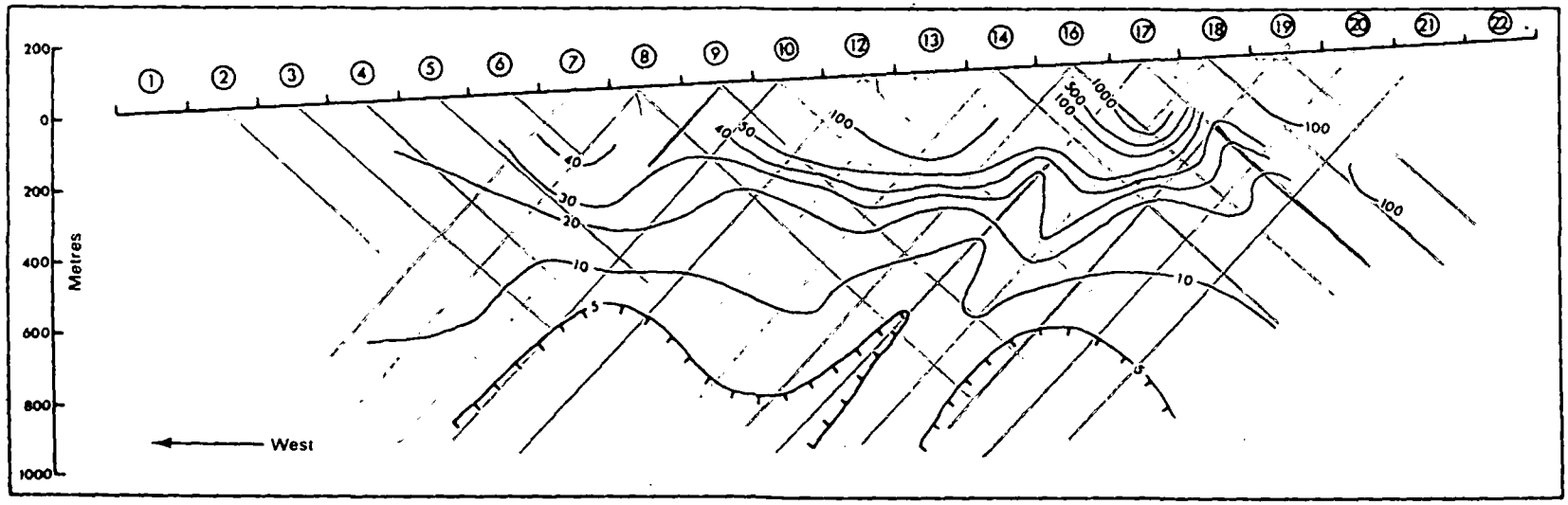

Fig. 9 Apparent resistivity cross section: Line 4, Gros Piton - Beausejour

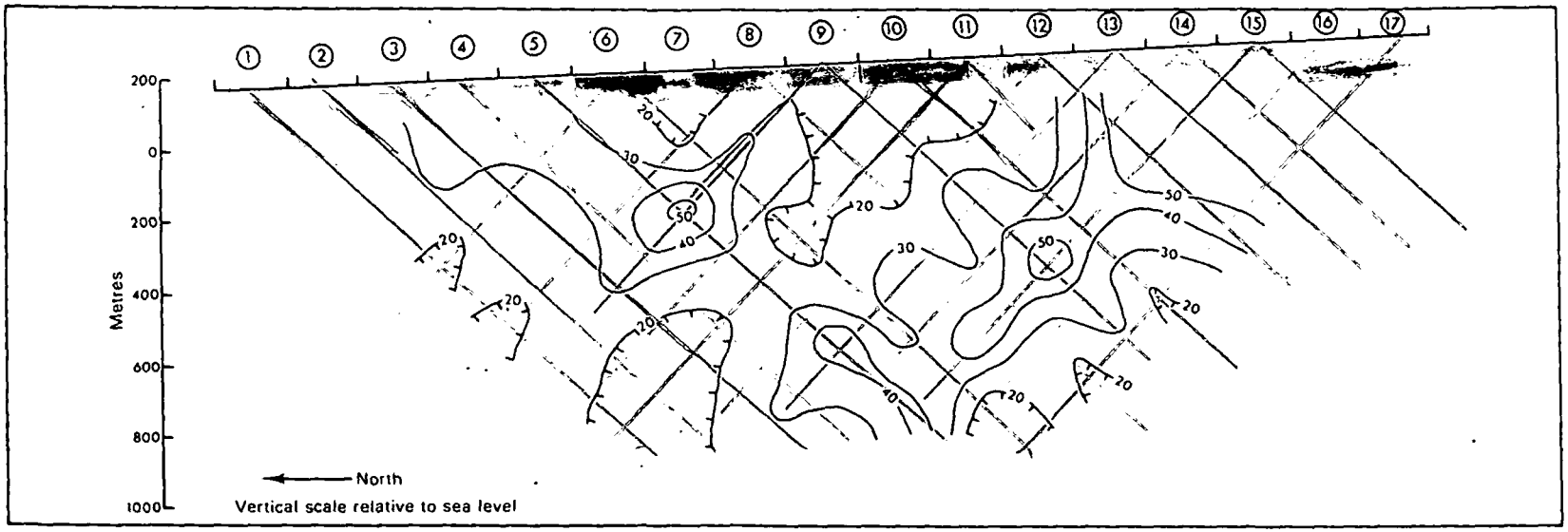

Fig. 10 Apparent resistivity cross section: Line 5, Coubaril - Rabot - Dauphine

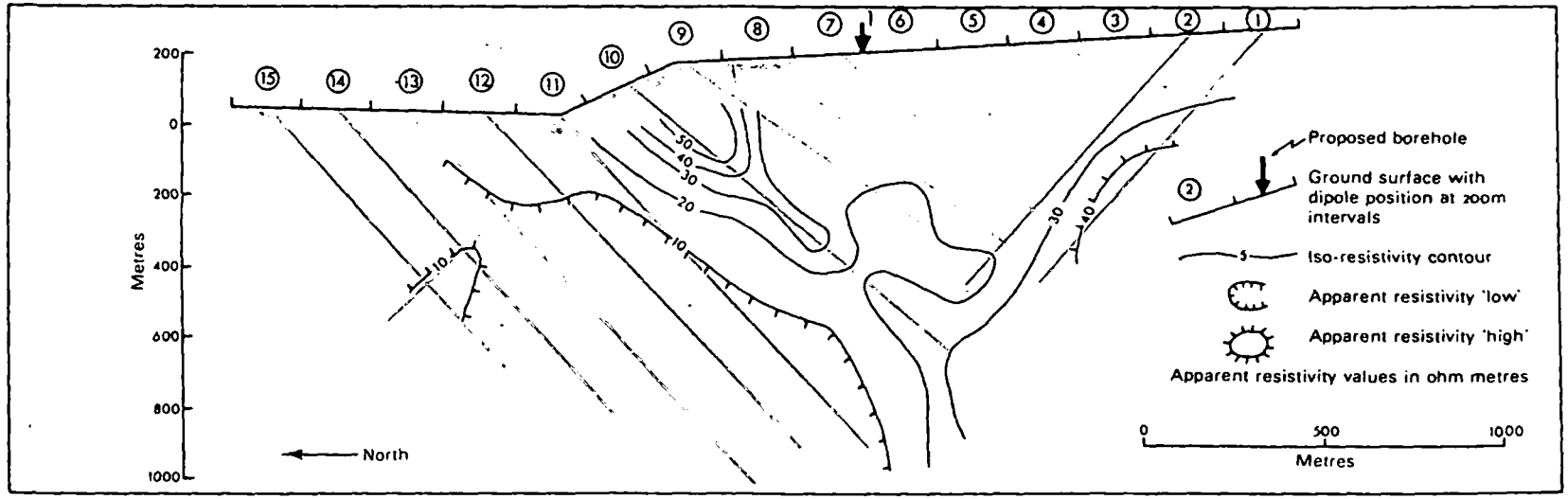

Fig. 11 Apparent resistivity cross section: Line 6, Rabot - Ruby

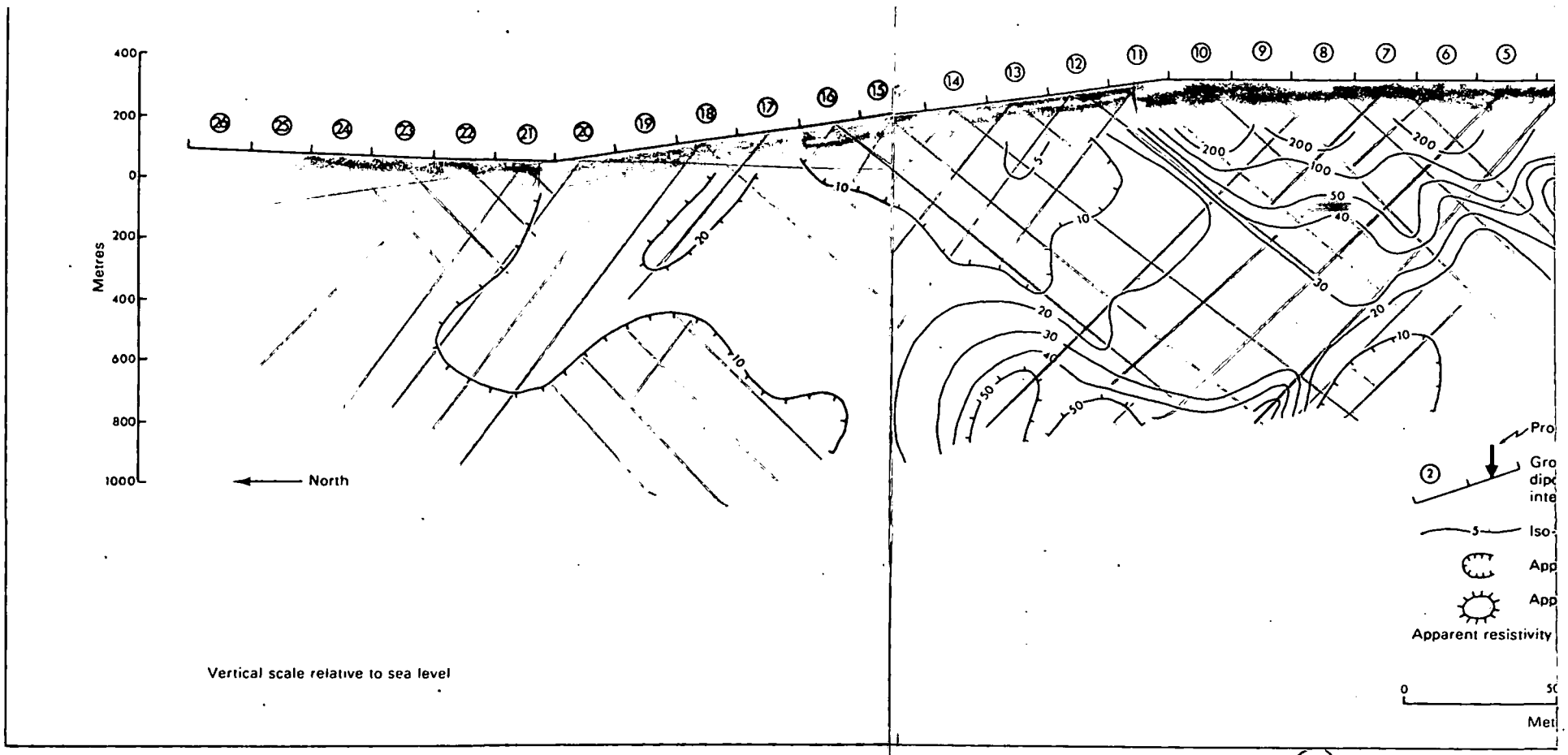

Fig. 12 Apparent resistivity cross section: Line 7, Ruby - Sulphur Springs - Fond Dou

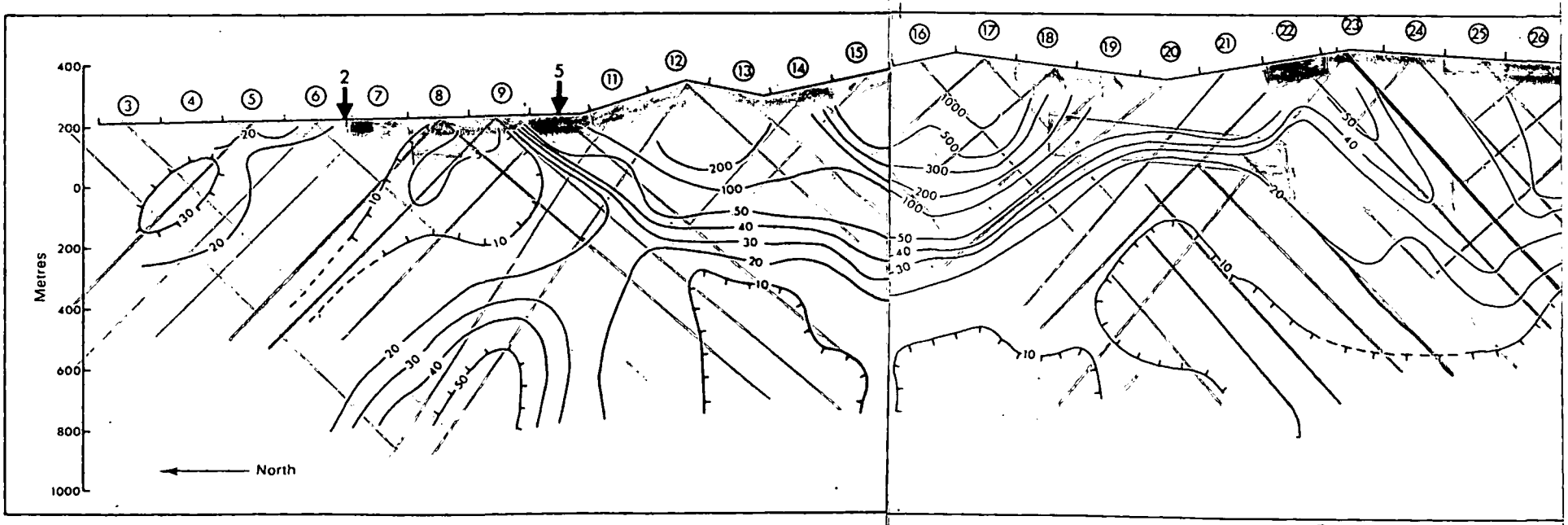

Apparent resistivity cross section: Line 9, Coubaril - Sulphur Springs - Mote

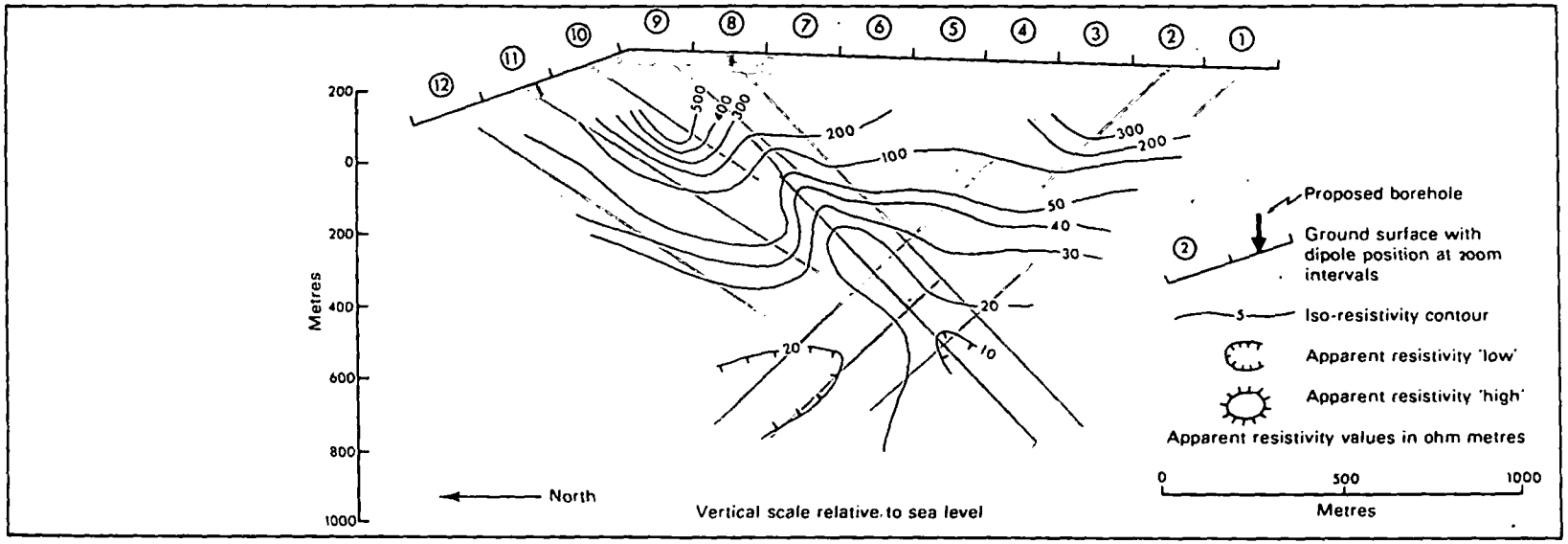

Fig. 14 Apparent resistivity cross section: Line 8, Esperance

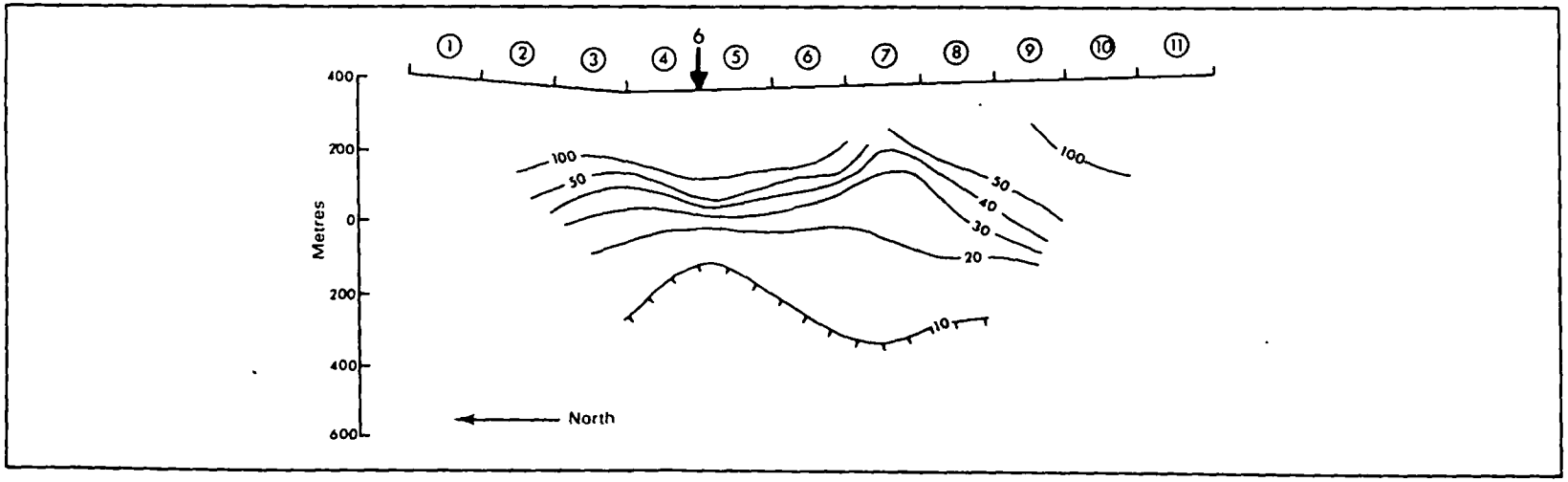

Fig. 15 Apparent resistivity cross section: Line 10, Belle Plaine - Victoria Junction

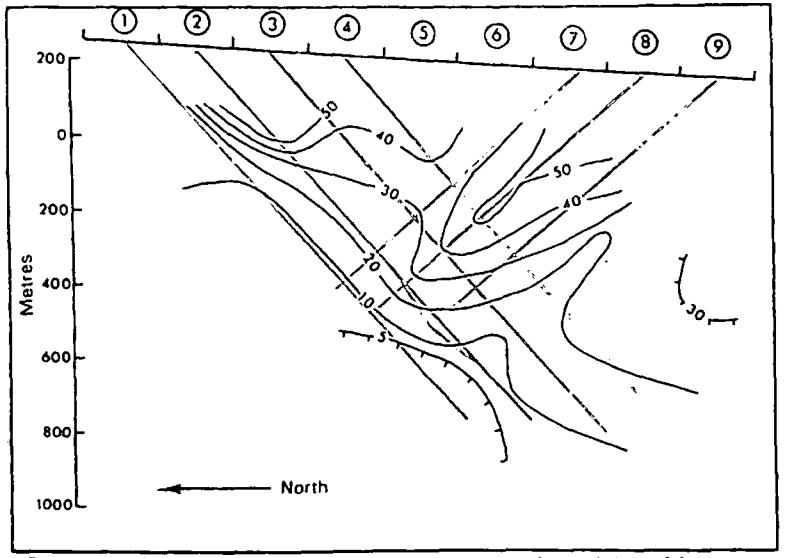

Fig. 16 Apparent resistivity cross section: Line 11, Gros Piton - Delcer

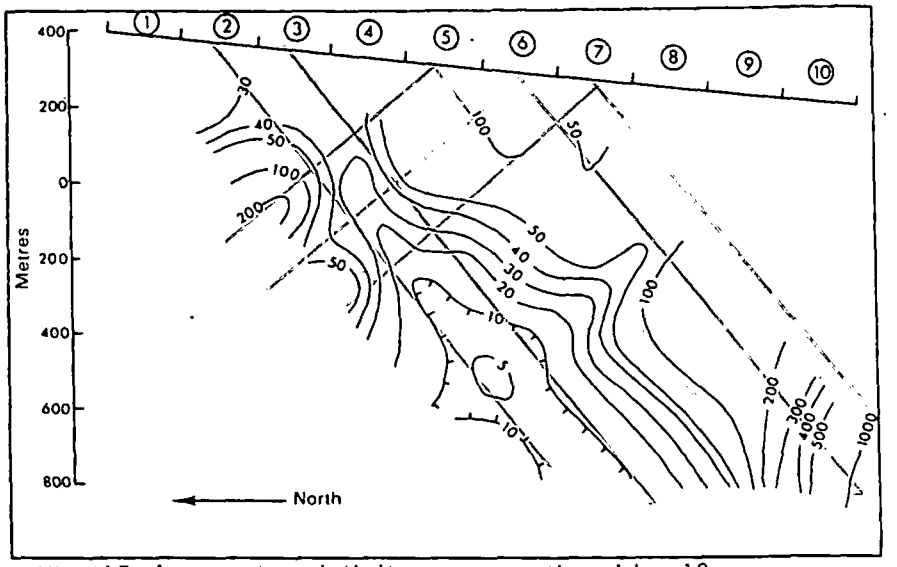

Fig. 17 Apparent resistivity cross section: Line 12, Victoria Junction - Le Riche

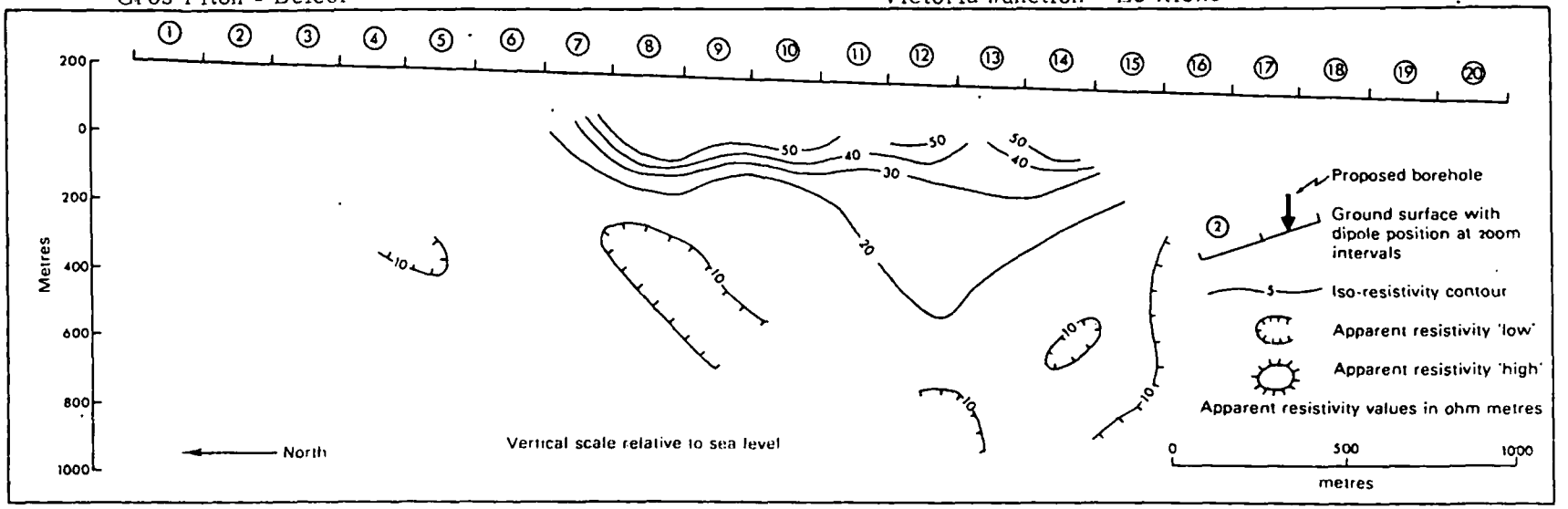

Fig. 18 Apparent resistivity cross section: Line 13, Londonderry

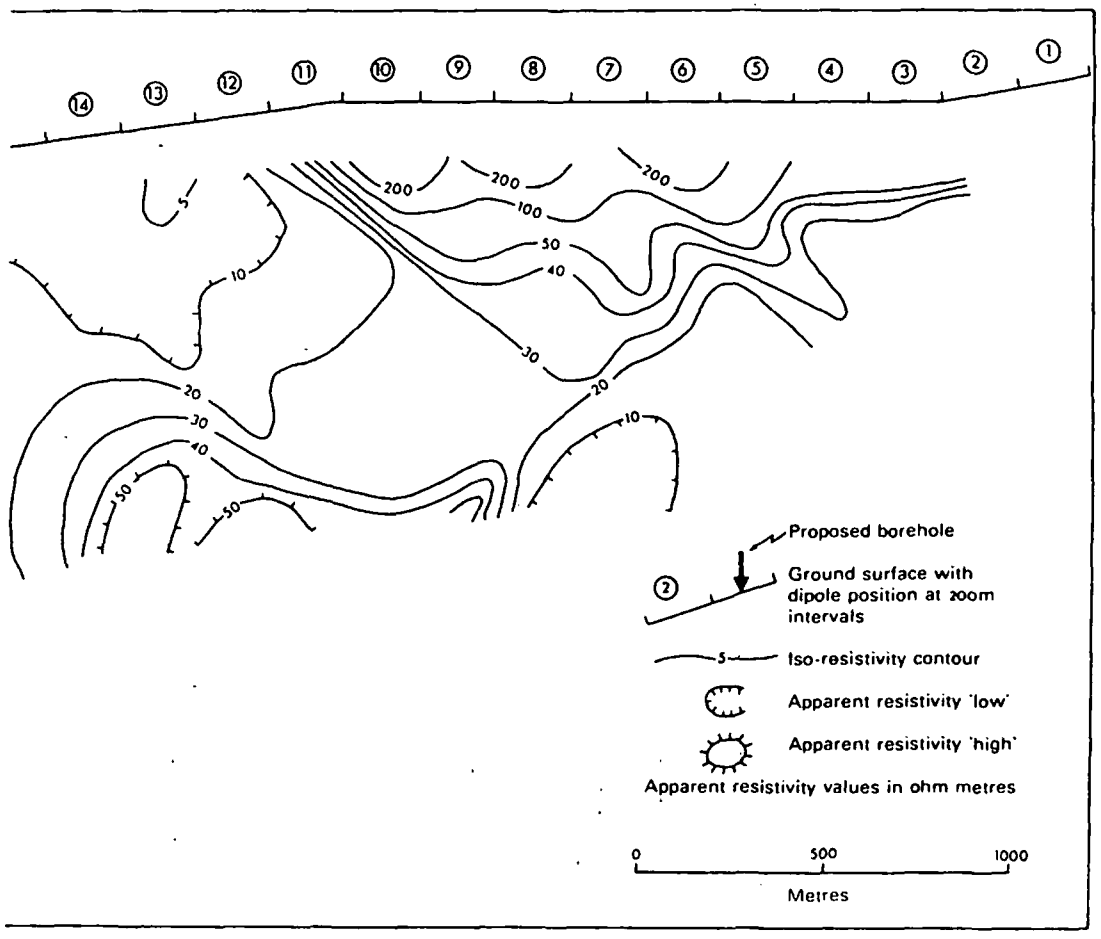
14 13 12 11 10 9 8 7 6 5 4 3 2 1
200
200
200
100
50
40
30
20
10
5
20
30
40
50
50
10
Proposed borehole
Ground surface with dipole position at 200m intervals
5
Iso-resistivity contour
Apparent resistivity 'low'
Apparent resistivity 'high'
Apparent resistivity values in ohm metres
0
500
1000
Metres

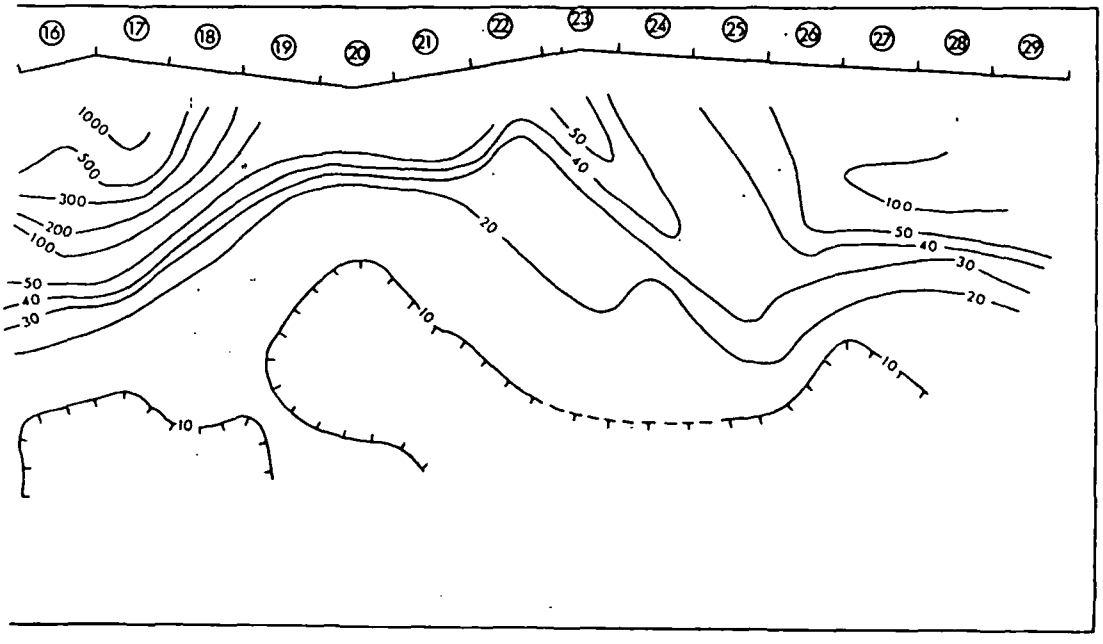
16 17 18 19 20 21 22 23 24 25 26 27 28 29
1000
500
300
200
100
50
40
30
20
50
40
100
50
40
30
20
10
10
10

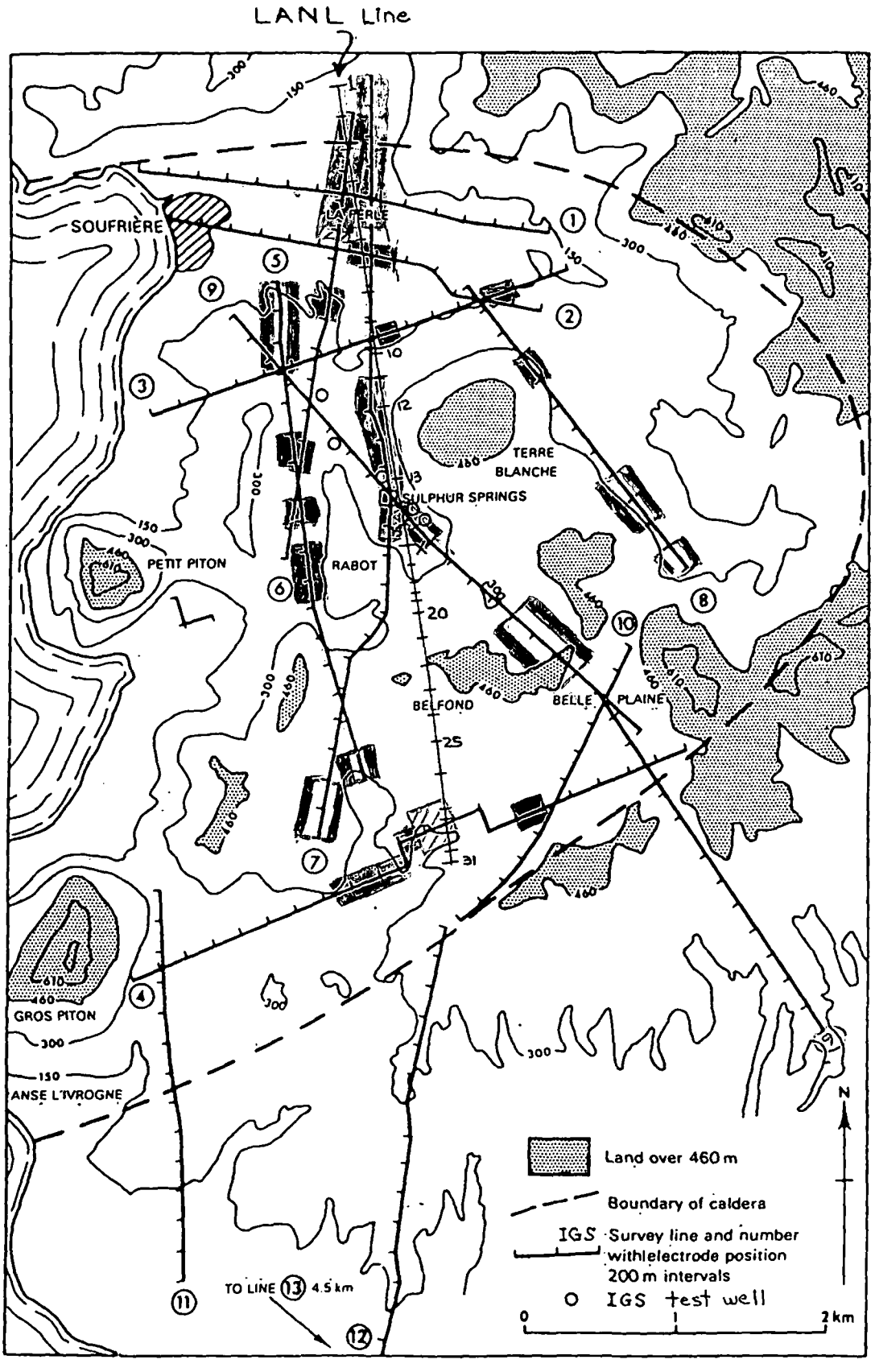

Fig. 1 Soufrière area, St Lucia showing geophysical survey lines

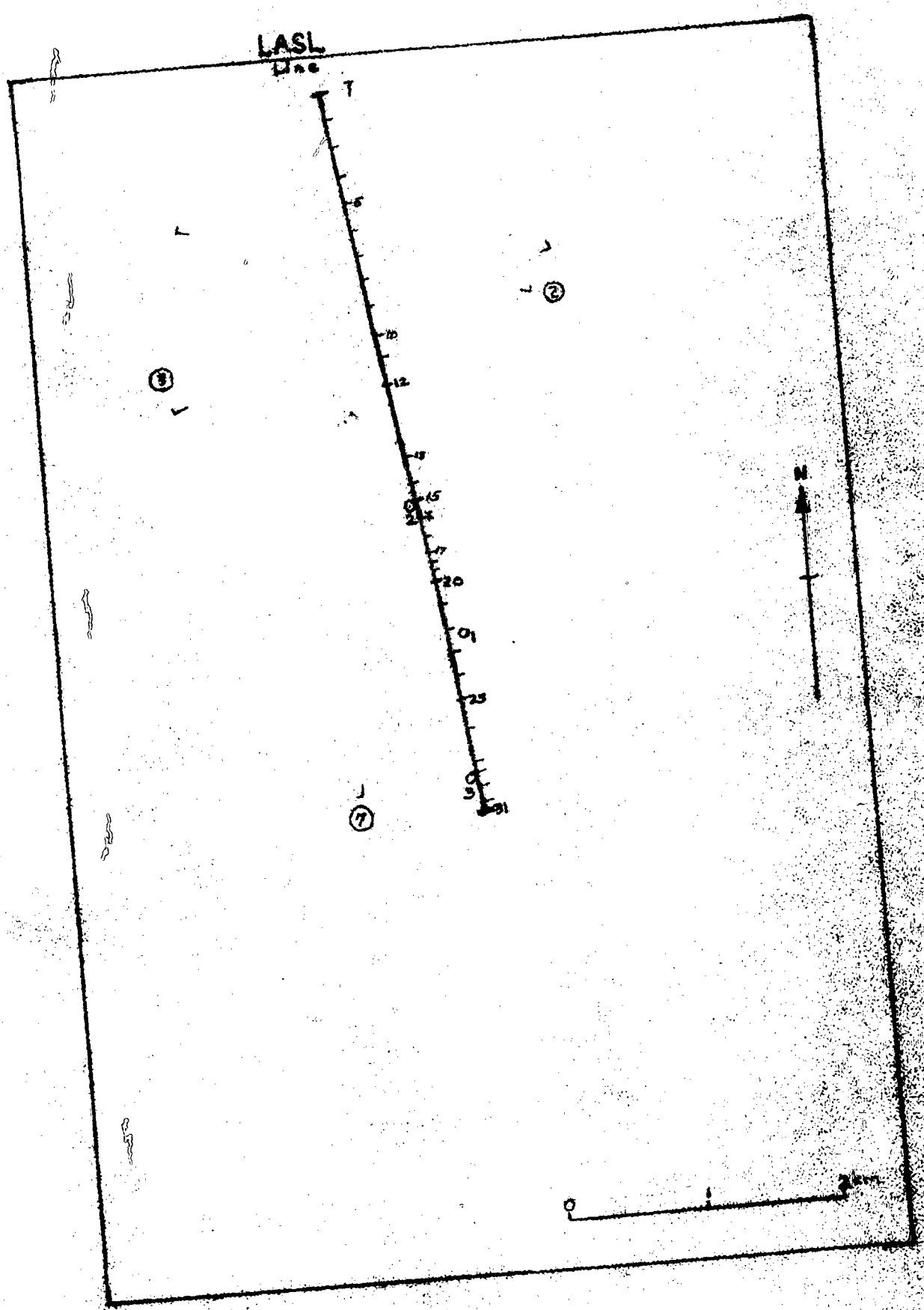
LASL
Line
T
5
10
12
15
17
20
23
31
N
0
1
2 km

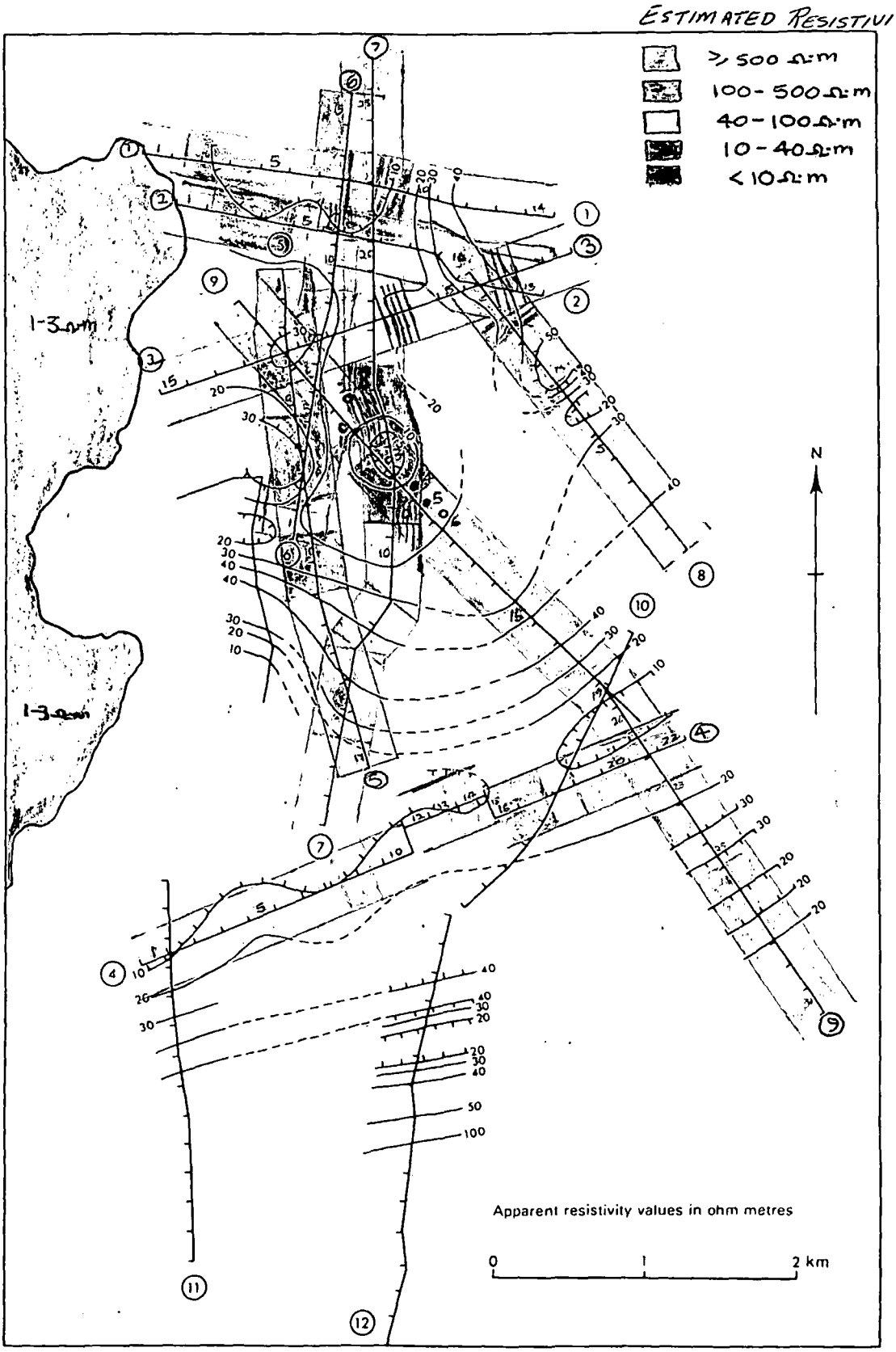

Fig. 4 Soufrière area: Apparent resistivity contours at 200m below sea level

Estimated Intrinsic resistivity, Shallow, 0 - 1a

1)=1-3 response

0-200m

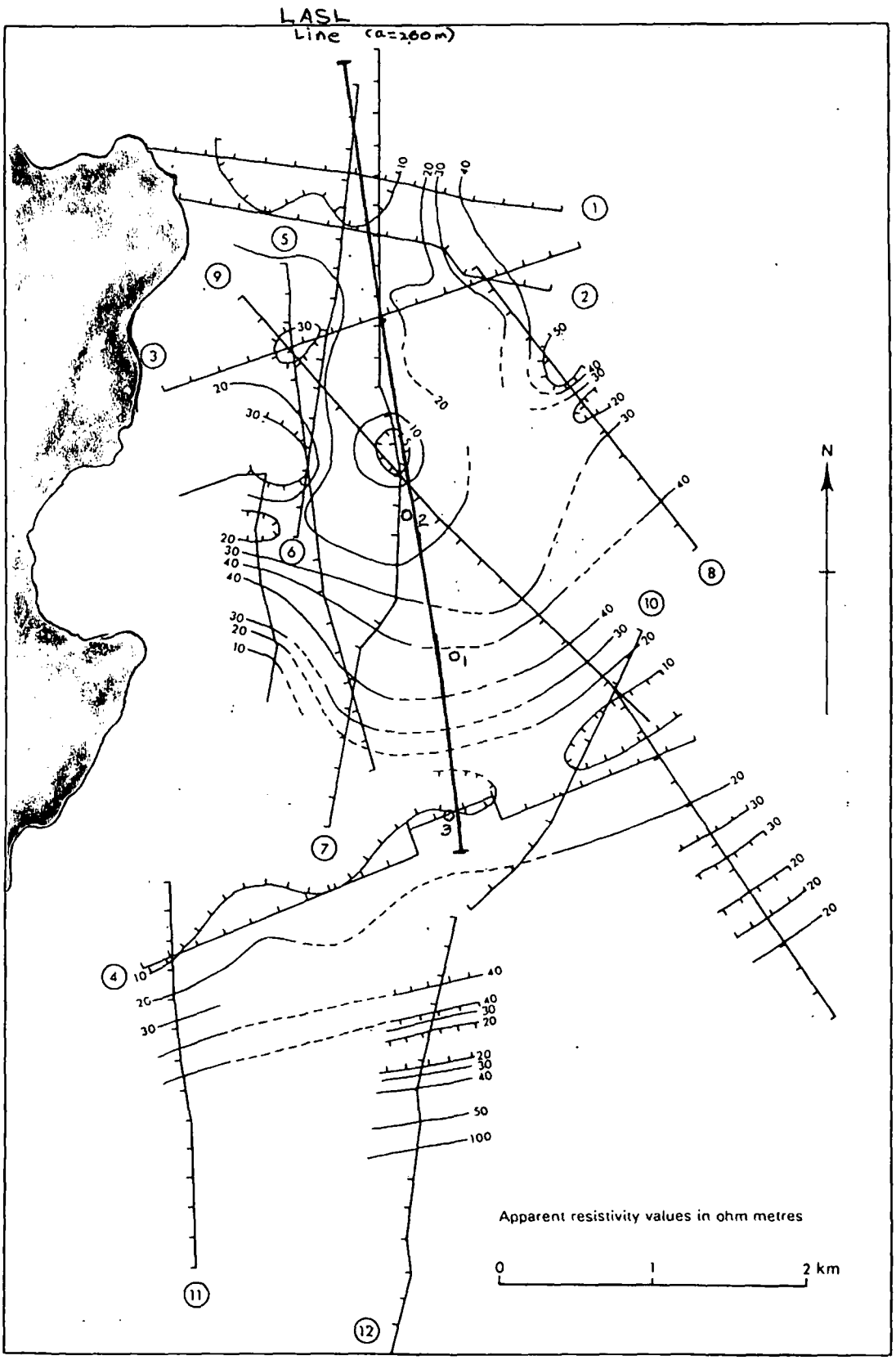

Fig. 4 Soufrière area: Apparent resistivity contours at 200m below sea level

APPENDIX A

Topographic-Effect Resistivity Anomalies for Valley, Ridge, and Slope Models

The apparent resistivity anomalies, in percent, for a valley (V), a ridge (R), and a slope (S), have been computed for slope lengths (SL) of 0.5, 1.0, 1.5, 2.0, 3.0, and 6.0 in units of dipole length and for slope angles (SA) of 10, 20, 30, and 40 degrees. Starting with valley cases, the models are coded in the form V-SL0.5-SA10, etc.

Case	Page	Var. from 100 +	−
V-SL0.5-SA10	A1	+11	1
V-SL1.0-SA10	A2	9	23
V-SL1.5-SA10	A3	15	27
V-SL2.0-SA10	A4	18	27
V-SL3.0-SA10	A5	+22	27
V-SL6.0-SA10	A6	14	18
V-SL0.5-SA20	A7	3	6
V-SL1.0-SA20	A8	20	38
V-SL1.5-SA20	A9	32	46
V-SL2.0-SA20	A10	+40	−45
V-SL3.0-SA20	A11	48	43
V-SL6.0-SA20	A12	23	13
V-SL0.5-SA30	A13	4	7
V-SL1.0-SA30	A14	27	49
V-SL1.5-SA30	A15	49	59
V-SL2.0-SA30	A16	62	58
V-SL3.0-SA30	A17	79	60
V-SL6.0-SA30	A18	49	44
V-SL0.5-SA40	A19	7	5
V-SL1.0-SA40	A20	35	55
V-SL1.5-SA40	A21	70	69
V-SL2.0-SA40	A22	188	67
V-SL3.0-SA40	A23	114	70
V-SL6.0-SA40	A24	66	54
R-SL0.5-SA10	A25	1	3
R-SL1.0-SA10	A26	9	8
R-SL1.5-SA10	A27	29	15
R-SL2.0-SA10	A28	30	18
R-SL3.0-SA10	A29	38	20
R-SL6.0-SA10	A30	21	16
R-SL0.5-SA20	A31	7	7
R-SL1.0-SA20	A32	27	12
R-SL1.5-SA20	A33	74	29
R-SL2.0-SA20	A34	77	33
R-SL3.0-SA20	A35	96	39
R-SL6.0-SA20	A36	57	34
R-SL0.5-SA30	A37	16	7
R-SL1.0-SA30	A38	54	21
R-SL1.5-SA30	A39	141	41
R-SL2.0-SA30	A40	147	48
R-SL3.0-SA30	A41	137	55
R-SL6.0-SA30	A42	114	51
R-SL0.5-SA40	A43	29	10
R-SL1.0-SA40	A44	103	30
R-SL1.5-SA40	A45	259	55
R-SL2.0-SA40	A46	282	62
R-SL3.0-SA40	A47	337	72
R-SL6.0-SA40	A48	213	66
S-SL0.5-SA10	A49	4	4
S-SL1.0-SA10	A50	8	13
S-SL1.5-SA10	A51	13	16
S-SL2.0-SA10	A52	15	17
S-SL3.0-SA10	A53	18	16
S-SL6.0-SA10	A54	10	10
S-SL0.5-SA20	A55	10	9
S-SL1.0-SA20	A56	20	27
S-SL1.5-SA20	A57	29	28
S-SL2.0-SA20	A58	35	29
S-SL3.0-SA20	A59	37	29
S-SL6.0-SA20	A60	8	10
S-SL0.5-SA30	A61	16	10
S-SL1.0-SA30	A62	28	32
S-SL1.5-SA30	A63	45	39
S-SL2.0-SA30	A64	55	40
S-SL3.0-SA30	A65	68	40
S-SL6.0-SA30	A66	37	28
S-SL0.5-SA40	A67	24	14
S-SL1.0-SA40	A68	39	39
S-SL1.5-SA40	A69	65	49
S-SL2.0-SA40	A70	80	48
S-SL3.0-SA40	A71	99	49
S-SL6.0-SA40	A72	51	42

33

St. Lucia - British Well Info.

Well #	Depth	Phys. Prop	
		Cold;	700m No. of Sulphur Springs
1 Fig 15, L&G. LASL, p. 83	~350m 450m ?	66°C @ 450m	
2			LASL Fig. 3, pg. 9.
3 Fig 15, L&G	~125m		
4 L&G, #31, p.1 Fig 15	~600m 612m	Susessful; Steam, 300-360m; 203 °C @ 600m slugs of geothermal brine;	So. of emanations, in extension of Sulphur Springs Valley - Just NE of pLine 9. d-9, d-10
5 L&G, #31, p.1 Fig 15	~725m	Successful; Steam, 300-360m;	Loc. as for Well 4;
6 LASL, p. 66			~ 100 m S of Sulphur Springs
7 LASL, p. 66.			~ 100 m S of Sulphur Springs

DEEP RESISTIVITY MEASUREMENTS IN THE QUALIBOU CALDERA, ST. LUCIA, WEST INDIES

(Mark Ander)

A 5.2-km-long dipole-dipole DC resistivity survey was conducted along a north-south-trending line through the Qualibou caldera from just north of Ruby to just north of Victoria Junction. A nominal dipole length of 200 m was selected to obtain high resolution and measurements were made at a total of 32 electrode stations. To get resistivity data to a depth of 2 km, a 35-kW trailer-mounted DC transmitter was used. The survey was centered over Sulphur Springs and the profile location was selected on the basis of the previous British resistivity investigation and the detailed geologic evaluation performed by Wohletz and Heiken of Los Alamos. The apparent resistivity profile shows similar characteristics to the British dipole-dipole data in the upper 700 m. There is an apparent resistivity high of greater than 1000 ohm-m located below the Belfond area. Beneath this resistivity high, there is deeper low apparent resistivity material that is measured at less than 10 ohm-m. The regions containing less than 10 ohm-m material are highly suggestive of zones containing thermal waters. There is a zone of very low apparent resistivity, less than 1 ohm-m, underlying the Etangs area. The zone beneath Etangs is related to thermal upwelling along a fault, probably the caldera-bounding fault. Beneath Sulphur Springs, starting at a depth of approximately 600 m, there is higher apparent resistivity material ranging from 40 ohm-m up to 150 ohm-m in the center of a 1-km-diameter high-resistivity closure. Interpretation of the data strongly suggests the presence of a very hot dry steam field beneath Sulphur Springs. Based on the deep apparent resistivity data, the recommended drilling sites are at (1) Craters of Belfond, (2) Valley of Sulphur Springs, and (3) Etangs.

I. INTRODUCTION

Direct current (DC) electrical resistivity methods have been employed for geothermal exploration in many countries and have proved to be an invaluable adjunct to the drilling of shallow or deep holes. Numerous case studies indicate that high-quality (>200°C) liquid-dominated geothermal reservoirs are characterized by a resistivity of less than 10 ohm-m. This fact prevails regardless of the resistivity of the host rock, which may be many orders of

magnitude higher in resistivity than that of the high-quality reservoir. Field data from drilled geothermal fields such as Wairakei, Broadlands, East Mesa, Heber, Salton Sea, North Brawley, Niland, Yellowstone, Roosevelt, Dieng, and Kawah Kamojang show remarkable correlations between the resistivity anomaly and the occurrence of an economically viable hydrothermal reservoir (Hatherton et al., 1966; Lumb and MacDonald, 1970; Risk et al., 1970; Risk, 1975; Banwell and MacDonald, 1965; Meidav and Rex, 1970; Meidav and Furgerson, 1972; Meidav et al., 1976; Harthill, 1978).

The range of resistivities of rocks in geothermal environments varies over many orders of magnitude. The electrical resistivity of rocks is affected by six factors: 1) temperature, 2) porosity, 3) degree of fluid saturation of the pore space, 4) salinity of the saturating fluid, 5) pore space geometric factors, and 6) rock matrix resistivity (Keller and Frischnecht, 1966). Rocks such as granite, basalt, limestone and sandstone are essentially infinitely resistive at temperatures of less than 450-500°C. The electrical current conduction in rocks other than clays, shales, or massive metalliferous zones is carried through an electrolyte, or ground water, that fills the pore space. The interrelationship between electrical resistivity and the many factors that may influence it in a geothermal environment is very complex. Fortunately, many of these factors combine to enhance the resistivity contrast of the reservoir making DC resistivity a highly successful geothermal exploration tool.

II. DEEP RESISTIVITY MEASUREMENTS AS A GEOTHERMAL EXPLORATION TOOL

Electrical resistivity is a geophysical technique permitting the determination of the distribution of earth resistivities as a function of depth. Depth control is achieved through control of the geometry and spacing between a set of transmitting electrodes and another set of receiving electrodes. The earth's apparent resistivity (ρ_a) is defined as:

$$\rho_a = 2\pi \frac{V}{I} K$$

where I is the current injected in the ground at the transmitting electrodes, V is the voltage measured at the receiving electrodes, and K is a geometry factor given by:

$$K = \left(\frac{1}{R_{11}} + \frac{1}{R_{22}} - \frac{1}{R_{12}} - \frac{1}{R_{21}} \right) .$$

The R_{ij} are the distances between the ith voltage electrode and jth current electrode. The depth of current flow is a function of the inter-electrode distance. As the electrode distance is expanded, the current is forced to penetrate deeper and deeper into the ground.

The apparent resistivity is that which is measured when the earth is not homogeneous. The apparent resistivity may also be defined as the resistivity of a layered or heterogenous medium relative to the resistivity of a homogeneous medium. To obtain the actual resistivities in a layered or heterogeneous medium, the apparent resistivity data must be computer modeled.

There are many different standard arrays in which the current and voltage electrodes may be placed (Bhattacharya and Patra, 1968; Van Nostrand and Cook, 1966). The dipole-dipole array is often selected because of its ability to obtain an almost continuous cross section to total depth. Because of this, the dipole-dipole array has gained considerable popularity in geothermal exploration. The dipole-dipole array combines horizontal and depth profiling but requires long straight cable runs to achieve results. It is quite sensitive to lateral changes in resistivity. In this method, constant dipole lengths are usually employed for the transmitter and receiver dipoles. For geothermal exploration, dipole lengths of 200-1000 m are characteristic, although both shorter and longer spacings have been used.

A. Previous Resistivity Studies on St. Lucia

Shallow resistivity studies have been carried out in the Qualibou caldera of St. Lucia by the Institute of Geological Sciences, London, England (Greenwood and Lee, 1976). They performed 13 dipole-dipole DC resistivity profiles throughout the region, obtaining data to a maximum depth of 700 m. Low apparent resistivity values were found in the north around Soufrière, La Pearle, and Cresslands and other areas generally north of Sulphur Springs. Additional lows were centered in the south around Belle Plaine, Etangs, and Fond Doux. Apparent resistivity highs were associated with the Belfond area and beneath Sulphur Springs, starting at a depth of 600 m. The typically low apparent resistivity values are associated with the geothermal system. It was

suggested that the higher values seen at depths beneath the Sulphur Springs area may be due to a steam field.

B. Field Operations in the Qualibou Caldera

After evaluating all available data, Los Alamos performed a deep resistivity survey (to a depth of 2.0 km) centered on Sulphur Springs. The profile location was determined based on the previous British resistivity study and a geologic study performed by the Los Alamos National Laboratory. The decision was made to run a 5.2-km-long, north-south trending, dipole-dipole DC resistivity profile from just north of Ruby to just north of Victoria Junction (Fig. 1). This profile traverses extreme topography and dense jungle and was conducted during January 1984.

A nominal dipole length of 200 m was selected for the St. Lucia survey to obtain high resolution. Because of the difficult terrain on St. Lucia, it was impossible to keep a constant 200-m spacing. Two short regions along the profile have electrode spacings of less than 100 m, giving even higher resolution in these critical areas. The 5.2-km-long profile line across the Qualibou caldera contained a total of 32 electrode stations as depicted in Fig. 1.

To get resistivity data to a depth of 2 km, a 35-kW trailer-mounted DC transmitter (Fig. 2) was used. This transmitting system was built by the Los Alamos National Laboratory and is designed to handle high current output, up to 70 amps peak-to-peak, over a single dipole or to automatically alternate high current output over two separate dipoles. This capability permits the transmitter to be easily used in a wide variety of DC resistivity methods requiring both single and multiple current electrodes. The transmitter operates with an input of 440 to 480 V AC, three phase, 50 to 60 Hz at 35 amps or less. The transmitter output can be selected from 0 to 1000 V DC and from 0 to 70 amps peak-to-peak (maximum current is not available at maximum voltage). The output current is reversed positive/negative (to produce a square wave) at selectable times of 1 to 99 seconds. The negative current is selected so that it may have either the same duration as the positive current, or twice the positive current, thus allowing for polarity identification.

Figure 3 shows an electrical block diagram of the DC resistivity transmitter and Table I contains the detailed transmitter specifications. The

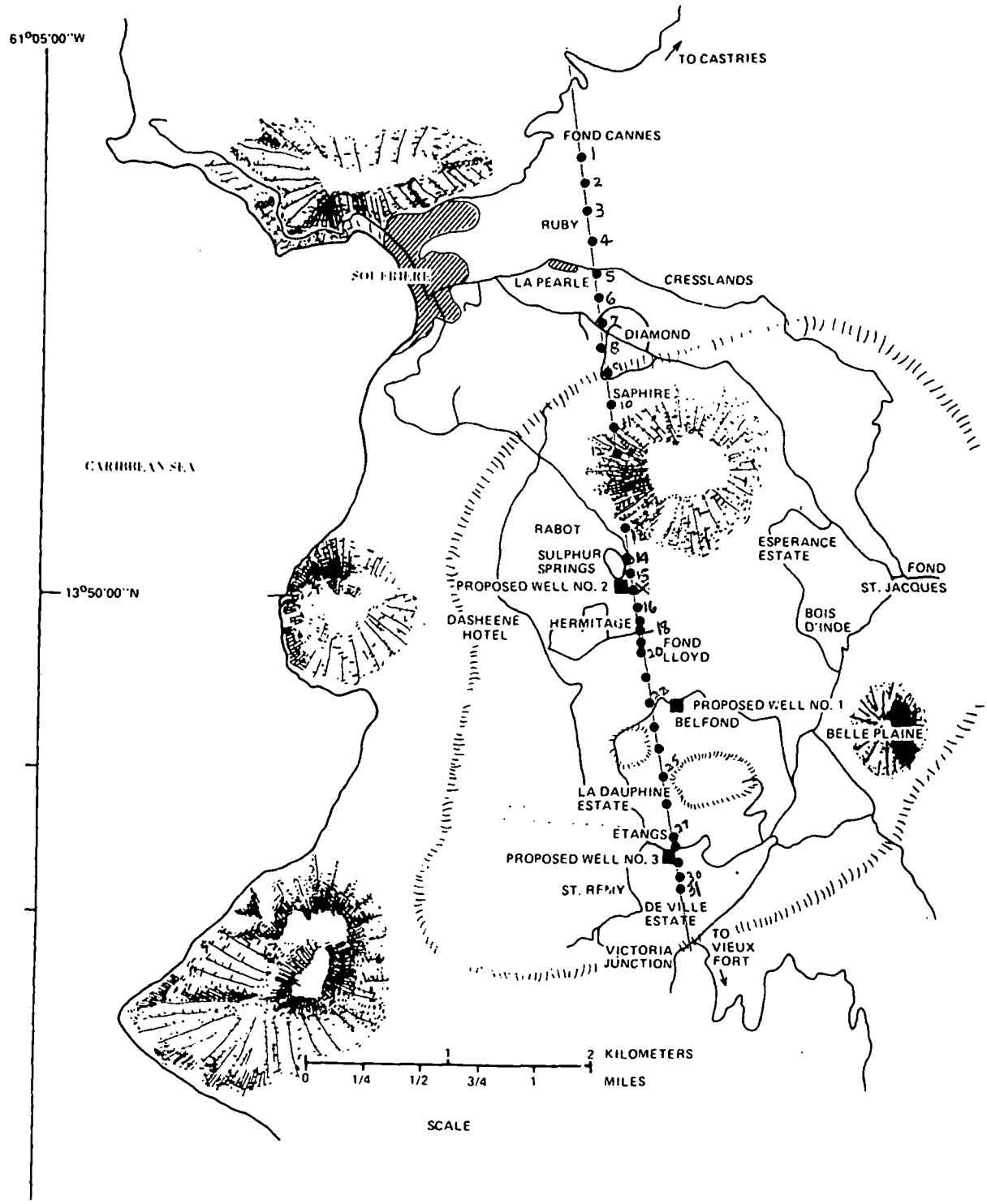

Fig. 1.
Location of the 5.2-km-long resistivity profile line (containing 32 electrode stations) across the Qualibou caldera.

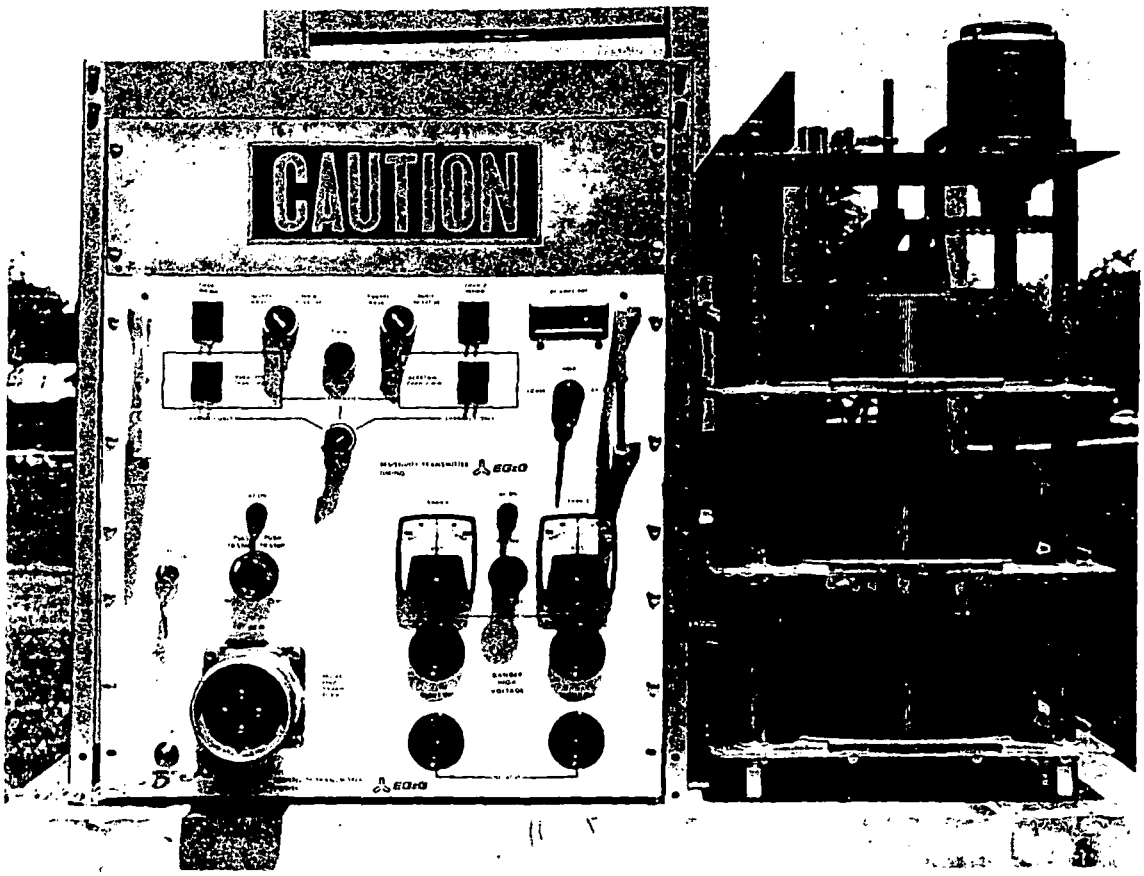

Fig. 2.
Photograph of the DC resistivity transmitter showing operator's console.

DC transmitter is powered by a trailer-mounted 60-kW diesel generator. The generator output is 480 V, 60 Hz, three phase.

Each of the four portable voltage measuring units (Fig. 4) consists of a voltage strip chart recorder and a DC voltage bucking box. The strip chart recorder and bucking box is shock mounted in a small portable aluminum transportainer. They are designed to apply a DC offset voltage to the incoming signal before it is plotted on the strip chart recorder. This is necessary to keep the measurements on scale because the currents produced by the DC transmitter (signal) are superimposed on natural earth currents (noise) known as telluric currents, which rapidly fluctuate in magnitude. Telluric currents have several sources. The two most important are inductions from the motion of charged particles in the ionosphere and the motion of charged

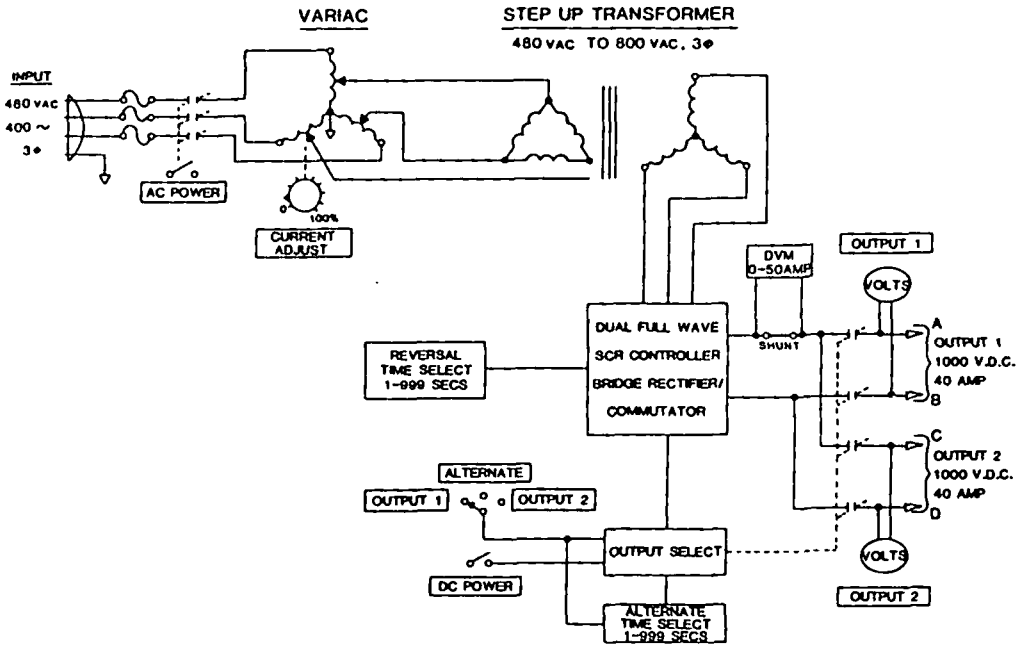

Fig. 3.
Electrical block diagram of the DC resistivity transmitter.

TABLE I

DEEP DC RESISTIVITY TRANSMITTER SPECIFICATIONS

INPUT:	440-480 VAC line-to-line Three phase WYE pulse neutral 50/60 Hz 35 amps 40 kVA or less
OUTPUT:	Adjustable 0 to 1000 VDC, isolated from input Ripple voltage less than 1%, at 720 Hz 0 to 70 amps peak-to-peak (max current not available at max voltage Two independent outputs isolated from chassis, each controllable as follows: - Output current reversed positive/negative at selectable time of 1-99 seconds. - Negative current selected for same or double the duration of the positive current. - Output on time selectable for 1-99 minutes. Either output may be selected, or the outputs may alternate at independently selected time durations.
SIZE:	Approximately 3 ft x 3 ft x 4 ft enclosed
WEIGHT:	Approximately 1500 lb (without trailer)
CONTROLS:	AC power on/off (panic button OFF) DC power on/off (panic button OFF) Digital OUTPUT CURRENT meter, 0-50 amp, 0.1 amp resolution Bipolar analog voltmeters on each output (2), ± 1000 V Output Select - Output 1 - Alternate - Output 2 Output 1 on time select 1-99 minutes Output 2 on time select 1-99 minutes Output 1 current reversal time select 1-99 seconds Output 2 current reversal time select 1-99 seconds Negative current time Normal/Doubled RESET TIME

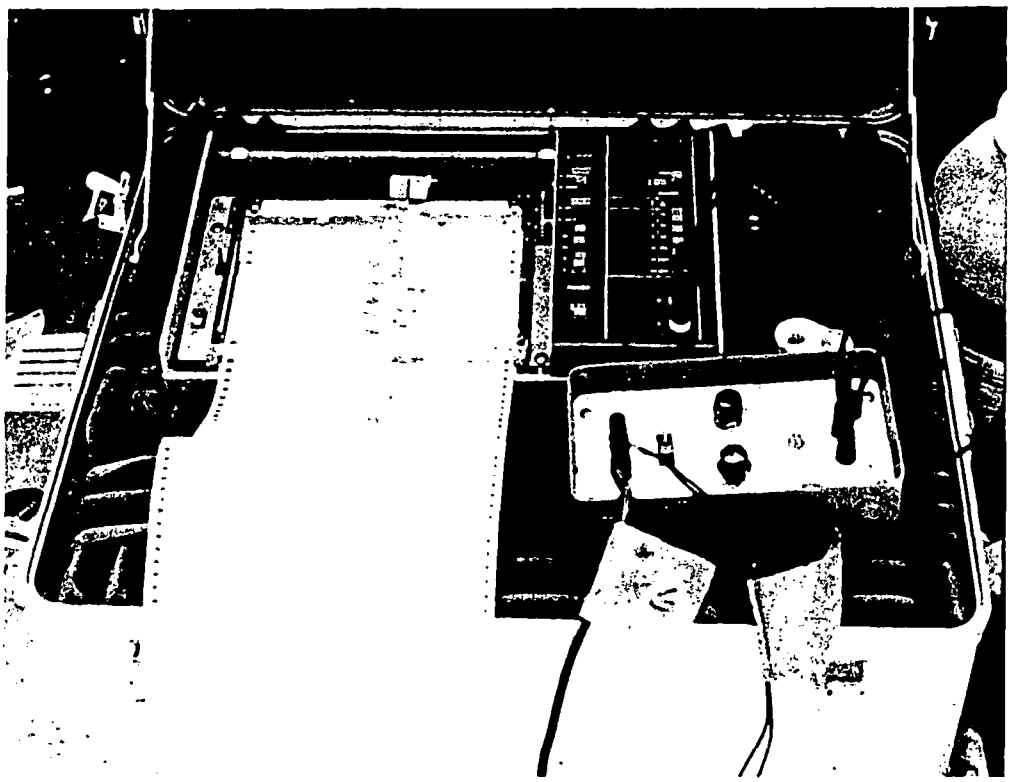

Fig. 4.
Photograph of a portable measuring unit showing voltage strip chart recorder and DC voltage bucking box.

clouds. The smallest signal that can be recorded by this receiving system is 2μV. The receiver system is powered by an internal rechargeable Ni-Cd battery, which gives approximately 10 hours of continuous use on a single charge.

How are data converted to depth?

III? RESISTIVITY DATA

The resulting apparent resistivity data from the dipole-dipole soundings are plotted as a function of depth in Fig. 5 (a plot of apparent resistivity versus depth is called a pseudosection). Also shown for comparison in Fig. 5 is the geologic cross section A-A' developed by Los Alamos. The geologic cross section is oriented approximately 10° counterclockwise relative to the dipole-dipole apparent resistivity cross section, with the sections intersecting at Sulphur Springs.

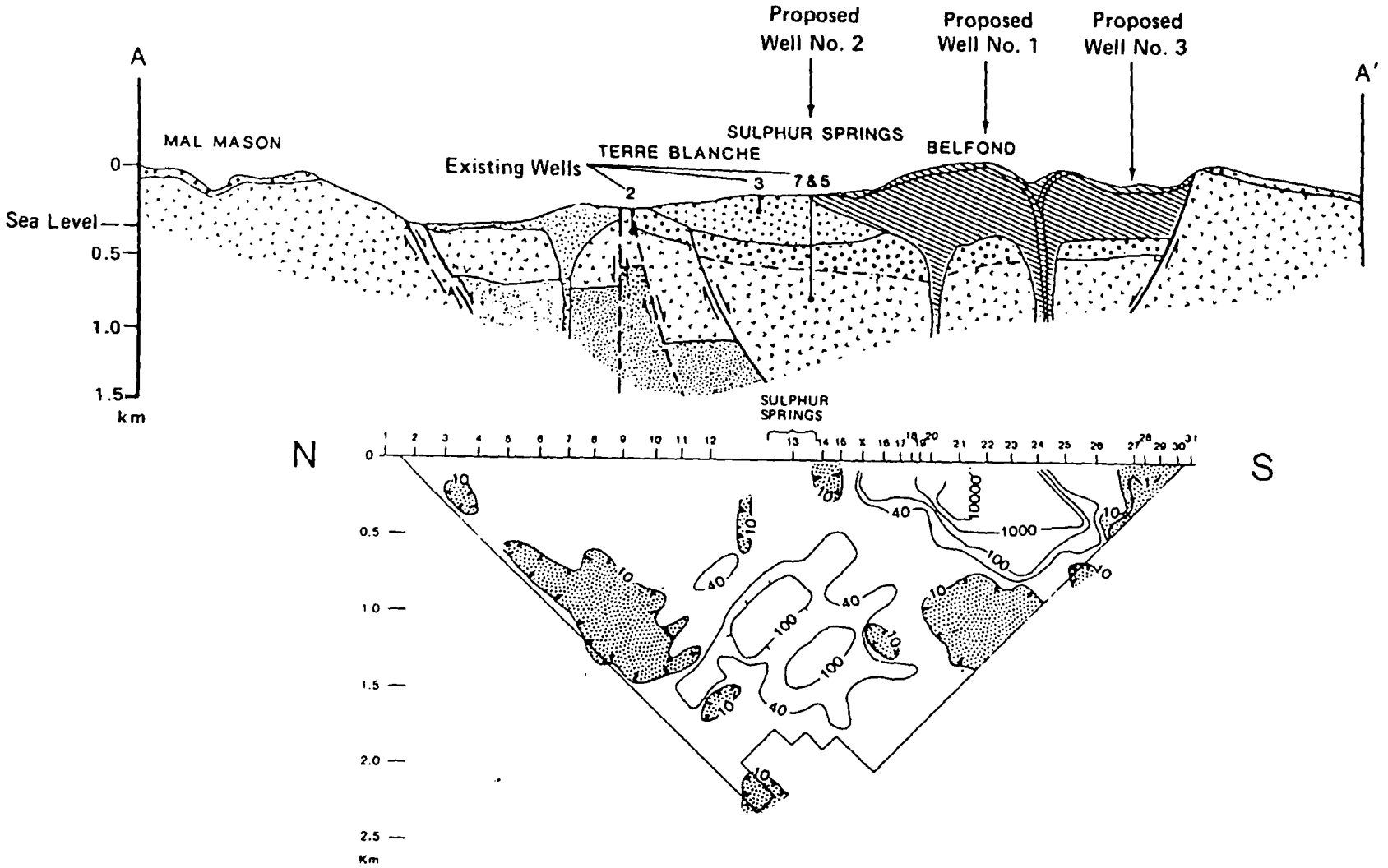

Fig. 5.
Apparent resistivity data from the dipole-dipole survey plotted as a function of depth. Resistivity values are in ohm-m and are shown beneath the appropriate geologic cross section. Shaded areas depict resistivity contours of 10 ohm-m or less.

The upper 700 m of the pseudosection shows similar characteristics to the British dipole-dipole data. In general, there is conductive material with a resisitivity less than 40 ohm-m located to the north of Sulphur Springs. There is an apparent resistivity high, greater than 1000 ohm-m, located below the Belfond area. Beneath this resistivity high, there is deeper low apparent resistivity material that is measured at less than 10 ohm-m. There is a zone of very low resistivity, less than 1 ohm-m, underlying the Etangs area. Beneath Sulphur Springs and starting at a depth of approximately 600 m, there is higher apparent resistivity material ranging from 40 ohm-m up to 150 ohm-m in the center of a 1-km-diameter high apparent resistivity closure.

IV. INTERPRETATION OF RESISTIVITY DATA

There are some interrelated interpretations possible from the apparent resistivity data. The regions containing less than 10 ohm-m material are highy suggestive of zones containing thermal waters. The zone beneath Etangs, containing material of less than 1 ohm-m, is related to thermal upwelling along a fault, probably the caldera-bounding fault, mapped earlier by Los Alamos geologists between Etangs and Belfond. A swampy area (at electrodes 30 and 31) located on a hillside with good drainage could be a surface manifestation of the fluid upwelling. The highly resistive shallow block associated with the Belfond area is a zone devoid of fluid penetration. It is fault bounded to the south and may also be fault bounded to the north. Beneath this highly resistive block, however, is a large zone of low apparent resistivity material (less than 10 ohm-m) that strongly suggests the presence of a large thermal reservoir. This region could not have been identified without the use of the deep DC resistivity survey. The location of Sulphur Springs is believed to be entirely fault controlled.

Based on the resistivity data alone, the deep higher resistivity zone located beneath Sulphur Springs can be interpreted in two ways: (1) the higher resistivity layer is due to a very not dry steam field; wet steam fields typically have resistivities around 30-60 ohm-m, while very hot dry steam fields can reach the higher resistivities measured in this area, (2) the higher resistivity zone beneath Sulphur Springs is due to a more

fluid impermeable caprock. The presence of steam in four of the seven shallow drill holes around Sulphur Springs and results from the hydrogeochemical studies suggest that the first interpretation is correct. The region between the two resistive zones (deep under Sulphur Springs and shallow under Belfond) most probably represents a fault along which thermal fluids are moving up dip from south to north to emerge in Sulphur Springs at the surface. This would suggest that the geothermal reservoir that feeds Sulphur Springs is located to the south beneath Belfond. This model is supported by the presence of upwelling, fault-controlled fluids in the Etangs area.

boiling at the water table ?

V. RECOMMENDATIONS FOR DRILLING IN THE QUALIBOU CALDERA

Based on the interpretation of the deep resistivity data, the following drilling recommendations are made:

(1) Craters of Belfond. The first well should be drilled in the Belfond area, preferably close to the location of the Belfond dance hall because of the ease of access for a drilling rig. The well is expected to encounter dry volcanic materials to a depth of 600-900 m where it is expected to pass through an impermeable hydrothermal boundary into a geothermal brine.

(2) Valley of Sulphur Springs. The second well should be drilled in the valley of Sulphur Springs, preferably south of the area of surface manifestations. This well is expected to encounter very hot dry steam between 600-1700 m and a geothermal brine by approximately 1800 m. It is also possible that a more impermeable, less fluid-bearing rock will be encountered instead of a steam zone above the deeper lying brine reservoir.

(3) Etangs. The third well should be drilled in the Etangs area, preferably south of the road near the Nutmeg Bar. This well should pass through the southern caldera-bounding fault and is expected to encounter geothermal fluids at shallow depths associated with the fault. The depth of the reservoir in this location could be as shallow as 1000 m.

REFERENCES

Banwell, C. J. and MacDonald, W. J. P., 1965. Resistivity surveying in New Zealand geothermal areas. Eighth Commonwealth Mining and Metallurgical Congress, Australia and New Zealand.

Bhattacharya, P. K. and Patra, H. P., 1968. Direct Current Geoelectric Sounding. Elsevier, 153 pp.

Greenwood, P. G. and Lee, M. K., 1976. Geophysical surveys in St. Lucia for geothermal resources. Institute of Geological Sciences, London, UK, 30 pp.

Harthill, N., 1978. A quadripole resistivity survey of the Imperial Valley, California. Geophysics 42: 1485-1500.

Hatherton, T., MacDonald, W. J. P., and Thompson, G., 1966. Geophysical methods in geothermal prospecting in New Zealand. Bull. Volcanalogique 29: 485.

Keller, G. V. and Frischnecht, F. C., 1966. Electrical Methods in Geophysical Prospecting. Pergamon Press, 519 pp.

Lumb, J. T. and MacDonald, W. J. P., 1970. Near surface resistivity surveys of geothemal areas using the electromagnetic method. Geothermics Special Issue 2: 311.

Meidav, T. and Rex, R. W., 1970. Geophysical investigations for geothermal resources, Imperial Valley, California, Phase 1: 1968 field project. Inst. of Geophysics and Planetary Physics, University of California, Riverside.

Meidav. T. and Furgerson, R., 1972. Electrical resistivity for geothermal exploration in the Imperial Valley. Geothermics 1(2): 47-62.

Meidav, T., West, R., Katzenstein, A., and Rotstein, Y., 1976. An electrical resistivity survey of the Salton Sea Geothermal Field Imperial Valley, California. Lawrence Livermore Laboratory.

Risk, G. F., MacDonald, W. J. P., and Dawson, G. B., 1970. D.C. resistivity surveys of the Broadlands geothermal region, New Zealand. Proceedings Second U.N. Symposium on the Development and Use of Geothermal Resources, San Francisco.

Risk, G. F., 1975. Monitoring the boundary of the Broadlands geothermal field, New Zealand. Proceedings Second U.N. Symposium on the Development and Use of Geothermal Resources, San Francisco.

Van Nostrand, R. G. and Cook, K. L., 1966. Interpretation of resistivity data. U.S. Geol. Surv. Prof. Paper 499, 310 pp.

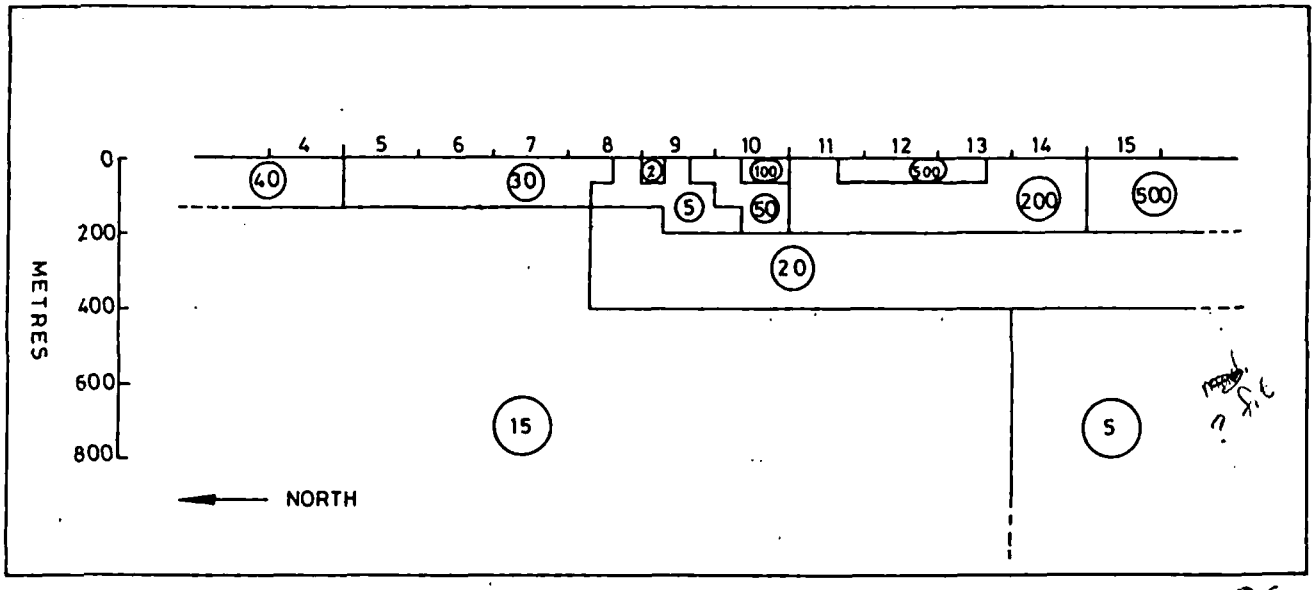

Fig. 11. Line 9 - true resistivity model 5

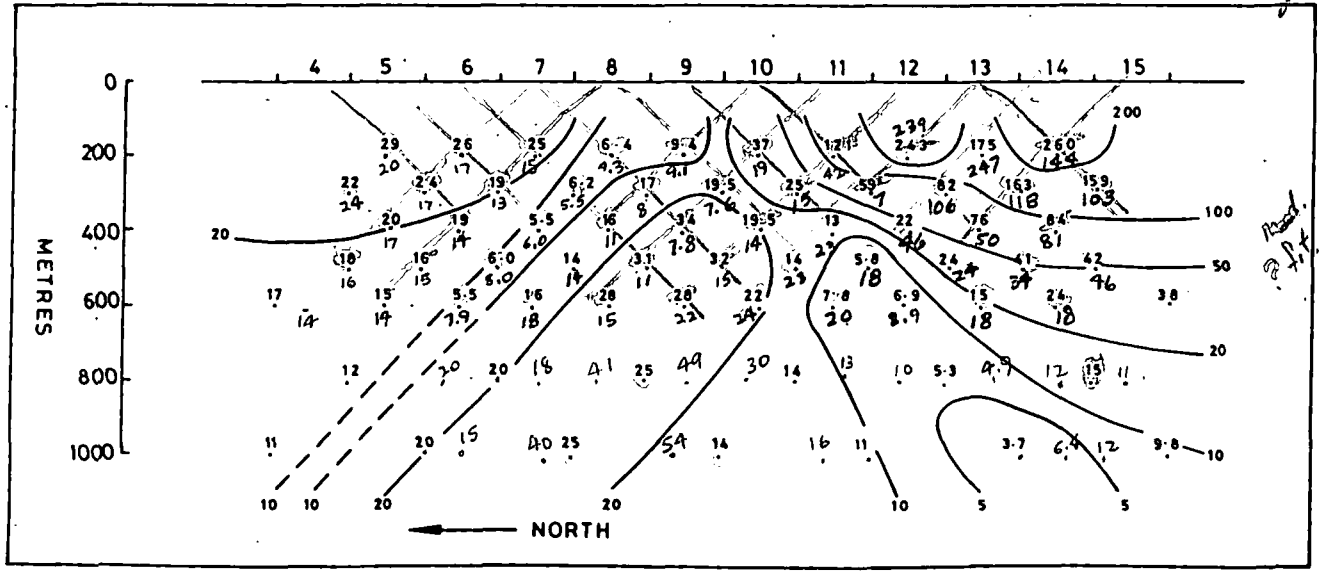

Fig. 12. Line 9 - computer generated section due to model 5

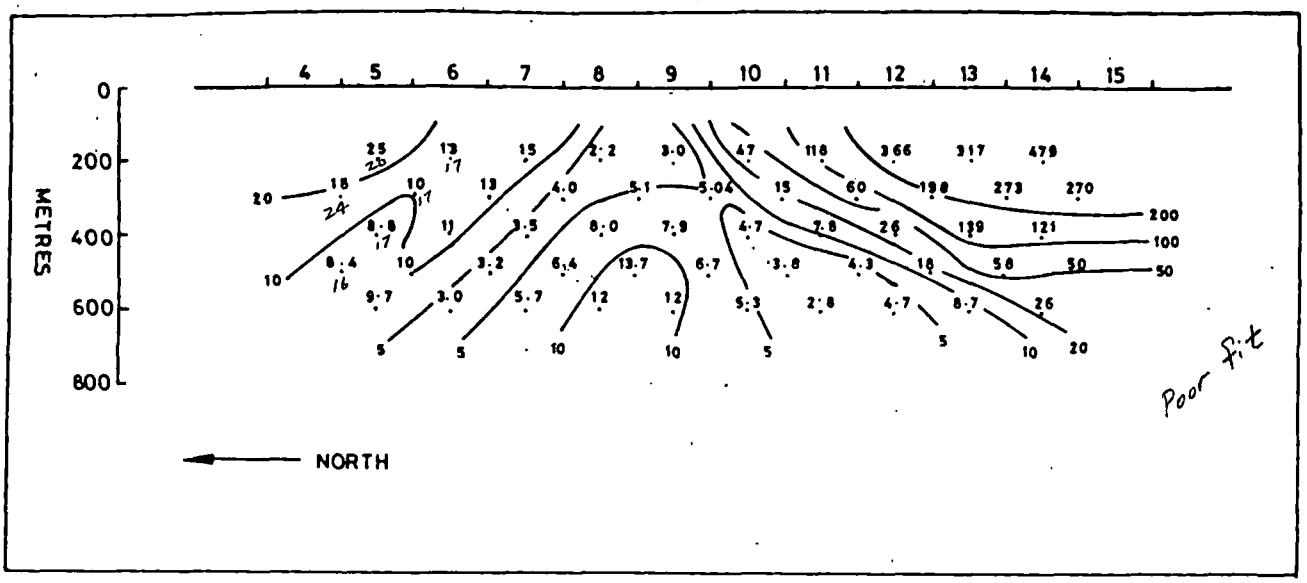

Fig. 4. Line 9 - computer generated section due to model 1

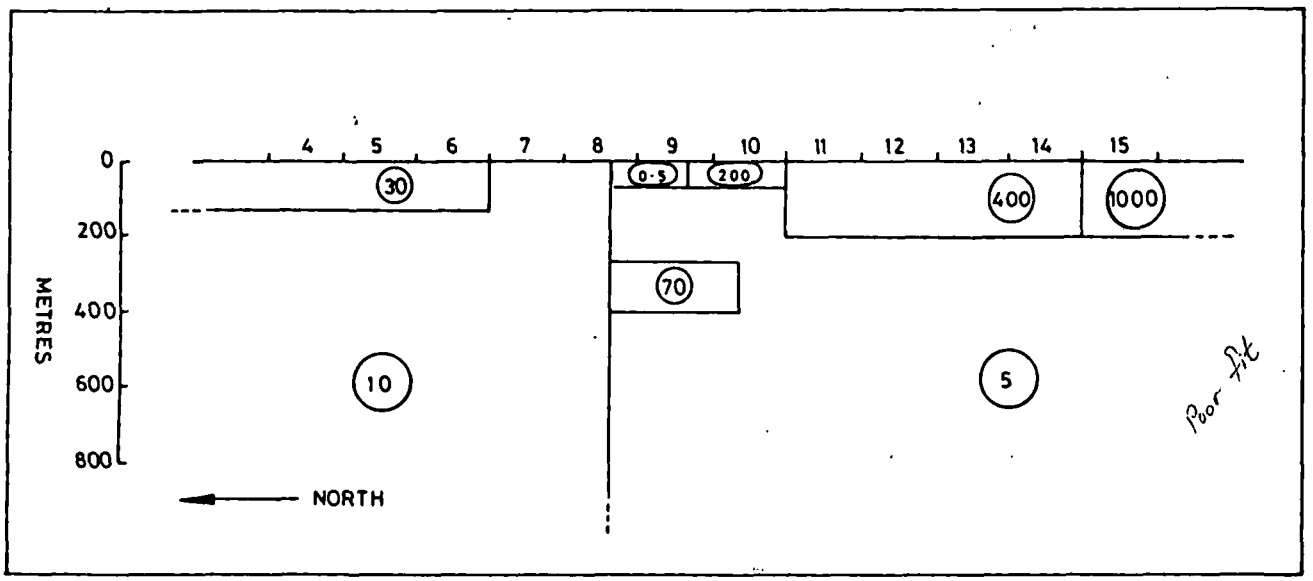

Fig. 5. Line 9 - true resistivity model 2

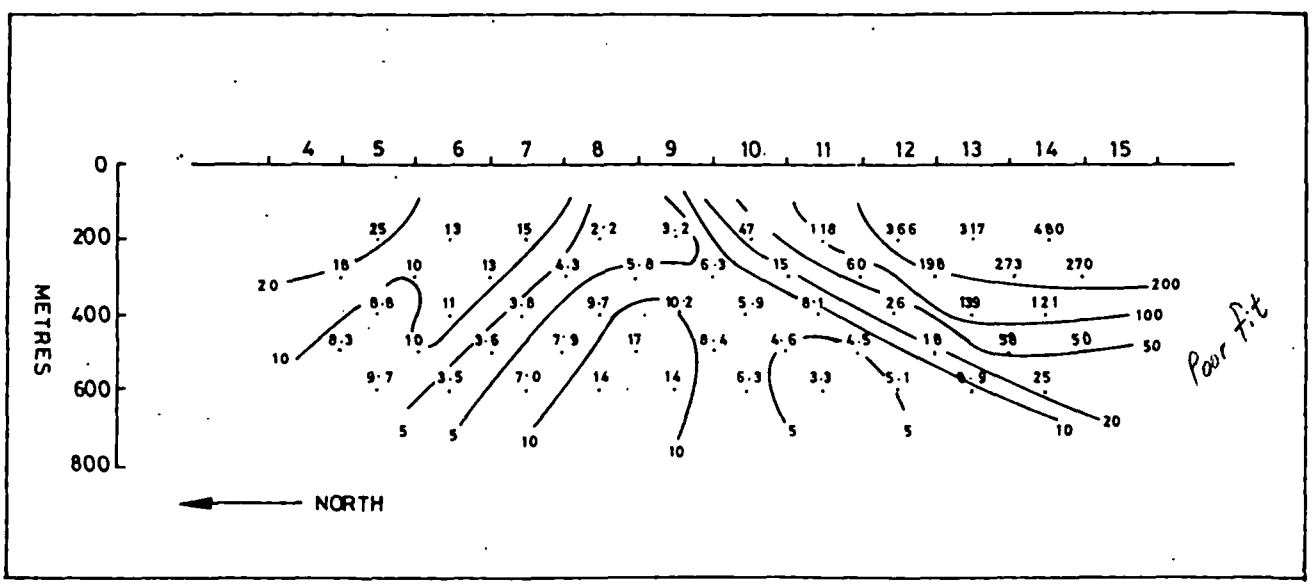

Fig. 6. Line 9 - computer generated section due to model 2

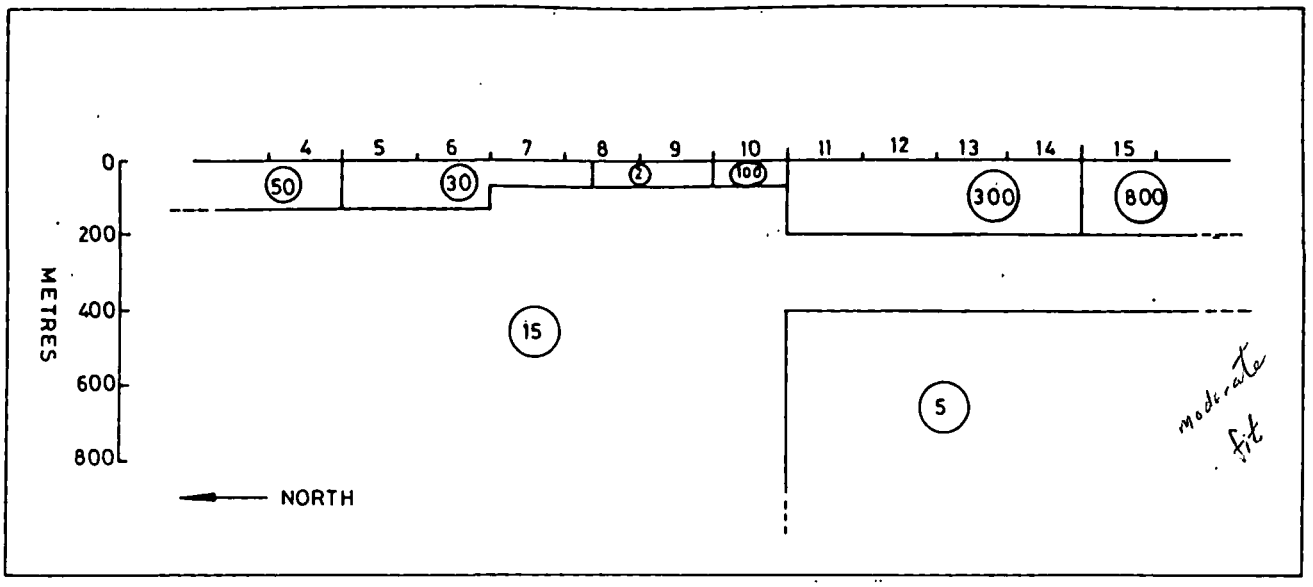

Fig. 7. Line 9 - true resistivity model 3

Computed two la
Computed two lay
good fit ± 20%

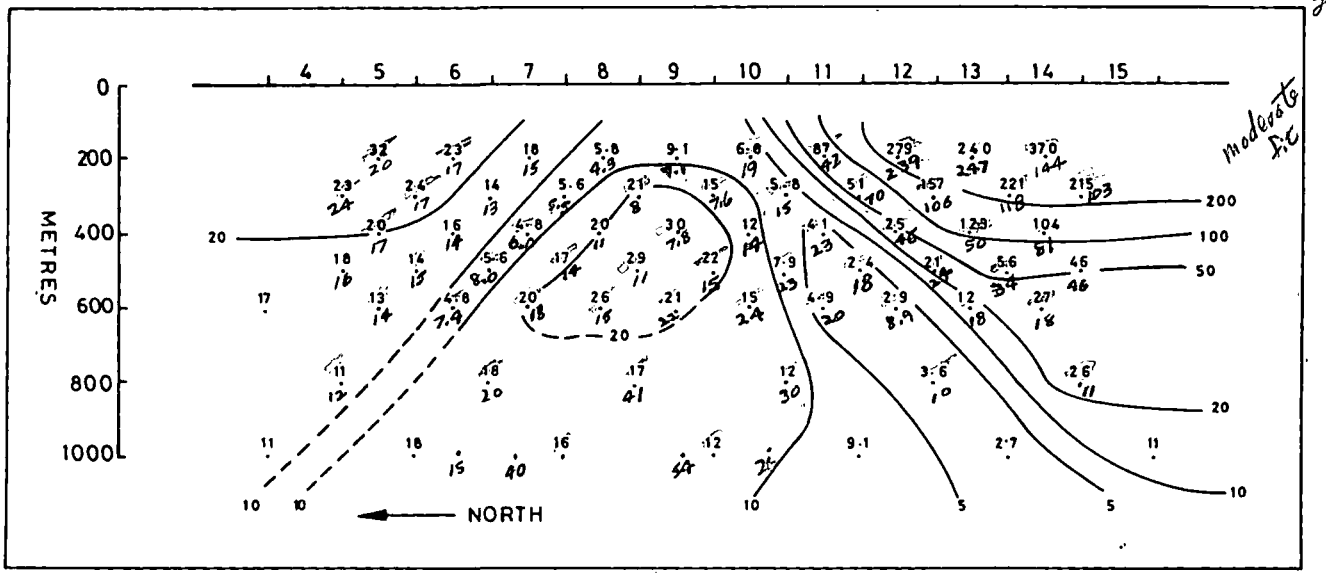

Fig. 8. Line 9 - computer generated section due to model 3

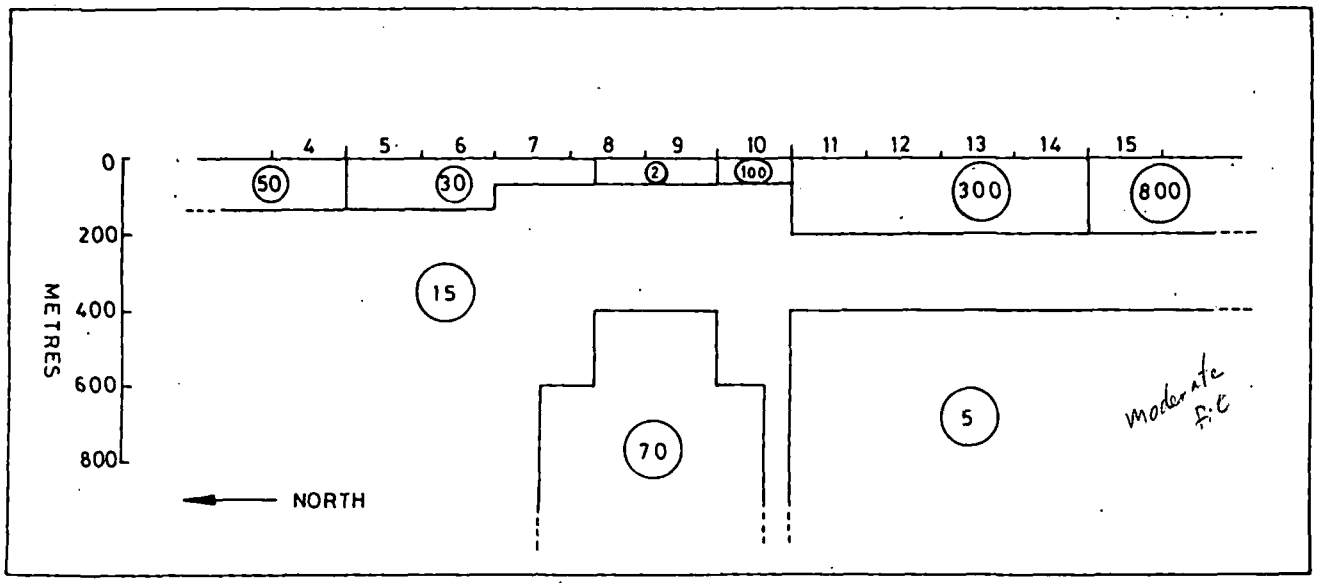

Fig. 9. Line 9 - true resistivity model 4

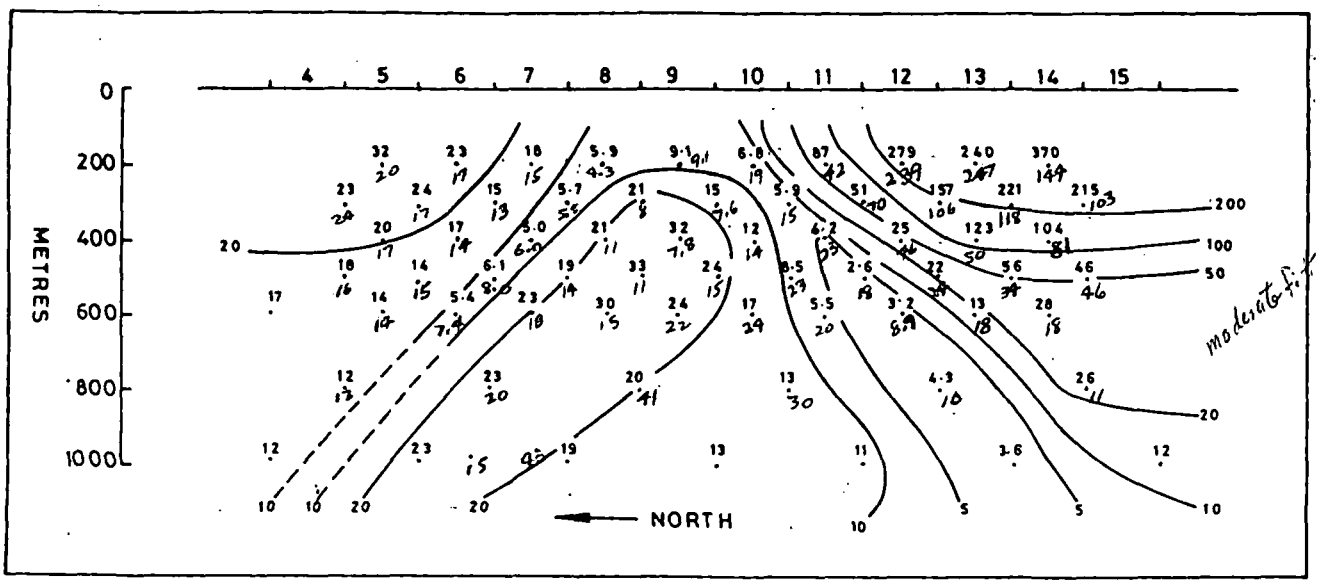

Fig. 10. Line 9 - computer generated section due to model 4

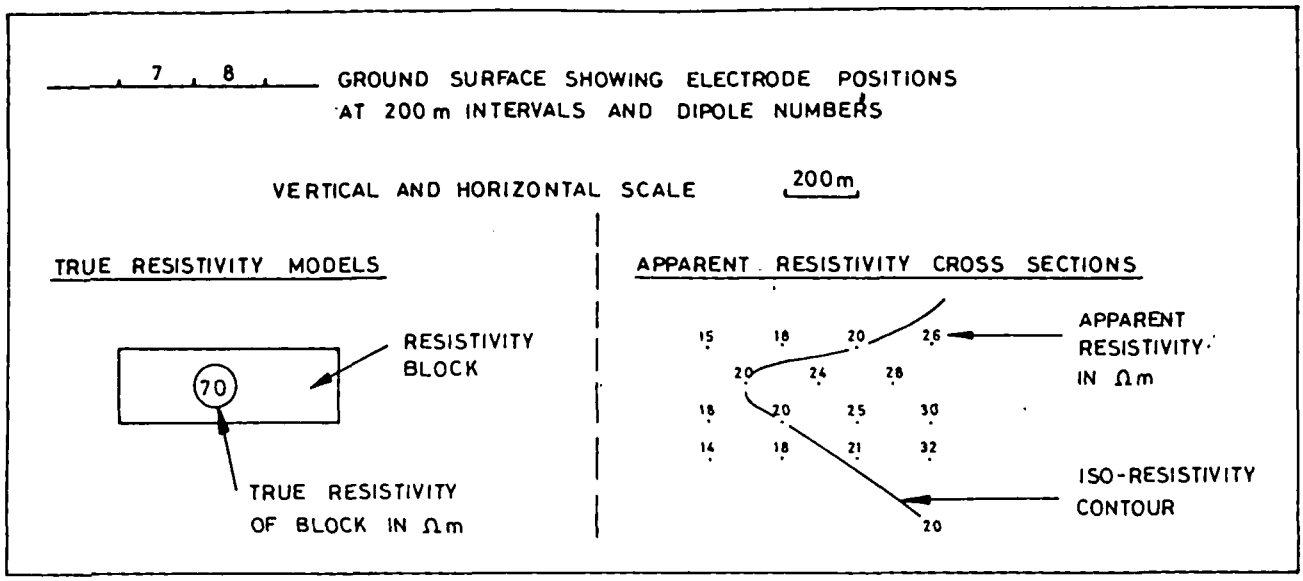

Fig. 1. Key to Figs. 2 to 14

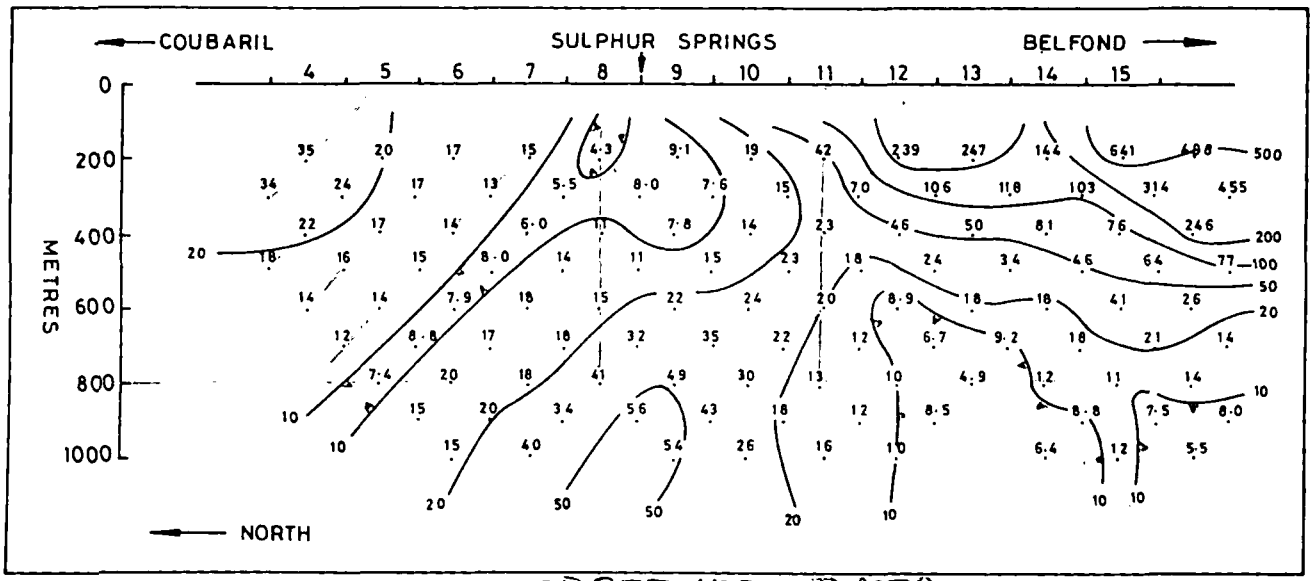

OBSERVED DATA

Fig. 2. Line 9 - apparent resistivity cross-section

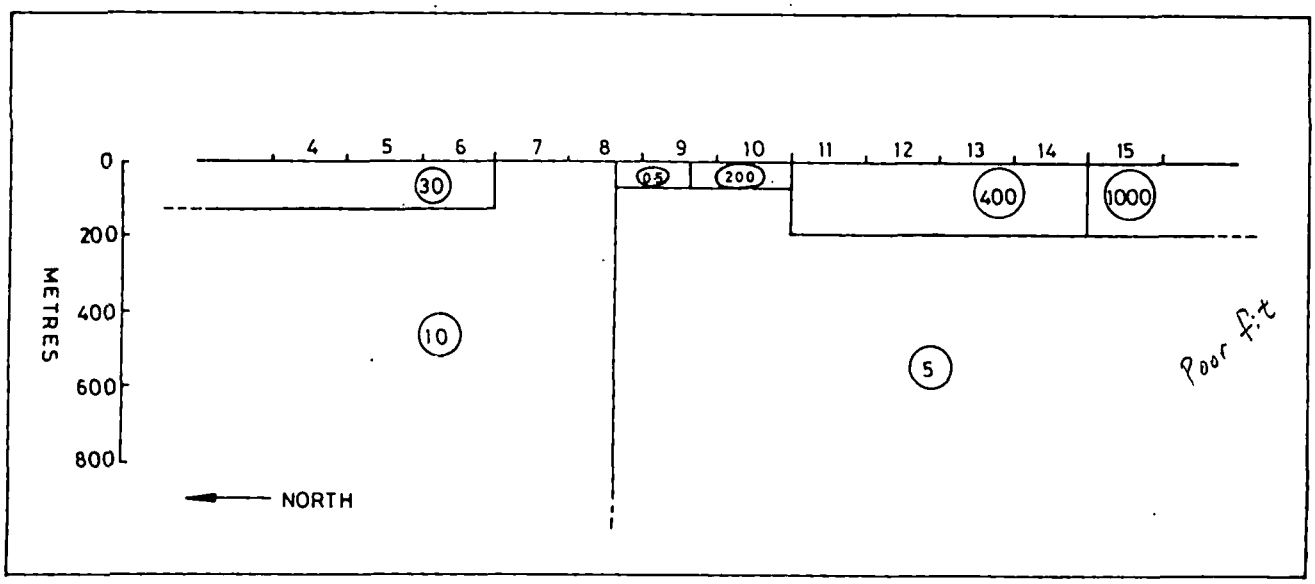

Fig. 3. Line 9 - true resistivity model 1

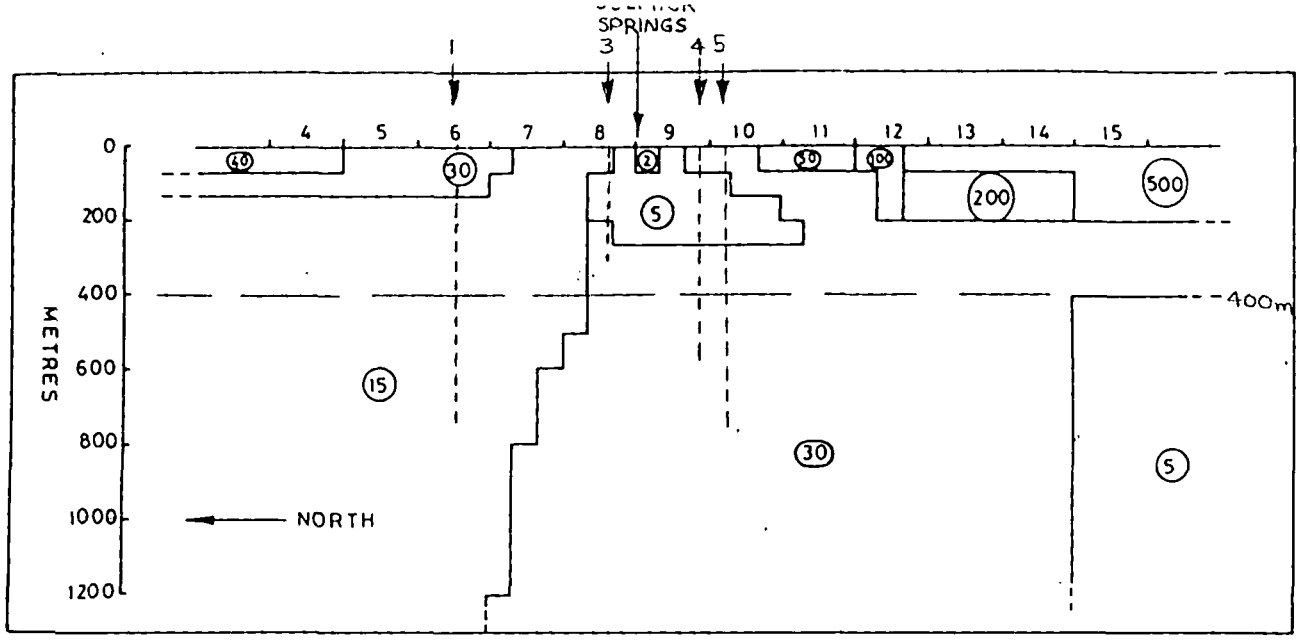

Fig. 2a Line 9 - true resistivity model 6

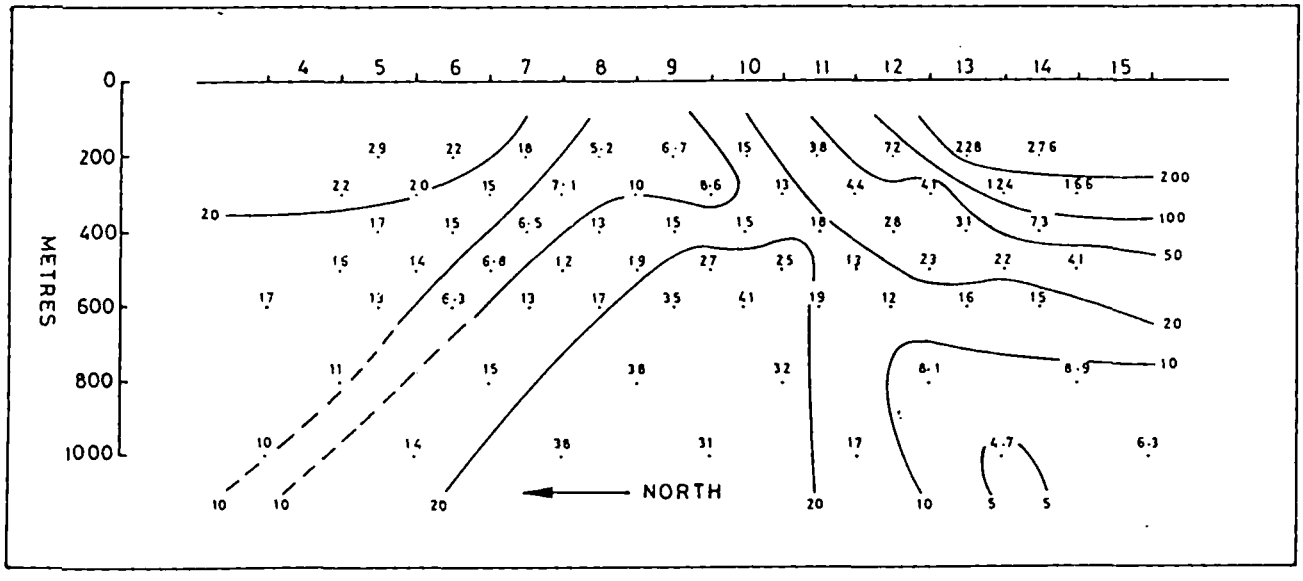

Fig. 2b Line 9 - computer generated section due to model 6

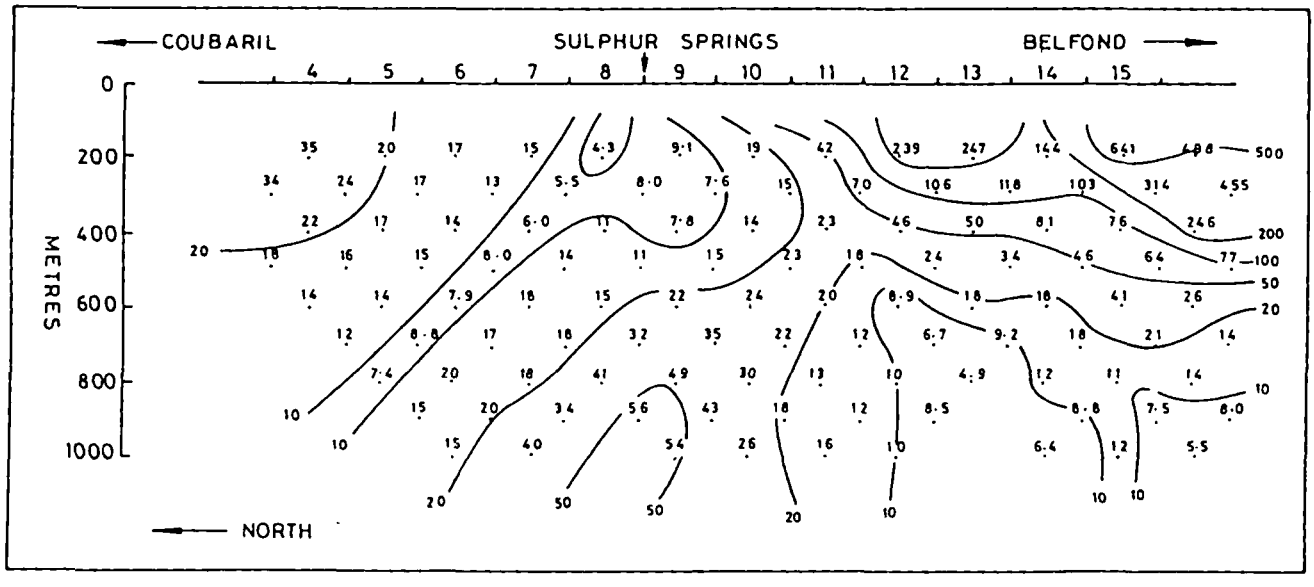

Fig. 2c Line 9 - apparent resistivity cross-section - observed

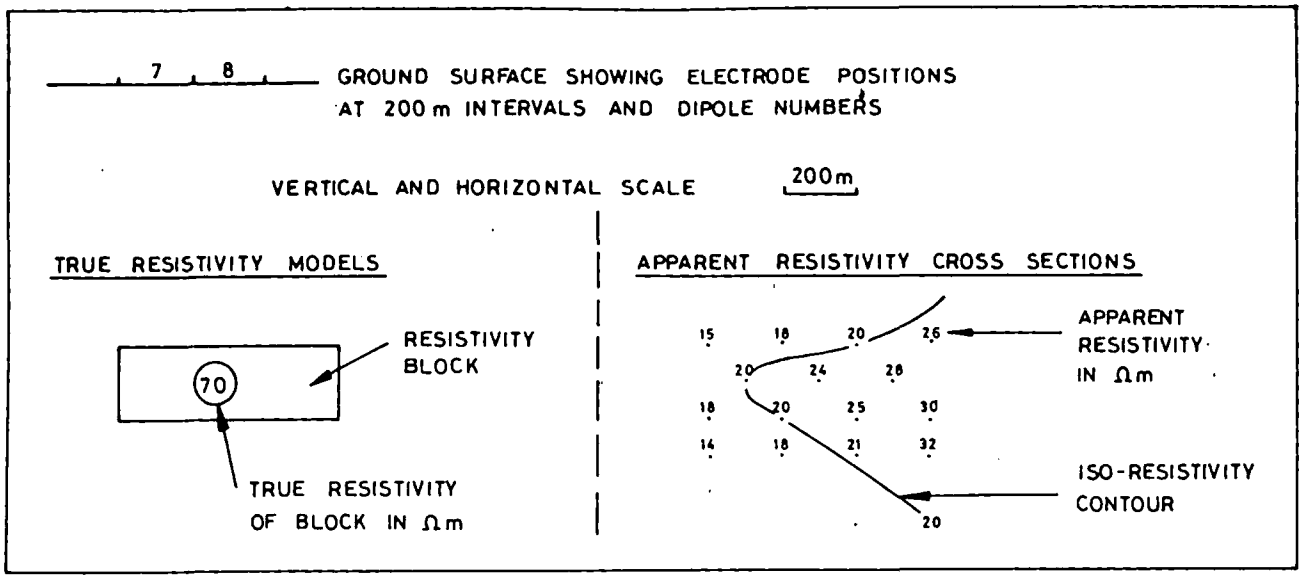

Fig. 1. Key to Figs. 2 to 14

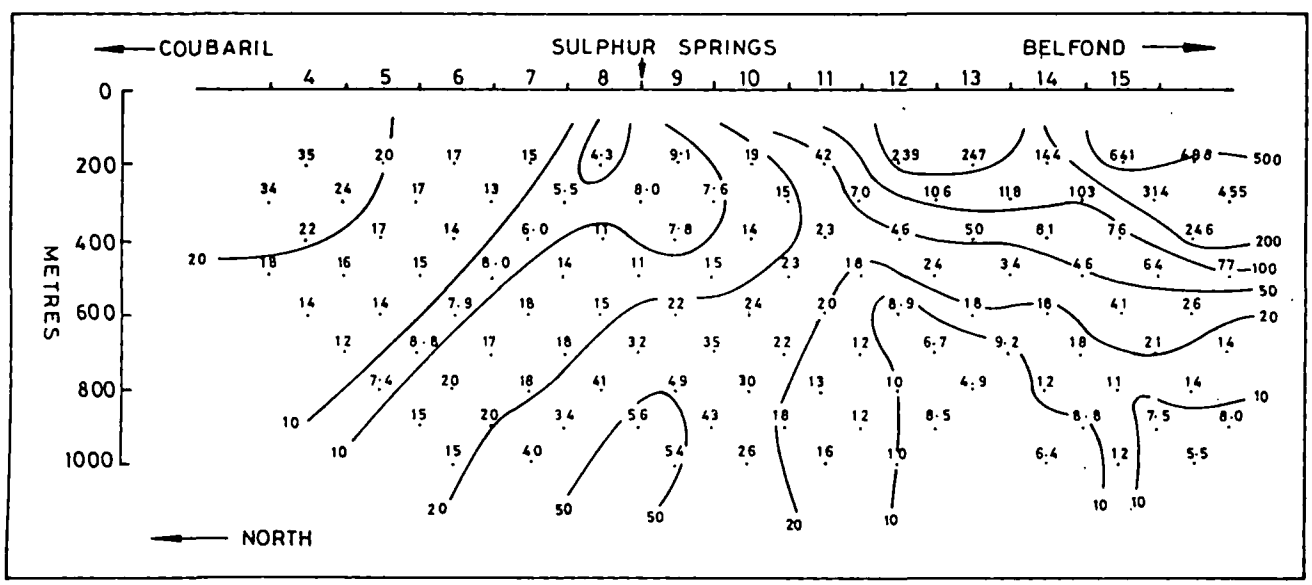

Fig. 2. Line 9 - apparent resistivity cross-section

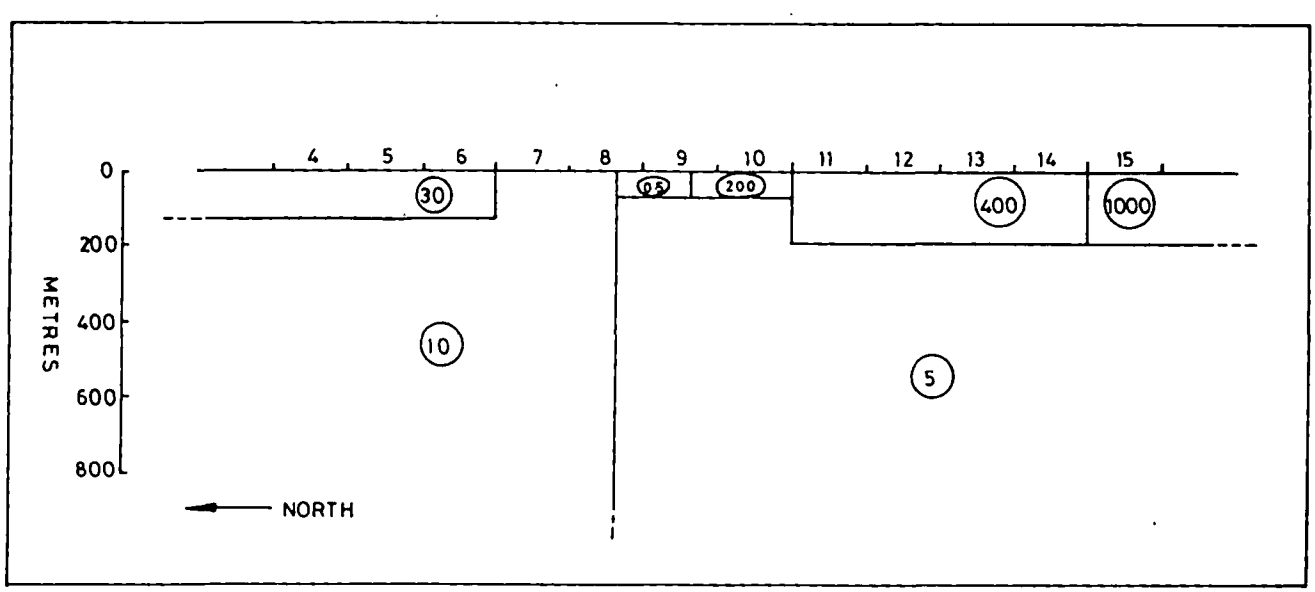

Fig. 3. Line 9 - true resistivity model 1

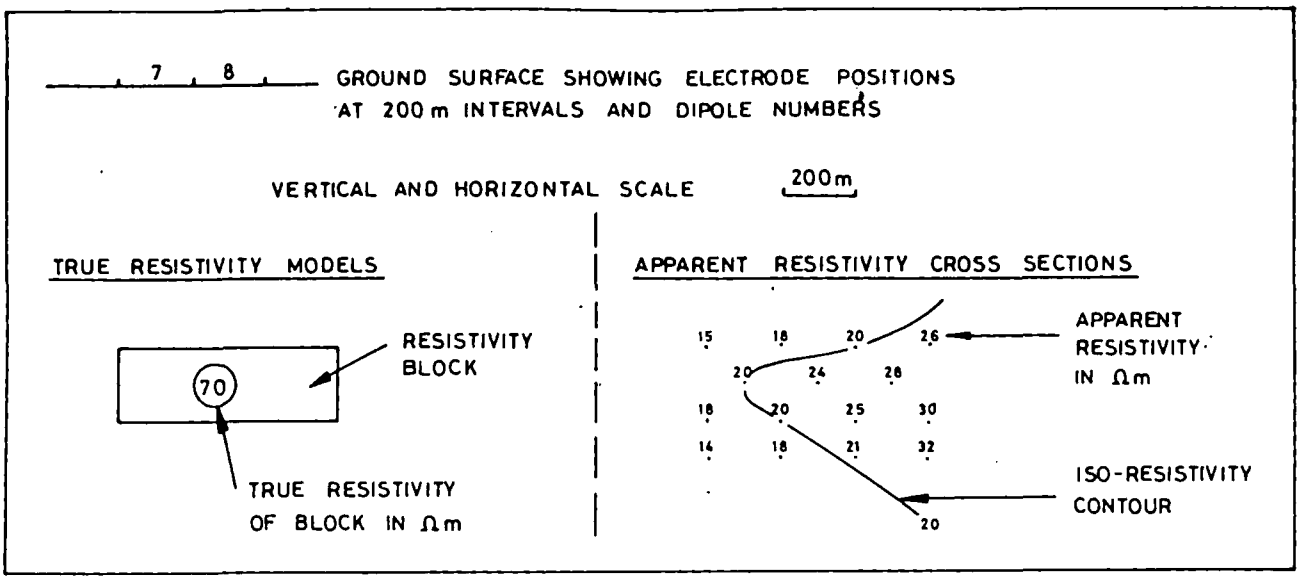

Fig. 1. Key to Figs. 2 to 14

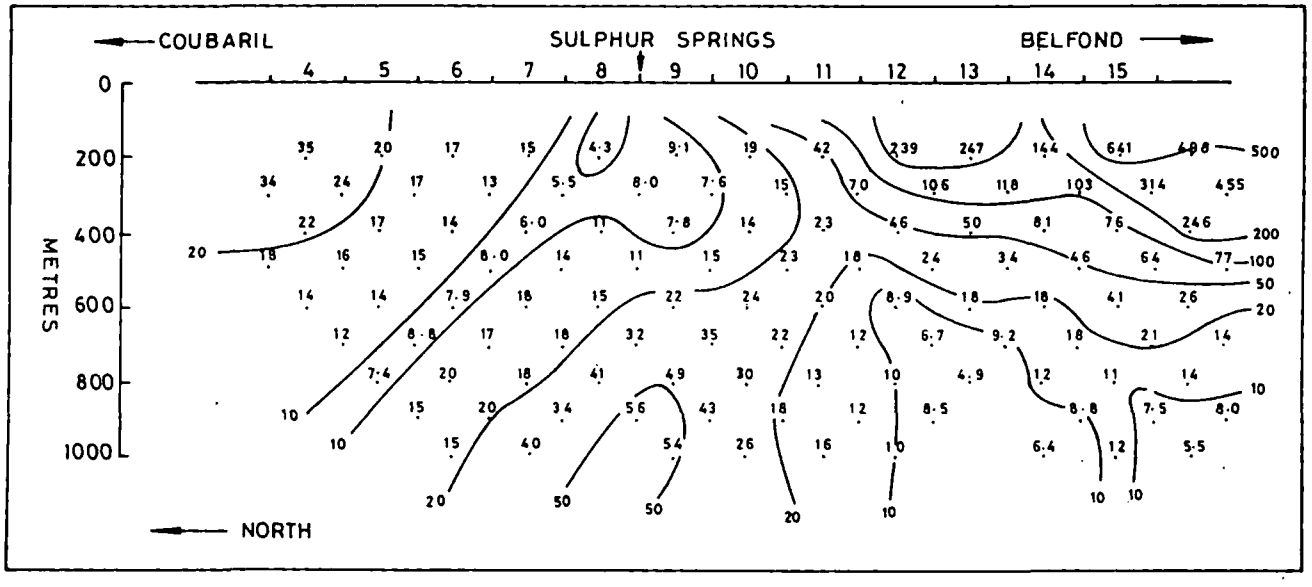

Fig. 2. Line 9 - apparent resistivity cross-section

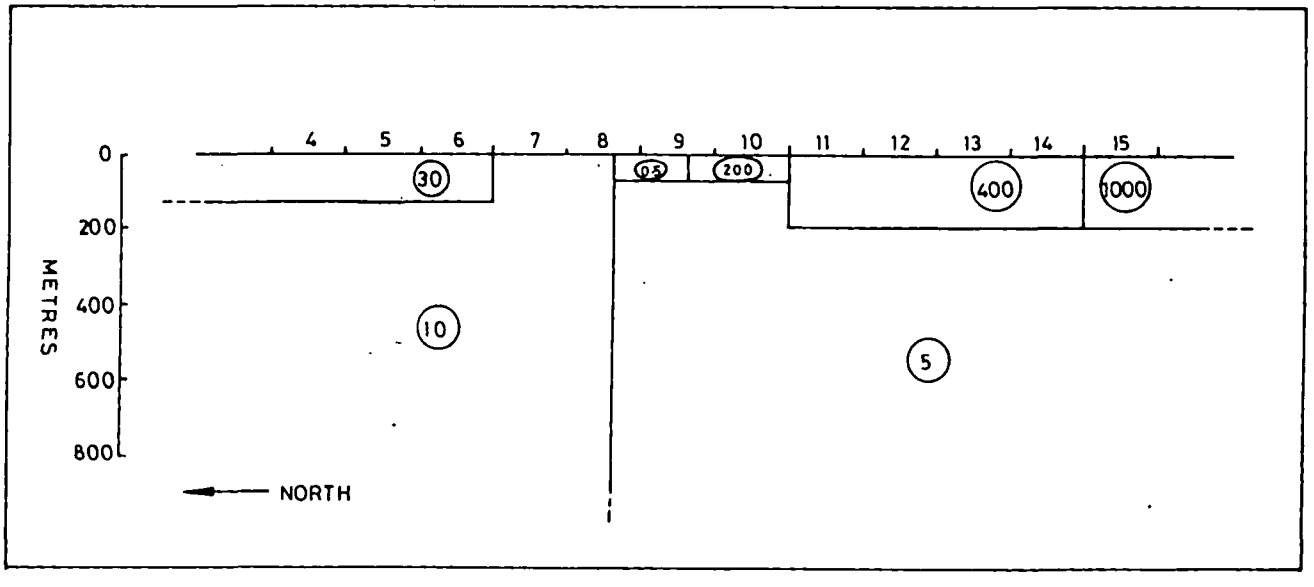

Fig. 3. Line 9 - true resistivity model 1

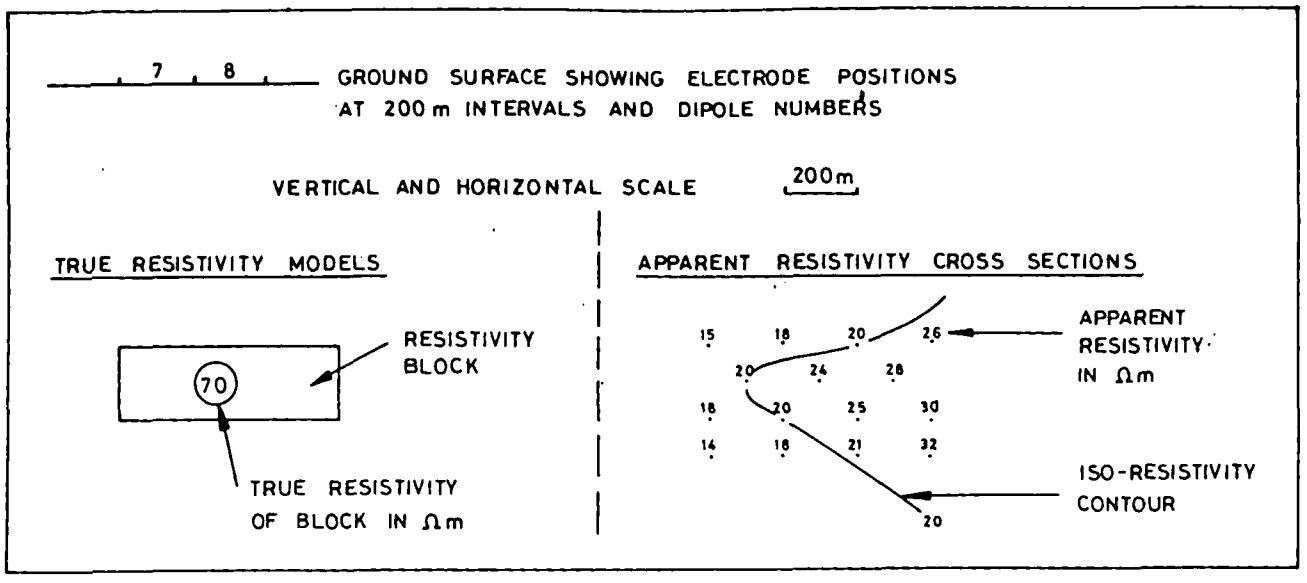

Fig. 1. Key to Figs. 2 to 14

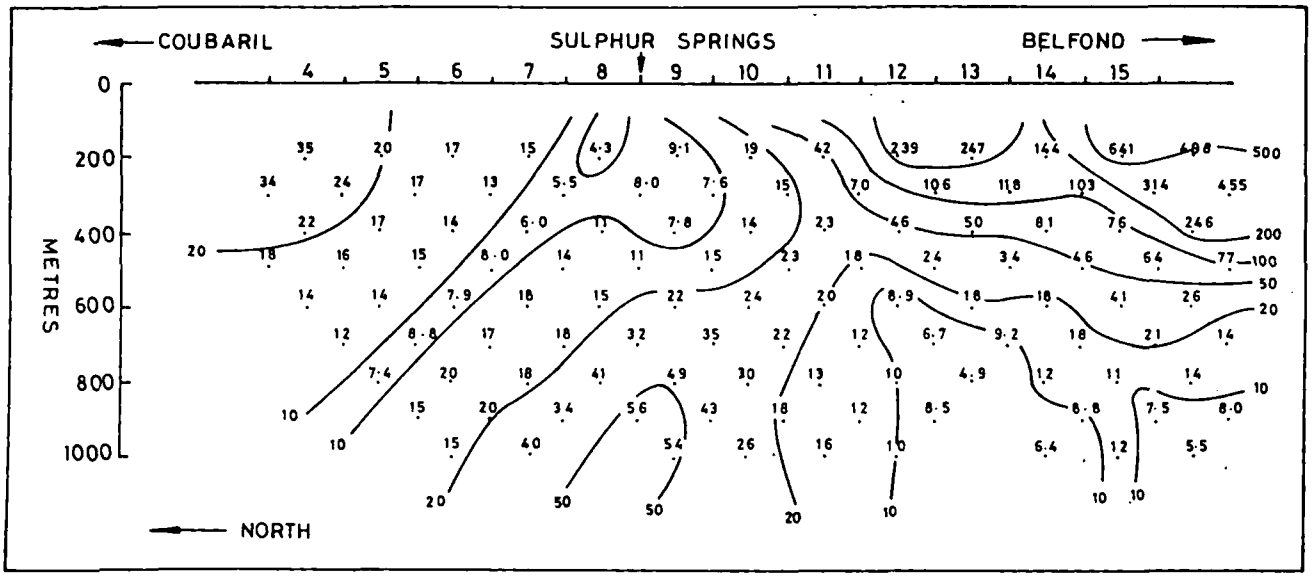

Fig. 2. Line 9 - apparent resistivity cross-section

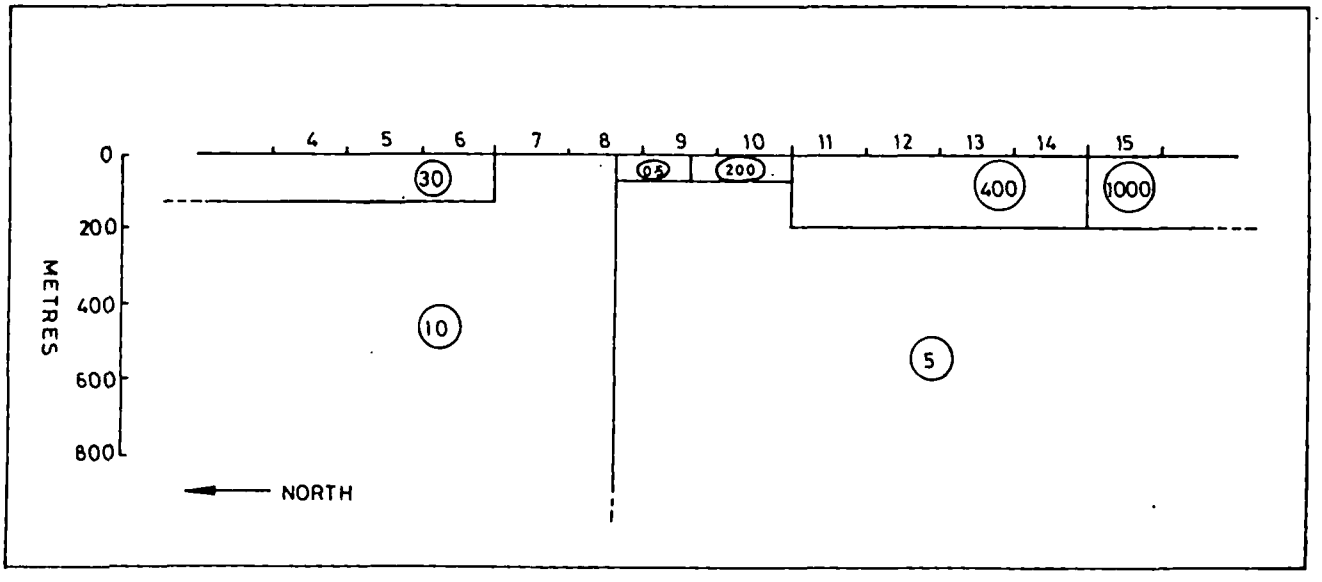

Fig. 3. Line 9 - true resistivity model 1

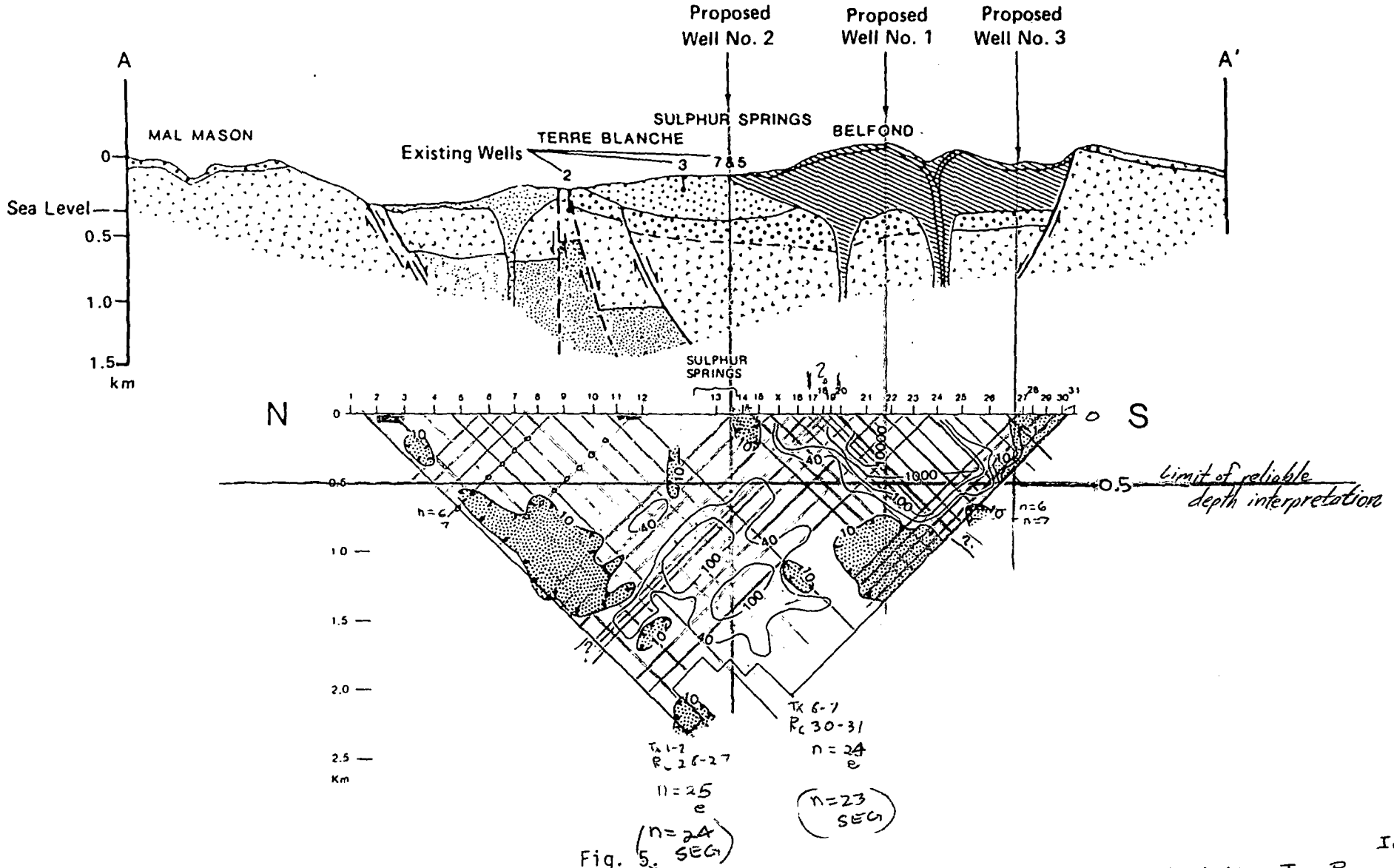

Fig. 5. Apparent resistivity data from the dipole-dipole survey plotted as a function of depth. Resistivity values are in ohm-m and are shown beneath the appropriate geologic cross section. Shaded areas depict resistivity contours of 10 ohm-m or less.

IGS

Tx	Rc	n
1-2	26-27	25
1-2	23-24	22
6-7	30-31	24

1-2 · 3-4

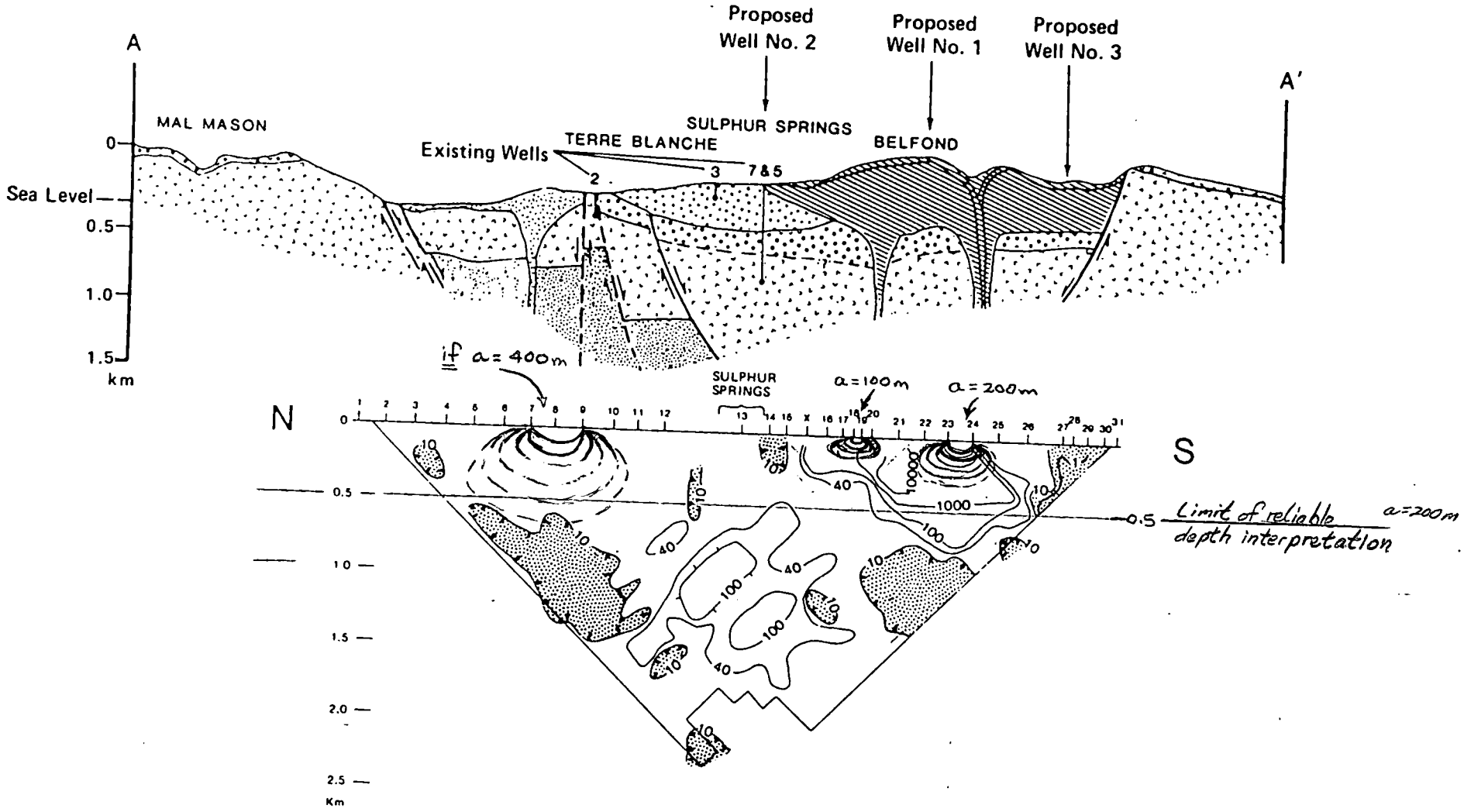

Fig. 5.
Apparent resistivity data from the dipole-dipole survey plotted as a function of depth. Resistivity values are in ohm-m and are shown beneath the appropriate geologic cross section. Shaded areas depict resistivity contours of 10 ohm-m or less.

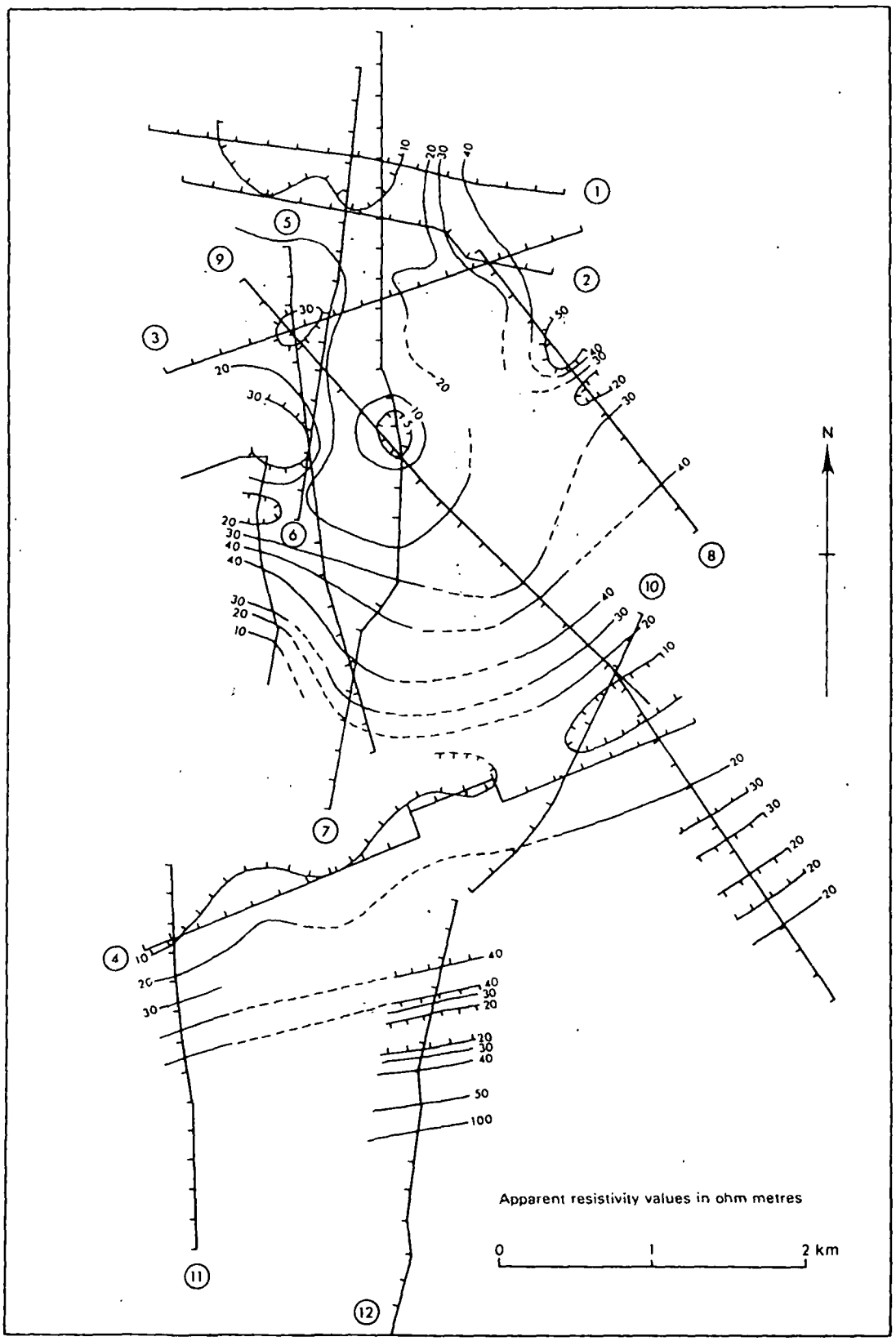

Fig. 4 Soufrière area: Apparent resistivity contours at 200m below sea level

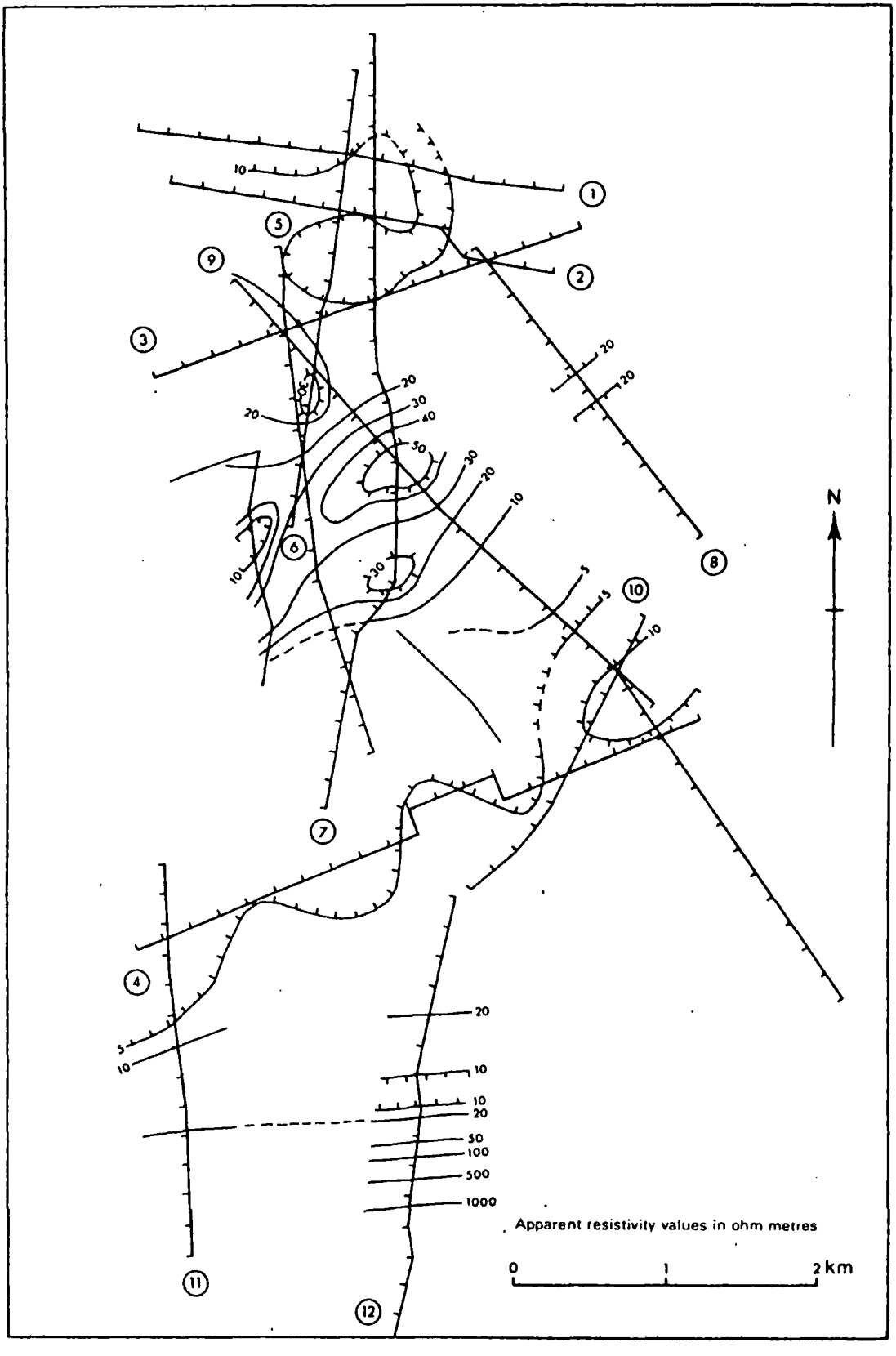

Fig. 5 Soufrière area: Apparent resistivity contours at 700m below sea level

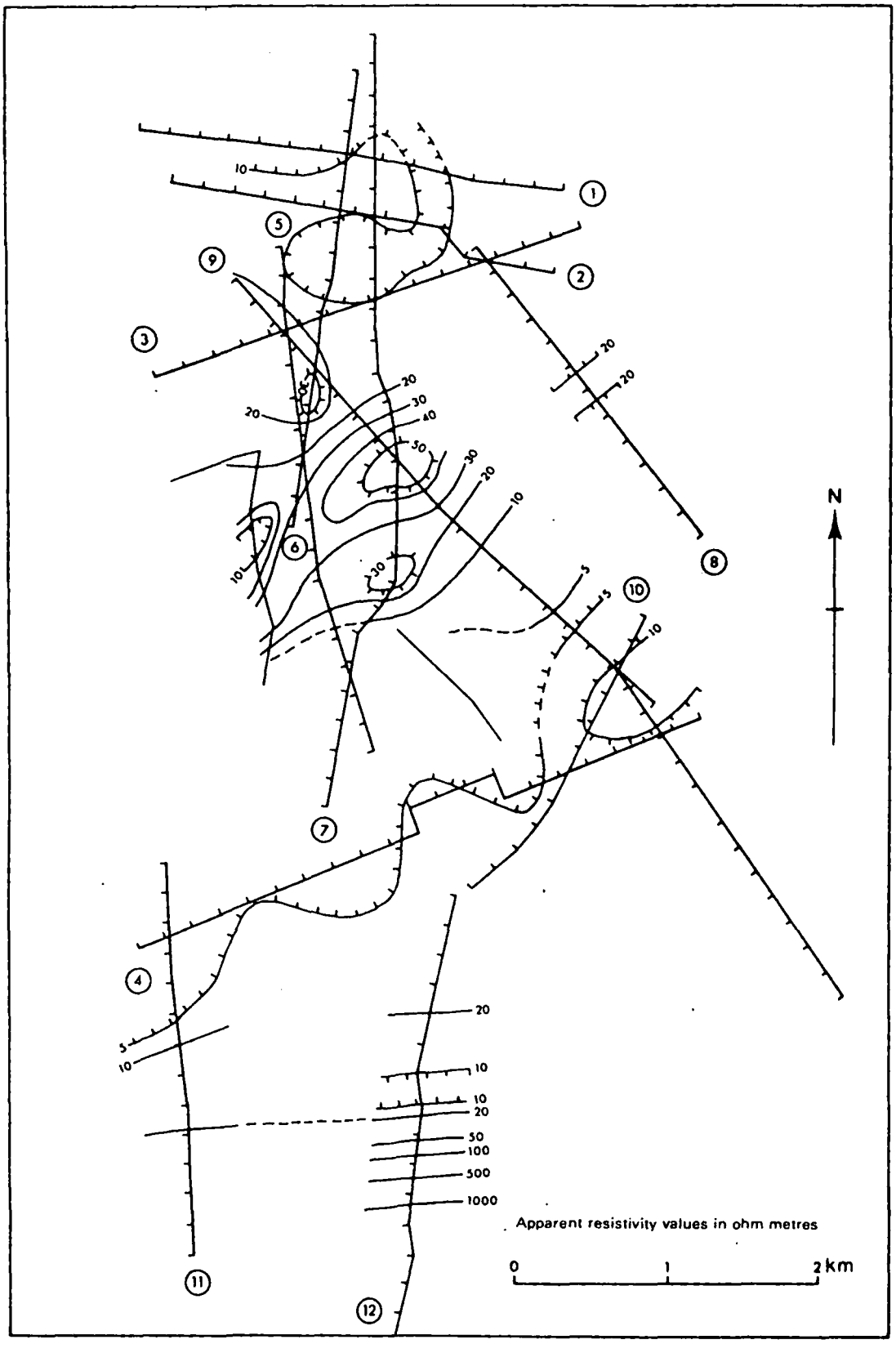

Fig. 5 Soufrière area: Apparent resistivity contours at 700m below sea level

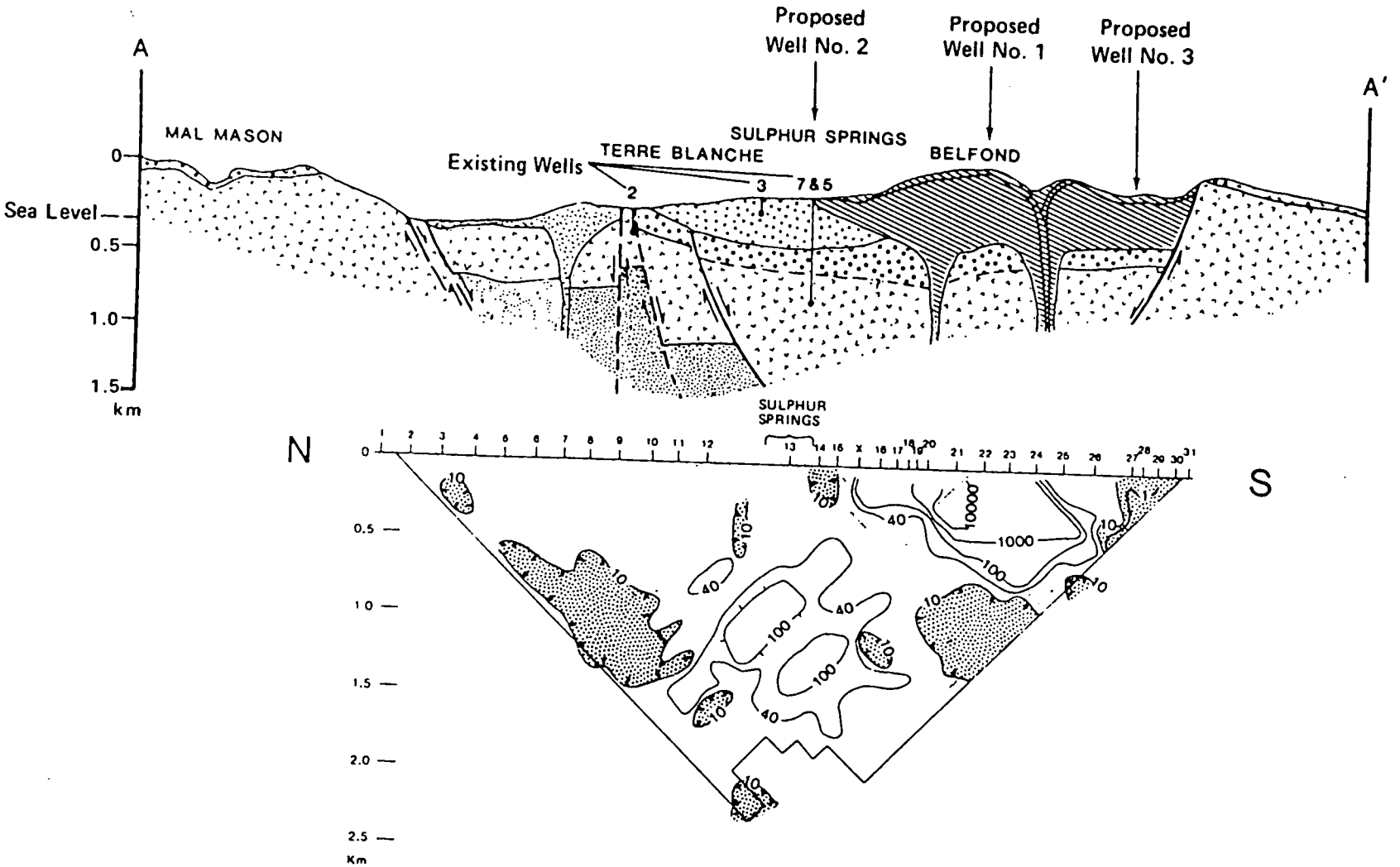

Fig. 5.
Apparent resistivity data from the dipole-dipole survey plotted as a function of depth. Resistivity values are in ohm-m and are shown beneath the appropriate geologic cross section. Shaded areas depict resistivity contours of 10 ohm-m or less.

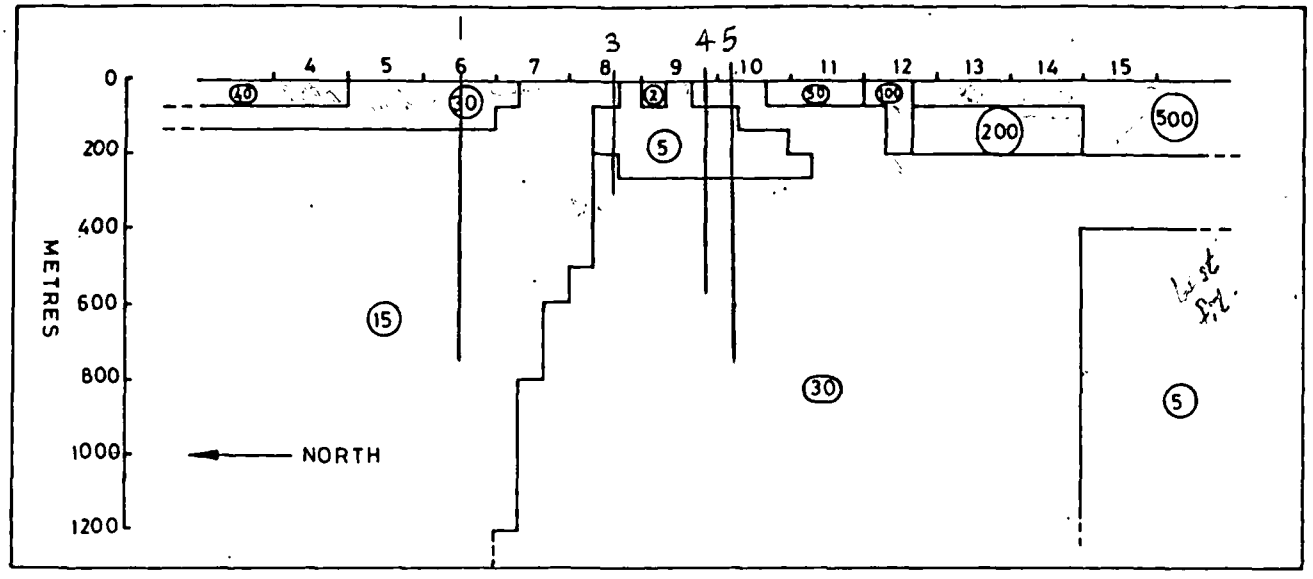

Fig. 13. Line 9 - true resistivity model 6

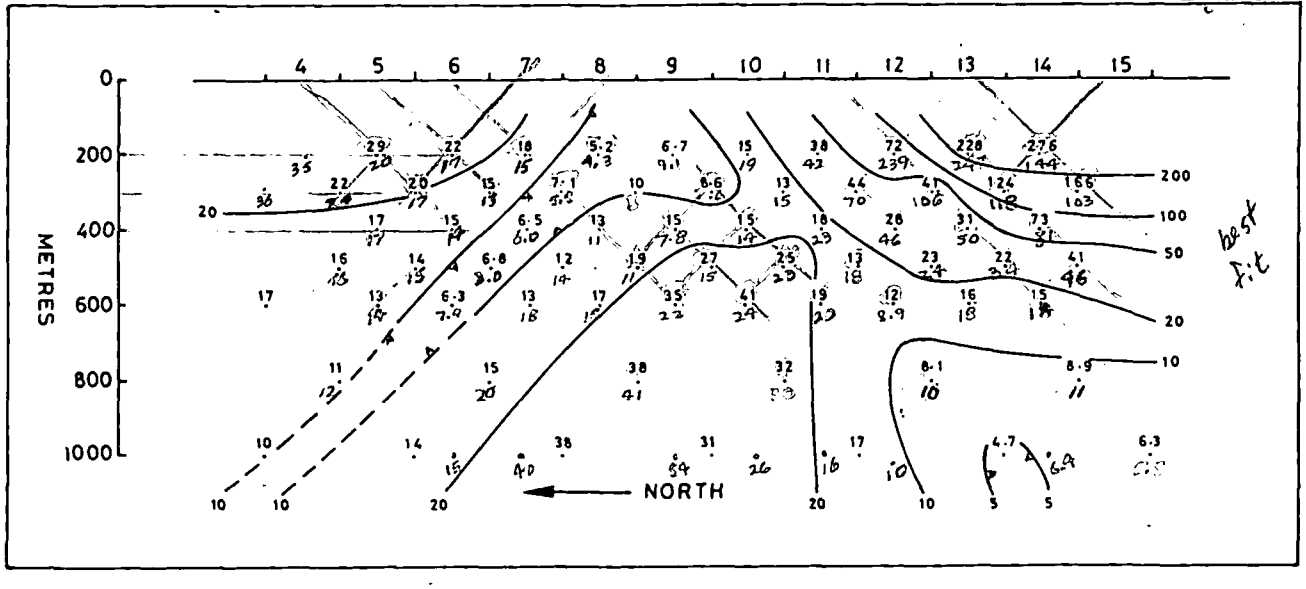

Fig. 14. Line 9 - computer generated section due to model 6

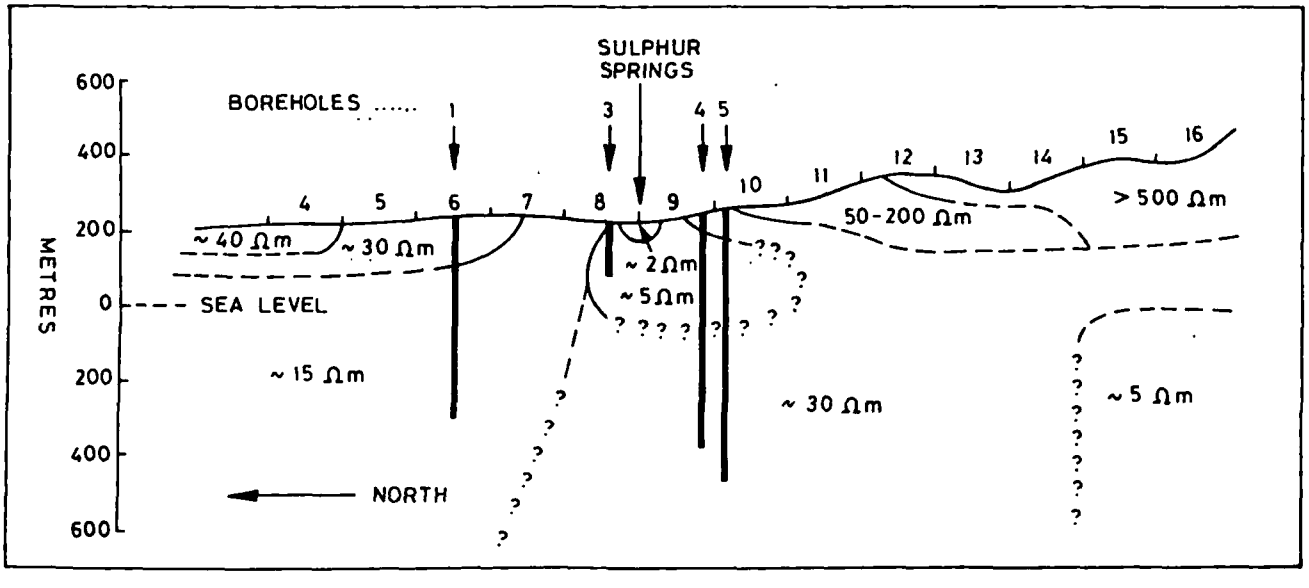

Fig. 15. Line 9 - estimated true resistivity section

Save For Island hydro. file

Q. J. Engng Geol. 1976 Vol 9 pp. 291-302 10 figs. Printed in Northern Ireland

A STUDY OF FRESH WATER LENS CONFIGURATION IN THE CAYMAN ISLANDS USING RESISTIVITY METHODS

Stephen Fredrick Bugg* & John William Lloyd†

*Richards and Dumbleton International, Consulting Civil Engineers, 4 Temple Row, Birmingham B2 5HR
†Department of Geological Sciences, University of Birmingham, P.O. Box 363, Birmingham B15 2TT

SUMMARY

The problems of identifying the base of fresh water lenses in oceanic islands are discussed. A study carried out in the Cayman Islands is described in which the lens base is defined in relation to potable water standards and mapped using surface resistivity measurements with salinity profile controls in boreholes. Using depth-salinity ratios the piezometric surface is then determined. The technique is considered to provide a reliable cheap and rapid method of obtaining lens geometry in oceanic islands particularly where fairly homogeneous lithologies are present.

Introduction

With increasing population and industrial development, the supply of water in many small oceanic islands is becoming increasingly critical. Desalinisation of sea water is proving feasible under certain circumstances but due to financial constraints reliance frequently has to be placed upon surface water retention schemes or groundwater abstraction. Sites for large surface reservoirs are normally few and the cost of construction and operation of numerous small storage dams is generally prohibitive so that the main usable sources of water usually prove to be groundwaters in the form of fresh water lenses resting upon saline water. The presence of such lenses can be readily determined but their configuration is usually difficult to ascertain economically and thus quantitative assessments rely heavily upon empiricism. As lens resources are often limited, less empiricism and better lens definition techniques are required in order that more reliable lens geometry can be determined as a basis for abstraction criteria.

The general theory of fresh water lens configuration under steady-state hydraulic conditions is well known through the Ghyben-Herzberg relationship of fresh water density to sea water density (Todd 1959). In small oceanic islands obviously only limited aereal development of lenses is possible; where, as is frequently the case, topography is low, lens formation is also severely restricted in depth due to the lack of physical height of the recharge mounds and to the density relationships. Thin lenses are thus formed which are

chiefly subjected to the dynamic effects of tide and recharge input. These lenses develop saline transition zones of significant thickness along their lower boundaries with the surrounding sea water, as described by Cooper (1959). The saline transition zones normally fall within the boundaries of fresh water lens configuration as defined by the theoretical Ghyben-Herzberg 1:40 relationship (Fig. 5) so that some reduction, to say 1:25 of the ratio, has to be applied for practical abstraction assessment purposes (Vacher 1974, Mather 1975). The modified ratio is applied to a measured piezometric surface and the lens base configuration determined with the additional aid of depth-salinity profiles based on limited numbers of boreholes. Although the method provides a moderately satisfactory approximation of lens geometry, two factors weaken its application and it could be improved by further boundary control techniques. The two complicating factors are:

(i) the determination of the piezometric surface requires that a large number of water levels have to be measured simultaneously over a full tidal cycle to obtain a mean surface, which on thin, flat, highly dynamic lenses can prove impossible, and

(ii) the application of a modified Ghyben-Herzberg ratio does not fully allow for lithological or permeability differences within the aquifer without comprehensive drilling control.

In the study discussed below these two factors have been largely discounted by direct mapping of the configuration of a suitably defined lens base. Geophysical techniques have been employed and the authors consider that these techniques can provide a reliable means of improving the definition of lens geometry under the circumstances stated. The study

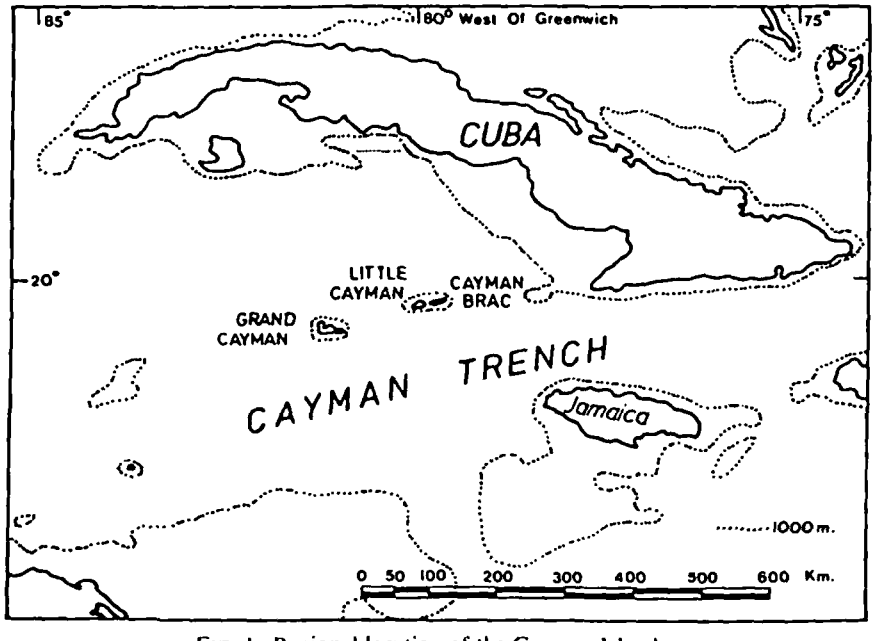

FIG. 1. Regional location of the Cayman Islands.

has been carried out in the Cayman Islands which consist largely of limestones. Application, however, is obviously not restricted to this one lithology.

Study area location

The Cayman Islands are located in the western Caribbean Sea 300 km south of Cuba (Fig. 1). They consist of three main islands situated in an isolated position on the northern edge of the Cayman Trench, a submarine depression extending from southern Cuba to the coast of Honduras. Land to sea gradients are steep with the 1000 m isobath usually occurring less than 2 km offshore. The main island is Grand Cayman which is about 40 km long from east to west and at maximum about 13 km wide. The maximum elevation on Grand Cayman is 20 m above sea level but most of the island is below 3 m and much of it is occupied by saline mangrove swamp. The islands of Little Cayman and Cayman Brac are much smaller than Grand Cayman although elevations reaching to 43 m above sea level on Cayman Brac form the highest points on the islands.

Geology of the Cayman Islands

The geological succession in the islands may be divided into three units as follows:

Age	*Formation*	*Lithology*
Recent	—	Sands and peat
Pleistocene	Ironshore	Limestone
Oligocene to Miocene	Bluff Limestone	Limestone

The Bluff Limestone was first designated as a formational name by Matley (1926) to describe the predominant limestone on the islands which is typically fossiliferous, medium to fine-grained and dominantly crystalline with soft chalky zoning. Bedding is sub-horizontal and poorly defined although the formation is well jointed. A highly developed microkarst characterises the limestone and the surface is a maze of honeycombed rock, pinnacles, ridges, fissures and sinkholes.

The Bluff Limestone Formation is overlain unconformably by the Ironshore Formation which occurs chiefly in coastal areas. Brunt *et al.* (1973) have subdivided these rocks into generally reef associated and lagoonal facies which consist predominantly of limestones with fine-grained chalky varieties typifying the lagoonal environment.

Superficial deposits are present in the form of unconsolidated marsh peats scattered throughout the islands while along the western side of Grand Cayman a major fine-grained sand beach ridge is developed. A simplified geological map of Grand Cayman is shown on Fig. 2.

The islands are not structurally complex. Brunt *et al.* (*op. cit*) consider that they may be structurally controlled by north-east to south-west trending faults and on Grand Cayman lineations are visible on air photographs which probably reflect master joint planes or minor faults.

Hydrogeology and Criteria for Lens Definition

Predominantly unconfined fresh groundwater bodies have been identified in the Islands by Mather (1971) and Wallace Evans (1974). Approximate boundaries to the lenses have been drawn but no confident lens base configurations have been detailed.

On Grand Cayman where the bulk of the present study under discussion was carried out, Mather (*op. cit*) recognized three significant lenses in the general localities as shown on Fig. 2. To consolidate Mather's work and in view of the fact that the main objective of the present study was to determine potable water resources, criteria for the definition of the

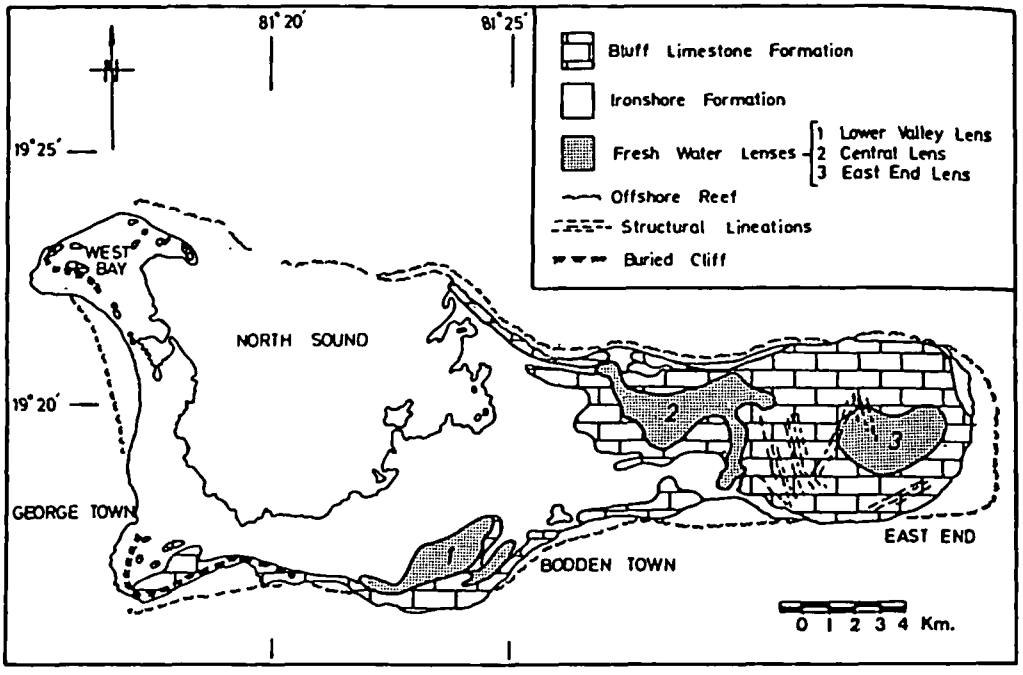

FIG. 2. Simplified geology and fresh water lenses of Grand Cayman.

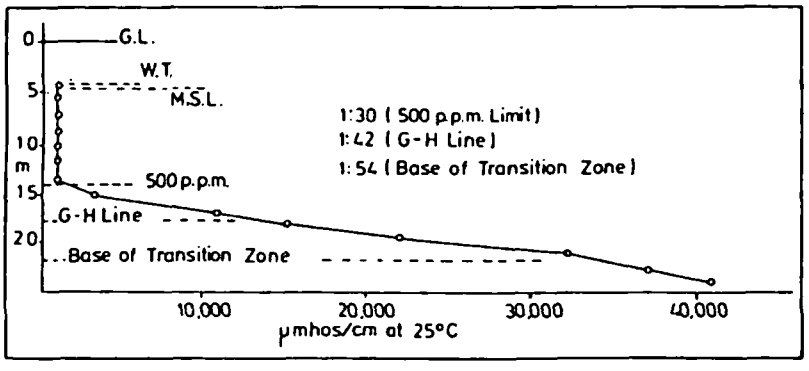

FIG. 3. Conductivity profile of a test borehole in the western lens (Lens 1).

three lenses were established based on quality. The World Health Organization potable limit for chloride, which is 600 parts per million (ppm), was taken as the initial guide together with depth-chloride profiles which indicate a rapid increase in chlorides beneath about 500 ppm where the transition zone becomes significant (Fig. 3). To allow a safety factor in the potable resources assessment a value of 500 ppm chloride was taken as defining fresh water. In the lenses where the potable limits are approached chloride is the dominant anion; when taken at 500 ppm together with other ions the total salinity does not exceed the value 1000–1100 ppm which is also within the World Health Organization standard. Other ionic concentrations do not prove hazardous within the established definition.

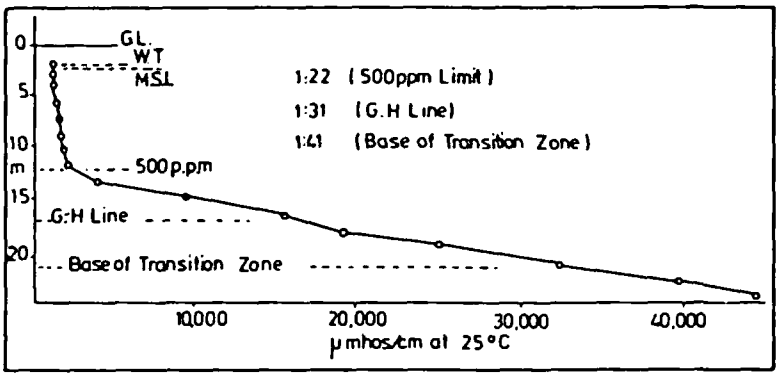

FIG. 4. Conductivity profile of test borehole No. 1 in the central lens (Lens 2).

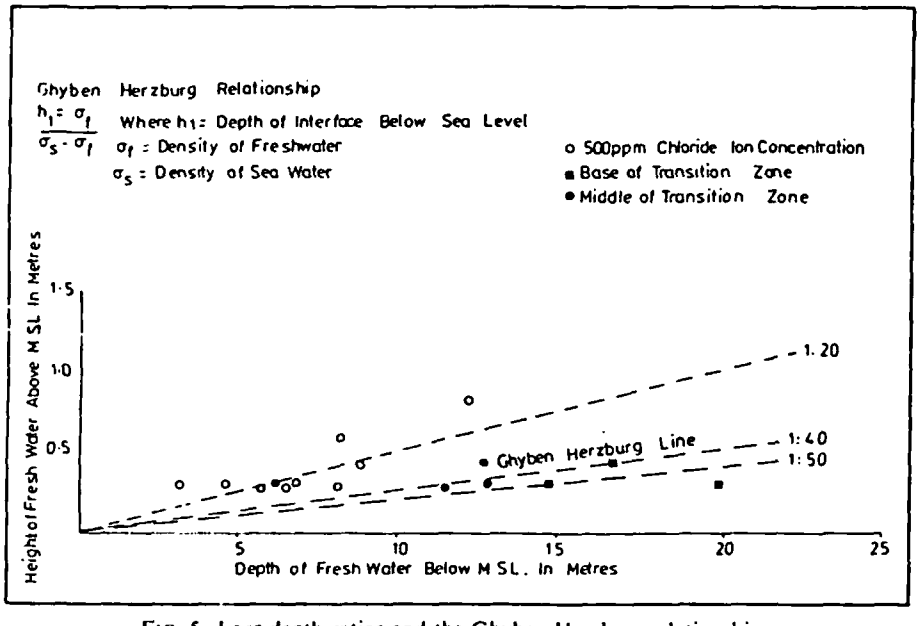

FIG. 5. Lens depth ratios and the Ghyben-Herzberg relationship.

Having defined limits, the study of the lens configuration was carried out using the following techniques:

(i) field measurements of electrical conductivity and chlorides,
(ii) borehole profiling of electrical conductivity,
(iii) borehole depth sampling for electrical conductivity and chloride measurements,
(iv) surface geophysical measurements, and
(v) limited simultaneous measurements of 'static' water levels.

For a large part, the lateral limits of the lenses in the Islands are determined by the presence of saline swamp areas so that the configuration of a lens boundary at the piezometric surface was largely based on direct chemical measurement although away from swamp areas the lens boundaries were determined by geophysical measurements. The lens bases were also determined from geophysical measurements and the piezometric surfaces were deduced from the base configurations on the basis of density relationships with limited water level control data.

Geophysical investigation

Various geophysical methods have been applied to groundwater investigations with seismic and electrical methods predominating. In the case of lens definition a significant change in electrical conductivity occurs at the top of the transition zone so that electrical methods, *viz.* electromagnetic, induced polarization and resistivity, might be considered. Electromagnetic methods suffer from the lack of a quantitative interpretation procedure particularly with regard to groundwater problems, while induced polarization equipment is

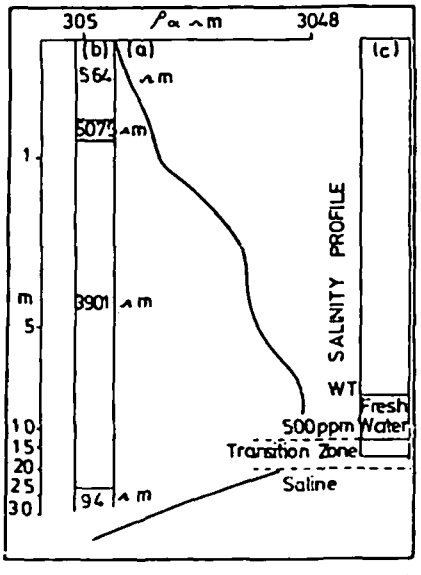

FIG. 6. Salinity interpretation of test borehole No. 1 in Lens 2 and layered model of apparent resistivity curve.

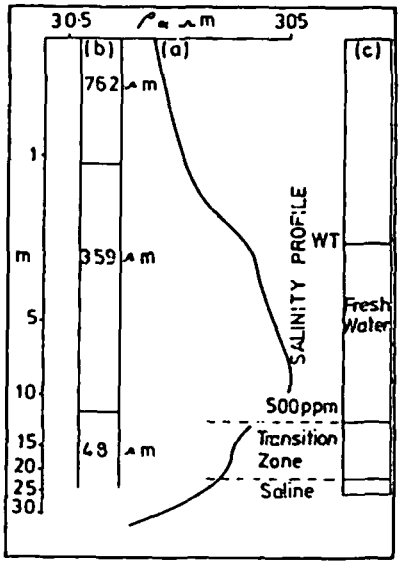

FIG. 7. Salinity interpretation of test borehole No. 2 in Lens 2 and layered model of apparent resistivity curve.

heavier and more complex than resistivity equipment and interpretation is also more complicated. The resistivity method, however, has proved successful in groundwater investigations (Swartz 1937, Flathe 1967) and was considered most practical for the environment under study. The method was therefore chosen with selection being based on the following main considerations:

(i) the presence of a high resistivity contrast at the base of a defined lens,
(ii) the resistivity method possesses adequate depth penetration to define a typical lens base,
(iii) interpretation methods give quantitative results,
(iv) the equipment is light, easily transported and does not require a vehicle for field operation, and
(v) the equipment is of a simple design amenable to local repair.

The resistivity survey was conducted using an A.B.E.M. Terrameter and a switching box to enable rapid tri-potential readings to be taken (Carpenter & Habberjam 1956). A contracting Wenner electrode configuration was used throughout with a maximum electrode separation of 58.5 m and a minimum electrode separation of 0.3 m. A total of 175 resistivity expansions were completed on Grand Cayman and nine expansions completed on Cayman Brac. Where expansions could not be carried out along the sides of roads and tracks, lines 182 m long were cut in the bush to enable the cables to be laid out and reeled in without breakage.

The field data were smoothed to minimize the effects of lateral inhomogeneities (Habberjam & Watkins 1967) and were interpreted using a partial curve matching technique

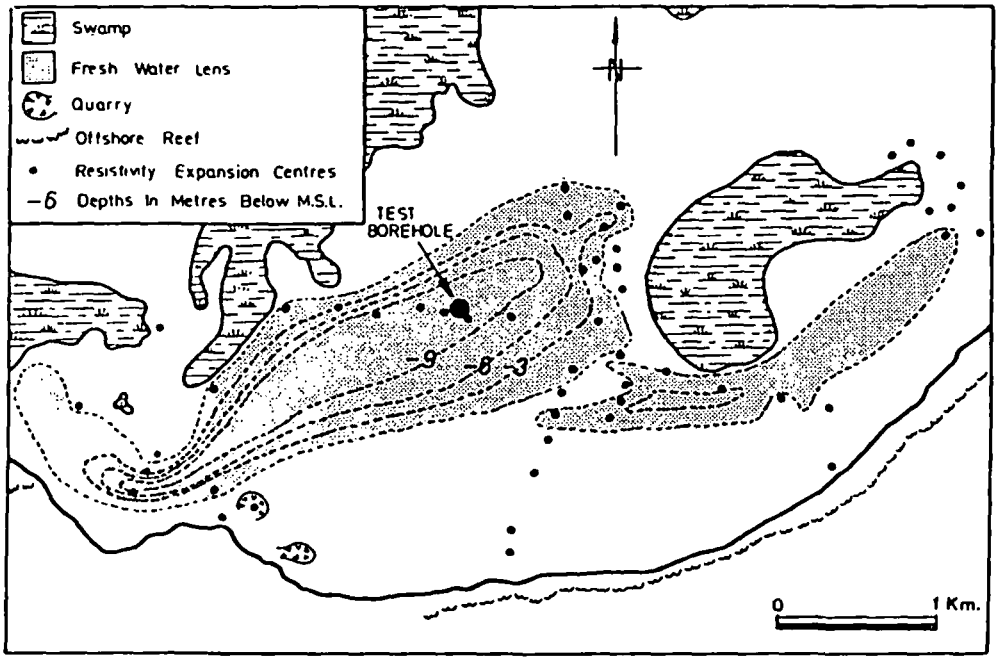

FIG. 8. Configuration of base of Lens 1.

(Koefoed 1960). Interpretations were then improved by a re-iterative process of curve re-generation and refitting (Ghosh 1971).

Six deep boreholes and many dug wells provide control over the results of the geophysical interpretation. Of the three lenses present only the central and western lenses could be tested by drilling as access other than on foot was not possible over the eastern lens. Within the deep boreholes the electrical conductivity and temperature of the groundwater were measured at 0.5 m intervals. Figures 3 and 4 illustrate the results of these conductivity profiles and the lens depth ratios measured for each case. Figure 5 shows the results from all the measured boreholes and affirms that the lens base in such a dynamic groundwater regime is more accurately represented by a reduced Ghyben-Herzburg relationship; in this case a ratio of 1:20 is more reasonable. In addition there is a suggestion from the limited data that the base of the transition zone related to a ratio of 1:50, and the depth ratio of the measured centre of the transition zone approximates to the 1:40, which would represent the fresh/saline water interface in an ideal static situation.

For interpretation purposes surface resistivity measurements were undertaken in the vicinity of the test boreholes. Figures 6 and 7 compare the field resistivity curves (b) and layered models derived from them (a) with the salinity profiles (c) derived from typical conductivity curves as shown in Figs. 3 and 4. The resistivity contrast between fresh and saline water is sufficiently great to cause a rapid change in apparent resistivity with depth, permitting location of the defined base of the fresh water lens. In a small number of cases the water table can be located, although resistivity measurements at small electrode separations may be more influenced by karstic limestone fissures filled with terra rosa than the by water table. The terra rosa infillings are recorded down to about 3 m below the surface.

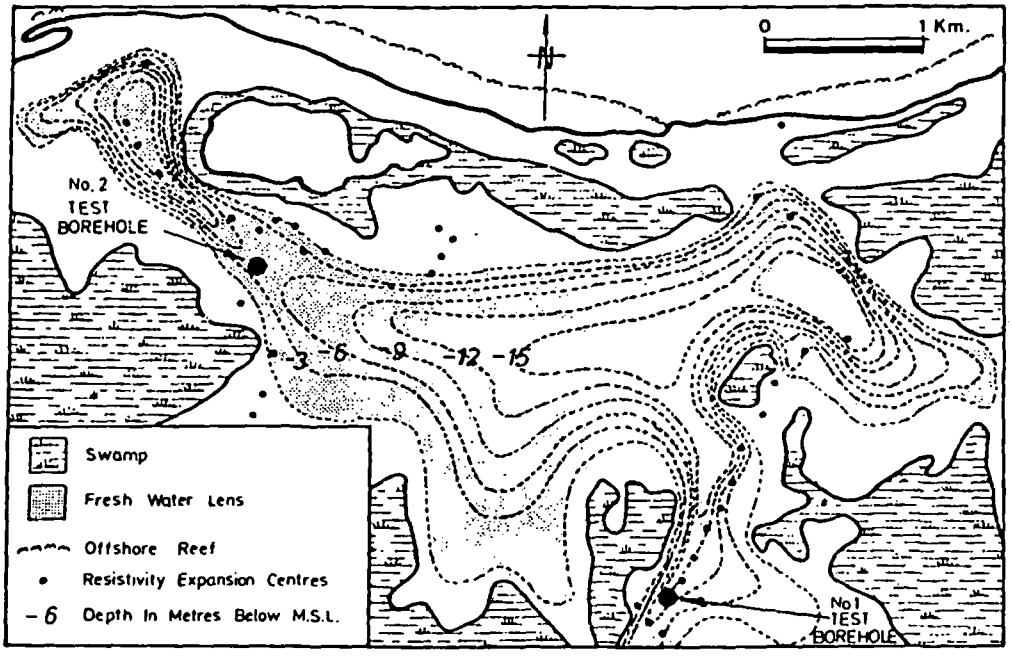

Fig. 9. Configuration of base of Lens 2.

In addition, the minor inflexions in the field curve below the main peak indicate the presence of the transition zone enabling the base of this zone to be inferred. The layered models derived from the resistivity curves accurately indicate the base of the fresh water lens in the majority of cases although problems of high contact resistance, and locally complex geology, result in some curves giving rise to hydrogeological models which are inconsistent with others from the same area.

One area where the problem of complex geology is encountered is in the western Lower Valley Lens (Lens 1, Fig. 8). Resistivity expansions located in the vicinity of the test borehole and along the eastern margin of the lens produce layered models in which the layer resistivities are of the order to tens of ohm-m as opposed to hundreds of ohm-m which is normally representative of the fresh water aquifer. Drilling results indicate that in these areas narrow chalky zones are present containing freshwater which give geophysical results notably different from those measured above karst limestone bedrock. The chalky zones in this area are not visible on the surface or identifiable on air photographs. It is not known whether the zones represent differing primary lithologies or are developed along lines of fracturing by preferential weathering. Similar zones, more intensely developed and without obscuring residual terra rose cover, are easily observable on air photographs of the eastern half of the islands, the softer weathered zones being occupied by mangrove swamps.

Lens 1 is bounded to the north-west by significant thickness of Ironshore Formation lagoonal facies and overlying swamps while the southern boundary is limited by the occurrence of a brackish transition zone developed in the highly permeable Bluff Limestone Formation. A total of sixty-two resistivity expansions were completed in the lens, access being

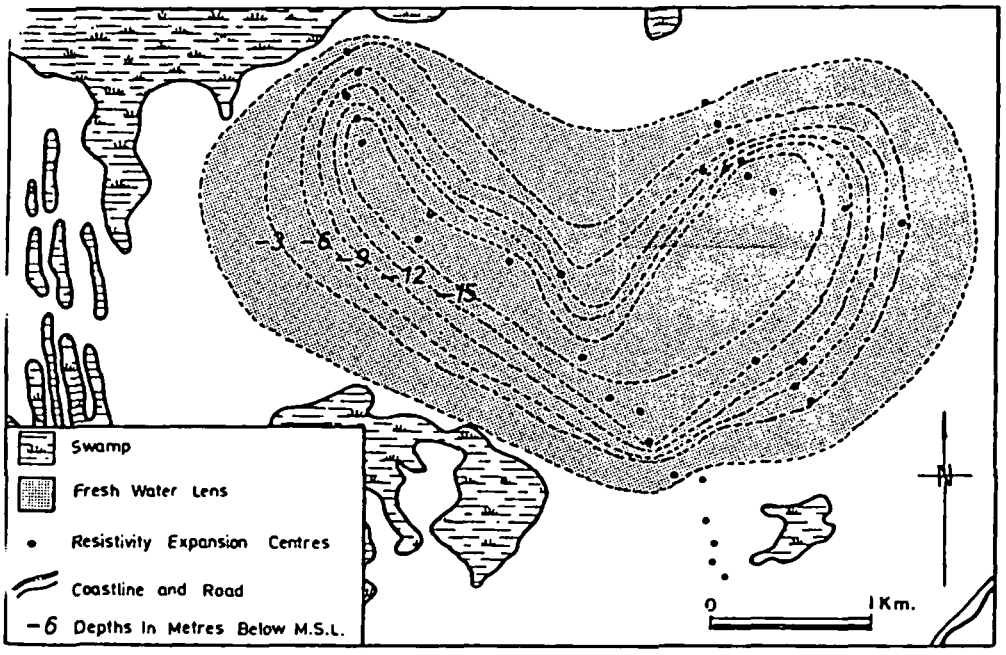

FIG. 10. Configuration of base of Lens 3.

easier than elsewhere in the interior of the island. Of these expansions, eleven failed to give interpretations which could be translated into meaningful hydrogeological models. Of the remaining expansions, not all gave results indicating the presence and thickness of the freshwater lens, but they could be interpreted in terms of brackish and/or saline groundwater and provided information about the lateral extent of the lens where swamps are not present.

In the central lens (Lens 2, Fig. 9) access was far more restricted than in the west. The central area of the lens is situated in rocks of the Bluff Limestone Formation, with Ironshore Formation deposits, commonly of the lagoonal facies, overlying the limestone in peripheral areas. Thickness of the Ironshore Formation rocks is of the order of 3 m or less. The boundary of the lens is controlled in all directions by the existence of brackish to saline swamps, developed in surrounding lower ground. The swamps are found occupying ground on both geological formations.

The Bluff Limestone Formation in this area shows an extreme development of the micro-karst topography of the islands, with deep sink holes, solution widened fissures and a honeycombed mass of porous near surface limestone. Where attempts were made to carry out resistivity expansions in these interior micro-karst areas it was found that the lack of suitable grounding medium necessitated electrodes being hammered into the rock or into crevices. High electrode to ground contact resistances occurred in such areas but usually disappeared after a few minutes, allowing reliable measurements. In some instances, however, the erratic nature of the resistances measured resulted in failure of the expansion. The difficulties in these cases are attributed to the high degree of air-filled cavities, solution holes and fissures acting as a near surface layer of extremely high resistivity.

Because of the inaccessibility of the Bluff Limestone Formation in the centre of Lens 2, many of the boreholes and resistivity expansions were completed around the more accessible fringes of the lens. Results gained in the accessible areas were extrapolated in the interior, where few data were available. A total of fifty resistivity expansions were completed of which seventeen gave rise to interpretations which did not provide meaningful hydrogeological models.

An example of this failure to provide a suitable model is illustrated in the case of test borehole No. 2 drilled on the crest of an east to west trending ridge of Bluff Limestone present along the northern boundary of the lens. The surface elevation at the borehole is 10.05 m above sea level and the water table was not encountered until 9.45 m below surface. The results of a resistivity expansion carried out at this location (Fig. 7) indicate that the observed unsmoothed field curve is representative of changes in the water quality, and can be used to infer depths to the base of the freshwater lens, and transition zone. Layered models derived from the smoothed apparent resistivity curve did not, however, reveal the existence of any fresh water. It appears that in this case the thin fresh water lens below a fairly thick unit of very high resistivity of the order of thousands of ohm-m and above a zone of very low resistivity, was "suppressed", i.e. failed to influence the curve to the extent that its existence could be deduced from the curve after smoothing.

The largest fresh water lens occurring on Grand Cayman (Lens 3) is situated in the interior of the eastern end of the island. It occurs entirely within the Bluff Limstonse Formation and has developed a broad transition zone around its perimeter (Fig. 10). The area is totally undeveloped and without roads. As a result, no drilling control was possible so

that resistivity methods were the only feasible means of determining the base of the lens using control relationships established elsewhere in the island together with depth-salinity profiles carried out in natural sink-holes.

A total of forty-eight resistivity expansions were completed of which ten could not be translated into meaningful hydrogeological models. In an attempt to achieve a suitable density of data points over the postulated lens area, resistivity expansions were completed in areas where terra rosa soils are not present to act as good grounding medium. In these locations the results tend to suffer from a high degree of lateral inhomogeneity and the depth estimations are consequently less accurate than in areas where good electrode to ground contact is achieved, i.e. in areas where residual terra rosa is present.

Discussion and conclusions

On the basis of depth-salinity profiles in the control boreholes and natural sink-holes, it is readily apparent that a marked change in salinity occurs at the top of the transition zone which approximates to a 500 ppm chloride concentration in the Cayman Islands. From surface resistivity measurements taken against control profiles it is also apparent that this marked change has sufficient electrical contrast to be reliably identified. With accurate control, therefore, surface resistivity provides a rapid and cheap method of mapping the base of fresh water lenses. It reduces substantially the cost of drilling investigations and can be carried out in areas where rig access is not possible. In the survey described, the success rate for the reliable interpretation of surface spreads undertaken was 77 per cent. Such a rate is cost acceptable, the failures being attributed to poor electrode to ground contact, lateral inhomogeneity and locally complex geology.

In the Cayman Islands study, where the base of a lens was established by resistivity measurements, the piezometric surface was calculated using a Ghyben-Herzberg ratio of 1:20 as determined by salinity profiling. Seasonal fluctuations in the piezometric surface were monitored by continuous water level recorders. In areas where resistivity spreads were not carried out due to bad surface conditions water levels were recorded in sink holes and the 1:20 ratio applied to obtain the lens base. This latter technique is subjective but was only widely applied to the centre of the central lens as no alternative practical method was available. Its use, however, in this particular study does not detract from the value of the resistivity approach.

In all parts of the lenses where adequate resistivity measurements were obtained they revealed details of lens configurations which had previously not been established and which show a marked relationship to the postulated north-west and north-east structural controls in the islands (Brunt *et al. op cit*). In particular the steep north-east trending interfaces on the western lens and the overall shape and depth configuration of the eastern lens may be noted. The emergence of these features together with the determination of similarly disposed directions of preferential permeability found during modelling of the lenses (Richards & Dumbleton 1975) add substance to the reliability and value of the resistivity survey.

In conclusion, therefore, the authors believe that surface resistivity surveys can substantially improve knowledge of the base configuration of fresh water lenses and by inference, with density relationships, indicate the shape of the piezometric surface in

unconfined aquifers where the lithologies are relatively homogeneous. Such surveys are quantitative, rapid and cheap and are eminently suitable for oceanic island studies. It is believed that their adoption will greatly assist in determining the extent of fresh water lens resources in such islands.

Acknowledgements: The authors would like to thank the Goverment of the Cayman Islands for permission to publish the paper. The work comprises part of a groundwater survey carried out by Richards and Dumbleton International, Consulting Engineers, Birmingham, England who have also kindly given permission for publication. The authors would further like to thank Mr. K. Nunn of the Department of Geological Sciences, University of Birmingham for his helpful comments on the manuscript.

References

Brunt, M. A., Gigliolt, M. E. C., Mather, J. D., Piper, D. J. W., & Richards, H. G., 1973. The Pleistocene rocks of the Cayman Islands. *Geol. Mag.* **110**, 209–304.

Carpenter, E. W., & Habberjam, 1956. A tripotential method of resistivity prospecting. *Geophysics* **21**, 455–69.

Cooper, H. H., 1959. A hypothesis concerning the dynamic balance of fresh water and salt water in a coastal aquifer. *Journal Geophysical Research*, **64**, 461–67.

Flathe', H., 1967. Interpretation of geoelectrical resistivity measurements for solving hydrogeological problems. *Canadian Geological Survey Economic Geology Rept.* **26**, 580–97.

Ghosh, G. P., 1971. Application of linear filter theory to resistivity sounding. *Geophysical Prospecting*, **19**, 193–217.

Habberjam, G. M., & Watkins, G. E., 1967. The reduction of lateral effects in resistivity probing. *Geophysical Prospecting*, **15**, 221–35.

Koefoed, O., 1960. A generalised Ciagnard Graph for the interpretation of geoelectric sounding data. *Geophysical Prospecting*, **8**, 459–69.

Matley, C. A., 1926. The geology of the Cayman Islands (B.W.I.) and their relation to the Bartlett Trough *Q. Jl Geol. Soc. Lond.* **82**, 352–87.

Mather, J. D., 1971. A preliminary survey of the groundwater resources of the Cayman Islands with recommendations for their develop ment. *Rept. of Hydrogeological Dept., Institute of Geological Sciences, London*, 91 pp (Unpublished).

——, 1975. Development of the groundwater resources of small limestone islands *Q. Jl Engng Geol.* **8**, 141–50.

Richards & Dumbleton International, 1975. Feasibility study for water supply, sewerage and storm water drainage. Vols. 1 & 2. Rept. to Government of Cayman Islands 250 pp (Unpublished).

Swartz, J. H., 1937. Resistivity studies of some salt water boundaries in the Hawaiian Islands. *Transactions American Geophysical Union*. **18**, 387–93.

Todd, D. K. 1959. *Groundwater Hydrology*. Wiley Inc., New York.

Vacher, H. L. ,1974. Groundwater Hydrology of Bermuda. Rept. to Government of Bermuda 70 pp (Unpublished).

Wallace Evans & Partners, 1974. Grand Cayman Mains Water Supply Feasibility Study. Rept. to Government of Cayman Islands 64 pp. (Unpublished).